NASA TECHNICAL NOTE

NASA TN D-7677

NASA TN D-7677

LIBRARY
RESEARCH CENTER
MOFFETT FIELD, CALIF
1974
COPY 2

DYNAMICS OF TILTING PROPROTOR AIRCRAFT IN CRUISE FLIGHT

by Wayne Johnson

Ames Research Center

and

U.S. Army Air Mobility R&D Laboratory

Moffett Field, Calif. 94035

NATIONAL AERONAUTICS AND SPACE ADMINISTRATION • WASHINGTON, D. C. • MAY 1974

1. Report No.	2. Government Accession No.	3. Recipient's Catalog No.
D- 7677		

4. Title and Subtitle	5. Report Date
DYNAMICS OF TILTING PROPROTOR AIRCRAFT IN CRUISE FLIGHT	MAY 1974
	6. Performing Organization Code

7. Author(s)	8. Performing Organization Report No.
Wayne Johnson	A-5032
	10. Work Unit No.
	760-63-03

9. Performing Organization Name and Address	11. Contract or Grant No.
NASA Ames Research Center and U. S. Army Air Mobility R&D Laboratory Moffett Field, Calif., 94035	
	13. Type of Report and Period Covered
	Technical Note

12. Sponsoring Agency Name and Address	14. Sponsoring Agency Code
National Aeronautics and Space Administration Washington, D. C., 20546	

15. Supplementary Notes

16. Abstract

A nine degree-of-freedom theoretical model is developed for investigations of the dynamics of a proprotor operating in high inflow axial flight on a cantilever wing. The basic characteristics of the rotor high inflow aerodynamics and the resulting rotor aeroelastic behavior are discussed. The problems of classical whirl flutter, the two-bladed rotor, and the influence of the proprotor on the stability derivatives of the aircraft are treated briefly. The influence of various elements of the theoretical model is discussed, including the modeling used for the blade and wing aerodynamics, and the influence of the rotor lag degree of freedom. The results from tests of two full-scale proprotors - a gimballed, stiff-inplane rotor and a hingeless, soft-inplane rotor - are presented; comparisons with the theoretical results show good correlation.

17. Key Words (Suggested by Author(s))	18. Distribution Statement
Rotary wing dynamics Tilt-rotor aircraft Proprotor	Unclassified - Unlimited CAT. 02

19. Security Classif. (of this report)	20. Security Classif. (of this page)	21. No. of Pages	22. Price*
Unclassified	Unclassified	253	$6.50

*For sale by the National Technical Information Service, Springfield, Virginia 22151

TABLE OF CONTENTS

	Page
NOMENCLATURE	v
SUMMARY	1
INTRODUCTION	1
SECTION 1: BASIC THEORY FOR PROPROTOR DYNAMICS	4
Four-Degree-of-Freedom Model	4
SECTION 2: THEORETICAL MODEL FOR A ROTOR IN HIGH INFLOW	27
Equations of Motion and Forces for the Rotor	27
The Rotor Aerodynamic Coefficients	40
SECTION 3: BEHAVIOR OF ROTORS IN HIGH INFLOW	60
Elementary Dynamic Behavior	60
Whirl Flutter	76
Two-Bladed Rotor	90
Aircraft Stability Derivatives	93
SECTION 4: NINE-DEGREE-OF-FREEDOM MODEL FOR A PROPROTOR ON A CANTILEVER WING	106
Wing Equations of Motion	106
Air Resonance	132
SECTION 5: RESULTS OF THE THEORY AND COMPARISON WITH FULL-SCALE TESTS	135
Proprotor Dynamic Characteristics	135
The Gimballed, Stiff-Inplane Rotor	145
The Hingeless, Soft-Inplane Rotor	151
SECTION 6: COMPARISONS WITH OTHER INVESTIGATIONS	156
CONCLUDING REMARKS	159
REFERENCES	161
FIGURES	165

NOMENCLATURE

Conventional helicopter notation is followed in this report, for example, for the rotor force and moment coefficients. Quantities are made dimensionless with ρ, Ω, and R (air density, rotor rotational speed, and rotor radius).

a rotor blade section two-dimensional lift curve slope

A rotor disk area, πR^2

c rotor blade chord

c_d blade section drag coefficient

c_ℓ blade section lift coefficient

c_w wing chord

C_p wing torsion structural damping

C_{q_1} wing vertical bending structural damping

C_{q_2} wing chordwise bending structural damping

C_x pylon yaw structural damping

C_y pylon pitch structural damping

C_H rotor vertical force coefficient, $\dfrac{H}{\rho\pi R^2(\Omega R)^2}$

C_{M_x} rotor lateral moment coefficient, $\dfrac{M_x}{\rho\pi R^3(\Omega R)^2}$

C_{M_y} rotor longitudinal moment coefficient, $\dfrac{M_y}{\rho\pi R^3(\Omega R)^2}$

C_P rotor power coefficient, $\dfrac{P}{\rho\pi R^2(\Omega R)^3}$

C_Q rotor torque coefficient, $\dfrac{Q}{\rho\pi R^3(\Omega R)^2}$

C_T rotor thrust coefficient, $\dfrac{T}{\rho\pi R^2(\Omega R)^2}$

C_Y rotor side force coefficient, $\frac{Y}{\rho \pi R^2 (\Omega R)^2}$

D blade section drag force per unit length

EI section modulus/moment product

f aircraft equivalent parasite drag area

F_r blade section radial aerodynamic force per unit length

F_x blade section inplane aerodynamic force per unit length

F_z blade section out of plane aerodynamic force per unit length

g_s structural damping coefficient

h rotor mast height, wing tip spar to rotor hub

h_{EA} rotor mast height, wing tip effective elastic axis to rotor hub

H rotor vertical force; also rotor aerodynamic coefficient

$H_{\dot{\beta}}^*$ $H_{\dot{\beta}} - \frac{C_T}{\sigma a}$

I_b characteristic inertia of blade bending, used to normalize rotor and support inertias

I_o $\int_0^R r^2 m \, dr$

I_{p_w} wing torsion generalized mass

I_{P_x} pylon yaw moment of inertia

I_{P_y} pylon pitch moment of inertia

I_{q_w} wing bending generalized mass

I_x pylon yaw moment of inertia (including rotor, for four-degree-of-freedom model)

I_y pylon pitch moment of inertia (including rotor, for four-degree-of-freedom model)

I_β $\int_0^R \eta_\beta{}^2 m\, dr$, blade flap inertia

$I_{\beta\alpha}$ $\int_0^R \eta_\beta r m\, dr$

I_ζ $\int_0^R \eta_\zeta{}^2 m\, dr$, blade lag inertia

$I_{\zeta\alpha}$ $\int_0^R \eta_\zeta r m\, dr$

K_p wing torsion spring constant

K_{q_1} wing vertical bending spring constant

K_{q_2} wing chordwise bending spring constant

K_x pylon yaw spring constant

K_y pylon pitch spring constant

K_P rotor blade pitch/flap coupling, tan δ_3

L blade section lift force per unit length

m blade section mass per unit length

m_P pylon mass

M rotor flap moment aerodynamic coefficient

M Mach number

M_b $\int_0^R m\, dr$, blade mass

M_x rotor lateral (yaw) hub moment

M_y rotor longitudinal (yaw) hub moment

M_F blade flap moment

M_L blade lag moment

M_{tip} tip Mach number, ΩR divided by the speed of sound

N number of blades

N_* $\dfrac{I_\beta * \left(\nu^2_{\beta_e} - 1\right)}{-\gamma M_{\dot{\beta}}}$

p wing torsion degree of freedom

q_1 wing vertical bending degree of freedom

q_2 wing chordwise bending degree of freedom

Q rotor torque; also rotor torque and lag moment aerodynamic coefficient

r blade radial station

r_e effective radius

R rotor blade radius

R rotor radial force aerodynamic coefficient

s Laplace variable in transfer functions

$sgn\ \Omega$ direction of rotation of rotor on right wing: +1 for clockwise and -1 for counterclockwise

S_w wing bending/torsion inertial coupling, $m_P z_{P_{EA}} y_{T_w}$

S_β $\displaystyle\int_0^R \eta_\beta m\, dr$

S_ζ $\displaystyle\int_0^R \eta_\zeta m\, dr$

T rotor thrust; also rotor aerodynamic coefficient

u_G longitudinal aerodynamic gust velocity

u_P blade section out of plane velocity

u_R blade section radial velocity

u_T blade section inplane velocity

U blade section resultant velocity, $\left(u_T^2 + u_P^2\right)^{1/2}$

v rotor-induced inflow; when dimensionless, the inflow ratio (forward speed divided by rotor tip speed)

V rotor or aircraft forward velocity

x vertical axis

x_P rotor shaft vertical displacement

x_w wing chordwise displacement

y lateral axis

y_P rotor shaft lateral displacement

y_{B_w} wing sweep station

y_{T_w} cantilever wing length (wing semispan)

y_w wing spanwise station

Y rotor side force

z longitudinal axis

z_{EA} wing tip elastic axis vertical shift due to dihedral

z_P rotor shaft longitudinal displacement

$z_{P_{EA}}$ pylon center-of-gravity location, forward of wing tip effective elastic axis

z_w wing vertical displacement

α blade section angle of attack

$\overline{\alpha}$ rotor blade mean angle of attack

α_G vertical aerodynamic gust velocity

α_x rotor shaft yaw angle at pivot

α_y rotor shaft pitch angle at pivot

α_z rotor shaft roll angle at pivot

β blade flap angle

β-1 low-frequency rotor flap mode

$\beta+1$ high-frequency rotor flap mode

β_G lateral aerodynamic gust velocity

β_0 rotor coning degree of freedom

β_{1C} rotor longitudinal flap degree of freedom

β_{1S} rotor lateral flap degree of freedom

γ Lock number, $\frac{\rho a c R^4}{I_b}$

$\delta( )$ small change in a quantity

δu_{P_A} component of perturbation of u_P independent of r

δu_{P_B} component of perturbation of u_P proportional to r

δu_R perturbation or u_R (independent of r)

δu_{T_A} component of perturbation of u_T proportional to r

δu_{T_B} component of perturbation of u_T independent of r

δ_{w_1} wing dihedral angle

δ_{w_2} wing angle of attack

δ_{w_2} wing sweep angle

δ_3 rotor blade pitch/flap coupling, $K_P = \tan \delta_3$

ζ blade lag angle

ζ damping ratio of oscillation, fraction of critical damping

$\zeta-1$ low-frequency rotor lag mode

$\zeta+1$ high-frequency rotor lag mode

ζ_0 rotor collective lag (or rotor speed perturbation) degree of freedom

ζ_{1C} rotor cyclic lag degree of freedom

ζ_{1S} rotor cyclic lag degree of freedom

η_β blade flap mode shape

η_ζ blade lag mode shape

η_w wing bending mode shape

θ blade pitch angle

θ_w wing torsion angle

θ_0 rotor collective pitch input

θ_{1C} rotor lateral cyclic pitch input

θ_{1S} rotor longitudinal cyclic pitch input

λ eigenvalue

ν_β blade flap rotating natural frequency

ν_{β_e} effective flap frequency, including pitch/flap coupling

ν_ζ blade lag rotating natural frequency

ξ_w wing torsion mode shape

ρ air density

σ rotor solidity, $\frac{Nc}{\pi R}$

τ time constant of a real root, $\frac{-1}{\lambda}$

ϕ blade inflow angle, $\tan^{-1} \frac{u_P}{u_T}$

ψ rotor blade azimuth angle, dimensionless time variable

ω frequency

Ω rotor rotational speed

Subscripts

o trim

θ blade pitch

μ hub inplane velocity

$\dot{\beta}$ blade flapwise velocity

λ hub out-of-plane velocity

$\dot{\zeta}$ blade lagwise velocity

$o, nc, ns, \frac{N}{2}$	rotor nonrotating degrees of freedom
0	collective rotor mode
$1C$	cyclic rotor mode
$1S$	cyclic rotor mode
m	blade index, $m = 1, \ldots, N$

Superscripts

$*$	normalized (usually by dividing by I_b or $\frac{N}{2} I_b$)
m	blade index, $m = 1, \ldots, N$

Derivatives

$(\dot{})$	$\frac{d}{d\psi}$
$(\,)'$	$\frac{d}{dr}$
$(\,)_\alpha$	$\frac{d}{d\alpha}$
$(\,)_M$	$\frac{d}{dM}$

DYNAMICS OF TILTING PROPROTOR AIRCRAFT IN CRUISE FLIGHT

Wayne Johnson

Ames Research Center
and
U.S. Army Air Mobility R&D Laboratory

SUMMARY

A theoretical model is developed for a proprotor on a cantilever wing, operating in high inflow axial flight. This theory is used to investigate the dynamic characteristics of tilting proprotor aircraft in cruise flight. The model, with a total of nine degrees of freedom, consists of first mode flap and lag blade motions of a rotor with three or more blades and the lowest frequency wing bending and torsion motions; rotor blade pitch control and aerodynamic gust excitation are included. The equations of motion for a four-degree-of-freedom model (lateral and longitudinal tip path plane tilt, pylon pitch and yaw) are obtained, primarily to introduce the methods and formulation to be used in deriving the rotor and cantilever wing equations. The basic characteristics of the rotor high inflow aerodynamics and the resulting rotor aeroelastic behavior are discussed. The problems of classical whirl flutter (a truly rigid propeller on a pylon) and the two-bladed rotor are discussed briefly. The influence of the proprotor on the stability derivatives of the aircraft is considered. The theoretical dynamic behavior of two full-scale proprotors is studied, and comparisons are made with the results of tests of these rotors in the Ames 40- by 80-Foot Wind Tunnel and with the results of other theories. These studies show the sensitivity of the theoretical results to several features and parameters of the proprotor configuration and to various elements in the theoretical model. In particular, these studies demonstrate the important influence of the rotor blade lag degree of freedom on the dynamics of both stiff inplane and soft inplane proprotor configurations, the dominance of the section lift curve slope (c_{ℓ_α}) terms in the high inflow aerodynamics of a rotor and the importance of a good structural model of the rotor blade and the wing in predicting the dynamic behavior of a proprotor. The comparisons also establish the theoretical model developed as an adequate representation of the basic proprotor and wing dynamics, which then will be a useful tool for further investigations.

INTRODUCTION

The tilting proprotor aircraft is a promising concept for short-haul V/STOL missions. This aircraft uses low disk loading rotors located on the wing tips to provide lift and control in hover and low-speed flight; it uses the same rotors to provide propulsive force in high-speed cruise, the lift then being supplied by a conventional wing. Such operation requires a 90° change in the rotor thrust angle, which is accomplished by mechanically tilting the rotor shaft axis. The rotor is vertical for helicopter mode

operation - landing and takeoff, hover, and low-speed flight - and is tilted forward for airplane mode, high-speed cruise flight. Thus the aircraft combines the efficient VTOL capability of the helicopter with the efficient, high-speed cruise capability of a turboprop aircraft. With the flexible blades of low disk loading rotors, the out-of-plane and inplane (flap and lag) motions of the blades are significant, so the blade motion is as important an aspect of tilt rotor dynamics as it is for helicopters. When in the cruise mode (axial flight at high forward speed), the rotor is operating at high inflow ratio (ratio of axial velocity to rotor tip speed); this introduces aerodynamic phenomena not encountered with the helicopter rotor, which is characterized by low inflow. The combination of flapping rotors operating at a high inflow ratio on the tips of flexible wings leads to dynamic and aerodynamic characteristics unique to this configuration, and which must be considered in the design of the aircraft. The combination of efficient VTOL and high-speed cruise capabilities is very attractive, so it is important to establish a clear understanding of the behavior of this aircraft and to formulate adequate methods for predicting it, to enable a confident design of the aircraft. Experimental and theoretical investigations have been conducted over several years to provide this capability (refs. 1 to 30). This report develops a model of the aeroelastic system for use in some initial studies of the system character and behavior. Of particular interest are the features specific to the configuration: high inflow aerodynamics of a flapping rotor in axial flow and the coupled dynamics of the rotor/pylon/wing aeroelastic system. Therefore, this work concentrates on the proprotor in airplane configuration: axial flow and high inflow ratio. In addition, rigid body degrees of freedom of the aircraft are not considered, only the elastic motion of a cantilevered wing. Many features of the coupled wing and rotor motion can be studied with such a model, theoretically and experimentally, with the understanding, of course, that the model must eventually incorporate the entire aircraft.

An introduction to the problems characteristic of a high inflow proprotor is provided by the following discussion (found in the early proprotor literature, e.g., refs. 3 and 8). Consider the behavior of the rotor in response to shaft pitch or yaw angular velocity, with the rotor operating in high inflow axial flight. A moment on the rotor disk is required to precess it to follow the shaft motion. With an articulated rotor (a rotor with a flap hinge at the center of rotation), this moment cannot be due to structural restraint between the shaft and the blade root, so it must be provided by aerodynamic forces on the blade. For example, pitch angular velocity of the shaft will require a yaw aerodynamic moment on the disk to precess it to follow the shaft. The aerodynamic moment is due to incremental lift changes on the blade sections; the component normal to the disk plane provides the yawing moment required. For high inflow flight, this incremental blade section lift also has a large inplane component and, as a result, the moment to precess the disk is accompanied by a net inplane force on the rotor hub. This force is directed to increase the rotor shaft angular velocity, so it is a negative damping force that increases with the inflow ratio. There is also the usual rotor positive damping due to tip path plane tilt of the thrust vector, plus the damping due to the hub moment for a hingeless rotor. If the inflow is high enough, the negative inplane force (H force) damping can dominate. The rotor and aircraft can be designed so that the velocity for any instability is well above the

flight regime, but the high inflow aerodynamics are always important in the analysis and design.

The behavior of the proprotor in high inflow (as outlined above) implies the following characteristics: decreased rotor/pylon/wing aeroelastic stability since the negative H force damping of the high inflow aerodynamics can reduce the dynamic stability at high forward velocity; decreased damping of the aircraft short period modes, again due to the negative H force damping contribution of the rotor; and large flapping in maneuvers and gusts. (The last arises because the moment to precess the rotor to follow the shaft is due to the flapping motion of the blades with respect to the shaft; a given shaft velocity requires a fixed component of the section aerodynamic force normal to the disk, which means then that increased incremental lift is required at high inflow and thus more flapping since flapping is the source of the lift.) These features were first delineated in the studies with the XV-3 aircraft (refs. 1 to 3), the first experimental tilting proprotor aircraft. Investigations of the concept and its problems with the XV-3 provided the initial impetus for further theoretical and experimental work with the configuration, much of which is still in progress. The work with proprotor dynamics has its basis in propeller/nacelle whirl flutter investigations (refs. 4 to 7); however, the flapping motion of the rotor introduces many new features into the dynamics. Experimental and theoretical work has been done by several organizations in the helicopter industry on the various features of tilting proprotor aircraft dynamics, aerodynamics, and design (refs. 8 to 24). This work has culminated in tests of full-scale, flight-worthy proprotors (refs. 25 and 26) and preliminary design of prototype demonstrator vehicles (refs. 27 and 28) as part of the current NASA/Army-sponsored tilt rotor research aircraft program. However, in the literature there is little concerning the details of the analysis of proprotor behavior. There are some early reports on very simple analytical models (e.g., refs. 8 and 18), and some recent reports on the most sophisticated analyses available (refs. 29 and 30). Further exploration of the basic characteristics of the proprotor dynamics is therefore desirable.

The objectives of this report are to establish a verified method to predict the dynamic behavior of the tilting proprotor aircraft in cruise flight; to develop an understanding of the dynamics of the vehicle and of the theory required to predict it; and to assess the applicability, validity, and accuracy of the model developed. The model of the wing/rotor system developed here will be useful for future investigations as well as for these initial studies. The primary application of the theory in this report is a comparison with tests in the Ames 40- by 80-Foot Wind Tunnel of two full-scale proprotors. The analysis begins with a treatment of the four-degree-of-freedom case: pylon pitch and yaw plus rotor longitudinal and lateral flapping (i.e., tip path plane pitch and yaw). With this derivation as a guide, the equations of motion are derived for a rotor with flap and lag degrees of freedom and a six-degree-of-freedom shaft motion. The high inflow aerodynamics involved are discussed, followed by some elementary considerations of the rotor behavior in high inflow. Next, the special cases of classical whirl flutter (no blade motion degrees of freedom) and the two-bladed rotor are considered briefly; the implications of the basic rotor behavior concerning the aircraft stability are investigated. After these preliminary discussions, the development of the rotor and cantilever wing model is resumed. The equations of motion for a

cantilever wing with the rotor at the tip are obtained and combined with the rotor equations of motion to produce a nine-degree-of-freedom model for tilting proprotor aircraft wing/rotor dynamics. This model is applied to two proprotor designs, in order to examine the basic features of the rotor and wing dynamics. Finally, the results of the theory are correlated with those from full-scale tests of these two proprotors in the 40- by 80-Foot Wind Tunnel.

The author wishes to thank Troy M. Gaffey of the Bell Helicopter Company and H. R. Alexander of the Boeing Vertol Company for their help in collecting the descriptions of the full-scale rotors given in table III and figures 14 to 17.

SECTION 1: BASIC THEORY FOR PROPROTOR DYNAMICS

Four-Degree-of-Freedom Model

Consider a flapping rotor on a pylon with pitch and yaw degrees of freedom operating in high inflow axial flight. Eventually, at least a few more degrees of freedom must be added to this model for both the rotor and the support. This limited model is examined first, however, to demonstrate the methods used to derive the equations of motion, and because this case is studied in the literature.

The model is shown in figure 1. The pylon has rigid-body pitch and yaw motion about a pivot, with the rotor forces acting at the hub forward of the pivot. The pylon degrees of freedom are pitch angle α_y, positive for upward rotation of the hub, and yaw angle α_x, positive for left rotation of the hub. The rigid-body pitch and yaw motion has inertia, damping, and elastic restraint about the pivot. At the hub, a distance h forward of the pylon pivot (h is the mast height) is a rotor with N blades. The rotor has clockwise rotation when viewed from the rear, with azimuth angle ψ measured from vertically upward. The azimuth position of the mth blade, $m = 1, 2, \ldots, N$ is $\psi_m = \psi + \Delta\psi$ where $\Delta\psi = 2\pi/N$ is the angle between succeeding blades. The rotor degrees of freedom are the out-of-plane motion given by the flapping angles $\beta^{(m)}$ for each blade, defined positive for forward displacement of the blade tip from the disk plane (upward in helicopter mode, which is the usual helicopter convention). The blade out-of-plane deflection is assumed to be the result of rigid-body rotation of the blade about a point at the center of rotation (by the angle $\beta^{(m)}$). The dimensionless rotating natural frequency of the flap motion is allowed to be greater than 1/rev so that blades with cantilever root constraint may be treated as well as articulated blades (which have an actual hinge at or near the center of rotation). The mode shape for the flap motion is assumed proportional to the radial distance r, that is, rigid-body rotation. The net forces exerted by the rotor on the hub from all N blades are rotor thrust T, rotor vertical force H, and rotor side force Y. It is assumed in the derivation of the equations of motion that an engine governor

supplies the torque required to hold the rotor rotational speed Ω constant during any perturbed motion, and that the pivot supplies the reaction to the rotor thrust T. The pivot also reacts the rotor vertical and side forces so that the only pylon motion is pitch and yaw about the pivot. With a flap natural frequency greater than 1/rev, as with cantilever root restraint or with a flap hinge offset or spring, blade flap motion results in a moment on the hub. The rotor pitch moment on the hub is M_y and the rotor yaw moment, M_x.

The rotor is assumed to be operating in purely axial flow in the equilibrium, unperturbed state, at velocity V. The inflow ratio $V/\Omega R$ (which may be written simply V, with the nondimensionalization implied) is assumed to be of order 1. Only rotor aerodynamics are considered; any pylon aerodynamic forces are neglected.

Equilibrium of forces and moments gives the equations of motion: flap moment equilibrium for each blade and pylon pitch and yaw moment equilibrium (about the pivot). The linearized equations of motion, that is, for small angles of the blade and pylon displacement, are then:

mth blade ($m = 1, \ldots, N$):

$$I_b[\ddot{\beta}^{(m)} + \nu_\beta{}^2\beta^{(m)} - (\ddot{\alpha}_y - 2\Omega\dot{\alpha}_x)\cos\psi_m + (\ddot{\alpha}_x + 2\Omega\dot{\alpha}_y)\sin\psi_m] = M_{F_m} \tag{1}$$

Yaw:

$$I_x\ddot{\alpha}_x + C_x\dot{\alpha}_x + K_x\alpha_x = M_x - hY \tag{2}$$

Pitch:

$$I_y\ddot{\alpha}_y + C_y\dot{\alpha}_y + K_y\alpha_y = M_y + hH \tag{3}$$

where

I_b flapping moment of inertia of the blade

$\beta^{(m)}$ flap motion of mth blade with respect to the hub

M_{F_m} aerodynamic flap moment on the blade

ν_β rotating natural frequency of flap motion (1/rev for an articulated blade with no hinge spring or offset; greater than 1/rev for a cantilever blade)

I_y, I_x pitch and yaw moment of inertia of the pylon about the pivot, including the mass of the rotor (as a point mass at the hub)

C_y, C_x pitch and yaw damping

K_y, K_x pitch and yaw spring restraint of pylon motion about pivot

These equations are now made dimensionless with ρ, Ω, and R; the inertias are normalized by dividing the flap equation of motion by I_b and the pylon equations of motion by $(N/2)I_b$. The normalization of the pylon inertia, damping, and spring constants (division by $(N/2)I_b$) are denoted by a superscript $*$; for example, $I_y^* = I_y/(N/2)I_b$. The rotor Lock number $\gamma = \rho a c R^4/I_b$ and solidity $\sigma = Nc/\pi R$ are introduced; the Lock number represents the ratio of aerodynamic to inertia forces on the rotor blade, and the solidity is the ratio of total blade area to disk area. Also notice that the normalized and dimensionless hub force H may be written in terms of the rotor coefficient:

$$\frac{H/\rho\Omega^2R^4}{(N/2)I_b/\rho R^5} = \frac{\rho a c R^4}{I_b}\frac{\pi R}{Nc}\frac{2}{a}\frac{H}{\rho\pi R^2(\Omega R)^2} = \gamma\frac{2C_H}{\sigma a}$$

and, similarly, for the other forces and moments. The equations of motion then become

$$\left.\begin{aligned} \ddot{\beta}^{(m)} + \nu_\beta^2\beta^{(m)} - (\ddot{\alpha}_y - 2\dot{\alpha}_x)\cos\psi_m + (\ddot{\alpha}_x + 2\dot{\alpha}_y)\sin\psi_m &= \gamma\frac{M_{F_m}}{ac} \\ I_x^*\ddot{\alpha}_x + C_x^*\dot{\alpha}_x + K_x^*\alpha_x &= \gamma\left(\frac{2C_{M_x}}{\sigma a} - h\frac{2C_Y}{\sigma a}\right) \\ I_y^*\ddot{\alpha}_y + C_y^*\dot{\alpha}_y + K_y^*\alpha_y &= \gamma\left(\frac{2C_{M_y}}{\sigma a} + h\frac{2C_H}{\sigma a}\right) \end{aligned}\right\} \quad (4)$$

These equations are straightforward except perhaps for the pylon acceleration terms in the flap moment equilibrium. Blade flap with respect to space is composed of $\beta^{(m)}$, flap with respect to the hub plane, plus α_y and α_x, which give the tilt of the hub plane; hence the $\ddot{\alpha}_y$ and $\ddot{\alpha}_x$ contributions to the flapwise acceleration. The remaining terms are due to Coriolis acceleration; the blade has a velocity Ωr in the hub plane, which has an angular velocity $\dot{\alpha}_x\cos\psi_m + \dot{\alpha}_y\sin\psi_m$ due to pylon motion, and the cross-product of these gives a flapwise Coriolis acceleration of the blade. In the flap equation, the dimensionless aerodynamic flap moment $M_{F_m}/\rho\Omega^2R^5$ is written as M_{F_m} for simplicity; that is, the nondimensionalization is now implicit in the notation M_{F_m}. This practice is followed in the following equations.

Now introduce a coordinate transform of the Fourier type, defining the new degrees of freedom as

$$\left.\begin{aligned} \beta_o &= \frac{1}{N}\sum_{m=1}^{N}\beta^{(m)} & \beta_{nc} &= \frac{2}{N}\sum_{m=1}^{N}\beta^{(m)}\cos n\psi_m \\ \beta_{ns} &= \frac{2}{N}\sum_{m=1}^{N}\beta^{(m)}\sin n\psi_m & \beta_{N/2} &= \frac{1}{N}\sum_{m=1}^{N}\beta^{(m)}(-1)^m \end{aligned}\right\} \quad (5)$$

so that

$$\beta^{(m)} = \beta_0 + \sum_n (\beta_{nc} \cos n\psi_m + \beta_{ns} \sin n\psi_m) + \beta_{N/2}(-1)^m \qquad (6)$$

The coning angle is β_0; β_{1C} and β_{1S} are tip path plane tilt coordinates; and $\beta_{N/2}$ is the reactionless flapping mode. The summation over n goes from 1 to $(N - 1)/2$ for N odd, and from 1 to $(N - 2)/2$ for N even; the $\beta_{N/2}$ degree of freedom appears only if N is even.

The quantities β_0, β_{nc}, β_{ns}, and $\beta_{N/2}$ are degrees of freedom, that is, functions of time (which, when dimensionless, is the rotor azimuth angle ψ) just as the quantities $\beta^{(m)}$ are. These degrees of freedom describe the rotor motion as seen in the nonrotating frame, while the $\beta^{(m)}$ terms describe the motion in the rotating frame. This coordinate transform must be accompanied by a conversion of the equations of motion for $\beta^{(m)}$ from the rotating frame to the nonrotating frame. This is accomplished by operating on the equations of motion with the summation operators:

$$\frac{1}{N}\sum_m (\ldots), \quad \frac{2}{N}\sum_m (\ldots)\cos n\psi_m, \quad \frac{2}{N}\sum_m (\ldots)\sin n\psi_m, \quad \frac{1}{N}\sum_m (\ldots)(-1)^m$$

The usefulness of the Fourier coordinate transformation lies in the simplifications it produces in the equations of motion. The above equations of motion have periodic coefficients because of the nonrotating degrees of freedom in the rotating equations of motion and vice versa; the periodic coefficients only appear explicitly so far with the pylon inertia terms in the flapping equation, but there are actually many more in the aerodynamic forces in all the equations. Since the Fourier coordinate transform converts the rotor degrees of freedom and equations of motion to the nonrotating frame, the result is constant coefficients for the inertia terms, and also for the aerodynamic terms for axial flow through the rotor (as considered here). In addition, only a limited number of the rotor nonrotating degrees of freedom couple with the pylon degrees of freedom; in this case, only the β_{1C} and β_{1S} degrees of freedom couple with α_y and α_x. The other rotor degrees of freedom are coupled from the pylon motion and represent only internal rotor motion. Thus the transformation reduced a set of $N + 2$ equations with periodic coefficients to four equations (considering only those influenced by the pylon motion) with constant coefficients. The rotor behavior for this problem is basically part of the nonrotating system, so the transformation which converts the rotor degrees of freedom and equations of motion to that frame is the appropriate one.

Operating with $(1/N)\sum_m (\ldots)$, $(2/N)\sum_m (\ldots)\cos\psi_m$, and $(2/N)\sum_m (\ldots)\sin\psi_m$ on the blade flapping equations gives the nonrotating equations for coning and tip path plane tilt motion, assuming that $N = 3$;

$$\left.\begin{aligned} \ddot{\beta}_0 + \nu_\beta^2\beta_0 &= \gamma \frac{M_{F_0}}{ac} \\ \ddot{\beta}_{1C} + 2\dot{\beta}_{1S} + (\nu_\beta^2 - 1)\beta_{1C} - \ddot{\alpha}_y + 2\dot{\alpha}_x &= \gamma \frac{M_{F_{1C}}}{ac} \\ \ddot{\beta}_{1S} - 2\beta_{1C} + (\nu_\beta^2 - 1)\beta_{1S} + \ddot{\alpha}_x + 2\dot{\alpha}_y &= \gamma \frac{M_{F_{1S}}}{ac} \end{aligned}\right\} \qquad (7)$$

where

$$M_{F_0} = \frac{1}{N}\sum_m M_{F_m}$$

$$M_{F_{1C}} = \frac{2}{N}\sum_m M_{F_m}\cos\psi_m$$

$$M_{F_{1S}} = \frac{2}{N}\sum_m M_{F_m}\sin\psi_m$$

The pitch and yaw moments on the rotor disk are $M_{F_{1C}}$ and $M_{F_{1S}}$, respectively. Note that the transformation introduces Coriolis and centrifugal acceleration terms into the β_{1C} and β_{1S} equations. The equation for β_0 does not couple inertially with α_y and α_x, nor will such coupling be found in the aerodynamics; hence it may be dropped. A set of four coupled equations remains for the degrees of freedom that describe the rotor tip path plane tilt and the pylon pitch and yaw motion: β_{1C}, β_{1S}, α_y, and α_x. If $N > 3$, the equations for β_0 β_{1C}, and β_{1S} remain as above. To these are added equations of motion for the degrees of freedom β_{2C}, β_{2S}, . . ., β_{nc}, β_{ns}, and $\beta_{N/2}$ as appropriate; like the β_0 equation, these equations are not coupled with α_y and α_x, so they may also be dropped from the set, since they represent only internal rotor motion. The four-degree-of-freedom model then is sufficient to represent the coupled rotor/pylon motion for the general case of a rotor with three or more blades. The exception is a two-bladed rotor, $N = 2$, which is considered separately in a later section.

The equations of motion for the four degrees of freedom (β_{1C}, β_{1S}, α_y, and α_x) are then

$$\begin{bmatrix} 1 & 0 & -1 & 0 \\ 0 & 1 & 0 & 1 \\ 0 & 0 & I_y^* & 0 \\ 0 & 0 & 0 & I_x^* \end{bmatrix} \begin{pmatrix} \beta_{1C} \\ \beta_{1S} \\ \alpha_y \\ \alpha_x \end{pmatrix}^{\cdot\cdot} + \begin{bmatrix} 0 & 2 & 0 & 2 \\ -2 & 0 & 2 & 0 \\ 0 & 0 & C_y^* & 0 \\ 0 & 0 & 0 & C_x^* \end{bmatrix} \begin{pmatrix} \beta_{1C} \\ \beta_{1S} \\ \alpha_y \\ \alpha_x \end{pmatrix}^{\cdot}$$

$$+ \begin{bmatrix} \nu_\beta^2 - 1 & 0 & 0 & 0 \\ 0 & \nu_\beta^2 - 1 & 0 & 0 \\ 0 & 0 & K_y^* & 0 \\ 0 & 0 & 0 & K_x^* \end{bmatrix} \begin{pmatrix} \beta_{1C} \\ \beta_{1S} \\ \alpha_y \\ \alpha_x \end{pmatrix} = \gamma \begin{pmatrix} M_{F_{1C}}/ac \\ M_{F_{1S}}/ac \\ 2C_{M_y}/\sigma a + h(2C_H/\sigma a) \\ 2C_{M_x}/\sigma a - h(2C_Y/\sigma a) \end{pmatrix} \tag{8}$$

The rotor aerodynamic forces (right-hand side) introduce much more coupling of the equations.

The hub pitch and yaw moments due to the rotor, M_y and M_x, might be found by integrating the forces on the blade (as is done for the other forces on the hub), but it is simpler to express them directly in terms of the rotor flapping motion. The source of the hub moment is the bending moment at the blade root due to flapping, $M_m = I_b(\nu_\beta^2 - 1)\beta^{(m)}$. Transforming the moment into the nonrotating frame and summing over all N blades gives the hub pitch and yaw moments:

$$\left.\begin{aligned} M_y &= \sum_m [-I_b(\nu_\beta^2 - 1)\beta^{(m)} \cos \psi_m] = -\frac{N}{2} I_b(\nu_\beta^2 - 1)\beta_{1C} \\ M_x &= \sum_m [I_b(\nu_\beta^2 - 1)\beta^{(m)} \sin \psi_m] = \frac{N}{2} I_b(\nu_\beta^2 - 1)\beta_{1S} \end{aligned}\right\} \tag{9}$$

where the definition of the tip path plane coordinates β_{1C} and β_{1S} has been applied; ν_β is the rotating natural frequency of the flap motion. If the rotor blade has a flap hinge at the center of rotation, then the only spring restraint of the blade is due to the centrifugal forces, resulting in $\nu_\beta = 1$; in that case, no moment on the hub is produced by tip path plane tilt β_{1C} and β_{1S} (except for the torque terms), as required for a hinged blade. With hinge offset, hinge spring, or a cantilever root, the natural frequency is greater than 1/rev and so tip path plane tilt produces a hub moment. Dividing by $\gamma(N/2)I_b$ gives

$$\left.\begin{aligned} \frac{2C_{M_y}}{\sigma a} &= -\frac{\nu_\beta^2 - 1}{\gamma} \beta_{1C} \\ \frac{2C_{M_x}}{\sigma a} &= \frac{\nu_\beta^2 - 1}{\gamma} \beta_{1S} \end{aligned}\right\} \tag{10}$$

Rotor aerodynamics- Consider now the rotor aerodynamics. Figure 2 shows the aerodynamic environment of the rotor blade section, and the definition of the section velocities and forces. A hub plane reference frame is used, that is, a coordinate frame fixed with respect to the shaft and tilting with pylon pitch and yaw (α_y and α_x). All forces and velocities are resolved with respect to the hub plane coordinate system, and the blade pitch angle and flap angle are measured from the hub plane. The velocities seen by the blade section are u_T (in the hub plane, positive in the blade drag direction), u_P (normal to the hub plane, positive rearward through the disk), and u_R (in the hub plane, radially outward along the blade). The resultant of u_P and u_T in the blade section is U. The blade pitch angle, θ, is composed of collective root pitch, built-in twist, and any increment due to control of the perturbed blade motion. The inflow angle is $\phi = \tan^{-1} u_P/u_T$, and the section angle of attack, $\alpha = \theta - \phi$. The aerodynamic forces on the blade section are lift L, drag D, and radial force F_r. The latter is positive outward (in the same direction as positive u_R) and has contributions from the tilt of the lift vector by blade flapping and from the radial drag due to u_R. The section lift and drag are resolved with respect to the hub plane into normal and inplane forces F_z and F_x.

The section aerodynamic lift and drag forces are expressed in terms of the lift and drag coefficients as

$$\left.\begin{aligned} L &= \frac{1}{2}\rho c(u_T^2 + u_P^2)c_\ell = \frac{c}{2}U^2 c_\ell \\ D &= \frac{1}{2}\rho c(u_T^2 + u_P^2)c_d = \frac{c}{2}U^2 c_d \end{aligned}\right\} \qquad (11)$$

Working with dimensionless quantities from this point on, the air density ρ has been dropped in the last step in equations (11). The coefficients are functions of the section angle of attack and Mach number:

$$c_\ell = c_\ell(\alpha, M)$$

$$c_d = c_d(\alpha, M)$$

where

$$\alpha = \theta - \tan^{-1}\frac{u_P}{u_T}$$

$$M = M_{tip}U$$

$$U^2 = u_T^2 + u_P^2$$

and M_{tip} is the tip Mach number, ΩR divided by the speed of sound. The section forces resolved into the hub plane are then

$$\left.\begin{aligned} F_z &= \frac{Lu_T - Du_P}{U} \\ F_x &= \frac{Lu_P + Du_T}{U} \\ F_r &= \frac{u_R D}{U} - \beta F_z \end{aligned}\right\} \tag{12}$$

The radial force F_r has terms due to radial drag and due to the tilt of F_z by the flap angle β. The radial drag term in F_r is derived assuming that the viscous drag force on the section has the same sweep angle as the local section velocity. Such a model for the radial drag force is only approximate, but is adequate for proprotors since this term is not important in high inflow aerodynamics. Substituting for L and D, and dividing by ac, where a is the two-dimensional section lift curve slope and c is the section chord, yields

$$\left.\begin{aligned} \frac{F_z}{ac} &= U\left(u_T \frac{c_\ell}{2a} - u_P \frac{c_d}{2a}\right) \\ \frac{F_x}{ac} &= U\left(u_P \frac{c_\ell}{2a} + u_T \frac{c_d}{2a}\right) \\ \frac{F_r}{ac} &= U u_R \frac{c_d}{2a} - \beta \frac{F_z}{ac} \end{aligned}\right\} \tag{13}$$

The net rotor aerodynamic forces are obtained by integrating the section forces over the span of the blade and summing over all N blades. The forces required are thrust, rotor vertical force, rotor side force, and flap moment:

$$\left.\begin{aligned} T &= \sum_m \int_0^1 F_z \, dr \\ H &= \sum_m \left(\cos \psi_m \int_0^1 F_r \, dr + \sin \psi_m \int_0^1 F_x \, dr\right) \\ Y &= \sum_m \left(\sin \psi_m \int_0^1 F_r \, dr - \cos \psi_m \int_0^1 F_x \, dr\right) \\ M_{F_m} &= \int_0^1 r F_z \, dr \end{aligned}\right\} \tag{14}$$

or, in coefficient form,

$$\left.\begin{aligned}
\frac{C_T}{\sigma a} &= \frac{1}{N}\sum_m \int_0^1 \frac{F_z}{ac}\,dr \\
\frac{2C_H}{\sigma a} &= \frac{2}{N}\sum_m \left(\cos\psi_m \int_0^1 \frac{F_r}{ac}\,dr + \sin\psi_m \int_0^1 \frac{F_x}{ac}\,dr\right) \\
\frac{2C_Y}{\sigma a} &= \frac{2}{N}\sum_m \left(\sin\psi_m \int_0^1 \frac{F_r}{ac}\,dr - \cos\psi_m \int_0^1 \frac{F_x}{ac}\,dr\right) \\
\frac{M_F}{ac} &= \int_0^1 r\,\frac{F_z}{ac}\,dr
\end{aligned}\right\} \qquad (15)$$

and for the flap equations of motion

$$M_{F_O} = \frac{1}{N}\sum_m M_{F_m}$$

$$M_{F_{1C}} = \frac{2}{N}\sum_m M_{F_m}\cos\psi_m$$

$$M_{F_{1S}} = \frac{2}{N}\sum_m M_{F_m}\sin\psi_m$$

The net blade forces required then are, if one substitutes for F_z, F_x, and F_r:

$$\left.\begin{aligned}
\int_0^1 \frac{F_z}{ac}\,dr &= \int_0^1 U\left(u_T\,\frac{c_\ell}{2a} - u_P\,\frac{c_d}{2a}\right)dr \\
\int_0^1 r\,\frac{F_x}{ac}\,dr &= \int_0^1 rU\left(u_P\,\frac{c_\ell}{2a} + u_T\,\frac{c_d}{2a}\right)dr
\end{aligned}\right\} \qquad (16)$$

(Eqs. (16) continued on next page.)

$$\left.\begin{aligned}
\int_0^1 \frac{F_x}{ac}\,dr &= \int_0^1 U\left(u_P \frac{c_\ell}{2a} + u_T \frac{c_d}{2a}\right)dr \\
\int_0^1 \frac{F_r}{ac}\,dr &= \int_0^1 U u_R \frac{c_d}{2a}\,dr - \beta \int_0^1 \frac{F_z}{ac}\,dr \\
\int_0^1 r\,\frac{F_z}{ac}\,dr &= \int_0^1 rU\left(u_T \frac{c_\ell}{2a} - u_P \frac{c_d}{2a}\right)dr
\end{aligned}\right\} \qquad (16)$$

The expressions in equations (16) give the net blade force normal to the hub plane (thrust) and its moment about the hub (flap moment), the net blade force in the hub plane (blade drag force), and the net blade radial force.

To evaluate the blade forces, the blade section pitch angle and the velocities seen by the blade section are required. Each velocity component has a trim component and a perturbation component, the latter due to the blade and pylon degrees of freedom. When the differential equations of motion are linearized, the perturbation components of the velocity are assumed to be small. The trim velocity components for operation in purely axial flow are

$$u_T = \Omega r$$

$$u_P = V + v$$

$$u_R = 0$$

The velocity u_T is due to the rotation of the blade; the rotor rotation speed Ω is included here to show the source of this velocity, but it is usually dropped when dimensionless quantities are used. The inflow u_P is composed of the forward velocity V plus the induced inflow v; the latter given by momentum theory as

$$v = -V/2 + \sqrt{(V/2)^2 + C_T/2} \qquad (17)$$

or

$$V + v = V/2 + \sqrt{(V/2)^2 + C_T/2}$$

$$\cong V + C_T/2V$$

where the last approximation is valid for large inflow V (really, the inflow ratio $V/\Omega R$, since it is dimensionless). The induced inflow will, in fact, be very small, $v/V \ll 1$, for typical proprotor operation; this is due to the high inflow V, and also to the low working C_T of a proprotor in cruise.

Consequently, induced inflow is not generally an important factor in high inflow proprotor aerodynamics, and the assumption of uniform induced inflow, or even neglecting it entirely, is reasonable for an investigation of the rotor aeroelastic behavior. Since the rotor in the unperturbed state is operating in purely axial flow, the radial velocity component u_R has no trim term. The trim blade pitch angle is determined by the collective pitch and the blade built-in twist.

The perturbation velocities are due to the rotor and pylon degrees of freedom (β, α_y, α_x here) and to the aerodynamic gusts. The convention used for the gust velocities is shown in figure 1. The gust velocities are normalized based on the forward speed V, so that the vertical and lateral gusts (α_G and β_G) are angles, and the longitudinal gust (u_G) is a fractional change in the forward speed. This convention follows the usual practice for aircraft stability and control investigations. The gust velocities are a small perturbation to the direction and magnitude of the forward velocity V, assumed uniform over the entire flow field. The gust influence is entirely aerodynamic; the gust velocities do not involve a change of the aircraft velocity with respect to an inertial frame, but only a change with respect to the air. Therefore, the gust velocities do not appear in the inertia terms of the equations of motion, but only in the aerodynamic terms. The perturbation velocities are

$$\left.\begin{aligned}
\delta u_T &= -h(\dot{\alpha}_y \sin\psi_m + \dot{\alpha}_x \cos\psi_m) \\
&\quad + (V + v)(\alpha_y \sin\psi_m + \alpha_x \cos\psi_m) \\
&\quad + V(\beta_G \cos\psi_m + \alpha_G \sin\psi_m) \\
\delta u_P &= r(\dot{\beta} - \dot{\alpha}_y \cos\psi_m + \dot{\alpha}_x \sin\psi_m) + V u_G \\
\delta u_R &= h(-\dot{\alpha}_y \cos\psi_m + \dot{\alpha}_x \sin\psi_m) \\
&\quad + (V + v)(\alpha_y \cos\psi_m - \alpha_x \sin\psi_m) \\
&\quad + V(-\beta_G \sin\psi_m + \alpha_G \cos\psi_m)
\end{aligned}\right\} \tag{18}$$

In δu_T and δu_R there are three terms: inplane hub velocity due to the angular velocity of the pylon about the pivot; inplane component of the forward velocity $V + v$ due to the tilt of the pylon; and the inplane velocity due to vertical and lateral gusts. In δu_P there are two terms: flapwise velocity with respect to the air, due to both flapping with respect to the shaft and angular velocity of the shaft (this term is proportional to r); and longitudinal gusts (this term is independent of r). If δu_P in equations (18) is written as

$$\delta u_P = r\delta u_{P_B} + \delta u_{P_A} \tag{18a}$$

then δu_T, δu_R, δu_{P_B}, and δu_{P_A} are all independent of r, and so may be factored out of the integrands in the aerodynamic forces. The perturbation of the blade pitch motion is

$$\delta\theta = \theta - K_P\beta \tag{19}$$

where now θ is just the perturbation of the blade pitch, an input variable in the equations of motion, also available for feedback control. Since this pitch perturbation is made through the control system, it is uniform over the blade span (independent of r). Also included above is pitch/flap coupling, with K_P the gain of negative feedback of blade flap angle to pitch angle. This feedback is usually accomplished by mechanical means inherent in the control-system geometry; it is then usually referred to as δ_3 coupling, where here $K_P = \tan\delta_3$.

It is now possible to find the perturbations of the aerodynamic forces on the blade, that is, the forces due to the rotor and pylon degrees of freedom and gusts. The following relations are made:

$$\left.\begin{aligned}
\delta c_\ell &= \frac{\partial c_\ell}{\partial\alpha}\delta\alpha + \frac{\partial c_\ell}{\partial M}\delta M \\
\delta c_d &= \frac{\partial c_d}{\partial\alpha}\delta\alpha + \frac{\partial c_d}{\partial M}\delta M \\
\delta\alpha &= \delta\theta - \frac{u_T\delta u_P - u_P\delta u_T}{U^2} \\
\delta U &= \frac{u_T\delta u_T + u_P\delta u_P}{U} \\
\delta M &= M_{tip}\delta U
\end{aligned}\right\} \tag{20}$$

where the coefficients of the perturbation quantities are evaluated at the trim state. Hence the net blade forces may be expended as linear combinations of the perturbations of the rotor blade velocity and pitch angle:

$$\left.\begin{aligned}
\int_0^1 \frac{F_z}{ac}\,dr &= T_o + T_\mu\delta u_T + T_{\dot\beta}\delta u_{P_B} + T_\lambda\delta u_{P_A} + T_\theta\delta\theta \\
\int_0^1 r\,\frac{F_z}{ac}\,dr &= M_o + M_\mu\delta u_T + M_{\dot\beta}\delta u_{P_B} + M_\lambda\delta u_{P_A} + M_\theta\delta\theta \\
\int_0^1 \frac{F_x}{ac}\,dr &= H_o + H_\mu\delta u_T + H_{\dot\beta}\delta u_{P_B} + H_\lambda\delta u_{P_A} + H_\theta\delta\theta \\
\int_0^1 \frac{F_r}{ac}\,dr &= R_\mu\delta u_R - \beta\int_0^1 \frac{F_z}{ac}\,dr
\end{aligned}\right\} \tag{21}$$

The coefficients are constants, independent of rotor azimuth ψ since trim axial flight is considered; they are integrals of the blade aerodynamics over the span (expressions for them are obtained later). The first terms, subscript o, are the trim forces and moments on the blade. The second terms, subscript μ, are forces and moments due to hub inplane velocity; the third terms, subscript $\dot{\beta}$, are due to flapwise velocity of the blade; the fourth terms, subscript λ, are due to axial velocity of the rotor; and the last terms, subscript θ, are due to blade pitch control. The thrust forces on the blade are T; the the flap moments, M; the blade drag forces, H; and the blade radial force R. In the blade radial force, the trim value of the coefficient of β ($\int_0^1 F_z/ac\, dr$) is required, which is just $C_T/\sigma a$; therefore,

$$\int_0^1 \frac{F_r}{ac}\, dr = R_\mu \delta u_R - \frac{C_T}{\sigma a}\beta \tag{22}$$

The last term is the radial tilt of the blade thrust vector.

The blade forces may now be summed over all N blades to find the net rotor forces. If the expressions for the blade forces (eqs. (21)) are substituted into those for the rotor forces (eqs. (15)), the aerodynamic coefficients are independent of m (blade index) so the summation operates only on the perturbations of the blade velocities and pitch. If the definitions of the rotor nonrotating degrees of freedom (the Fourier coordinate transform described above) are used, the following is obtained:

$$\left.\begin{aligned}
\frac{C_T}{\sigma a} &= T_o \\
\frac{2C_H}{\sigma a} &= (H_\mu + R_\mu)[-h\dot{\alpha}_y + (V + v)\alpha_y + V\alpha_G] \\
&\quad + H_{\dot{\beta}}(\dot{\beta}_{1S} - \beta_{1C} + \dot{\alpha}_x) \\
&\quad + H_\theta(\theta_{1S} - K_P\beta_{1S}) \\
&\quad - \frac{C_T}{\sigma a}\beta_{1C} \\
\frac{2C_Y}{\sigma a} &= -(H_\mu + R_\mu)[-h\dot{\alpha}_x + (V + v)\alpha_x + V\beta_G] \\
&\quad - H_{\dot{\beta}}(\dot{\beta}_{1C} + \beta_{1S} - \dot{\alpha}_y) \\
&\quad - H_\theta(\theta_{1C} - K_P\beta_{1C}) \\
&\quad - \frac{C_T}{\sigma a}\beta_{1S}
\end{aligned}\right\} \tag{23}$$

(Eqs. (23) continued on next page.)

$$\left.\begin{aligned}
\frac{M_{F_{1C}}}{ac} &= M_\mu[-h\dot{\alpha}_x + (V + v)\alpha_x + V\beta_G] \\
&\quad + M_{\dot{\beta}}(\dot{\beta}_{1C} + \beta_{1S} - \dot{\alpha}_y) \\
&\quad + M_\theta(\theta_{1C} - K_P\beta_{1C}) \\
\\
\frac{M_{F_{1S}}}{ac} &= M_\mu[-h\dot{\alpha}_y + (V + v)\alpha_y + V\alpha_G] \\
&\quad + M_{\dot{\beta}}(\dot{\beta}_{1S} - \beta_{1C} + \dot{\alpha}_x) \\
&\quad + M_\theta(\theta_{1S} - K_P\beta_{1S})
\end{aligned}\right\} \qquad (23)$$

The perturbations of the thrust are no longer needed (they are entirely reacted by the pivot) so only the trim term, T_O, is retained. Again, $N \geq 3$ has been assumed in evaluating the sums. The fixed frame coordinates for the blade pitch motion are

$$\left.\begin{aligned}
\theta_0 &= \frac{1}{N}\sum_m \theta^{(m)} \\
\theta_{1C} &= \frac{2}{N}\sum_m \theta^{(m)}\cos\psi_m \\
\theta_{1S} &= \frac{2}{N}\sum_m \theta^{(m)}\sin\psi_m
\end{aligned}\right\} \qquad (24)$$

These coordinates represent control inputs by means of the usual rotor swashplate mechanism: θ_0 is the rotor collective control, and θ_{1C} and θ_{1S} are rotor lateral and longitudinal cyclic control (control plane tilt).

The decoupling of the equations of motion (which has been seen in the inertia terms) is maintained by the aerodyanmics also because axial flow is assumed for the trim operating state. In the forces that excite the four-degree-of-freedom model (C_H, C_Y, $M_{F_{1C}}$, and $M_{F_{1S}}$) the only rotor degrees of freedom involved are β_{1C} and β_{1S}. The aerodynamic forces introduce some input variables, but even with these, there is limited coupling: only lateral/longitudinal control plane tilt (θ_{1C}, θ_{1S}) and lateral/longitudinal gusts appear in the four-degree-of-freedom set. As for the inertia terms, the aerodynamic terms due to the higher rotor degrees of freedom (β_{2C}, β_{2S}, . . ., β_{nc}, β_{ns}, $\beta_{N/2}$ as appropriate for $N > 3$) do not involve any coupling with the shaft motion or with the blade pitch control or gusts (assuming conventional

swashplate control inputs and uniform gusts); hence these degrees of freedom remain internal rotor dynamics.

From helicopter rotor aerodynamics, the tilt of the tip path plane (β_{1C} or β_{1S}) is expected to tilt the rotor thrust vector and hence give an inplane force on the rotor hub. The tip path plane tilt terms in C_H and C_Y are (from eqs. (23)):

$$\Delta \frac{2C_H}{\sigma a} = -\left(\frac{C_T}{\sigma a} + H_{\dot{\beta}}\right)\beta_{1C}$$

$$\Delta \frac{2C_Y}{\sigma a} = -\left(\frac{C_T}{\sigma a} + H_{\dot{\beta}}\right)\beta_{1S}$$

The first terms are the inplane forces due to radial tilt of the blade mean thrust vector by the blade flapping. They are only half that expected because of the tilt of the rotor thrust by tip path plane tilt, assuming that the thrust vector remains perpendicular to the tip path plane. The other half is in $H_{\dot{\beta}}$. Rotor tip path plane tilt β_{1C} or β_{1S}, steady in the fixed system, causes a flapping velocity in the rotating frame. This flapping velocity changes the blade angle of attack and so tilts the blade mean thrust vector in the chordwise direction (like induced drag). The inplane force due to flapping velocity, $H_{\dot{\beta}}$, may be written

$$H_{\dot{\beta}} = \frac{C_T}{\sigma a} + H_{\dot{\beta}}^{*} \tag{25}$$

where the first term is the tilt of the blade thrust, and $H_{\dot{\beta}}^{*}$ is due to the rotor inflow. Thus the inplane hub forces due to tip path plane tilt are, combining that due to direct radial tilt of the blade thrust by β, and that due to chordwise tilt of the blade thrust by $\dot{\beta}$:

$$\Delta \frac{2C_H}{\sigma a} = -\left(\frac{2C_T}{\sigma a} + H_{\dot{\beta}}^{*}\right)\beta_{1C}$$

$$\Delta \frac{2C_Y}{\sigma a} = -\left(\frac{2C_T}{\sigma a} + H_{\dot{\beta}}^{*}\right)\beta_{1S}$$

The first term is the inplane component of the rotor thrust due to tip path plane tilt, as expected, and the second is the inplane force due to the inflow term of $H_{\dot{\beta}}$ acting on $\dot{\beta}$. The inflow term $H_{\dot{\beta}}^{*}$ is negative, so it decreases the inplane force due to tip path plane tilt. For low inflow, the effect of $H_{\dot{\beta}}^{*}$ is small, but for large inflow (as considered here) it dominates the thrust vector tilt term. It is, in fact, the negative H force, already mentioned as an important feature in high inflow rotor aerodynamics. Notice that $H_{\dot{\beta}}$ acts on the blade flapwise velocity to produce an inplane force, regardless of the source; hence the angular velocity of the tip path plane (with respect to the

hub plane) or the shaft (the hub plane) also produces a hub force, with no corresponding term from the blade radial force.

Substituting now for the rotor forces and moments into equations (8), one obtains the equations of motion for the four-degree-of-freedom model:

$$
\begin{bmatrix} 1 & 0 & -1 & 0 \\ 0 & 1 & 0 & 1 \\ 0 & 0 & I_y^* & 0 \\ 0 & 0 & 0 & I_x^* \end{bmatrix} \begin{pmatrix} \beta_{1C} \\ \beta_{1S} \\ \alpha_y \\ \alpha_x \end{pmatrix}^{\cdot\cdot}
$$

$$
+ \begin{bmatrix} -\gamma M_{\dot\beta} & 2 & \gamma M_{\dot\beta} & 2+\gamma h M_\mu \\ -2 & -\gamma M_{\dot\beta} & 2+\gamma h M_\mu & -\gamma M_{\dot\beta} \\ 0 & -h\gamma H_{\dot\beta} & C_y^* + h^2\gamma(H_\mu + R_\mu) & -h\gamma H_{\dot\beta} \\ -h\gamma H_{\dot\beta} & 0 & h\gamma H_{\dot\beta} & C_x^* + h^2\gamma(H_\mu + R_\mu) \end{bmatrix} \begin{pmatrix} \beta_{1C} \\ \beta_{1S} \\ \alpha_y \\ \alpha_x \end{pmatrix}^{\cdot}
$$

$$
+ \begin{bmatrix} \nu_\beta^2 - 1 + K_P\gamma M_\theta & -\gamma M_{\dot\beta} & 0 & -\gamma(V+v)M_\mu \\ \gamma M_{\dot\beta} & \nu_\beta^2 - 1 + K_P\gamma M_\theta & -\gamma(V+v)M_\mu & 0 \\ \nu_\beta^2 - 1 + h\gamma\left(\frac{2C_T}{\sigma a} + H_{\dot\beta}^*\right) & K_P h\gamma H_\theta & K_y^* - h\gamma(V+v)(H_\mu + R_\mu) & 0 \\ K_P h\gamma H_\theta & -\left[\nu_\beta^2 - 1 + h\gamma\left(\frac{2C_T}{\sigma a} + H_{\dot\beta}^*\right)\right] & 0 & K_x^* - h\gamma(V+v)(H_\mu + R_\mu) \end{bmatrix} \begin{pmatrix} \beta_{1C} \\ \beta_{1S} \\ \alpha_y \\ \alpha_x \end{pmatrix} \tag{26}
$$

$$
= \begin{bmatrix} \gamma M_\theta & 0 \\ 0 & \gamma M_\theta \\ 0 & h\gamma H_\theta \\ h\gamma H_\theta & 0 \end{bmatrix} \begin{pmatrix} \theta_{1C} \\ \theta_{1S} \end{pmatrix} + \begin{bmatrix} \gamma V M_\mu & 0 \\ 0 & \gamma V M_\mu \\ 0 & h\gamma V(H_\mu + R_\mu) \\ h\gamma V(H_\mu + R_\mu) & 0 \end{bmatrix} \begin{pmatrix} \beta_{1C} \\ \beta_{1S} \end{pmatrix}
$$

The influence of the rotor aerodynamics in this set of equations is as follows: damping of the flap motion, $M_{\dot\beta}$, which also acts on flapping velocity due to shaft angular velocity and tip path plane tilt; speed stability flap moments M_μ due to hub velocity produced by angular velocity of the pylon about a pivot aft of the hub, and due to the inplane component of the forward velocity produced by the shaft tilt; positive damping and a negative spring on the pylon

motion due to $H_\mu + R_\mu$ (which is positive); and inplane hub forces on the pylon acting through $H_{\dot\beta}$, due to flapping velocity produced by tip path plane tilt (β_{1C}, β_{1S}) or angular velocity ($\dot\beta_{1C}$, $\dot\beta_{1S}$) or shaft angular velocity ($\dot\alpha_y$, $\dot\alpha_x$). The blade pitch input produces flap moments and hub forces through M_θ and H_θ; through pitch/flap coupling Kp these coefficients enter the coefficients of β_{1C} and β_{1S} also. Gusts produce flap moments and hub forces through the hub inplane velocity coefficients, M_μ and $H_\mu + R_\mu$.

Aerodynamic coefficients- The blade forces required are given in equations (16). Substitute for the velocities and section force coefficients in terms of the trim plus perturbation values, linearize about the trim state, and compare with the expanded forms (eqs. (21)) to identify the aerodynamic coefficients. For the moment, the effects of drag (c_d) and of compressibility (M) will be neglected. Moreover, only certain coefficients are required for the four-degree-of-freedom model, namely, T_O, Q_O, $M_{\dot\beta}$, M_μ, M_θ, $H_{\dot\beta}$, H_μ, and H_θ. Only these coefficients will be examined now; in fact, this set is sufficient to describe the general behavior of all the rotor aerodynamic coefficients required here.

If the drag coefficient is neglected (except for Q_O), the forces required are

$$\frac{C_T}{\sigma a} = T_O = \int_0^1 U u_T \frac{c_\ell}{2a}\, dr$$

$$\frac{C_Q}{\sigma a} = Q_O = \int_0^1 rU\left(u_P \frac{c_\ell}{2a} + u_T \frac{c_d}{2a}\right) dr$$

$$\int_0^1 r \frac{F_z}{ac}\, dr = \int_0^1 rU u_T \frac{c_\ell}{2a}\, dr$$

$$\int_0^1 \frac{F_x}{ac}\, dr = \int_0^1 U u_P \frac{c_\ell}{2a}\, dr$$

where $c_\ell = c_\ell(\alpha)$, $\alpha = \theta - \tan^{-1} u_P/u_T$, and $U^2 = u_T^2 + u_P^2$. With the perturbations about the trim state, the flap moment becomes

$$\int_0^1 r \frac{F_z}{ac} dr = \int_0^1 rUu_T \frac{c_\ell}{2a} dr$$

$$+ \int_0^1 r \left[\frac{c_\ell}{2a} (\delta U u_T + U \delta u_T) + U u_T \frac{c_{\ell_\alpha}}{2a} \delta\alpha \right] dr$$

$$= \int_0^1 rUu_T \frac{c_\ell}{2a} dr$$

$$+ \int_0^1 r \left[\frac{c_\ell}{2a} \left(\frac{u_T^2}{U} + U \right) + U u_T \frac{c_{\ell_\alpha}}{2a} \frac{u_P}{U^2} \right] dr \, \delta u_T$$

$$+ \int_0^1 r^2 \left[\frac{c_\ell}{2a} \frac{u_P u_T}{U} - U u_T \frac{c_{\ell_\alpha}}{2a} \frac{u_T}{U^2} \right] dr \, \delta u_{P_B}$$

$$+ \int_0^1 rUu_T \frac{c_{\ell_\alpha}}{2a} dr \, \delta\theta$$

$$= M_O + M_\mu \delta u_T + M_\beta \delta u_{P_B} + M_\theta \delta\theta$$

and, similarly, the blade drag force is

$$\int_0^1 \frac{F_x}{ac} dr = \int_0^1 Uu_P \frac{c_\ell}{2a} dr$$

$$+ \int_0^1 \left[\frac{c_\ell}{2a} (\delta U u_P + U \delta u_P) + U u_P \frac{c_{\ell_\alpha}}{2a} \delta\alpha \right] dr$$

$$= \int_0^1 Uu_P \frac{c_\ell}{2a} dr$$

$$+ \int_0^1 \left(\frac{c_\ell}{2a} \frac{u_T u_P}{U} + U u_P \frac{c_{\ell_\alpha}}{2a} \frac{u_P}{U^2} \right) dr \, \delta u_T$$

$$+ \int_0^1 r \left[\frac{c_\ell}{2a} \left(\frac{u_P^2}{U} + U \right) - U u_P \frac{c_{\ell_\alpha}}{2a} \frac{u_T}{U^2} \right] dr \, \delta u_{P_B}$$

$$+ \int_0^1 Uu_P \frac{c_{\ell_\alpha}}{2a} dr \, \delta\theta$$

$$= H_O + H_\mu \delta u_T + H_\beta \delta u_{P_B} + H_\theta \delta\theta$$

Also required is R_μ, but R_μ is due to blade radial drag force and since all drag terms are neglected for now, $R_\mu = 0$.

The coefficients are now:

$$\left.\begin{aligned}
\frac{C_T}{\sigma a} = T_O &= \int_0^1 U u_T \frac{c_\ell}{2a}\, dr \\
\frac{C_Q}{\sigma a} = Q_O &= \int_0^1 rU\left(u_P \frac{c_\ell}{2a} + u_T \frac{c_d}{2a}\right) dr \\
M_\mu &= \int_0^1 r\left[\frac{c_\ell}{2a}\left(U + \frac{u_T^2}{U}\right) + \frac{c_{\ell_\alpha}}{2a}\frac{u_T u_P}{U}\right] dr \\
M_\beta &= \int_0^1 r^2\left(\frac{c_\ell}{2a}\frac{u_T u_P}{U} - \frac{c_{\ell_\alpha}}{2a}\frac{u_T^2}{U}\right) dr \\
M_\theta &= \int_0^1 \frac{c_{\ell_\alpha}}{2a}\, rU u_T\, dr \\
H_\mu + R_\mu &= \int_0^1 \left(\frac{c_\ell}{2a}\frac{u_T u_P}{U} + \frac{c_{\ell_\alpha}}{2a}\frac{u_P^2}{U}\right) dr \\
H_\beta &= \int_0^1 r\left[\frac{c_\ell}{2a}\left(U + \frac{u_P^2}{U}\right) - \frac{c_{\ell_\alpha}}{2a}\frac{u_T u_P}{U}\right] dr \\
H_\theta &= \int_0^1 \frac{c_{\ell_\alpha}}{2a}\, U u_P\, dr
\end{aligned}\right\} \qquad (27)$$

The trim values of the velocities (u_T, u_P, and U) and of the blade loading (c_ℓ and c_{ℓ_α}) should be substituted into these expressions. For the velocities, the trim values are

$$u_T = r$$

$$u_P = V + v$$

$$V = \sqrt{r^2 + (V + v)^2}$$

For the lift coefficient and lift curve slope, assuming small angle of attack so that $c_{\ell_\alpha} = a$ (two-dimensional lift curve slope), the trim values are

$$\frac{c_\ell}{2a} = \frac{1}{2}$$

$$\frac{c_\ell}{2a} = \frac{\alpha}{2} = \frac{1}{2}\left[\theta - \tan^{-1}(V + v)/r\right]$$

where θ is here the trim collective value plus the built-in twist of the blade.

The inplane force due to flapping velocity is also written $H_{\dot\beta} = (C_T/\sigma a) + H_{\dot\beta}^*$; substituting the expression for $C_T/\sigma a$ from $H_{\dot\beta}$ (with $u_T = r$) yields

$$H_{\dot\beta}^* = \int_0^1 r\left(\frac{c_\ell}{2a}\frac{u_P^2}{U} - \frac{c_{\ell_\alpha}}{2a}\frac{u_T u_P}{U}\right)dr \tag{28}$$

Approximate expressions for the aerodynamic coefficients may be obtained by evaluating the integrands at an effective radius. Since the inflow angle is $\phi = \tan^{-1} u_P/u_T$, then also $u_T/U = \cos\phi$ and $u_P/U = \sin\phi$; from this, it is possible to substitute for u_P and U in the integrands, in terms of u_T and ϕ. Then c_ℓ and ϕ are evaluated at an effective radius r_e ($r_e = 0.75$ usually) and $u_T = r$ is used in the integrand; $c_{\ell_\alpha}/2a = 1/2$ may also be used. Then,

$$\frac{C_T}{\sigma a} = \int_0^1 \frac{r^2}{\cos\phi}\frac{\alpha}{2}\,dr \cong \frac{1}{\cos\phi}\frac{\bar\alpha}{6}$$

where $\bar\alpha$ is the rotor mean angle of attack. This expression is used to evaluate $\bar\alpha$ in the aerodynamic coefficients. The coefficient M_μ is approximately

$$M_\mu = \int_0^1 r\left[\frac{\alpha}{2}\frac{r}{\cos\phi}\left(1 + \frac{1}{\cos^2\phi}\right) + \frac{c_{\ell_\alpha}}{2a} r\sin\phi\right]dr$$

$$\cong \frac{\bar\alpha}{6\cos\phi}\left(1 + \frac{1}{\cos^2\phi}\right) + \frac{\sin\phi}{6}$$

$$\cong \frac{\sin\phi}{6} + \frac{2C_T}{\sigma a}$$

The last step follows since the C_T term ($\bar\alpha$ term) is significant only for low inflow, when ϕ is small; therefore, $[1 + (\cos\phi)^{-2}] \cong 2$. Similar approximations may be found for the other coefficients.

The aerodynamic coefficients are then approximately:

$$\left.\begin{aligned}
\frac{C_T}{\sigma a} &= \frac{\bar{\alpha}}{6\cos\phi} \\
M_\mu &= \frac{\sin\phi}{6} + \frac{2C_T}{\sigma a} \\
M_{\dot\beta} &= -\frac{\cos\phi}{8} \\
M_\theta &= \frac{1}{8\cos\phi} \\
H_\mu + R_\mu &= \frac{V\sin\phi}{2} + \frac{2C_T}{\sigma a}V \\
H_{\dot\beta} &= -\frac{\sin\phi}{6} + \frac{C_T}{\sigma a} \\
H_\theta &= \frac{V}{4\cos\phi}
\end{aligned}\right\} \qquad (29)$$

where ϕ is evaluated at r_e, so that

$$\cos\phi = r_e/\sqrt{r_e^2 + V^2}$$

$$\sin\phi = V/\sqrt{r_e^2 + V^2}$$

and usually $r_e = 3/4$ is satisfactory. The thrust coefficient (c_ℓ) terms in $M_{\dot\beta}$ (flap damping) are always negligible and were therefore dropped. There are no c_ℓ terms in the pitch coefficients M_θ and H_θ. For operation in high inflow, V is of order 1 and so cos ϕ and sin ϕ are of order 1 also; $C_T/\sigma a << 1$ (in fact, for proprotor operation in cruise, the blade loading is even lower than usual for helicopters). Hence for high inflow operation, the thrust effects on all the aerodynamic coefficients (c_ℓ terms) may reasonably be neglected compared with the c_{ℓ_α} terms. The reason the c_{ℓ_α} terms dominate the coefficients is that with high inflow both inplane and out-of-plane velocity perturbations give large angle-of-attack changes. Therefore they give (through c_{ℓ_α}) large section lift perturbations, which have significant components in both the out-of-plane and inplane directions. The high inflow thus allows a great simplification of the rotor aerodynamic derivatives.

Retaining now only the c_{ℓ_α} terms in equations (27), that is, assuming that V is of order 1 and $\alpha \ll 1$, and substituting for the trim velocities, one obtains the coefficients (writing V for $V + v$ for convenience):

$$M_\mu = \int_0^1 \frac{c_{\ell_\alpha}}{2a} \frac{r^2 V}{\sqrt{r^2 + V^2}}\, dr$$

$$M_\beta^{\cdot} = -\int_0^1 \frac{c_{\ell_\alpha}}{2a} \frac{r^4}{\sqrt{r^2 + V^2}}\, dr$$

$$M_\theta = \int_0^1 \frac{c_{\ell_\alpha}}{2a} r^2 \sqrt{r^2 + V^2}\, dr$$

$$H_\mu + R_\mu = \int_0^1 \frac{c_{\ell_\alpha}}{2a} \frac{V^2}{\sqrt{r^2 + V^2}}\, dr$$

$$H_\beta^{\cdot *} = -\int_0^1 \frac{c_{\ell_\alpha}}{2a} \frac{r^2 V}{\sqrt{r^2 + V^2}}\, dr$$

$$H_\theta = \int_0^1 \frac{c_{\ell_\alpha}}{2a} V\sqrt{r^2 + V^2}\, dr$$

$$\frac{C_T}{\sigma a} = \int_0^1 \frac{\alpha}{2} r\sqrt{r^2 + V^2}\, dr$$

If c_{ℓ_α} is assumed to be independent of r, that is, $c_{\ell_\alpha}/2a = 1/2$, the integrals may be evaluated exactly as

$$\left.\begin{aligned} M_\mu &= \frac{V}{4}\sqrt{1 + V^2} - \frac{V^3}{4} \ell n \frac{1 + \sqrt{1 + V^2}}{V} \\ M_\beta^{\cdot} &= -\frac{1}{2}\sqrt{1 + V^2}\ \frac{2 - 3V^2}{8} - \frac{3}{16} V^4 \ell n \frac{1 + \sqrt{1 + V^2}}{V} \\ M_\theta &= \frac{1}{16}\sqrt{1 + V^2}\ (2 + V^2) - \frac{V^4}{16} \ell n \frac{1 + \sqrt{1 + V^2}}{V} \end{aligned}\right\} \quad (31)$$

(Eqs. (31) continued on next page.)

$$
\left.
\begin{aligned}
H_\mu + R_\mu &= \frac{V^2}{2}\, \ell n\, \frac{1 + \sqrt{1 + V^2}}{V} \\
H_{\dot\beta}^{*} &= -\frac{V}{4}\sqrt{1 + V^2} + \frac{V^3}{4}\, \ell n\, \frac{1 + \sqrt{1 + V^2}}{V} \\
H_\theta &= \frac{V}{4}\sqrt{1 + V^2} + \frac{V^3}{4}\, \ell n\, \frac{1 + \sqrt{1 + V^2}}{V}
\end{aligned}
\right\} \qquad (31)
$$

and with a mean angle of attack,

$$
\frac{C_T}{\sigma a} = \frac{\bar\alpha}{6}\left[(1 + V^2)^{3/2} - V^3\right]
$$

The behavior of these coefficients is clearer from the expansions for small and large V:

	small V	large V
M_μ	$\frac{V}{4}$	$\frac{1}{6}$
$M_{\dot\beta}$	$-\frac{1}{8}(1 + V^2)$	$-\frac{1}{10V}$
M_θ	$\frac{1}{8}(1 - V^2)$	$\frac{V}{6}$
H_μ	$\frac{V^2}{2}\, \ell n\, \frac{2}{V}$	$\frac{V}{2}$
$H_{\dot\beta}^{*}$	$-\frac{V}{4}$	$-\frac{1}{6}$
H_θ	$\frac{V}{4}$	$\frac{V^2}{2}$
$\frac{6C_T/\sigma a}{\bar\alpha}$	$1 + \frac{3}{2}V^2$	$\frac{3}{2}V$

This behavior is also shown in the approximate expressions based on the inflow angle ϕ at an effective radius. These expressions (eqs. (29)) are in fact most convenient for examining the general behavior, since they contain (in simple form) the behavior over the complete range of inflow ratio. For numerical

work, it is straightforward to evaluate the coefficients by use of the exact integrals (eqs. (31)) or even more complete expressions (as derived in a later chapter).

The flap damping coefficient $M_{\dot{\beta}}$ is negative (which is positive damping); the inplane force due to flapping velocity $H_{\dot{\beta}}$ has the term $C_T/\sigma a$ as expected, and the inflow term $H_{\dot{\beta}}^*$ is negative and therefore opposes the contributions from tip path plane tilt of the rotor thrust. The speed stability coefficients, M_μ and H_μ, and pitch control power coefficients, M_θ and H_θ, are all positive. All coefficients are of order 1 for high inflow. For low inflow only, the flap damping and control, $M_{\dot{\beta}}$ and M_θ, are of order 1; the flap moment due to inplane velocity is an order V smaller in low inflow, and all inplane force coefficients are an order V smaller than the corresponding flap moment coefficients. Flap damping $M_{\dot{\beta}}$ and the mean blade angle of attack (for given rotor thrust) are decreased by high inflow, but remain the same order as for low inflow; the other coefficients increase with increased inflow ratio. For low inflow, the rotor thrust coefficient terms must be retained for M_μ, H_μ, and $H_{\dot{\beta}}$ (but not for $H_{\dot{\beta}}^*$; H_θ, of course, has only $c\ell_\alpha$ terms), but for high inflow, they may be neglected for all coefficients.

SECTION 2: THEORETICAL MODEL FOR A ROTOR IN HIGH INFLOW

Equations of Motion and Forces for the Rotor

With the procedures to be followed established from the derivation and discussion of the simpler four-degree-of-freedom model, consider now a more comprehensive model for the rotor motion. The blade motion is extended to both flap and lag (first mode out of plane and inplane) degrees of freedom, and the shaft motion to all six degrees of freedom; inputs from blade pitch and aerodynamic gusts complete the model. The equations of motion are derived for the rotor degrees of freedom, and expressions for the rotor forces and moments acting on the hub are obtained. In a later chapter, a wing is added to this model, thereby completing the equations for use in the study of proprotor dynamics.

The model considered and the conventions for the hub forces and moments, pylon motion, and aerodynamic gust are shown in figure 3. The pylon motion is defined about a pivot a distance h aft of the hub. The pivot linear displacement degrees of freedom are x_P, y_P, and z_P - vertical, lateral, and longitudinal, respectively. The angular degrees of freedom are α_x, α_y, and α_z (yaw, pitch, and roll). The forces and moments exerted by the rotor on the hub and the gust velocities are as defined in section 1. The torque reaction between the rotor and pylon is Q; following shaft-driven rotor convention, Q is the torque exerted by the shaft on the rotor, hence the torque moment on the hub due to the rotor is $-Q$ (as indicated in fig. 3). The rotor blade azimuth angle ψ is measured with respect to the pylon, which is rotated by α_z in roll; so the rotational velocity of the blade with respect to space is $\Omega + \dot{\alpha}_z$ (without blade flap or lag motion). The equilibrium velocity V with respect to the

air is assumed to be purely axial flow. The blade motion is defined by flap and lag (degrees of freedom) and pitch (input) motion with respect to the hub plane.

The blade motion is represented by two degrees of freedom per blade: flap and lag motion β and ζ, which are pure out-of-plane and pure inplane deflection of the blade spar, respectively. The motion is defined with respect to the hub plane. The mode shape of the blade deflection is $\eta_\beta(r)$ for flap and $\eta_\zeta(r)$ for lag. These modes are functions of r and are normalized to 1 at the tip. The out-of-plane deflection of the blade is then a distance $\beta(\psi)\eta_\beta(r)$ normal to the hub plane, with β defined positive for deflection above the hub plane (forward in airplane cruise mode). The inplane deflection is a distance $\zeta(\psi)\eta_\zeta(r)$ from the undeflected spar line, measured in the hub plane, with ζ defined positive for deflection opposing the rotor direction of rotation. Rotating mode shapes are used, that is, natural vibration modes including the centrifugal spring due to blade rotation. A major influence on the mode shape is the root restraint, that is, either a hinged or a cantilever root. However, the centrifugal stiffening is so strong that the effect of the root restraint on the lowest flap and lag mode shapes is restricted mainly to the root area. The influence of the root restraint on the natural frequencies of the modes is of primary importance. The first (lowest frequency) flap and lag bending modes even for a cantilever blade are then nearly $\eta = r$; near the root of a cantilever blade, the mode shape must deviate from this, of course, to satisfy the boundary condition of zero slope.

The final form for the equations of motion is in terms of the nonrotating rotor degrees of freedom. It is possible to have different mode shapes for the various nonrotating degrees of freedom, for example, one for the coning mode and one for the tip path plane tilt modes, depending on how the hub restraint appears during deflection of the blades in that particular rotor model. Two rotors are considered in applications of this theory; a cantilever rotor and a gimballed rotor. For the cantilever rotor, the mode shape for all nonrotating degrees of freedom of the blade is that of elastic bending with cantilever root restraint. For the gimballed rotor, the mode shape for tip path plane tilt degrees of freedom β_{1C} and β_{1S} is that of an articulated blade, namely, rigid-body motion about a hinge at the center of rotation, $\eta_\beta = r$. For all other nonrotating modes of the gimballed rotor (specifically, for the coning and blade lag modes), the rotor blade acts as a cantilever blade, with corresponding blade deflection mode shapes.

The motion of a cantilever rotor blade in elastic bending is actually more complex than the representation used here. The inplane and out-of-plane deflections are highly coupled by the collective pitch and built-in twist of the blade, which are large for the proprotor. Consequently, although the lowest bending modes are usually still identifiable as predominantly flap or lag motion, there is actually both inplane and out-of-plane motion in each mode. The neglect of this effect, by assuming that the blade flap and lag degrees of freedom are pure out-of-plane deflections and pure inplane deflections, respectively, is probably the severest limitation of the theory presented here. The basic features of the flap and lag motion are represented, so this model may be expected to predict proprotor behavior fairly well.

The equations of motion are derived for a constant rotor rotational speed Ω (with respect to the pylon); this is to be considered the model for powered operation of the rotor. The autorotation case - where the rotor rotates freely on the shaft, the rotor speed being determined by equilibrium of torques on the rotor - can also be handled with this model if the collective lag mode ζ_0 is used. This mode involves the simultaneous motion of all blades in the lag direction (opposite the rotor rotation direction); if there is no hub restraint for this mode, it will be equivalent to a perturbation of the rotor azimuth or rotational speed. If the mode shape for rigid-body rotation is used, and if the natural frequency in the rotating frame is set to zero ($\eta = r$ and $\nu = 0$ for the ζ_0 mode), then, indeed, $\dot{\zeta}_0$ will be just the degree of freedom that represents the rotor rotational speed perturbation. This is a good representation of the autorotation case. The other limit, a fixed rotor rotation speed Ω, will be considered as powered operation. With a constant rotor rotation speed the collective lag mode is then elastic bending of a cantilever blade with respect to the hub (which rotates at a constant speed). This limit is, in fact, the case of operation with a perfect governor on the engine or rotor speed. For an actual rotor in powered flight, the engine/drive train/governor dynamics must be included to give a complete representation of the behavior.

The blade also has pitch motion about the feathering axis at the blade root (given by θ), with the actual blade pitch measured from the hub plane. The pitch has trim and perturbation contributions as before. The trim value is due to root collective and built-in twist; the perturbation value is due to a control input and pitch/flap coupling. Pitch/flap coupling (δ_3) is included for the gimballed rotor.

The equations of motion for flap and lag degrees of freedom are obtained from equilibrium of moments on the blade. For the mth blade ($m = 1, \ldots, N$) in the rotating frame, the equations are

$$\left.\begin{aligned} I_\beta(\ddot{\beta} + \nu_\beta^2\beta) + I_{\beta\alpha}[-(\ddot{\alpha}_y - 2\dot{\alpha}_x)\cos\psi_m + (\ddot{\alpha}_x + 2\dot{\alpha}_y)\sin\psi_m] + S_\beta\ddot{z}_P &= M_F \\ I_\zeta(\ddot{\zeta} + \nu_\zeta^2\zeta) + S_\zeta[(\ddot{x}_P + h\ddot{\alpha}_y)\sin\psi_m - (\ddot{y}_P - h\ddot{\alpha}_x)\cos\psi_m] - I_{\zeta\alpha}\ddot{\alpha}_z &= M_L \end{aligned}\right\} \tag{32}$$

The flap and lag aerodynamic moments on the blade are

$$M_F = \int_0^1 \eta_\beta F_z \, dr$$

$$M_L = \int_0^1 \eta_\zeta F_x \, dr$$

and the inertia constants are integrals of the blade section mass:

$$I_\beta = \int_0^1 \eta_\beta{}^2 m \, dr$$

$$I_{\beta\alpha} = \int_0^1 \eta_\beta r m \, dr$$

$$S_\beta = \int_0^1 \eta_\beta m \, dr$$

$$I_\zeta = \int_0^1 \eta_\zeta{}^2 m \, dr$$

$$I_{\zeta\alpha} = \int_0^1 \eta_\zeta r m \, dr$$

$$S_\zeta = \int_0^1 \eta_\zeta m \, dr$$

The rotating natural frequencies of the flap and lag motions are ν_β and ν_ζ, respectively. A subscript o will be added to the mode shape, inertias, and natural frequency for the collective modes (coning or collective lag) since these terms may not be identical to those for the cyclic modes (e.g., for the gimballed rotor or the autorotation case).

The flap equation is forced by pure out-of-plane aerodynamic forces (F_z) and the lag by pure inplane forces (Fx), because of the assumption of decoupled flap and lag bending modes. The flap equation is as before, with the addition of the acceleration due to longitudinal motion of the shaft. The flap mode shape η_β influences the effective inertias of the flap motion and the shaft angular acceleration; with rigid-body flap motion, $\eta_\beta = r$, the equation reduces to that used for four-degree-of-freedom case. The lag motion couples with inplane acceleration of the rotor hub (resolved into the rotating frame) and with roll angular acceleration of the rotor shaft. The Coriolis inertial coupling of the flap and lag equations has been neglected. The coefficients of these terms would be proportional to the rotor trim coning angle, which is of order $\gamma C_T/\sigma a$. However, aerodynamic terms also contribute to this coupling, and for high inflow these coefficients are of order 1. Hence the Coriolis inertia coupling may be neglected compared with the high inflow aerodynamic forces.

Now let $I_b = \int_0^1 r^2 m \, dr$ and normalize the inertias by dividing by I_b; this normalization is denoted by superscript $*$, for example, $I_\beta{}^* = I_\beta / I_b$. The Lock

number is defined (as before) by $\gamma = \rho a c R^4 / I_b$. I_b is only a normalization factor - a representative moment of inertia of the blade. It is used in the blade Lock number (the ratio of blade aerodynamic to inertial forces) and to normalize the blade masses so they are of order 1. A convenient inertia is that of the blade about the shaft, that is, the rotary moment of inertia of the entire rotor divided by N. This inertia is a well-defined property of the rotor and also should be the largest possible moment of inertia of the blade.

This normalization yields the following equations:

$$\left.\begin{aligned} I_\beta^*(\ddot{\beta} + \nu_\beta^2 \beta) + I_{\beta\alpha}^*[-(\ddot{\alpha}_y - 2\dot{\alpha}_x)\cos\psi_m + (\ddot{\alpha}_x + 2\dot{\alpha}_y)\sin\psi_m] + S_\beta^* \ddot{z}_P &= \gamma \frac{M_F}{ac} \\ I_\zeta^*(\ddot{\zeta} + \nu_\zeta^2 \zeta) + S_\zeta^*[(\ddot{x}_P + h\ddot{\alpha}_y)\sin\psi_m - (\ddot{y}_P - h\ddot{\alpha}_x)\cos\psi_m] - I_{\zeta\alpha}^* \ddot{\alpha}_z &= \gamma \frac{M_L}{ac} \end{aligned}\right\} \quad (33)$$

If $\eta \cong r$ for the flap and lag modes, then the I^* terms are all nearly 1 and the S^* terms, nearly 3/2 (for constant mass distribution); with usual blade construction, the I^* terms are slightly less than 1, and the S^* terms around 1.

The Fourier coordinate transformation is now applied to convert the equations of motion and degrees of freedom of the rotor from the rotating frame to the nonrotating frame. Again, the nonrotating degrees of freedom above 0, $1C$, and $1S$ are not coupled with the shaft motion, so these higher rotor degrees of freedom involve just internal rotor motion. In studies of the coupled rotor and shaft motion then, the 0, $1C$, $1S$ set is sufficient to treat the general case of $N \geq 3$. The nonrotating equations of motion for the degrees of freedom β_0, β_{1C}, β_{1S}, ζ_0, ζ_{1C}, and ζ_{1S} are:

$$\left.\begin{aligned} I_{\beta_0}^*(\ddot{\beta}_0 + \nu_{\beta_0}^2 \beta_0) + S_{\beta_0}^* \ddot{z}_P &= \gamma \frac{M_{F_0}}{ac} \\ I_\beta^*[\ddot{\beta}_{1C} + 2\dot{\beta}_{1S} + (\nu_\beta^2 - 1)\beta_{1C}] + I_{\beta\alpha}^*(-\ddot{\alpha}_y + 2\dot{\alpha}_x) &= \gamma \frac{M_{F_{1C}}}{ac} \\ I_\beta^*[\ddot{\beta}_{1S} - 2\dot{\beta}_{1C} + (\nu_\beta^2 - 1)\beta_{1S}] + I_{\beta\alpha}^*(\ddot{\alpha}_x + 2\dot{\alpha}_y) &= \gamma \frac{M_{F_{1S}}}{ac} \\ I_{\zeta_0}^*(\ddot{\zeta}_0 + \nu_{\zeta_0}^2 \zeta_0) - I_{\zeta_0\alpha}^* \ddot{\alpha}_z &= \gamma \frac{M_{L_0}}{ac} \\ I_\zeta^*[\ddot{\zeta}_{1C} + 2\dot{\zeta}_{1S} + (\nu_\zeta^2 - 1)\zeta_{1C}] + S_\zeta^*(-\ddot{y}_P + h\ddot{\alpha}_x) &= \gamma \frac{M_{L_{1C}}}{ac} \\ I_\zeta^*[\ddot{\zeta}_{1S} - 2\dot{\zeta}_{1C} + (\nu_\zeta^2 - 1)\zeta_{1S}] + S_\zeta^*(\ddot{x}_P + h\ddot{\alpha}_y) &= \gamma \frac{M_{L_{1S}}}{ac} \end{aligned}\right\} \quad (34)$$

where the flap aerodynamic forcing moments are

$$M_{F_0} = \frac{1}{N} \sum_m M_{F_m}$$

$$M_{F_{1C}} = \frac{2}{N} \sum_m M_{F_m} \cos \psi_m$$

$$M_{F_{1S}} = \frac{2}{N} \sum_m M_{F_m} \sin \psi_m$$

and, similarly, for the lag moments. The flap modes are coning (β_0) and tip path plane tilt (β_{1C}, β_{1S}). The collective lag mode ζ_0 is simultaneous lagging motion of all the blades (with respect to the hub rotating at constant speed Ω, for the powered case; for the autorotation case, ζ_0 is the rotor speed perturbation degree of freedom). The cyclic lag modes ζ_{1C} and ζ_{1S} produce rectilinear inplane motion of the net rotor center of gravity, laterally for ζ_{1C} ($-y_h$ direction) and vertically for ζ_{1S} (x_h direction). Note that the equations separate into a lateral/vertical group ($1C$, $1S$, x, y) and a longitudinal group (0, z), with no inertia coupling between them. This decoupling is maintained by the aerodynamics also (because of the trim axial flow); the shaft motion due to the actual wing degrees of freedom will, in general, couple the two groups of equations.

The hub moment due to the rotor may be expressed (as before) in terms of tip path plane tilt β_{1C} and β_{1S}:

$$\begin{pmatrix} \frac{-2C_{M_y}}{\sigma a} \\ \\ \frac{2C_{M_x}}{\sigma a} \end{pmatrix} = \frac{I_\beta^*(\nu_\beta^2 - 1)}{\gamma} \begin{pmatrix} \beta_{1C} \\ \\ \beta_{1S} \end{pmatrix} \tag{35}$$

The inertia contributions to the rotor drag, side force, thrust, and torque acting on the hub are

$$\left.\begin{aligned} H_{inertia} &= -\frac{N}{2} S_\zeta \ddot{\zeta}_{1S} - NM_b(\ddot{x}_P + h\ddot{\alpha}_y) \\ Y_{inertia} &= \frac{N}{2} S_\zeta \ddot{\zeta}_{1C} - NM_b(\ddot{y}_P - h\ddot{\alpha}_x) \\ T_{inertia} &= -NS_{\beta_0}\ddot{\beta}_0 - NM_b\ddot{z}_P \\ Q_{inertia} &= -NI_{\zeta_0\alpha}\ddot{\zeta}_0 + NI_O\ddot{\alpha}_z \end{aligned}\right\} \tag{36}$$

The drag and side forces are the net inplane acceleration of the rotor due to the motion of the shaft and blade; similarly, the thrust is the net longitudinal acceleration of the rotor; and the torque, the net angular acceleration. The new inertia constants are

$$I_O = \int_0^1 r^2 m \, dr$$

$$M_b = \int_0^1 m \, dr$$

Therefore, NI_O is the moment of inertia of the entire rotor about the shaft, and NM_b, the mass of the entire rotor. When normalized (divided by I_b), $I_O{}^*$ is nearly 1 (exactly 1 if I_O is used for I_b) and $M_b{}^*$ is around 3 for a uniform mass distribution ($M_b{}^*$ is greater than 3 for usual rotors). In coefficient form, dividing the side and drag forces by $(N/2)I_b\gamma$ and the thrust and torque by $NI_b\gamma$, these forces are

$$\left.\begin{aligned}
\left(\frac{2C_H}{\sigma a}\right)_{inertia} &= -\frac{S_\zeta{}^*}{\gamma}\ddot{\zeta}_{1S} - \frac{2}{\gamma}M_b{}^*(\ddot{x}_P + h\ddot{\alpha}_y) \\
\left(\frac{2C_Y}{\sigma a}\right)_{inertia} &= \frac{S_\zeta{}^*}{\gamma}\ddot{\zeta}_{1C} - \frac{2}{\gamma}M_b{}^*(\ddot{y}_P - h\ddot{\alpha}_x) \\
\left(\frac{C_T}{\sigma a}\right)_{inertia} &= -\frac{S^*_{\beta_0}}{\gamma}\ddot{\beta}_0 - \frac{M_b{}^*}{\gamma}\ddot{z}_P \\
\left(\frac{C_Y}{\sigma a}\right)_{inertia} &= -\frac{I^*_{\zeta_0\alpha}}{\gamma}\ddot{\zeta}_0 + \frac{I_O{}^*}{\gamma}\alpha_z
\end{aligned}\right\} \qquad (37)$$

Rotor aerodynamics- The analysis follows that of the previous section; the section aerodynamic environment, with the conventions for forces and velocities, remains as shown in figure 2. With the present degrees of freedom and shaft motion, the perturbation velocities are

$$\left.\begin{aligned}
\delta u_T &= r(\dot{\alpha}_z - \dot{\zeta}) - h(\dot{\alpha}_y \sin\psi_m + \dot{\alpha}_x \cos\psi_m) \\
&\quad + (V + v)(\alpha_y \sin\psi_m + \alpha_x \cos\psi_m) + V(\beta_G \cos\psi_m + \alpha_G \sin\psi_m) \\
&\quad + (\dot{y}_P \cos\psi_m - \dot{x}_P \sin\psi_m) \\
&= r\delta u_{T_A} + \delta u_{T_B} \\
\delta u_P &= r(\dot{\beta} - \dot{\alpha}_y \cos\psi_m + \dot{\alpha}_x \sin\psi_m) + (Vu_G + \dot{z}_P) \\
&= r\delta u_{P_B} + \delta u_{P_A} \\
\delta u_R &= h(-\dot{\alpha}_y \cos\psi_m + \dot{\alpha}_x \sin\psi_m) + (V + v)(\alpha_y \cos\psi_m - \alpha_x \sin\psi_m) \\
&\quad + V(-\beta_G \sin\psi_m + \alpha_G \cos\psi_m) - (\dot{y}_P \sin\psi_m + \dot{x}_P \cos\psi_m)
\end{aligned}\right\} \qquad (38)$$

and the blade pitch perturbation is as before, including control and pitch/flap coupling K_P:

$$\delta\theta = \theta - K_P\beta \tag{39}$$

The trim velocities are, again, for equilibrium axial flow: $u_T = r$, $u_P = V + v$, and $u_R = 0$.

The rotor motion contributions to the velocity perturbations (in δu_{T_A} and δu_{P_B}) assume that $\eta_\beta = \eta_\zeta = r$ for the flap and lag mode shapes. This approximation is satisfactory for the aerodynamic forces. The first modes of flap and lag are nearly this anyway, even for a cantilever blade. Also, this approximate mode shape is correct at and near the tip, where the most important aerodynamic loading occurs. The mode shapes $\eta_\beta = \eta_\zeta = r$ are used in the aerodynamic moments on the blade so that

$$M_F = \int_0^1 rF_z \, dr$$

$$M_L = \int_0^1 rF_x \, dr$$

The use of this mode shape for the aerodynamic greatly simplifies the aerodynamic coefficients involved or, at least, reduces the number of coefficients required. With the correct η_β and η_ζ, separate coefficients are required for blade motion and shaft angular motion, and for the lag moments and torque moments on the blade. With $\eta_\beta = \eta_\zeta = r$, only r (to some power) appears in the integrands of the aerodynamic coefficients, never η or η^2; hence the evaluation of the coefficients is also simplified.

The expressions for the section aerodynamic forces (L, D, and F_r, their decomposition into the hub plane F_z and F_x, and the rotor forces and moments (T, Y, H, Q, and M_F) in terms of the net rotating forces on the blade are the same as in the previous section. Again, the net blade forces may be expanded as linear combinations of the velocity and pitch perturbations:

$$\left.\begin{aligned}
\int_0^1 r\frac{F_z}{ac}\,dr &= M_o + M_\mu\delta u_{T_B} + M_\zeta\delta u_{T_A} + M_\lambda\delta u_{P_A} + M_\beta\delta u_{P_B} + M_\theta\delta\theta \\
\int_0^1 \frac{F_x}{ac}\,dr &= H_o + H_\mu\delta u_{T_B} + H_\zeta\delta u_{T_A} + H_\lambda\delta u_{P_A} + H_\beta\delta u_{P_B} + H_\theta\delta\theta \\
\int_0^1 \frac{F_z}{ac}\,dr &= T_o + T_\mu\delta u_{T_B} + T_\zeta\delta u_{T_A} + T_\lambda\delta u_{P_A} + T_\beta\delta u_{P_B} + T_\theta\delta\theta \\
\int_0^1 r\frac{F_x}{ac}\,dr &= Q_o + Q_\mu\delta u_{T_B} + Q_\zeta\delta u_{T_A} + Q_\lambda\delta u_{P_A} + Q_\beta\delta u_{P_B} + Q_\theta\delta\theta \\
\int_0^1 \frac{F_r}{ac}\,dr &= R_\mu\delta u_R - \beta\frac{C_T}{\sigma a}
\end{aligned}\right\} \tag{40}$$

where M is the flap moment; H, the blade inplane force (drag direction); T, the blade thrust; Q, the blade torque moment; and R, the radial force. The subscripts denote the source of the force or moment; subscript o indicates trim values; subscript μ, hub inplane velocity (speed); $\dot{\zeta}$, blade rotational velocity (lag damping); $\dot{\beta}$, flapwise velocity (flap damping); λ, hub longitudinal velocity (inflow); and θ, blade pitch control. The coefficients may be grouped as inplane and out-of-plane forces, so the H and Q terms have similar behavior, and the M and T terms have similar behavior. Alternatively the coefficients may be grouped as inplane and out-of-plane velocities so the coefficients with subscripts μ and $\dot{\zeta}$ have similar behavior, and those with subscripts $\dot{\beta}$ and λ have similar behavior. The only difference between the coefficients within a particular group (say, the out-of-plane forces due to out-of-plane velocities: $M_{\dot{\beta}}$, M_{λ}, $T_{\dot{\beta}}$, and T_{λ}) is a factor of r more or less in the spanwise integration (the difference between the force and moment, and between the translation and rotational velocities), hence just slightly different numerical constants. The behavior of the coefficients with a variation in the parameters (in particular, with forward velocity V) is basically the same within a group; that is, it is determined primarily by whether an inplane or out-of-plane force is involved, and whether an inplane or out-of-plane velocity or blade pitch control is the input. The fundamental set of coefficients is considered to be the M and H terms with subscripts μ, $\dot{\beta}$, and θ - one each of inplane and out-of-plane types- together with T_O and Q_O for the trim values. Then the behavior of all other coefficients may be inferred from a knowledge of the behavior of this set.

Again, the inplane force due to flapping velocity is written:

$$H_{\dot{\beta}} = \frac{C_T}{\sigma a} + H_{\dot{\beta}}^{*} \tag{41}$$

to show explicitly the contribution due to the thrust vector tilt.

The blade forces can now be summed over all N blades to find the net rotor forces. The aerodynamic coefficients are independent of ψ_m, so the summation operates only on the blade velocity perturbations. With the definitions of the rotor nonrotating degrees of freedom, the flap and lag moments required for the equations of motion are

$$\left.\begin{aligned}
\frac{M_{F_0}}{ac} &= M_O + M_{\dot{\zeta}}(\dot{\alpha}_z - \dot{\zeta}_0) + M_{\dot{\beta}}\dot{\beta}_0 \\
&\quad + M_{\lambda}(Vu_G + \dot{z}_P) + M_{\theta}(\theta_0 - K_P\beta_0) \\
\frac{M_{F_{1C}}}{ac} &= M_{\mu}[-h\dot{\alpha}_x + (V + v)\alpha_x + V\beta_G + \dot{y}_P] \\
&\quad + M_{\dot{\zeta}}(-\dot{\zeta}_{1C} - \zeta_{1S}) + M_{\dot{\beta}}(\dot{\beta}_{1C} + \beta_{1S} - \dot{\alpha}_y) \\
&\quad + M_{\theta}(\theta_{1C} - K_P\beta_{1C}) \\
\frac{M_{F_{1S}}}{ac} &= M_{\mu}[-h\dot{\alpha}_y + (V + v)\alpha_y + V\alpha_G - \dot{x}_P] \\
&\quad + M_{\dot{\zeta}}(-\dot{\zeta}_{1S} + \zeta_{1C}) + M_{\dot{\beta}}(\dot{\beta}_{1S} - \beta_{1C} + \dot{\alpha}_x) \\
&\quad + M_{\theta}(\theta_{1S} - K_P\beta_{1S})
\end{aligned}\right\} \tag{42}$$

and, similarly, for the lag moments, with the M terms replaced by $\dot{Q}$ terms, The aerodynamic contributions to the rotor drag force, side force, thrust, and torque on the hub are

$$\left.\begin{aligned}
\left(\frac{2C_H}{\sigma a}\right)_{aero} &= (H_\mu + R_\mu)[-h\dot{\alpha}_y + (V + v)\alpha_y + V\alpha_G - \dot{x}_P] \\
&\quad + H_{\dot{\zeta}}(-\dot{\zeta}_{1S} + \zeta_{1C}) + H_{\dot{\beta}}(\dot{\beta}_{1S} + \dot{\alpha}_x) \\
&\quad + H_\theta(\theta_{1S} - K_P\beta_{1S}) - \left(\frac{2C_T}{\sigma a} + H_{\dot{\beta}}^*\right)\beta_{1C} \\
\left(\frac{2C_Y}{\sigma a}\right)_{aero} &= -(H_\mu + R_\mu)[-h\dot{\alpha}_x + (V + v)\alpha_x + V\beta_G + \dot{y}_P] \\
&\quad - H_{\dot{\zeta}}(-\dot{\zeta}_{1C} - \zeta_{1S}) - H_{\dot{\beta}}(\dot{\beta}_{1C} - \dot{\alpha}_y) \\
&\quad - H_\theta(\theta_{1C} - K_P\beta_{1C}) - \left(\frac{2C_T}{\sigma a} + H_{\dot{\beta}}^*\right)\beta_{1S} \\
\left(\frac{C_T}{\sigma a}\right)_{aero} &= T_o + T_{\dot{\zeta}}(\dot{\alpha}_z - \dot{\zeta}_0) + T_{\dot{\beta}}\dot{\beta}_0 \\
&\quad + T_\lambda(Vu_G + \dot{z}_P) + T_\theta(\theta_0 - K_P\beta_0) \\
\left(\frac{C_Q}{\sigma a}\right)_{aero} &= Q_o + Q_{\dot{\zeta}}(\dot{\alpha}_z - \dot{\zeta}_0) + Q_{\dot{\beta}}\dot{\beta}_0 \\
&\quad + Q_\lambda(Vu_G + \dot{z}_P) + Q_\theta(\theta_0 - K_P\beta_0)
\end{aligned}\right\} \qquad (43)$$

The aerodynamics maintain the separation into lateral/vertical and longitudinal groups because of the purely axial flow in the trim state.

Equations of motion- The complete equations of motion can now be obtained by combining the aerodynamic and inertia terms. For the lateral/vertical motion group, the equations of motion are

$$
\begin{bmatrix} I_\beta^* & 0 & 0 & 0 \\ 0 & I_\beta^* & 0 & 0 \\ 0 & 0 & I_\zeta^* & 0 \\ 0 & 0 & 0 & I_\zeta^* \end{bmatrix} \begin{pmatrix} \beta_{1C} \\ \beta_{1S} \\ \zeta_{1C} \\ \zeta_{1S} \end{pmatrix}^{\cdot\cdot} + \begin{bmatrix} -\gamma M_{\dot\beta} & 2I_\beta^* & \gamma M_{\dot\zeta} & 0 \\ -2I_\beta^* & -\gamma M_{\dot\beta} & 0 & \gamma M_{\dot\zeta} \\ -\gamma Q_{\dot\beta} & 0 & \gamma Q_{\dot\zeta} & 2I_\zeta^* \\ 0 & -\gamma Q_{\dot\beta} & -2I_\zeta^* & \gamma Q_{\dot\zeta} \end{bmatrix} \begin{pmatrix} \beta_{1C} \\ \beta_{1S} \\ \zeta_{1C} \\ \zeta_{1S} \end{pmatrix}^{\cdot}
$$

$$
+ \begin{bmatrix} I_\beta^*(\nu_\beta^2-1)+K_P\gamma M_\theta & -\gamma M_{\dot\beta} & 0 & \gamma M_{\dot\zeta} \\ \gamma M_{\dot\beta} & I_\beta^*(\nu_\beta^2-1)+K_P\gamma M_\theta & -\gamma M_{\dot\zeta} & 0 \\ K_P\gamma Q_\theta & -\gamma Q_{\dot\beta} & I_\zeta^*(\nu_\zeta^2-1) & \gamma Q_{\dot\zeta} \\ \gamma Q_{\dot\beta} & K_P\gamma Q_\theta & -\gamma Q_{\dot\zeta} & I_\zeta^*(\nu_\zeta^2-1) \end{bmatrix} \begin{pmatrix} \beta_{1C} \\ \beta_{1S} \\ \zeta_{1C} \\ \zeta_{1S} \end{pmatrix}
$$

$$
+ \begin{bmatrix} -I_{\beta\alpha}^* & 0 \\ 0 & I_{\beta\alpha}^* \\ 0 & S_\zeta^* h \\ S_\zeta^* h & 0 \end{bmatrix} \begin{pmatrix} \alpha_y \\ \alpha_x \end{pmatrix}^{\cdot\cdot} + \begin{bmatrix} \gamma M_{\dot\beta} & 2I_{\beta\alpha}^* + \gamma h M_\mu \\ 2I_{\beta\alpha}^* + \gamma h M_\mu & -\gamma M_{\dot\beta} \\ \gamma Q_{\dot\beta} & \gamma h Q_\mu \\ \gamma h Q_\mu & -\gamma Q_{\dot\beta} \end{bmatrix} \begin{pmatrix} \alpha_y \\ \alpha_x \end{pmatrix}^{\cdot}
$$

$$
+ \begin{bmatrix} 0 & -\gamma(V+v)M_\mu \\ -\gamma(V+v)M_\mu & 0 \\ 0 & -\gamma(V+v)Q_\mu \\ -\gamma(V+v)Q_\mu & 0 \end{bmatrix} \begin{pmatrix} \alpha_y \\ \alpha_x \end{pmatrix} + \begin{bmatrix} 0 & 0 \\ 0 & 0 \\ -S_\zeta^* & 0 \\ 0 & S_\zeta^* \end{bmatrix} \begin{pmatrix} y_P \\ x_P \end{pmatrix}^{\cdot\cdot} + \begin{bmatrix} -\gamma M_\mu & 0 \\ 0 & \gamma M_\mu \\ -\gamma Q_\mu & 0 \\ 0 & \gamma Q_\mu \end{bmatrix} \begin{pmatrix} y_P \\ x_P \end{pmatrix}^{\cdot}
$$

$$
= \begin{bmatrix} \gamma M_\theta & 0 \\ 0 & \gamma M_\theta \\ \gamma Q_\theta & 0 \\ 0 & \gamma Q_\theta \end{bmatrix} \begin{pmatrix} \theta_{1C} \\ \theta_{1S} \end{pmatrix} + \begin{bmatrix} \gamma V M_\mu & 0 \\ 0 & \gamma V M_\mu \\ \gamma V Q_\mu & 0 \\ 0 & \gamma V Q_\mu \end{bmatrix} \begin{pmatrix} \beta_G \\ \alpha_G \end{pmatrix} \tag{44}
$$

with the hub moment,

$$\begin{pmatrix} -\frac{2C_{M_y}}{\sigma a} \\ \frac{2C_{M_x}}{\sigma a} \end{pmatrix} = \frac{I_\beta^*(\nu_\beta^2-1)}{\gamma} \begin{pmatrix} \beta_{1C} \\ \beta_{1S} \end{pmatrix} \tag{45}$$

and the vertical and lateral forces on the hub,

$$\begin{pmatrix} \frac{2C_H}{\sigma a} \\ \frac{2C_Y}{\sigma a} \end{pmatrix} = \begin{bmatrix} 0 & H_\beta^* \\ -H_\beta^* & 0 \end{bmatrix} \begin{pmatrix} \beta_{1C} \\ \beta_{1S} \end{pmatrix}^{\cdot} + \begin{bmatrix} -\left(\frac{2C_T}{\sigma a} + H_\beta^*\right) & -K_P H_\theta \\ K_P H_\theta & -\left(\frac{2C_T}{\sigma a} + H_\beta^*\right) \end{bmatrix} \begin{pmatrix} \beta_{1C} \\ \beta_{1S} \end{pmatrix}$$

$$+ \begin{bmatrix} 0 & -\frac{1}{\gamma} S_\zeta^* \\ \frac{1}{\gamma} S_\zeta^* & 0 \end{bmatrix} \begin{pmatrix} \zeta_{1C} \\ \zeta_{1S} \end{pmatrix}^{\cdot\cdot} + \begin{bmatrix} 0 & -H_\zeta^* \\ H_\zeta^* & 0 \end{bmatrix} \begin{pmatrix} \zeta_{1C} \\ \zeta_{1S} \end{pmatrix}^{\cdot} + \begin{bmatrix} H_\zeta^* & 0 \\ 0 & H_\zeta^* \end{bmatrix} \begin{pmatrix} \zeta_{1C} \\ \zeta_{1S} \end{pmatrix}$$

$$+ \begin{bmatrix} -\frac{2}{\gamma} M_b^* h & 0 \\ 0 & \frac{2}{\gamma} M_b^* h \end{bmatrix} \begin{pmatrix} \alpha_y \\ \alpha_x \end{pmatrix}^{\cdot\cdot} + \begin{bmatrix} -h(H_\mu+R_\mu) & H_\beta^* \\ H_\beta^* & h(H_\mu+R_\mu) \end{bmatrix} \begin{pmatrix} \alpha_y \\ \alpha_x \end{pmatrix}^{\cdot}$$

$$+ \begin{bmatrix} (V+v)(H_\mu+R_\mu) & 0 \\ 0 & -(V+v)(H_\mu+R_\mu) \end{bmatrix} \begin{pmatrix} \alpha_y \\ \alpha_x \end{pmatrix} + \begin{bmatrix} 0 & -\frac{2}{\gamma} M_b^* \\ -\frac{2}{\gamma} M_b^* & 0 \end{bmatrix} \begin{pmatrix} y_P \\ x_P \end{pmatrix}^{\cdot\cdot}$$

$$+ \begin{bmatrix} 0 & -(H_\mu+R_\mu) \\ -(H_\mu+R_\mu) & 0 \end{bmatrix} \begin{pmatrix} y_P \\ x_P \end{pmatrix}^{\cdot} + \begin{bmatrix} 0 & H_\theta \\ -H_\theta & 0 \end{bmatrix} \begin{pmatrix} \theta_{1C} \\ \theta_{1S} \end{pmatrix}$$

$$+ \begin{bmatrix} 0 & V(H_\mu+R_\mu) \\ -V(H_\mu+R_\mu) & 0 \end{bmatrix} \begin{pmatrix} \beta_G \\ \alpha_G \end{pmatrix} \tag{46}$$

The longitudinal equations of motion are

$$\left.\begin{aligned} I^*_{\beta_0}\ddot{\beta}_0 - \gamma M_{\dot{\beta}}\dot{\beta}_0 + (I^*_{\beta_0}\nu^2_{\beta_0} + K_P\gamma M_\theta)\beta_0 + \gamma M_{\dot{\zeta}}\dot{\zeta}_0 - \gamma M_{\dot{\zeta}}\dot{\alpha}_z + S^*_{\beta_0}\ddot{z}_P - \gamma M_\lambda \dot{z}_P \\ = \gamma M_\theta \theta_0 + \gamma V M_\lambda u_G + \gamma M_o \\ I^*_{\zeta_0}\ddot{\zeta}_0 + \gamma Q_{\dot{\zeta}}\dot{\zeta}_0 + I^*_{\zeta_0}\nu^2_{\zeta_0}\zeta_0 - \gamma Q_{\dot{\beta}}\dot{\beta}_0 + K_P\gamma Q_\theta\beta_0 - I^*_{\zeta_0\alpha}\ddot{\alpha}_z - \gamma Q_{\dot{\zeta}}\dot{\alpha}_z - \gamma Q_\lambda \dot{z}_P \\ = \gamma Q_\theta \theta_0 + \gamma V Q_\lambda u_G + \gamma Q_o \end{aligned}\right\} \quad (47)$$

with the thrust and torque,

$$\left.\begin{aligned} \frac{C_T}{\sigma a} &= T_o + T_{\dot{\zeta}}(\dot{\alpha}_z - \dot{\zeta}_0) + T_{\dot{\beta}}\dot{\beta}_0 + T_\lambda(Vu_G + \dot{z}_P) \\ &\quad + T_\theta(\theta_0 - K_P\beta_0) - \frac{1}{\gamma}S^*_{\beta_0}\ddot{\beta}_0 - \frac{1}{\gamma}M_b{}^*\ddot{z}_P \\ \frac{C_Q}{\sigma a} &= Q_o + Q_{\dot{\zeta}}(\dot{\alpha}_z - \dot{\zeta}_0) + Q_{\dot{\beta}}\dot{\beta}_0 + Q_\lambda(Vu_G + \dot{z}_P) \\ &\quad + Q_\theta(\theta_0 - K_P\beta_0) - \frac{1}{\gamma}I^*_{\zeta_0\alpha}\ddot{\zeta}_0 + \frac{1}{\gamma}I_o{}^*\ddot{\alpha}_z \end{aligned}\right\} \quad (48)$$

Note that if, in $C_Q/\sigma a$, the substitution is made for ζ_0 from the equation of motion:

$$\begin{aligned} \frac{C_Q}{\sigma a} &= I^*_{\zeta_0}\frac{\nu^2_{\zeta_0}}{\gamma}\zeta_0 - \frac{I^*_{\zeta_0\alpha} - I^*_{\zeta_0}}{\gamma}\ddot{\zeta}_0 + \frac{I_o{}^* - I^*_{\zeta_0\alpha}}{\gamma}\ddot{\alpha}_z \\ &= I^*_{\zeta_0}\frac{\nu^2_{\zeta_0}}{\gamma}\zeta_0 \end{aligned} \quad (49)$$

where the last expression holds if $\eta_{\zeta_0} = r$ is assumed for the inertias, as it was for the aerodynamic terms. That assumption is consistent with the use of only one blade lag mode; this result is comparable to that for the hub moments M_x and M_y in terms of rotor tip path plane tilt β_{1C} and β_{1S}.

The present model may be used for the case of the rotor operating in autorotation, as is frequently done for proprotor dynamics wind-tunnel tests, by use of the collective lag mode for the rotor speed perturbation degree of freedom. It is important to include that degree of freedom so that proper representation of the autorotation dynamics is obtained. In fact, the

representation used for the powered case, assuming that the rotor hub rotational speed Ω is fixed by the engine and that the collective lag motion is elastic rotor deflection with respect to the hub, can only be considered a limiting case of a perfect governor. A model with true engine/governor/drive train dynamics would always allow some rotor speed perturbation, and hence that motion would also have an important influence on the powered case.

Autorotation operation means no restraint of the rotor rotation about the hub. Therefore, no rotor torque is transmitted to the shaft, and no pylon roll motion is transmitted to the rotor. The collective lag degree of freedom is then rigid-body rotation of the entire rotor about the shaft. The collective lag mode shape is then $\eta_{\zeta_0} = r$; with no restraint of this degree of freedom, $\nu_{\zeta_0} = 0$. The lag motion of the blade is defined with respect to the pylon, which is rolled by α_z, rather than with respect to an inertia frame; there will then be a response of ζ_0 to pylon roll α_z, but the zero spring rate for collective lag motion ($\nu_{\zeta_0} = 0$) assures that this motion will be only that required to hold the rotor fixed with respect to space. Since no torque is transmitted through the rotor shaft during autorotation, any C_Q forcing terms in the pylon/wing equations of motion should be dropped. This would automatically be accomplished by the zero spring rate ($\nu_{\zeta_0} = 0$, as in eq. (49)), but actually dropping C_Q would result in a better conditioned numerical problem. With $\eta_{\zeta_0} = r$, it follows that $I^*_{\zeta_0} = I^*_{\zeta_0\alpha} = I_O{}^*$ (and all are equal to 1 if $I_b = I_O$ is used); and the zero collective lag spring rate means that $\nu_{\zeta_0} = 0$. These changes are all that are required in the equations of motion to accommodate the autorotation case.

The Rotor Aerodynamic Coefficients

In this section, the aerodynamic coefficients of the rotor forces defined in equations (40) are derived and discussed. The derivation follows that used for the four-degree-of-freedom model; all the coefficients required will now be derived, and the effects of drag and compressibility retained. First, the basic set of coefficients is considered; the M and H terms (out-of-plane and inplane forces) with subscripts μ, $\dot{\beta}$, and θ (inplane and out-of-plane velocities and blade pitch control), with T_O and Q_O for the trim forces. The trim thrust and torque follow directly from integration of the section forces (no perturbation process required) as

$$\frac{C_T}{\sigma a} = T_O = \int_0^1 U\left(u_T \frac{c_\ell}{2a} - u_P \frac{c_d}{2a}\right) dr$$

$$\frac{C_Q}{\sigma a} = Q_O = \int_0^1 rU\left(u_P \frac{c_\ell}{2a} + u_T \frac{c_d}{2a}\right) dr$$

From the perturbations about the trim state, the flap moment is

$$\int_0^1 r \frac{F_z}{ac}\, dr = \int_0^1 rU\left(u_T \frac{c_\ell}{2a} - u_P \frac{c_d}{2a}\right) dr$$

$$+ \int_0^1 r\left[\frac{c_\ell}{2a}\left(\delta U u_T + U\delta u_T\right) + U u_T \frac{c_{\ell_\alpha}}{2a}\,\delta\alpha\right.$$

$$+ U u_T \frac{c_{\ell_M}}{2a}\,\delta M - \frac{c_d}{2a}\left(\delta U u_P + U\delta u_P\right)$$

$$\left. - U u_P \frac{c_{d_\alpha}}{2a}\,\delta\alpha - U u_P \frac{c_{d_M}}{2a}\,\delta M\right] dr$$

$$= \int_0^1 rU\left(u_T \frac{c_\ell}{2a} - u_P \frac{c_d}{2a}\right) dr$$

$$+ \int_0^1 r\left[\frac{c_\ell}{2a}\left(\frac{u_T^2}{U} + U\right) + \frac{c_{\ell_\alpha}}{2a}\frac{u_T u_P}{U} + \frac{Mc_{\ell_\alpha}}{2a}\frac{u_T^2}{U}\right.$$

$$\left. - \frac{c_d}{2a}\frac{u_T u_P}{U} - \frac{c_{d_\alpha}}{2a}\frac{u_P^2}{U} - \frac{Mc_{d_M}}{2a}\frac{u_T u_P}{U}\right] dr\ \delta u_{T_B}$$

$$+ \int_0^1 r^2\left[\frac{c_\ell}{2a}\frac{u_P u_T}{U} - \frac{c_{\ell_\alpha}}{2a}\frac{u_T^2}{U} + \frac{Mc_{\ell_M}}{2a}\frac{u_P u_T}{U}\right.$$

$$\left. - \frac{c_d}{2a}\left(\frac{u_P^2}{U} + U\right) + \frac{c_{d_\alpha}}{2a}\frac{u_P u_T}{U} - \frac{Mc_{d_M}}{2a}\frac{u_P^2}{U}\right] dr\ \delta u_{P_B}$$

$$+ \int_0^1 r\left(U u_T \frac{c_{\ell_\alpha}}{2a} - U u_P \frac{c_{d_\alpha}}{2a}\right) dr\ \delta\theta$$

$$= M_o + M_\mu \delta u_{T_B} + M_\beta \delta u_{P_B} + M_\theta \delta\theta$$

and, for the blade drag force,

$$\int_0^1 \frac{F_x}{ac}\,dr = \int_0^1 U\left(u_P\,\frac{c_\ell}{2a} + u_T\,\frac{c_d}{2a}\right)dr$$

$$+ \int_0^1 \left[\frac{c_\ell}{2a}\,(\delta U u_P + U\delta u_P) + U u_P\,\frac{c_{\ell_\alpha}}{2a}\,\delta\alpha\right.$$

$$+ U u_P\,\frac{c_{\ell_M}}{2a}\,\delta M + \frac{c_d}{2a}\,(\delta U u_T + U\delta u_T)$$

$$\left. + U u_T\,\frac{c_{\ell_\alpha}}{2a}\,\delta\alpha + U u_T\,\frac{c_{d_M}}{2a}\,\delta M\right]dr$$

$$= \int_0^1 U\left(u_P\,\frac{c_\ell}{2a} + u_T\,\frac{c_d}{2a}\right)dr$$

$$+ \int_0^1 \left[\frac{c_\ell}{2a}\,\frac{u_T u_P}{U} + \frac{c_{\ell_\alpha}}{2a}\,\frac{u_P^2}{U} + \frac{Mc_{\ell_M}}{2a}\,\frac{u_P u_T}{U}\right.$$

$$\left. + \frac{c_d}{2a}\left(\frac{u_T^2}{U} + U\right) + \frac{c_{d_\alpha}}{2a}\,\frac{u_P u_T}{U} + \frac{Mc_{d_M}}{2a}\,\frac{u_T^2}{U}\right]dr\;\delta u_{T_B}$$

$$+ \int_0^1 r\left[\frac{c_\ell}{2a}\left(\frac{u_P^2}{U} + U\right) - \frac{c_{\ell_\alpha}}{2a}\,\frac{u_T u_P}{U} + \frac{Mc_{\ell_M}}{2a}\,\frac{u_P^2}{U}\right.$$

$$\left. + \frac{c_d}{2a}\,\frac{u_P u_T}{U} - \frac{c_{d_\alpha}}{2a}\,\frac{u_T^2}{U} + \frac{Mc_{\ell_M}}{2a}\,\frac{u_T u_P}{U}\right]dr\;\delta u_{P_B}$$

$$+ \int_0^1 U\left(u_P\,\frac{c_{\ell_\alpha}}{2a} + u_T\,\frac{c_{d_\alpha}}{2a}\right)dr\;\delta\theta$$

$$= H_O + H_\mu\,\delta u_{T_B} + H_\beta\,\delta u_{P_B} + H_\theta\,\delta\theta$$

The radial force is simply

$$\int_0^1 \frac{F_r}{ac}\,dr = \left(\int_0^1 U\,\frac{c_d}{2a}\,dr\right)\delta u_R - \beta\,\frac{C_T}{\sigma a}$$

$$= R_\mu\,\delta u_R - \beta\,\frac{C_T}{\sigma a}$$

The coefficients may be identified now; the trim values of the blade section force coefficients (c_ℓ, c_d, and their derivatives, evaluated at the angle of attack and Mach number of the radical station) must be used in the integrands, and the trim velocities are

$$u_T = r$$

$$u_P = V + v$$

$$U = \sqrt{r^2 + (V + v)^2}$$

For convenience, $V + v$ will be written as V in the following expressions. If one substitutes for the trim velocities, the rotor aerodynamic coefficients are

$$\left.\begin{aligned}
\frac{C_T}{\sigma a} &= \int_0^1 U\left(r\,\frac{c_\ell}{2a} - V\,\frac{c_d}{2a}\right)dr \\
\frac{C_Q}{\sigma a} &= \int_0^1 rU\left(V\,\frac{c_\ell}{2a} + r\,\frac{c_d}{2a}\right)dr \\
M_\mu &= \int_0^1 r\left[\frac{c_\ell}{2a}\,U + \left(\frac{c_\ell}{2a} + \frac{Mc_{\ell_M}}{2a}\right)\frac{r^2}{U} - \left(\frac{c_d}{2a} + \frac{Mc_{d_M}}{2a}\right)\frac{rV}{U}\right. \\
&\qquad \left. + \left(r\,\frac{c_{\ell_\alpha}}{2a} - V\,\frac{c_{d_\alpha}}{2a}\right)\frac{V}{U}\right]dr \\
M_{\dot\beta} &= \int_0^1 r^2\left[\left(\frac{c_\ell}{2a} + \frac{Mc_{\ell_M}}{2a}\right)\frac{rV}{U} - \frac{c_d}{2a}\,U - \left(\frac{c_d}{2a} + \frac{Mc_{d_M}}{2a}\right)\frac{V^2}{U}\right. \\
&\qquad \left. - \left(r\,\frac{c_{\ell_\alpha}}{2a} - V\,\frac{c_{d_\alpha}}{2a}\right)\frac{r}{U}\right]dr \\
M_\theta &= \int_0^1 rU\left(r\,\frac{c_{\ell_\alpha}}{2a} - V\,\frac{c_{d_\alpha}}{2a}\right)dr
\end{aligned}\right\} \quad (50)$$

(Eqs. (50) continued on next page.)

$$
\left.
\begin{aligned}
H_\mu + R_\mu &= \int_0^1 \left[\left(\frac{c_\ell}{2a} + \frac{Mc_{\ell_M}}{2a} \right) \frac{rV}{U} + \frac{c_d}{2a} 2U + \left(\frac{c_d}{2a} + \frac{Mc_{d_M}}{2a} \right) \frac{r^2}{U} \right. \\
&\quad \left. + \left(V \frac{c_{\ell_\alpha}}{2a} + r \frac{c_{d_\alpha}}{2a} \right) \frac{V}{U} \right] dr \\
H_{\dot\beta}^* &= \int_0^1 r \left[\left(\frac{c_\ell}{2a} + \frac{Mc_{\ell_M}}{2a} \right) \frac{V^2}{U} + \frac{c_d}{2a} \frac{VU}{r} + \left(\frac{c_d}{2a} + \frac{Mc_{d_M}}{2a} \right) \frac{rV}{U} \right. \\
&\quad \left. - \left(V \frac{c_{\ell_\alpha}}{2a} + r \frac{c_{d_\alpha}}{2a} \right) \frac{r}{U} \right] dr \\
H_\theta &= \int_0^1 U \left(V \frac{c_{\ell_\alpha}}{2a} + r \frac{c_{d_\alpha}}{2a} \right) dr
\end{aligned}
\right\} \qquad (50)
$$

where $U = (r^2 + V^2)^{1/2}$. The expression for $H_{\dot\beta}^*$ was obtained from $H_\beta = C_T/\sigma a + H_{\dot\beta}^*$ using the result for $C_T/\sigma a$. The effect of R_μ in the sum $H_\mu + R_\mu$ is just a term $(c_d/2a)U$ in the integrand. So R_μ only adds to the drag terms of H_μ, which are usually negligible for high inflow aerodynamics anyway. The following expressions for H_μ and $H_{\dot\beta}$ are also required, at least to find the other coefficients:

$$
\left.
\begin{aligned}
H_\mu &= \int_0^1 \left[\left(\frac{c_\ell}{2a} + \frac{Mc_{\ell_M}}{2a} \right) \frac{rV}{U} + \frac{c_d}{2a} U + \left(\frac{c_d}{2a} + \frac{Mc_{d_M}}{2a} \right) \frac{r^2}{U} \right. \\
&\quad \left. + \left(V \frac{c_{\ell_\alpha}}{2a} + r \frac{c_{d_\alpha}}{2a} \right) \frac{V}{U} \right] dr \\
H_{\dot\beta} &= \int_0^1 r \left[\frac{c_\ell}{2a} U + \left(\frac{c_\ell}{2a} + \frac{Mc_{\ell_M}}{2a} \right) \frac{V^2}{U} + \left(\frac{c_d}{2a} + \frac{Mc_{d_M}}{2a} \right) \frac{rV}{U} \right. \\
&\quad \left. - \left(V \frac{c_{\ell_\alpha}}{2a} + r \frac{c_{d_\alpha}}{2a} \right) \frac{r}{U} \right] dr
\end{aligned}
\right\} \qquad (51)
$$

The behavior of (and the expressions for) all the other coefficients can be inferred from a knowledge of the above set. The other coefficients follow immediately from the fact that, in the spanwise integration, the T terms have one less r than the M terms, the Q terms have one more r than the H terms, subscripts $\dot\zeta$ have one more r than subscripts μ, and subscripts λ have one less r than subscripts $\dot\beta$. The basic behavior of the coefficient is determined by whether it is an out-of-plane force or an inplane force, produced by an

out-of-plane or inplane velocity or blade pitch control. The combinations $H_\mu + R_\mu$ and $H_{\dot\beta}^* = H_{\dot\beta} - C_T/\sigma a$ are special effects that do not have comparable forms in the other coefficients. There is no radial drag due to blade lagging velocity (no δu_R) and no torque moment due to the radial drag force, so there are no R contributions to $H_{\dot\zeta}$ or any of the Q terms. The inplane force due to flapping velocity is written $H_\beta = C_T/\sigma a + H_{\dot\beta}^*$ only to show explicitly the term due to tilt of the thrust vector, so it is not extended to H_λ or any of the Q terms. Hence the coefficients H_μ and $H_{\dot\beta}$ are used to derive the other coefficients, not $H_\mu + R_\mu$ and $H_{\dot\beta}^*$.

If all terms but c_ℓ and c_{ℓ_α} are dropped from these expressions (and the degrees of freedom reduced to β_{1C}, β_{1S}, α_y, and α_x), the results of the previous section are recovered.

Evaluation of the coefficients- Approximate expressions for the aerodynamic coefficients are obtained by evaluating the integrands at an effective radius, with the techniques of the previous section. The results for the complete set of coefficients required are (dropping terms that are negligible for both high and low inflow):

$$
\left.
\begin{aligned}
M_o &= (3/4)(C_T/\sigma a) \\
M_\mu &= (\sin\phi)/6 + 2C_T/\sigma a \\
M_{\dot\zeta} &= (\sin\phi)/8 + 3/2(C_T/\sigma a) \\
M_{\dot\beta} &= -(\cos\phi)/8 \\
M_\lambda &= -(\cos\phi)/6 \\
M_\theta &= 1/(8\cos\phi) \\
T_o &= C_T/\sigma a = \bar\alpha/(6\cos\phi) \\
T_\mu &= (\sin\phi)/4 + 3C_T/\sigma a \\
T_{\dot\zeta} &= (\sin\phi)/6 + 2C_T/\sigma a \\
T_{\dot\beta} &= -(\cos\phi)/6 \\
T_\lambda &= -(\cos\phi)/4 \\
T_\theta &= 1/(6\cos\phi) \\
H_o &= (4/3)(C_Q/\sigma a) \\
H_\mu + R_\mu &= (V\sin\phi)/2 - 4V(C_T/\sigma a) + 6(C_Q/\sigma a) \\
H_{\dot\zeta} &= (V\sin\phi)/4 - (4/3)V(C_T/\sigma a) + (8/3)(C_Q/\sigma a) \\
H_{\dot\beta} &= -(\sin\phi)/6 + C_T/\sigma a
\end{aligned}
\right\} \qquad (52)
$$

(Eqs. (52) continued on next page.)

$$
\left.
\begin{aligned}
H_\lambda &= -(\sin\phi)/4 + (3/2)(C_T/\sigma a) \\
H_\theta &= V/(4\cos\phi) \\
Q_o &= C_Q/\sigma a = V(C_T/\sigma a) + c_d/8a \\
Q_\mu &= (V\sin\phi)/4 - (4/3)V(C_T/\sigma a) + (8/3)(C_Q/\sigma a) \\
Q_\zeta &= (V\sin\phi)/6 - V(C_T/\sigma a) + 2C_Q/\sigma a \\
Q_\beta &= -(\sin\phi)/8 + (3/4)(C_T/\sigma a) \\
Q_\lambda &= -(\sin\phi)/6 + C_T/\sigma a \\
Q_\theta &= V/(6\cos\phi)
\end{aligned}
\right\} \qquad (52)
$$

where the inflow angle is evaluated at an effective radius r_e ($r_e = 0.75$ usually works well) so that

$$\sin\phi = V/\sqrt{r_e^2 + V^2}$$

$$\cos\phi = r_e/\sqrt{r_e^2 + V^2}$$

$$\alpha(r_e) = \theta(r_e) - \tan^{-1} V/r_e$$

Wherever V occurs in these expressions, $V + v$ is really meant, but the effect of the induced velocity v is important only for low inflow. The similar behavior of the coefficients within a group (as discussed above) appears in these approximations.

The $c_d(C_Q)$ terms are important only for the inplane forces due to inplane velocities at low inflow. The $c_\ell(C_T)$ terms are important for low V, but never for the out-of-plane forces due to out-of-plane velocities. All C_T and C_Q terms may be dropped for high inflow, where V is of order 1; in that case, $V + v$ may be replaced by V also. The compressibility influence, especially c_{d_M} and c_{ℓ_M}, may result in important contributions from the lift and drag terms even in high inflow; stalled flow may affect c_{ℓ_α} and c_{d_α}. In general, however, for high inflow the behavior of the coefficients is given primarily by the c_{ℓ_α} terms alone; this is expected to occur so long as significant stall or compressibility effects in the trim operating state are avoided.

The basic features of the rotor aerodynamic coefficients in high inflow are obtained then the c_{ℓ_α} terms. Of particular interest is the variation with forward speed V. If it is assumed that $V/\Omega R$ is of order 1, that all the blade section coefficients are small compared with c_{ℓ_α}, and that $c_{\ell_\alpha}/2a = 1/2$, then the coefficients reduce to

$$
\left.
\begin{aligned}
M_\mu &= \frac{1}{2}\int_0^1 \frac{r^2 V}{\sqrt{r^2+V^2}}\,dr \\
M_{\dot\beta} &= -\frac{1}{2}\int_0^1 \frac{r^4}{\sqrt{r^2+V^2}}\,dr \\
M_\theta &= \frac{1}{2}\int_0^1 r^2\sqrt{r^2+V^2}\,dr \\
H_\mu &= \frac{1}{2}\int_0^1 \frac{V^2}{\sqrt{r^2+V^2}}\,dr \\
H_{\dot\beta} &= -\frac{1}{2}\int_0^1 \frac{r^2 V}{\sqrt{r^2+V^2}}\,dr \\
H_\theta &= \frac{1}{2}\int_0^1 V\sqrt{r^2+V^2}\,dr
\end{aligned}
\right\} \tag{53}
$$

These coefficients were obtained in the discussion of the aerodynamics for the four-degree-of-freedom model, and the integrals were evaluated in that section (eqs. (31)). The variation of these coefficients with forward velocity is shown in figure 4. The behavior of any of the remaining coefficients is similar to one in this set, but with slightly different numerical constants.

If only the c_{ℓ_α} terms are retained and with $c_{\ell_\alpha}/2a = 1/2$, the entire set of aerodynamic coefficients is

$$
\left.
\begin{aligned}
M_\mu &= Vf_2 & H_\mu &= V^2 f_0 \\
M_{\dot\zeta} &= Vf_3 & H_{\dot\zeta} &= V^2 f_1 \\
M_{\dot\beta} &= -f_4 & H_{\dot\beta} &= H_{\dot\beta}^* = -Vf_2 \\
M_\lambda &= -f_3 & H_\lambda &= -Vf_1 \\
M_\theta &= g_2 & H_\theta &= Vg_0 \\
T_\mu &= Vf_1 & Q_\mu &= V^2 f_1 \\
T_{\dot\zeta} &= Vf_2 & Q_{\dot\zeta} &= V^2 f_2 \\
T_{\dot\beta} &= -f_3 & Q_{\dot\beta} &= -Vf_3 \\
T_\lambda &= -f_2 & Q_\lambda &= -Vf_2 \\
T_\theta &= g_1 & Q_\theta &= Vg_1
\end{aligned}
\right\} \tag{54}
$$

where

$$f_n = \frac{1}{2} \int_0^1 \frac{r^n \, dr}{\sqrt{r^2 + V^2}}$$

$$g_n = \frac{1}{2} \int_0^1 r^n \sqrt{r^2 + V^2} \, dr$$

The integrals required are

$$f_0 = \frac{1}{2} \ell n \frac{1 + \sqrt{1 + V^2}}{V}$$

$$f_1 = \frac{1}{2} (\sqrt{1 + V^2} - V)$$

$$f_2 = \frac{1}{4} \sqrt{1 + V^2} - \frac{1}{2} V^2 f_0$$

$$f_3 = \frac{1}{6} [\sqrt{1 + V^2} (1 - 2V^2) + 2V^3]$$

$$f_4 = \frac{1}{16} \sqrt{1 + V^2} (2 - 3V^2) + \frac{3}{8} V^4 f_0$$

$$g_0 = \frac{1}{4} \sqrt{1 + V^2} + \frac{1}{2} V^2 f_0$$

$$g_1 = \frac{1}{6} [(\sqrt{1 + V^2})^3 - V^3]$$

$$g_2 = \frac{1}{16} \sqrt{1 + V^2} (2 + V^2) - \frac{1}{8} V^4 f_0$$

The aerodynamic coefficients can also be evaluated using the exact expressions (eqs. (50)), including the effects of the blade lift and drag, and of stall and compressibility - the only approximation then being in the knowledge of the section aerodynamics. To evaluate the coefficients requires the blade section force coefficients and their derivatives with respect to angle of attack and Mach number: $c_{\ell_\alpha}/2a$, $c_\ell/2a$, $c_d/2a$, $c_{d_\alpha}/2a$, $c_\ell/2a + Mc_{\ell_M}/2a$, and $c_d/2a + Mc_{d_M}$. The coefficients are to be evaluated at the blade trim angle of attack and Mach number:

$$\alpha = \theta - \tan^{-1}(V + v)/r$$

$$M = M_{tip}\sqrt{r^2 + (V + v)^2}$$

The blade twist and the collective pitch required for a given flight condition are then required to evaluate the section aerodynamic, in contrast to the results with only c_{ℓ_α} terms where only V is required. The section coefficients may be evaluated from tables of airfoil section data, appropriate to the rotor blade being considered.

Alternatively, representative analytic expressions may be used for the blade section coefficients. While a particular section may not be considered then, a representation that includes typical stall and compressibility effects will allow a general study of the influence of these effects on the rotor aeroelastic behavior. The following expressions for the section coefficients are used here. Below a stall angle of attack α_s (typically 12°), a constant lift curve slope is assumed, with a Prandtl-Glauert correction for compressibility, so that $c_\ell = a\alpha(1 - M^2)^{-1/2}$, and the lift coefficients required are

$$\left.\begin{aligned} \frac{c_{\ell_\alpha}}{2a} &= \frac{1}{2}(1 - M^2)^{-1/2} \\ \frac{c_\ell}{2a} &= \frac{\alpha}{2}(1 - M^2)^{-1/2} \\ \frac{c_\ell}{2a} + \frac{Mc_{\ell_M}}{2a} &= \frac{\alpha}{2}(1 - M^2)^{-3/2} \end{aligned}\right\} \tag{55}$$

In practice, the Prandtl-Glauert factor $(1 - M^2)^{-1/2}$ is truncated at its value at $M = 0.95$, say, to avoid numerical problems near $M = 1$. The drag for unstalled flow is

$$\left.\begin{aligned} c_d &= 0.0065 - 0.0216\alpha + 0.4\alpha^2 + \Delta c_d \\ \Delta c_d &= \begin{cases} 0.43(M + |\alpha|/0.26 - 0.9) & \text{if } |\alpha| > \alpha_{div} = 0.26(0.9 - M) \\ 0 & \text{otherwise} \end{cases} \end{aligned}\right\} \tag{56a}$$

This is the classical result of Bailey (ref. 31) with a lower $c_{d_{min}}$ as appropriate for current proprotor sections, and with a compressibility term obtained from section tests on rotating blades. The compressibility drag increment has a critical Mach number of 0.9 at zero angle of attack; above the critical Mach number, there is a large increase in c_d. The drag coefficient and its derivatives must be divided by $2a$; $a = 5.7$ is used for the two-dimensional lift curve slope. For stalled flow, $|\alpha| > \alpha_s$, the following approximation is used:

$$\left.\begin{aligned} c_\ell &= c_{\ell_s}\, sgn(\alpha) \\ c_d &= c_{d_s}(\sin\alpha)^2 \end{aligned}\right\} \qquad (56b)$$

where, typically, $c_{\ell_s} = 1.0$ and $c_{d_s} = 2.0$. Combined compressibility and stall effects are not included. A very important influence of stalled flow is that possibly $c_{\ell_\alpha} = 0$ there, so the c_ℓ, c_d, c_{d_α}, c_{ℓ_M}, and c_{d_M} terms in the coefficients dominate the behavior even in high inflow (if a large enough portion of the blade is stalled).

With these analytical, semiempirical expressions for the section aerodynamics, the influence of the drag and lift terms and of stall and compressibility on the rotor aerodynamic coefficients is examined. For the design of a specific rotor and the prediction of its behavior, the section characteristics appropriate for the actual blade sections should be used. For the present work, it is desired only to check the relative importance of these effects so approximate lift and drag coefficients are satisfactory. The influence of these effects on the rotor coefficients is shown in figure 5, for H_θ, H_μ, $H_{\dot\beta}$, M_θ, M_μ, and $M_{\dot\beta}$. The coefficients were calculated using the exact expressions (eqs. (50)), with the above approximations for the section aerodynamics, for two rotors.[1] The collective required to give the rotor thrust for equilibrium cruise at a given V is used. In figure 5, the results for these two rotors are compared with the coefficients found using only the c_{ℓ_α} terms. The coefficients with only the c_{ℓ_α} terms are given by equations (31) (fig. 4); the approximation is the same for the two rotors since it is independent of the section characteristics. The most important difference between the two rotors so far as the behavior of the coefficients is concerned is that they have different tip speeds. Therefore for a given forward speed $V/\Omega R$, the blades have a different resultant Mach number $M = M_{tip}(r^2 + V^2)^{1/2}$ at a section. The tip resultant Mach number $M = M_{tip}(1 + V^2)^{1/2}$ is shown in figure 5(b) for the two rotors.

The exact coefficients in figure 5 show a significant difference from the coefficients based only on the c_{ℓ_α} terms; the difference is particularly large when the tip critical Mach number (0.9 for $\alpha = 0$ with the section characteristics used) is exceeded. The following conclusions are reached then: the c_{ℓ_α} terms in the rotor aerodynamic coefficients give the basic behavior, at least so long as the section critical Mach number is not exceeded; the other terms in the coefficients are not negligible, however, and should be included to properly evaluate the behavior of a real rotor, especially when operating at high section α or M. When the section aerodynamics other than c_{ℓ_α} are required, actual section characteristics should be used rather than representative expressions.

Three methods for evaluating the rotor aerodynamic coefficients have been described:

---

[1]Specifically, this is for the two full-scale rotors examined in later chapters, hence the labels "Bell" and "Boeing" in figure 5.

(a) Approximations based on evaluating the integrands at an equivalent radius.
(b) Approximations based on the retention of only the c_{ℓ_α} terms, with $c_{\ell_\alpha}/2a = 1/2$; the integrals may be evaluated, giving the coefficients as functions of V alone.
(c) Approximations based on analytical expressions for the blade section aerodynamics in the exact coefficients; representative stall and compressibility effects are included, but no specific section is modeled.

The coefficients based on the equivalent radius approximation (method (a)) are used only for the expository development, never in the calculations. Method (b) treats the c_{ℓ_α} terms correctly and exactly, and if the other terms are required method (c) should be used rather than method (a). The coefficients based on just the c_{ℓ_α} terms (method (b)) will normally be used in the calculations here. These coefficients include the basic behavior with inflow ratio, which is of primary interest here. In fact, this level is usually a good approximation for calculating the dynamic behavior (as shown later). Method (c), the coefficients based on the exact expressions (eqs. (50)), is used here only to check the influence of the terms other than c_{ℓ_α}.

The method used here allows the derivation of rotor aerodynamic coefficients, including the influence of lift and drag and of stall and compressibility, with no more difficulty than a derivation that includes only c_{ℓ_α} terms. Therefore, a good representation of the rotor aerodynamics is available if one chooses to use it (and if enough information on the section aerodynamics is available). Evaluation of the coefficients in method (c), or even including tabular data for the actual blade sections used, requires numerical integration over the span, but that is no problem for numerical work. There is only one real complication in evaluating the coefficients by the exact expressions: the trim angle-of-attack distribution is required, which means that the blade collective pitch at the given operating state must be known. Hence a preliminary solution of the rotor performance to find the collective pitch is required before the coefficients can be evaluated for the dynamics. In contrast, with only the c_{ℓ_α} terms (method (b)), only $V/\Omega R$ is required to evaluate the coefficients.

Discussion of the coefficients- Some properties of the coefficients are discussed here; in particular, certain useful equivalence among the coefficients are derived. A helicopter rotor in hover (low inflow axial flight) exhibits equivalence of control plane, hub plane, and tip path plane tilt; that is, these inputs produce the same forces on the helicopter (with certain exceptions). This behavior translates into certain equalities among the rotor aerodynamic coefficients. The influence of high inflow operation on the behavior of the rotor, and on the basic set of coefficients in general is examined now.

Consider the longitudinal moment on the rotor disk due to tip path plane tilt (β_{1C}, β_{1S}), hub plane tilt (α_y, α_x), and control plane tilt (θ_{1C}, θ_{1S}); from equation (42), this moment is

$$\frac{M_{F_{1S}}}{ac} = (V + v)M_\mu \alpha_y + M_{\dot\beta}(\dot\beta_{1S} - \beta_{1C} + \dot\alpha_x) + M_\theta \theta_{1S}$$

Hub plane tilt α_y gives an inplane component of $V + v$, hence a flap moment through the speed stability coefficient M_μ. Tip path plane tilt β_{1C} (with respect to the hub plane) gives a flapping velocity in the rotating frame, hence a flap moment through the flap damping coefficient $M_{\dot\beta}$. Control plane tilt θ_{1S} produces a flap moment through the pitch control power coefficient M_θ. For low inflow,

$$M_\theta = -M_{\dot\beta} = \frac{1}{8}$$

so the flapping produced by blade pitch is $\beta_{1C}/\theta_{1S} = M_\theta/-M_{\dot\beta} = 1$ (if $\nu_\beta = 1$). That is the familiar result of helicopter hover control (with a low inflow rotor): the tip path plane remains parallel to the control plane. In high inflow operation, however, M_θ and $-M_{\dot\beta}$ are not equal. Based on the equivalent radius approximation,

$$M_\theta = \frac{1}{8\cos\phi}$$

$$M_{\dot\beta} = -\frac{\cos\phi}{8}$$

so that

$$\frac{M_\theta}{-M_{\dot\beta}} = \frac{1}{\cos^2\phi}$$

Pitch control power M_θ increases with V, while the flap damping $M_{\dot\beta}$ decreases; the ratio then increases with V. For a $V/\Omega R$ up to 1 or so, there are no drastic changes in the magnitudes of the coefficients, but the effect is important. Based on just the c_{ℓ_α} terms, the coefficients are

$$M_\theta = \int_0^1 r u_T U \frac{c_{\ell_\alpha}}{2a}\, dr$$

$$-M_{\dot\beta} = \int_0^1 r^2 \frac{u_T^2}{U^2} \frac{c_{\ell_\alpha}}{2a}\, dr$$

The integrand of $M_{\dot\beta}$ is a factor $u_T r/U^2 = r^2/(r^2 + V^2)$ smaller than that of M_θ; therefore, the ratio of the coefficients is of the order $r_e^2/(r_e^2 + V^2) = \cos^2\phi$ (as above). This high inflow effect results from the fact that the $\delta\alpha$ due to $\dot\beta$ is not the same as that due to θ when the inflow angle ϕ is large. The flapping term comes from $\delta u_P = r\dot\beta$ so that

$$\delta\alpha = \delta\theta - \frac{u_T \delta u_P}{U^2} = \delta\theta - \frac{u_T r}{U^2}\dot\beta$$

which gives the additional factor $u_T r/U^2$ in $M_{\dot\beta}$.

Consider now the hub moment in terms of flapping with respect to space (in an inertia frame), that is,

$$\beta_{1C_I} = \beta_{1C} - \alpha_y$$

$$\beta_{1S_I} = \beta_{1S} + \alpha_x$$

so that the longitudinal moment on the rotor disk due to flapping (with respect to space), hub plane tilt, and control plane tilt is

$$\frac{M_{F_{1S}}}{ac} = [-M_{\dot{\beta}} + (V + v)M_\mu]\alpha_y + M_{\dot{\beta}}(\dot{\beta}_{1S_I} - \beta_{1S_I}) + M_\theta \theta_{1S}$$

Flapping with respect to space acts through $M_{\dot{\beta}}$ to give a hub moment as usual. The moment due to hub plane tilt α_y is $[-M_{\dot{\beta}} + (V + v)M_\mu]$, while that due to control plane tilt is M_θ. In high inflow, these moments are not equal, for while both α_y and θ_{1S} tilt the control plane, only α_y tilts the hub plane reference frame also. The difference is, in fact, small. From the definitions of the coefficients (eqs. (50)), it follows that

$$-M_{\dot{\beta}} + (V + v)M_\mu = \int_0^1 r\left[\frac{c_d}{2a} rU + \left(r\frac{c_{\ell_\alpha}}{2a} - V\frac{c_{d_\alpha}}{2a}\right)\frac{r^2}{U} + \frac{c_\ell}{2a} VU + \left(r\frac{c_{\ell_\alpha}}{2a} - V\frac{c_{d_\alpha}}{2a}\right)\frac{V^2}{U}\right]dr$$

$$= M_\theta + \int_0^1 rU\left(V\frac{c_\ell}{2a} + r\frac{c_d}{2a}\right)dr$$

Hence

$$-M_{\dot{\beta}} + (V + v)M_\mu = M_\theta + \frac{C_Q}{\sigma a} \tag{57}$$

Now $M_\theta \cong 1/(8 \cos \phi)$, so that $M_\theta >> C_Q/\sigma a$ (which is of the order of $VC_T/\sigma a$) for all V, both high and low inflow. So for all V,

$$-M_{\dot{\beta}} + (V + v)M_\mu \cong M_\theta$$

which means that hub plane tilt and control plane tilt are equivalent. For low inflow, $(V + v)M_\mu$ is of order V^2 small, while $M_{\dot{\beta}}$ and M_θ are of order 1 and both equal 1/8.

Similar results may be obtained for the inplane forces. Consider the vertical hub force due to flapping, hub plane tilt, and control plane tilt:

$$\frac{2C_H}{\sigma a} = (V + v)(H_\mu + R_\mu)\alpha_y + H_{\dot\beta}(\dot\beta_{1S} + \dot\alpha_x) - \left(\frac{2C_T}{\sigma a} + H_{\dot\beta}^*\right)\beta_{1C} + H_\theta\theta_{1S}$$

Tip path plane tilt β_{1C} gives an inplane hub force by tilt of the thrust vector, while blade pitch control has no such effect. The corresponding hub forces due to flapping and pitch, $H_{\dot\beta}^*$ and H_θ, are equal for low inflow where

$$H_\theta = -H_{\dot\beta}^* \cong \frac{V}{4}$$

In high inflow, these forces, like the flap moments, are no longer equal. On the basis of the equivalent radius approximation,

$$H_\theta = \frac{V}{4\cos\phi}$$

$$H_{\dot\beta}^* = -\frac{\sin\phi}{6}$$

so that

$$\frac{H_\theta}{-H_{\dot\beta}^*} \cong \frac{1}{\cos^2\phi}$$

Both forces increase with V, but H_θ increases faster by a factor $(\cos\phi)^{-2} = (r_e^2 + V^2)/r_e^2$. On the basis of just the c_{ℓ_α} terms, the coefficients are

$$H_\theta = \int_0^1 U u_P \frac{c_{\ell_\alpha}}{2a}\,dr$$

$$-H_{\dot\beta}^* = \int_0^1 r\,\frac{u_T u_P}{U}\,\frac{c_{\ell_\alpha}}{2a}\,dr$$

The integrand of $H_{\dot\beta}^*$ is a factor $u_T r/U^2 = r^2/(r^2 + V^2)$ smaller than that of H_θ, which agrees with the result from the equivalent radius expressions. Also, it is the same factor found between the integrands of $M_{\dot\beta}$ and M_θ, as expected since the difference between the coefficients has the same source in both cases, namely, the difference between $\delta\alpha$ due to θ and due to $\dot\beta$ when the inflow ϕ is large. In terms of flapping with respect to space, the hub force is

$$\frac{2C_H}{\sigma a} = \left[-\left(\frac{2C_T}{\sigma a} + H_{\dot\beta}^*\right) + (V + v)(H_\mu + R_\mu)\right]\alpha_y + H_{\dot\beta}\dot\beta_{1C_I} - \left(\frac{2C_T}{\sigma a} + H_{\dot\beta}^*\right)\beta_{1C_I} + H_\theta\theta_{1S}$$

The equivalence of hub plane tilt and control plane tilt may again be demonstrated; from the expressions for the coefficients, there follows exactly

$$-H_{\dot{\beta}}^{*} + (V + v)(H_{\mu} + R_{\mu}) = H_{\theta} + (V + v)R_{\mu} \tag{58}$$

which is, for all V, approximately

$$-H_{\dot{\beta}}^{*} + (V + v)(H_{\mu} + R_{\mu}) \cong H_{\theta}$$

and if only high inflow is considered, so $H_{\dot{\beta}} \cong H_{\dot{\beta}}^{*}$, it follows that

$$-H_{\dot{\beta}} + (V + v)(H_{\mu} + R_{\mu}) \cong H_{\theta}$$

The speed stability coefficients M_{μ} and $H_{\mu} + R_{\mu}$ produce moments and forces due to hub inplane velocity - that is, due to shaft linear velocity, aerodynamic gusts, or angular velocity of the pylon about a pivot aft of the hub. For low inflow, these coefficients are an order V smaller than the other moments and forces. For high inflow, however, the speed stability coefficients are of the same order as the others, and this difference between the low inflow and high inflow aerodynamics may be expected to have an important influence on the aeroelastic behavior. The speed stability coefficients usually produce positive damping of the motion (see, e.g., the four-degree-of-freedom model, eqs. (26)). With high inflow, hub plane tilt results in an inplane component of V that produces forces and moments through the speed stability coefficients. These forces are in the same direction as the displacement, so they act as negative springs (eqs. (26) again). The speed stability coefficients often appear in the equations of motion as coupling terms rather than as direct damping or spring terms. In such cases, the effect of the coefficients may be significant since their magnitude is of order 1 in high inflow, the overall effect may be stabilizing or destabilizing, depending on the coupled motion involved.

The inplane forces on the hub due to tip path plane tilt have contributions from the direct tilt of the thrust vector ($2C_T/\sigma a$ term) and from the inflow ($H_{\dot{\beta}}$ term). From the equivalent radius approximation, the relative size of these two terms is

$$\frac{2C_T/\sigma a}{H_{\dot{\beta}}^{*}} = \frac{\bar{\alpha}/(3 \cos \phi)}{(\sin \phi)/6} = \frac{3}{2} \frac{\bar{\alpha}}{V \cos^2 \phi}$$

Thus the ratio is of order $\bar{\alpha}/V$. In high inflow, $C_T/\sigma a$ may be neglected since V is of order 1, and also because the working angle of attack $\bar{\alpha}$ of the prop-rotor is low. These terms are very important for flapping rotor dynamics. The response of the rotor to low-frequency excitation, say, control plane tilt or shaft motion, is tilt of the tip path plane. Through $2C_T/\sigma a + H_{\dot{\beta}}^{*}$, the tip path plane tilt gives a hub inplane force that couples the rotor and vehicle motion or is used to control the vehicle. For high inflow, $H_{\dot{\beta}}^{*}$ dominates the

thrust term, so the inplane force on the hub is not only an order larger, but also of opposite sign. This effect is expected to produce dynamic behavior significantly different from that of low inflow rotors. Hub plane angular velocity and tip path plane angular velocity act through $H_{\dot{\beta}}$ to produce inplane forces also. In high inflow, the thrust term may be neglected, so $H_{\dot{\beta}} \cong H_{\dot{\beta}}{}^*$; the coefficient is then the same as for tip path plane tilt.

Consider now the cross derivatives M_μ and $H_{\dot{\beta}}$, which are out-of-plane force due to inplane velocity and inplane force due to out-of-plane velocity, respectively. On the basis of only the c_{ℓ_α} terms, these coefficients are equal:

$$M_\mu = -H_{\dot{\beta}} = \int_0^1 \frac{r^2 V}{\sqrt{r^2 + V^2}} \frac{c_{\ell_\alpha}}{2a}\, dr$$

This equality is useful in simplifying the whirl flutter equations of motion in a later chapter. Examine, therefore, whether it remains valid with the more complete expressions for the coefficients. From equations (50),

$$M_\mu + H_{\dot{\beta}} = \frac{3C_T}{\sigma a} + \int_0^1 U\left(r \frac{Mc_{\ell_M}}{2a} + 3V \frac{c_d}{2a} - r \frac{c_{d_\alpha}}{2a}\right) dr \tag{59}$$

The right-hand side is negligible for large V, compared with M_μ or $H_{\dot{\beta}}$; for high inflow, one has always then

$$M_\mu \cong -H_{\dot{\beta}}$$

High inflow, $V/\Omega R$ of order 1, influences the rotor aerodynamic coefficients substantially. It follows then that the features of high inflow aerodynamics are an important factor in the aeroelastic behavior of the rotor and wing system. In summary, the combinations of the coefficients derived are

$$\left.\begin{aligned} -M_{\dot{\beta}} + (V + v)M_\mu &\cong M_\theta \\ -H_{\dot{\beta}}{}^* + (V + v)(H_\mu + R_\mu) &\cong H_\theta \\ M_\mu &\cong -H_{\dot{\beta}} \end{aligned}\right\} \tag{60}$$

The first two approximations are valid for all V, while the last is only for high inflow; to these may also be added $H_{\dot{\beta}} \cong H_{\dot{\beta}}{}^*$ for high inflow.

Performance considerations- The evaluation of the rotor aerodynamic coefficients for the analysis of the proprotor dynamics requires a consideration of the proprotor performance. First, to obtain the rotor collective

pitch value requires a solution for the performance in a specified operating state, for example, cruise flight (C_T given by the airplane drag) or autorotation ($C_Q = 0$). The rotor collective pitch is needed only to evaluate the complete expressions for the coefficients, however (eqs. (50), described as method (c) previously). Second, the total axial velocity $V + v$, a major parameter in the coefficients, includes the induced inflow v, which is related to the rotor thrust and operating state. Two topics are now considered: the expressions required for an elementary analysis of the proprotor performance (C_T and C_Q) to find the collective pitch; and an evaluation of the rotor-induced inflow.

In the previous analysis, expressions were obtained (eqs. (50)) for the rotor thrust and torque coefficients in terms of the blade section aerodynamic forces. Using the identity of the power and torque coefficients for the rotor ($C_P = C_Q$ since $P = Q\Omega$), these expressions are

$$\left.\begin{aligned} \frac{C_T}{\sigma a} &= \int_0^1 U\left[r\,\frac{c_\ell}{2a} - (V + v)\,\frac{c_d}{2a}\right] dr \\ \frac{C_P}{\sigma a} &= \int_0^1 rU\left[(V + v)\,\frac{c_\ell}{2a} + r\,\frac{c_d}{2a}\right] dr \end{aligned}\right\} \tag{61}$$

where $U^2 = r^2 + (V + v)$. If uniform induced inflow v, is assumed, the power expression is

$$C_P = (V + v)C_T + \int_0^1 \frac{\sigma c_d}{2}\, U^3\, dr \tag{62}$$

which is the usual result for the power required by a rotor operating in axial flow. The first term is the sum of the induced power loss and the useful work done:

$$C_{P_i} = (V + v)C_T \cong (V + C_T/2V)C_T \tag{63}$$

For high inflow, the induced loss term $vC_T \cong C_T{}^2/2V$ is negligible (see discussion below); then C_{P_i} is proprotional to C_T, in contrast to hover operation where the induced inflow is important and for which C_{P_i} is proportional to $C_T{}^{3/2}$.

The second term in equation (62) is the rotor profile power loss; if the section drag coefficient is constant over the span (or if an effective mean value of c_d is used), then

$$
\left.
\begin{aligned}
C_{P_o} &= \int_0^1 \frac{\sigma c_d}{2} \left[r^2 + (V + v)^2\right]^{3/2} dr \\
&= \frac{\sigma c_d}{8} \left\{ \sqrt{1 + (V + v)^2} \left[1 + \frac{5}{2} (V + v)^2\right] \right. \\
&\quad \left. + \frac{3}{2} (V + v)^4 \, \ell n \, \frac{1 + \sqrt{1 + (V + v)^2}}{V + v} \right\} \\
&\cong \begin{cases}
\dfrac{\sigma c_d}{8} \left[1 + 3(V + v)^2\right] & \text{low } V \\
\dfrac{\sigma c_d}{8} (6.27) & V + v = 1 \\
\dfrac{\sigma c_d}{8} (4V^3) & \text{high } V
\end{cases}
\end{aligned}
\right\} \tag{64}
$$

The two rotor operating conditions of primary interest here are: operation with the rotor providing the propulsive force required for equilibrium cruise flight, and autorotation operation (no net power supplied to the rotor through the shaft). The latter corresponds to the condition in which dynamic tests of the proprotor and wing are often performed. The performance problem involved is then to find the rotor collective pitch required (and the other coefficient) for a given C_T (thrust required for equilibrium cruise flight) or C_Q (zero for autorotation).

The rotor aerodynamic coefficients require an estimate of the rotor induced velocity v. For high inflow, however, the induced velocity is much less than the forward speed of the rotor (as shown below), so great attention to the inflow calculation is not required to satisfactorily evaluate the coefficients. The assumption of uniform inflow is adequate then, and it may, in fact, be possible to neglect the induced inflow entirely. The rotor C_T required in cruise flight is obtained by equating the rotor thrust (for two rotors) with the aircraft drag, and expressing the drag in terms of an equivalent flat-plate area f for the aircraft ($D = (1/2)\rho V^2 f$). Therefore, for the thrust required of the rotor,

$$C_T = \frac{1}{4} \frac{f}{A} V^2$$

where A is the disk area of the rotor. Momentum theory can be used to estimate the induced inflow; the usual result (ref. 32) for axial flow operation at thrust C_T is:

$$V + v = V/2 + \sqrt{(V/2)^2 + C_T/2} \tag{65}$$

Substituting for C_T yields

$$\frac{v}{V} = \frac{\sqrt{1 + (f/2A)} - 1}{2}$$

or, since f/A and hence C_T/V^2 is small,

$$\frac{v}{V} \cong \frac{C_T}{2V^2} = \frac{1}{8}\frac{f}{A}$$

Typical values of proprotor aircraft drag and radius give $f/A \cong 0.0033$; it follows then that $v/V \cong 0.0017$ typically, which is indeed much less than 1. For the proprotor in equilibrium cruise flight, neglecting v/V is a reasonable approximation then.

When the rotor is operated in autorotation, the performance requirement is that $C_Q = 0$, which requires that $C_T = -C_{Q_O}/(V + v) \cong -C_{Q_O}/V$. With the high inflow result for the profile power, $C_{Q_O} \cong (\sigma c_d/2)V^3$, the thrust required in autorotation is

$$C_T = -\frac{\sigma c_d}{2} V^2$$

For the proprotor in axial flight at high inflow, autorotation occurs in the windmill brake state (i.e., at $V > 2\sqrt{|C_T|/2}$, or $|C_T/2V^2| \cong |v/V| < 1/4$); hence momentum theory may again be used to estimate the induced inflow (ref. 32). The same conventions are used for the directions of V and C_T (so the C_T required in autorotation is negative, as given previously); the momentum theory result is

$$V + v = \frac{V}{2} + \sqrt{\left(\frac{V}{2}\right)^2 + \frac{C_T}{2}} \tag{66}$$

Substituting for the required C_T yields

$$\frac{v}{V} \cong \frac{C_T}{2V^2} \cong -\frac{\sigma c_{d_o}}{4}$$

Typical values of proprotor drag coefficient and solidity yield $\sigma c_{d_o}/2 \cong 0.0004$. Hence the typical induced inflow $v/V \cong -0.0002$, which is smaller than in cruise flight. Again, the induced inflow may be neglected.

The effect of the induced inflow on the blade load distribution (that required to evaluate the aerodynamic coefficients for the dynamics analysis), may be investigated by considering the change in angle of attack due to v/V:

$$\delta\alpha = \delta \tan^{-1}\frac{V + v}{\Omega r} = \frac{v}{V}\frac{V/\Omega r}{1 + (V/\Omega r)^2}$$

which has a maximum value of $\delta\alpha = (1/2)v/V$. Use of the momentum theory result $v/V \cong C_T/2V^2$ (valid for both powered and autorotation operation in

high inflow) and the mean angle of attack $\bar{\alpha} = 6C_T/\sigma a$ yield the maximum change in angle of attack:

$$\frac{\delta\alpha}{\alpha} \cong \frac{\sigma a}{24V^2}$$

For typical values of rotor solidity, $\delta\alpha/\alpha \cong 0.02V^{-2}$, which is a small fraction for high inflow (V of order 1).

Numerical calculations were performed to verify that $V + v \cong V$ is a good approximation in the calculation of the aerodynamic coefficients. The important consideration in the dynamics analysis is that the performance calculation and the calculation of the aerodynamic coefficients be consistent, either neglecting the induced inflow v/V or using the same estimate of v/V for both calculations. Any error in estimating the rotor performance or the collective pitch required is not relevant to the dynamics analysis. The aerodynamic coefficients that correspond to the operation of the rotor at a given value of C_T or C_Q are obtained, the only error being a small change in the angle-of-attack distribution over the blade.

SECTION 3: BEHAVIOR OF ROTORS IN HIGH INFLOW

In the next four chapters, several topics on the behavior of high inflow proprotors are investigated, based on the equations of motion derived previously. The development of the proprotor and cantilever wing model is resumed in section 4. The reader interested in that topic may skip the four chapters in this section.

Elementary Dynamic Behavior

Some aspects of the dynamic behavior typical of proprotor aircraft are examined. First, the fundamental stability of the blade motion is examined through the eigenvalues of the uncoupled blade motion. Then the influence of the transformation to nonrotating degrees of freedom and equations of motion on the eigenvalues of the rotor is examined. The actual coupled motion of the proprotor and wing system is considerably more complex, but these considerations are useful in the interpretation of the results for the complete model. The equations of motion and the hub forces for the rotor were found to separate into longitudinal and lateral/vertical groups (eqs. (44) to (48)). The wing motion, in fact, couples these groups, but it is useful for a preliminary study of the dynamics to neglect that coupling, and examine the rotor response to shaft motion, gust, or blade pitch control in the longitudinal or in the lateral/vertical systems. Attention is directed to the low-frequency response, since that response is useful in evaluating the influence of the proprotor on the aircraft stability.

Blade stability- Consider the uncoupled, shaft fixed flapping motion of a single blade. The equation of motion (in the rotating frame) is

$$I_\beta^* \ddot{\beta} - \gamma M_{\dot{\beta}} \dot{\beta} + (I_\beta^* \nu_\beta^2 + K_P \gamma M_\theta)\beta = \gamma M_\theta \theta \tag{67}$$

The roots (eigenvalues) of this equation are

$$\lambda = \frac{\gamma M_{\dot{\beta}}}{2I_\beta^*} \pm i \sqrt{\nu_\beta^2 + K_P \frac{\gamma M_\theta}{I_\beta^*} - \left(\frac{\gamma M_{\dot{\beta}}}{2I_\beta^*}\right)^2} \tag{68}$$

For low inflow, $-M_{\dot{\beta}} = M_\theta = 1/8$, and equation (68) reduces then to the usual result for the flapping motion of a hovering rotor. The flap damping is positive, $M_{\dot{\beta}} < 0$, so the real part of λ is negative and the flap motion is stable. As $V/\Omega R$ increases, the flap damping $-M_{\dot{\beta}}$ decreases and the pitch control power M_θ increases. Then the real part of λ decreases in magnitude as $V/\Omega R$ increases, and the stability of the flapping motion decreases. The change is not great for $V/\Omega R$ of order 1, however; and $M_{\dot{\beta}}$ is always negative (at least the c_{ℓ_α} contribution is) so the motion remains stable for even extremely high inflow.

Pitch/flap coupling K_P introduces a flap spring term through the aerodynamic force M_θ, which changes the effective flap natural frequency:

$$\nu_{\beta_e}^2 = \nu_\beta^2 + K_P \frac{\gamma M_\theta}{I_\beta^*} \tag{69}$$

Negative pitch/flap coupling, $K_P > 0$, increases the effective flap frequency $\nu_{\beta e}$. Increasing $V/\Omega R$ increases M_θ, and so increases the effectiveness of K_P. Again, the influence is not great for $V/\Omega R$ of order 1 or less.

Consider the uncoupled lag motion with the rotating equation of motion (homogeneous form):

$$I_\zeta^* \ddot{\zeta} + \gamma Q_{\dot{\zeta}} \dot{\zeta} + I_\zeta^* \nu_\zeta^2 \zeta = 0 \tag{70}$$

The roots for this motion are

$$\lambda = -\frac{\gamma Q_{\dot{\zeta}}}{2I_\beta^*} \pm i \sqrt{\nu_\zeta^2 - \left(\frac{\gamma Q_{\dot{\zeta}}}{2I_\zeta^*}\right)^2} \tag{71}$$

The lag damping $Q_{\dot{\zeta}}$ is positive, $Q_{\dot{\zeta}} > 0$, so the motion is stable. The coefficient $Q_{\dot{\zeta}}$ increases with $V/\Omega R$, hence the stability of the lag motion increases. For low inflow, the lag aerodynamic damping is very low. For high inflow, however, there is a significant increase in lag damping, which is important in proprotor dynamics. In high inflow, the source of lag damping is the same as for the flap damping, namely, the lift change due to angle-of-attack

perturbations (i.e., the c_{ℓ_α} terms). Therefore, both flap damping and lag damping are of the same order in high inflow.

The flap and lag motions of the blade are strongly coupled by the aerodynamic forces in high inflow; specifically, they are coupled by the cross aerodynamic coefficients $M_\zeta^\cdot$ and $Q_\beta^\cdot$, which are of order 1 in high inflow (like all the coefficients).

Nonrotating system eigenvalues- Consider the blade uncoupled flap motion, as observed in the nonrotating frame. The coning mode β_0 has an equation of motion (eqs. (47)) identical to that of the blade in the rotating frame, so the eigenvalues of its motion are the same as those given previously. The equations of motion for the tip path plane tilt coordinates, β_{1C} and β_{1S}, are modified by the transformation to the nonrotating frame; centrifugal and Coriolis terms are introduced, which have the effect of coupling the β_{1C} and β_{1S} motions.

The homogeneous equations of motion in Laplace form for β_{1C} and β_{1S} are (from eqs. (44)):

$$\begin{bmatrix} I_\beta^* s^2 - \gamma M_{\dot\beta}^\cdot s + I_\beta^*(\nu_\beta^2 - 1) + K_P \gamma M_\theta & 2I_\beta^* s - \gamma M_{\dot\beta}^\cdot \\ -(2I_\beta^* s - \gamma M_{\dot\beta}^\cdot) & I_\beta^* s^2 - \gamma M_{\dot\beta}^\cdot s + I_\beta^*(\nu_\beta^2 - 1) + K_P \gamma M_\theta \end{bmatrix} \begin{pmatrix} \beta_{1C} \\ \beta_{1S} \end{pmatrix} = 0 \qquad (72)$$

The characteristic equation for this system is the fourth-order polynomial:

$$\Delta = [I_\beta^* \lambda^2 - \gamma M_{\dot\beta}^\cdot \lambda + I_\beta^*(\nu_\beta^2 - 1) + K_P \gamma M_\theta]^2 + (2I_\beta^* \lambda - \gamma M_{\dot\beta}^\cdot)^2 = 0 \qquad (73)$$

The eigenvalues are then the solutions of this polynomial; writing the roots of the flapping motion in the rotating frame (eq. (68)) as $\lambda = \lambda_R, \bar{\lambda}_R$, the nonrotating system eigenvalues (roots of eq. (73)) are then

$$\lambda_{NR} = \lambda_R \pm i \qquad (74)$$

and the conjugates. The nonrotating eigenvalues have the same real parts as the rotating roots, but the frequency is greater or less than that of the rotating roots by 1/rev. On the root locus plane ($Im\lambda$ vs. $Re\lambda$), the nonrotating roots are then shifted vertically by ±1/rev from the rotating roots.

For a three-bladed rotor, the rotating roots on the λ-plane are a pair of triple poles at λ_R and its conjugate. The nonrotating roots are a single pair at λ_R and its conjugate for the β_0 mode, plus a pair at $\lambda_R + i$ and $\lambda_R - i$ and their conjugates for the β_{1C} and β_{1S} modes. In both the rotating and nonrotating frame, there are then six roots, corresponding to the three blades each with a second-order differential equation. The eigenvectors of equation (72) give the coupled motion of β_{1C} and β_{1S} corresponding to the eigenvalues. There are two modes (and their conjugates); each eigenvector defines a wobbling motion of the tip path plane, at frequency $Im\lambda_R$ - 1/rev for the

low-frequency mode and at frequency $Im\lambda_R$ + 1/rev for the high-frequency mode. The high-frequency mode wobbles in the same direction as the rotor rotational direction, and so is called a progressive mode. The low-frequency mode wobbles opposite the rotor direction if $Im\lambda_R$ > 1/rev, so it is a regressive mode. If $Im\lambda_R$ < 1/rev, however, the low-frequency mode wobbles in the same direction as the rotor rotation and so is another progressive mode. The two modes are denoted here by $\beta \pm 1$ for the flap modes at frequencies $Im\lambda_R \pm$ 1/rev, respectively.

The behavior of the roots of the lag motion in the nonrotating frame is similar to that of the flap motion (the influence of the transformation from the rotating to nonrotating frame is a general result for all rotor degrees of freedom). The coupled motion of ζ_{1C} and ζ_{1S} is a low-frequency and high-frequency mode, denoted by $\zeta \pm 1$, each a whirling of the net rotor center of gravity about the shaft. This motion has an important role in proprotor dynamics. The blade flap and lag motions are, of course, highly coupled, with each other and with the shaft degrees of freedom. The basic flap and lag roots remain identifiable even for the coupled motion, however, both by the frequency of the eigenvalue and by the participation of the degrees of freedom in the eigenvectors. The characteristic location of the nonrotating roots, at the low-frequency and high-frequency rotor modes, remains an important feature of the dynamics.

Longitudinal system - Consider the longitudinal dynamics of the rotor, described by equations (47) and (48). It consists of two degrees of freedom (coning β_0 and collective lag ζ_0) excited by longitudinal shaft motion (hub velocity z_P and roll angle α_z), longitudinal gust (Vu_G), and rotor collective pitch control (θ_0). The influence of the rotor is transmitted to the shaft as a thrust force and a torque moment (C_T and C_Q) acting on the hub.

The equations of motion for the longitudinal system are, in transfer function form (and matrix notation),

$$\begin{bmatrix} I^*_{\beta_0} s^2 - \gamma M^{\cdot}_{\beta} s + I^*_{\beta_0} \nu^2_{\beta_0} + \gamma K_P M_\theta & \gamma M^{\cdot}_{\zeta} s \\ -\gamma Q^{\cdot}_{\beta} s + \gamma K_P Q_\theta & I^*_{\zeta_0} s^2 + \gamma Q^{\cdot}_{\zeta} s + I^*_{\zeta_0} \nu^2_{\zeta_0} \end{bmatrix} \begin{pmatrix} \beta_0 \\ \zeta_0 \end{pmatrix}$$

$$= \begin{bmatrix} \gamma M_\theta \\ \gamma Q_\theta \end{bmatrix} \theta_0 + \begin{bmatrix} \gamma V M_\lambda \\ \gamma V Q_\lambda \end{bmatrix} u_G + \begin{bmatrix} \gamma M^{\cdot}_{\zeta} s \\ I^*_{\zeta_0 \alpha} s^2 + \gamma Q^{\cdot}_{\zeta} s \end{bmatrix} \alpha_z + \begin{bmatrix} -S^*_{\beta_0} s^2 + \gamma M_\lambda s \\ \gamma Q_\lambda s \end{bmatrix} z_P \qquad (75)$$

The thrust and torque are

$$\left.\begin{aligned}
\frac{C_T}{\sigma a} &= T_\theta \theta_0 + V T_\lambda u_G + T_{\dot\zeta} s \alpha_z + \left(- \frac{M_b^*}{\gamma} s^2 + T_\lambda s \right) z_P \\
&\quad - \frac{1}{\gamma} \left(S_{\beta_0}^* s^2 - \gamma T_{\dot\beta} s + K_P \gamma T_\theta \right) \beta_0 - T_{\dot\zeta} s \zeta_0 \\
\frac{C_Q}{\sigma a} &= I_{\zeta_0}^* \frac{\nu_{\zeta_0}^2}{\gamma} \zeta_0
\end{aligned}\right\} \tag{76}$$

To simplify the notation, subscript 0 on the inertias and frequencies is dropped in the rest of the discussion of the longitudinal system; only the longitudinal dynamics are involved, so the values appropriate to the coning and collective lag modes are implied throughout.

For the low-frequency response, the equations of motion to lowest order in s reduce to

$$\begin{bmatrix} I_\beta^* \nu_{\beta_e}^2 & 0 \\ \gamma K_P Q_\theta & I_\zeta^* \nu_\zeta^2 \end{bmatrix} \begin{pmatrix} \beta_0 \\ \zeta_0 \end{pmatrix} = \begin{pmatrix} \gamma M_\theta \\ \gamma Q_\theta \end{pmatrix} \theta_0 + \begin{pmatrix} \gamma M_\lambda \\ \gamma Q_\lambda \end{pmatrix} (V u_G + \dot z_P) + \begin{pmatrix} \gamma M_{\dot\zeta} \\ \gamma Q_{\dot\zeta} \end{pmatrix} \dot\alpha_z \tag{77}$$

The rotor thrust and torque are

$$\left.\begin{aligned}
\frac{C_T}{\sigma a} &= T_\theta \theta_0 + T_\lambda (V u_G + \dot z_P) + T_{\dot\zeta} \dot\alpha_z - K_P T_\theta \beta_0 \\
\frac{C_Q}{\sigma a} &= \frac{I_\zeta^* \nu_\zeta^2}{\gamma} \zeta_0
\end{aligned}\right\} \tag{78}$$

The solution for the low-frequency response of the rotor coning mode to collective pitch, longitudinal gusts, and shaft motion is then

$$\beta_0 = \frac{1}{I_\beta^* \nu_\beta^2} \left[\gamma M_\theta \theta_0 + \gamma M_\lambda (V u_G + \dot z_P) + \gamma M_{\dot\zeta} \dot\alpha_z \right] \tag{79}$$

The response of the rotor thrust to these inputs, including the influence of the rotor dynamics, is obtained by substituting for β_0 in the expression for $C_T/\sigma a$ (eqs. (78)):

$$\frac{C_T}{\sigma a} = \left(T_\theta - M_\theta \frac{K_P \gamma T_\theta}{I_\beta {}^* \nu_\beta{}^2 + K_P \gamma M_\theta} \right) \theta_0 + \left(T_\lambda - M_\lambda \frac{K_P \gamma T_\theta}{I_\beta {}^* \nu_\beta{}^2 + K_P \gamma M_\theta} \right) (V u_G + \dot{z}_P) + \left(T_{\dot{\zeta}} - M_{\dot{\zeta}} \frac{K_P \gamma T_\theta}{I_\beta {}^* \nu_\beta{}^2 + K_P \gamma M_\theta} \right) \dot{\alpha}_z \tag{80}$$

This result can be simplified by use of the relations:

$$M_\theta T_{\dot{\zeta}} - M_{\dot{\zeta}} T_\theta \cong \frac{1}{8 \cos \phi} \frac{\sin \phi}{6} - \frac{\sin \phi}{8} \frac{1}{6 \cos \phi} = 0$$

and, similarly, $M_\theta T_\lambda - M_\lambda T_\theta \cong 0$. With these relations, the expression for thrust reduces to

$$\frac{C_T}{\sigma a} \cong \left[T_\theta \theta_0 + T_\lambda (V u_G + \dot{z}_P) + T_{\dot{\zeta}} \dot{\alpha}_z \right] \frac{\nu_\beta{}^2}{\nu_{\beta_e}^2} \tag{81}$$

The factor in brackets is the direct response of the rotor thrust to the inputs. The only influence of the rotor flap dynamics (β_0 term in eqs. (78)) is to reduce (if $K_P > 0$) the direct low-frequency response by the ratio $\nu_\beta{}^2/\nu_{\beta_e}^2$. The effective flap frequency ν_{β_e} includes the aerodynamic spring due to pitch/flap coupling K_P. The ratio $\nu_\beta/\nu_{\beta_e} = 1$ if $K_P = 0$ and, for values of ν_{β_0} and K_P typical of proprotor coning mode, it will always be nearly 1.

With a procedure similar to that used for the rotor thrust, the flap dynamics are eliminated from the low-frequency lag response to give

$$\zeta_0 = \frac{1}{I_\zeta {}^* \nu_\zeta{}^2} \left[\gamma Q_\theta \theta_0 + \gamma Q_\lambda (V u_G + \dot{z}_P) + \gamma Q_{\dot{\zeta}} \dot{\alpha}_z - \gamma K_P Q_\theta \beta_0 \right]$$

$$\cong \frac{1}{I_\zeta {}^* \nu_\zeta{}^2} \left[\gamma Q_\theta \theta_0 + \gamma Q_\lambda (V u_G + \dot{z}_P) + \gamma Q_{\dot{\zeta}} \dot{\alpha}_z \right] \frac{\nu_\beta{}^2}{\nu_{\beta_e}^2} \tag{82}$$

Again, the only influence of the flap dynamics on the direct response is the factor $\nu_\beta{}^2/\nu_{\beta_e}^2$. The rotor torque follows directly from the solution for ζ_0.

The low-frequency response of the rotor coning and collective lag motion to collective pitch, longitudinal gust, and shaft motion is then

$$\begin{pmatrix} \beta_0 \\ \zeta_0 \end{pmatrix} = \begin{bmatrix} \frac{1}{I_\beta^* \nu_\beta^2} & \\ & \frac{1}{I_\zeta^* \nu_\zeta^2} \end{bmatrix} \left[\begin{pmatrix} \gamma M_\theta \\ \gamma Q_\theta \end{pmatrix} \theta_0 + \begin{pmatrix} \gamma M_\lambda \\ \gamma Q_\lambda \end{pmatrix} (V u_G + \dot{z}_P) + \begin{pmatrix} \gamma M_{\dot{\zeta}} \\ \gamma Q_{\dot{\zeta}} \end{pmatrix} \dot{\alpha}_z \right] \frac{\nu_\beta^2}{\nu_{\beta_e}^2} \tag{83}$$

The low-frequency response of the rotor thrust and torque is

$$\begin{pmatrix} \frac{C_T}{\sigma a} \\ \frac{C_Q}{\sigma a} \end{pmatrix} = \left[\begin{pmatrix} T_\theta \\ Q_\theta \end{pmatrix} \theta_0 + \begin{pmatrix} T_\lambda \\ Q_\lambda \end{pmatrix} (V u_G + \dot{z}_P) + \begin{pmatrix} T_{\dot{\zeta}} \\ Q_{\dot{\zeta}} \end{pmatrix} \dot{\alpha}_z \right] \frac{\nu_\beta^2}{\nu_{\beta_e}^2} \tag{84}$$

An important term in the response is the shaft torque due to longitudinal gust. The direct response has the magnitude $VQ_\lambda \cong -(V \sin \phi)/6$. The aerodynamic torque VQ_λ increases greatly with inflow (the behavior of Q_λ is similar to that of $H_{\dot{\beta}}$, which is shown in fig. 4; in fact, with only the c_{ℓ_α} terms, $Q_\lambda = H_{\dot{\beta}}$ exactly) - the source of a fundamental problem of the high inflow rotor response to longitudinal gusts, namely, a great increase in shaft and drive train loads with forward speed.

The rotor aerodynamic coefficients T_λ and $Q_{\dot{\zeta}}$ result in hub thrust and torque terms that damp the z_P and α_z motions, respectively. Since $T_\lambda \cong -(\cos \phi)/4$ and $Q_{\dot{\zeta}} \cong (V \sin \phi)/6$, the damping of z_P decreases slightly as V increases (its behavior is like that of $M_{\dot{\beta}}$), while the damping of α_z increases greatly with V (its behavior is like that of H_μ). The thrust force due to inflow T_λ is a usual feature of rotor dynamics; the influence of the torque due to rotational speed $Q_{\dot{\zeta}}$ is much different than for low inflow rotors, however, because the coefficient is orders of magnitude larger in high inflow.

In the derivation of the low-frequency results, it was assumed that $\nu_{\zeta_0} \neq 0$; for the autorotation case, however, $\nu_{\zeta_0} = 0$. Then $C_Q = 0$ always; and the characteristic equation has a factor s, that is, one root at the origin, which indicates that the proper degree of freedom is $\dot{\zeta}_0$, the rotor speed perturbation. The other root of the collective lag mode is at $\lambda = -\gamma Q_{\dot{\zeta}}/2I_{\zeta_0}^*$ (uncoupled), that is, a real root with time constant $\tau = 2I_{\zeta_0}^*/\gamma Q_{\dot{\zeta}} \cong 12/\gamma V \sin \phi$. The low-frequency response of $\dot{\zeta}_0$ is then

$$\dot{\zeta}_0 = \frac{1}{Q_{\dot{\zeta}}} \left[Q_\theta \theta_0 + Q_\lambda (V u_G + \dot{z}_P) + Q_{\dot{\zeta}} \dot{\alpha}_z \right] \tag{85}$$

There is a response of $\dot{\zeta}_0$ to shaft roll $\dot{\alpha}_z$ even though $\nu_{\zeta_0} = 0$, because ζ_0 has been defined with respect to the rolled shaft position; the response is such that $\dot{\zeta}_0 - \dot{\alpha}_z$, the rotor speed perturbation with respect to space, is exactly zero. From the expressions for the coefficients with only the c_{ℓ_α} terms, it

follows that $VQ_\lambda/Q_{\dot{\zeta}} = -V^2 f_2/V^2 f_2 = -1$ exactly (eqs. (54)); hence the response of the rotor speed perturbation to a longitudinal gust (at low frequency) is

$$\frac{\dot{\zeta}_0}{u_G} = -1 \tag{86}$$

This is the response required to keep the inflow ratio constant, including the velocity and rotational speed perturbations, as shown in the following analysis:

$$\delta\left(\frac{V}{\Omega R}\right) = \frac{\delta V}{\Omega R} - \frac{V\delta(\Omega R)}{(\Omega R)^2}$$

$$= \frac{V}{\Omega R}\left[\frac{\delta V}{V} - \frac{\delta(\Omega R)}{\Omega R}\right]$$

$$= \frac{V}{\Omega R}\left(u_G + \dot{\zeta}_0\right)$$

Hence $\delta(V/\Omega R) = 0$ implies $\dot{\zeta}_0/u_G = -1$ as given above. This result holds even for the complete model of the rotor and cantilever wing.

Lateral/vertical system: Flap response- Consider the lateral/vertical group of degrees of freedom, inputs, and hub forces (eqs. (44) to (46)). The cyclic lag degrees of freedom, ζ_{1C} and ζ_{1S}, are dropped to obtain a manageable set of equations. The rotor motion is then described by two degrees of freedom (tip path plane tilt β_{1C} and β_{1S}) excited by lateral and vertical shaft motions (shaft tilt, α_x and α_y and hub inplane velocity, $\dot{x}_P$ and $\dot{y}_P$), aerodynamic gust (angle of attack α_G and sideslip β_G), and cyclic pitch control (θ_{1C} and θ_{1S}). The influence of the rotor is transmitted to the shaft as rotor drag force and side force (C_H and C_Y) and pitch and yaw moments (C_{M_y} and C_{M_x}) acting on the hub.

The low-frequency response is of interest here so that the basic response of the rotor in high inflow can be examined, and also as a basis for investigating (in a later section) the influence of the rotor forces on the aircraft stability and control characteristics. For stability and control problems, it is convenient to obtain the equations of motion in a body-axis system rather than in the inertia axis system used so far (the inertia axes are most convenient for the cantilever wing problem, which is the main subject of this report). In body axes, the trim velocity of the rotor $(V + v)$ remains axial during shaft tilt by α_x and α_y; then converting to body axes requires that the terms in the equations of motion and hub forces due to the inplane component of $(V + v)$ produced by the shaft tilt (i.e., the $(V + v)\alpha_x$ and $(V + v)\alpha_y$ terms) be dropped. The shaft angular velocity $\dot{\alpha}_x$ and $\dot{\alpha}_y$ must then involve a centrifugal acceleration in order to turn the vector $(V + v)$ to keep it aligned with the shaft. This may be accounted for by simply adding the rotor mass to the aircraft mass; hence the equations presented here do not incorporate these centrifugal acceleration terms. The perturbations to the aircraft velocity $(V + v)$ are given by the hub velocities $\dot{x}_P$, $\dot{y}_P$, and $\dot{z}_P$. These motions and

aerodynamic gusts are the only sources of inplane velocity of the hub in body axes.

The equations of motion for β_{1C} and β_{1S} (in transfer function form with the α_x and α_y terms dropped as discussed previously) are

$$\begin{bmatrix} I_\beta^* s^2 - \gamma M_{\dot\beta} s + I_\beta^*(\nu_\beta^2 - 1) + K_P \gamma M_\theta & 2I_\beta^* s - \gamma M_{\dot\beta} \\ -(2I_\beta^* s - \gamma M_{\dot\beta}) & I_\beta^* s^2 - \gamma M_{\dot\beta} s + I_\beta^*(\nu_\beta^2 - 1) + K_P \gamma M_\theta \end{bmatrix} \begin{pmatrix} \beta_{1C} \\ \beta_{1S} \end{pmatrix}$$

$$= \gamma M_\theta \begin{pmatrix} \theta_{1C} \\ \theta_{1S} \end{pmatrix} + \gamma V M_\mu \begin{pmatrix} \beta_G \\ \alpha_G \end{pmatrix} + \gamma M_\mu \begin{pmatrix} \dot y_P \\ -\dot x_P \end{pmatrix} + \begin{bmatrix} I^*_{\beta\alpha} s - \gamma M_{\dot\beta} & -(2I^*_{\beta\alpha} + \gamma h M_\mu) \\ -(2I^*_{\beta\alpha} + \gamma h M_\mu) & -(I^*_{\beta\alpha} s - \gamma M_{\dot\beta}) \end{bmatrix} \begin{pmatrix} \dot\alpha_y \\ \dot\alpha_x \end{pmatrix} \tag{87}$$

Consider the response of the rotor to cyclic control, gust, inplane hub velocity, and shaft angular velocity. For the low-frequency response, only the lowest order terms in s are required and the equations become

$$\begin{bmatrix} I_\beta^*(\nu_\beta^2 - 1) + K_P \gamma M_\theta & -\gamma M_{\dot\beta} \\ \gamma M_{\dot\beta} & I_\beta^*(\nu_\beta^2 - 1) + \gamma M_\theta K_P \end{bmatrix} \begin{pmatrix} \beta_{1C} \\ \beta_{1S} \end{pmatrix}$$

$$= \gamma M_\theta \begin{pmatrix} \theta_{1C} \\ \theta_{1S} \end{pmatrix} + \gamma M_\mu \begin{pmatrix} \dot y_P + V\beta_G - h\dot\alpha_x \\ -\dot x_P + V\alpha_G - h\dot\alpha_y \end{pmatrix} + \begin{bmatrix} -\gamma M_{\dot\beta} & -2I^*_{\beta\alpha} \\ -2I^*_{\beta\alpha} & \gamma M_{\dot\beta} \end{bmatrix} \begin{pmatrix} \dot\alpha_y \\ \dot\alpha_z \end{pmatrix} \tag{88}$$

Only the steady-state terms in the flap response are retained. A steady tip path plane tilt gives a flapping velocity in the rotating frame so there are moments through $M_{\dot\beta}$; since shaft angular velocity involves a Coriolis acceleration of the rotating blades in the hub plane (β_{1C} and β_{1S} are flapping with respect to the hub plane), inertia terms also appear.

Inverting the matrix on the left-hand side of equation (88) gives the solution for β_{1C} and β_{1S}:

$$\begin{pmatrix} \beta_{1C} \\ \beta_{1S} \end{pmatrix} = \frac{\begin{bmatrix} 1 & N_* \\ -N_* & 1 \end{bmatrix}}{1 + N_*^2} \left[\frac{M_\theta}{-M_{\dot\beta}} \begin{pmatrix} -\theta_{1S} \\ \theta_{1C} \end{pmatrix} + \frac{M_\mu}{-M_{\dot\beta}} \begin{pmatrix} \dot x_P - V\alpha_G + h\dot\alpha_y \\ \dot y_P + V\beta_G - h\dot\alpha_x \end{pmatrix} + \frac{2I^*_{\beta\alpha}}{-\gamma M_{\dot\beta}} \begin{pmatrix} \dot\alpha_y \\ -\dot\alpha_x \end{pmatrix} + \begin{pmatrix} \dot\alpha_x \\ \dot\alpha_y \end{pmatrix} \right] \tag{89}$$

where

$$N_* = \frac{I_\beta^*(\nu_\beta^2 - 1) + K_P \gamma M_\theta}{-\gamma M_{\dot\beta}} \tag{90}$$

The parameter N_* is a measure of the lateral/vertical coupling of the rotor response (lateral/longitudinal for helicopter orientation); $N_* = 0$ for $\nu_\beta = 1$ and $K_P = 0$, that is, for an articulated rotor with no hinge spring or offset, and no pitch/flap coupling. From equation (69), it also follows that N_* can be written $N_* = I_\beta^*(\nu_\beta^2 - 1)/-\gamma M_{\dot\beta}$, so the parameter is a measure of the (effective) structural restraint of the blade flapping motion.

In the flapping response (eq. (89)), the bracketed quantities give the basic effectiveness of each kind of excitation, while the factor involving N_* accounts for the rotor flapping dynamics. Inside the brackets, most of the Lock number factors cancelled, indicating that the response is mainly a balance of aerodynamic forces; the exception is the third term, which is a balance of the inertial forces ($2I_{\beta\alpha}^*$) due to shaft angular velocity $\dot\alpha_x$ and $\dot\alpha_y$ and aerodynamic forces ($-\gamma M_{\dot\beta}$) due to tip path plane tilt β_{1C} and β_{1S}. Cyclic pitch control, hub inplane velocity, and hub plane angular velocity result in aerodynamic moments on the disk. These moments cause the rotor to flap until the moment on the disk due to the flapping cancels the applied moment, thus achieving equilibrium deflection. The coefficient $M_{\dot\beta}$ is the effectiveness of flapping in producing a moment on the rotor disk, hence its appearance in the denominators always. Blade cyclic pitch produces an aerodynamic moment on the disk through M_θ, so the net control effectiveness is $M_\theta/-M_{\dot\beta}$. Hub inplane velocity produces an aerodynamic moment on the disk through M_μ, with a net effectiveness of $M_\mu/-M_{\dot\beta}$. With the present model, there are three sources of hub inplane velocity: shaft velocity $\dot x_P$ and $\dot y_P$, vertical and lateral aerodynamic gusts α_G and β_G (which are angles, so $V\alpha_G$ and $V\beta_G$ are the corresponding velocity perturbations), and angular velocity of the shaft about a pivot a distance h aft of the hub producing hub velocities $h\dot\alpha_x$ and $h\dot\alpha_y$.

Consider the response to shaft angular velocity $\dot\alpha_x$ and $\dot\alpha_y$. The inplane velocity due to angular velocity about a pivot aft of the hub gives a moment on the disk (hence flapping) through M_μ as discussed previously. The third term in equation (89), with effectiveness $2I_{\beta\alpha}^*/-\gamma M_{\dot\beta}$, is the lag of the tip path plane required to precess the rotor to follow the shaft (β_{1C} and β_{1S} are flapping with respect to the shaft). For the tip path plane to follow the angular velocity of the hub plane requires a Coriolis acceleration of the disk of magnitude $2I_{\beta\alpha}^*\alpha_y$ because of the rotation of the blades. A moment is required to produce this acceleration, that is, to precess the rotor disk, and that moment is supplied by aerodynamic forces on the disk that result from the flapping velocity of the rotating blades. The tip path plane tilts back, lagging the shaft tilt, until the aerodynamic moment due to flapping (of magnitude $-\gamma M_{\dot\beta}\beta_{1C}$) is just large enough to provide the required acceleration. There is a 90° azimuthal phase difference in the response, characteristic of rotor or gyro dynamics: shaft pitch $\dot\alpha_y$ requires a lateral moment on the disk to precess it; that lateral moment is supplied by the flapping velocity in the rotating frame due to steady tip path plane pitch β_{1C}. The flapping dynamics also introduce a phase shift if $N_* \neq 0$.

The last term in equation (89) is also a flapping response due to shaft angular velocity. Hub plane angular velocity due to $\dot{\alpha}_y$ or $\dot{\alpha}_x$ produces a flapping velocity of the rotating blade, hence a moment on the disk through $-\gamma M_{\dot{\beta}}$. The rotor flaps until the moment on the disk due to tip path plane tilt, which also acts through $-\gamma M_{\dot{\beta}}$, is just large enough to cancel the exciting moment. Both moments in the equilibrium are aerodynamic, so the Lock numbers cancel. Both are due to the flapwise velocity of the blade so the coefficients $M_{\dot{\beta}}$ also cancel. The net effectiveness, then, is exactly 1. The last term in equation (89) results in a coupling of the lateral and vertical response of the rotor to shaft angular velocity ($\dot{\alpha}_x$ and $\dot{\alpha}_y$), even if $N_* = 0$. The basic flapping dynamics in the nonrotating frame (as discussed previously) consists of low-frequency and high-frequency flapping modes ($\beta \pm 1$), each of which appears as a wobble in the tip path plane. The basic response of the rotor then involves coupling of the lateral and vertical motion, a fundamental characteristic that results from the rotation of the blades. The low-frequency response should involve only excitation of the low-frequency flap mode ($\beta - 1$), but the lateral/vertical coupling is still expected.

When $N_* = 0$, the first factor in equation (89), representing the influence of the rotor flap dynamics, reduces to a unity matrix. With a hingeless rotor ($\nu_\beta > 1$) or pitch/flap coupling ($K_P \neq 0$), N_* is no longer zero and the flap dynamics matrix introduces a phase shift and a magnitude change in the flapping response. An example is the response to cyclic pitch control, θ_{1C} and θ_{1S}. The diagonal terms in the flap dynamics matrix produce a tip path plane tilt following the control plane tilt, through equilibrium of the aerodynamic moments due to blade pitch and flapping. The off-diagonal terms correspond to lateral/vertical coupling of the tip path plane/control plane tilt, which results from the aerodynamic pitch moment being reacted by a moment due to structural flap restraint ($\nu_\beta > 1$) or pitch/flap coupling ($K_P \neq 0$), hence due to $N_* \neq 0$. The two sources of tip path plane tilt produced by control plane tilt (or any other excitation) have a 90° azimuthal phase difference because the diagonal terms are due to flapping velocity (in the rotating frame), while the off-diagonal terms are due to flapping displacement.

Consider the individual terms in the flap responses - each has the form of a basic control power multiplied by a factor (involving N_*) that accounts for the flap dynamics. The effectiveness of cyclic pitch is given by (using the approximations based on the inflow at an effective radius)

$$\frac{M_\theta}{-M_{\dot{\beta}}} \cong \frac{1}{\cos^2 \phi} = 1 + \tan^2 \phi = 1 + \left(\frac{V}{r_e}\right)^2 \tag{91}$$

The pitch control power increases with V then, due to both an increase in the pitch moment M_θ and a decrease in the flap damping $M_{\dot{\beta}}$ (as shown in fig. 4); the increase is slow for the usual range of V (up to 1 or so). With the influence of the flap dynamics, the response to control is

$$\left.\begin{aligned} \frac{\partial \beta_{1C}}{\partial \theta_{1S}} &= -\frac{M_\theta/-M_{\dot\beta}}{1 + N_*^2} \\ \frac{\partial \beta_{1C}}{\partial \theta_{1S}} &= \frac{(M_\theta/-M_{\dot\beta})N_*}{1 + N_*^2} \end{aligned}\right\} \tag{92}$$

and similarly for β_{1S}. The total flapping response to cyclic pitch then has a magnitude

$$\frac{\partial |\beta|}{\partial |\theta|} = \frac{M_\theta/-M_{\dot\beta}}{\sqrt{1 + N_*^2}} \tag{93}$$

and an azimuthal phase shift of

$$\Delta\psi = \tan^{-1} N_* \tag{94}$$

Then if $N_* \neq 0$, the magnitude of the response is always decreased (by a factor $(1 + N_*^2)^{-1/2}$) whether N_* is positive or negative ($\nu_\beta^2 - 1$ is always positive, but the pitch flap coupling K_P can be positive or negative); and N_* produces a phase shift of the response, the sign of which depends on the sign of N_*. The coupling parameter N_* is approximately

$$N_* = \frac{I_\beta^*(\nu_\beta^2 - 1)}{-\gamma M_{\dot\beta}} + K_P \frac{M_\theta}{-M_{\dot\beta}} \cong \frac{\nu_\beta^2 - 1}{\gamma(\cos\phi)/8} + \frac{K_P}{\cos^2\phi} \tag{95}$$

so N_* increases somewhat with the inflow ratio V. The effect of the flap dynamics (N_*) on the response to all the inputs follows that on the cyclic pitch (a magnitude decrease and an azimuthal phase shift), so, for the remaining terms, only the basic control power is examined.

The response to inplane hub velocity is given by

$$\frac{\partial \beta_{1C}}{\partial \dot{x}_P} = \frac{M_\mu}{-M_{\dot\beta}} \cong \frac{4}{3}\tan\phi = \frac{V}{r_e^2} \tag{96}$$

The flapping due to hub inplane velocity increases substantially with V then primarily because of the increase in the speed stability M_μ but also because of the decreased flap damping $M_{\dot\beta}$ (fig. 4). This important influence of the high inflow aerodynamics produces significant differences in the dynamics from that of low inflow rotors. The response to aerodynamic gust is

$$-\frac{\partial \beta_{1C}}{\partial \alpha_G} = \frac{M_\mu}{-M_{\dot\beta}} \cong \tan^2\phi = \left(\frac{V}{r_e}\right)^2 \tag{97}$$

This is the response to angle-of-attack changes rather than just velocity perturbations, hence the extra factor of V (though both are hub inplane velocity changes). The substantial increase in high inflow of the flapping produced by hub velocity results in problems characteristic of the proprotor aircraft: high flapping or blade loads in maneuvers and gusts and substantial coupling of the rotor dynamics with the shaft motion.

The flapping response to shaft angular velocity $\dot{\alpha}_y$ is (for $N_* = 0$)

$$\frac{\partial \beta_{1C}}{\partial \dot{\alpha}_y} = \frac{2I^*_{\beta\alpha}}{-\gamma M^{\cdot}_{\beta}} + h\,\frac{M_{\mu}}{-M^{\cdot}_{\beta}} \cong \frac{16}{\gamma \cos\phi} + h\,\frac{4}{3}\tan\phi \tag{98}$$

The second term is due to the hub inplane velocity with shaft angular motion about the pivot a distance h aft of the hub (its behavior was discussed previously). The first term is the flapping required to produce a moment to precess the disk to follow the hub plane; it increases somewhat with V because of the decrease in the flap damping $H^{\cdot}_{\beta}$. The response to $\dot{\alpha}_x$ is

$$\frac{\partial \beta_{1C}}{\partial \dot{\alpha}_x} = -1 \tag{99}$$

the equilibrium of the moment due to flapping velocity due to $\dot{\alpha}_x$ and β_{1C}, which does not change with V. For values of the Lock number, mast height, and inflow velocity (γ, h, V) typical of proprotor operation, the primary contribution to the flapping response due to angular velocity of the shaft is the term required to precess the disk:

$$\frac{\partial |\beta|}{\partial \dot{\alpha}_y} \cong \frac{\partial \beta_{1C}}{\partial \dot{\alpha}_y} \cong \frac{16}{\gamma \cos\phi} \tag{100}$$

With only the inertia term of the response to shaft tilt, the influence of N_* is the same as for the response to cyclic pitch.

Lateral/vertical system: Hub forces and moments- Consider the lateral/vertical hub forces and moments: rotor drag force C_H, side force C_Y, hub pitch moment C_{M_y}, and hub yaw moment C_{M_x}. Retaining only the flap degrees of freedom, dropping the α_x and α_y terms (giving inplane components of $V + v$) to convert to body axes, and then retaining only the lowest order terms in s, yields the following hub forces:

$$-\begin{pmatrix} \frac{2C_H}{\sigma a} \\ \frac{2C_Y}{\sigma a} \end{pmatrix} = \begin{bmatrix} \left(\frac{2C_T}{\sigma a} + H_{\dot{\beta}}^{*}\right) & H_\theta K_P \\ -H_\theta K_P & \left(\frac{2C_T}{\sigma a} + H_{\dot{\beta}}^{*}\right) \end{bmatrix} \begin{pmatrix} \beta_{1C} \\ \beta_{1S} \end{pmatrix} + H_\theta \begin{pmatrix} -\theta_{1S} \\ \theta_{1C} \end{pmatrix} + V(H_\mu + R_\mu) \begin{pmatrix} -\alpha_G \\ \beta_G \end{pmatrix}$$

$$+ (H_\mu + R_\mu) \begin{pmatrix} \dot{x}_P \\ \dot{y}_P \end{pmatrix} + \begin{bmatrix} h(H_\mu + R_\mu) & H_{\dot{\beta}} \\ -H_{\dot{\beta}} & h(H_\mu + R_\mu) \end{bmatrix} \begin{pmatrix} \dot{\alpha}_y \\ -\dot{\alpha}_x \end{pmatrix} \tag{101}$$

The hub moments are simply

$$\begin{pmatrix} -\frac{2C_{M_y}}{\sigma a} \\ \frac{2C_{M_x}}{\sigma a} \end{pmatrix} = \frac{I_\beta^{*}(\nu_\beta^{2} - 1)}{\gamma} \begin{pmatrix} \beta_{1C} \\ \beta_{1S} \end{pmatrix} \tag{102}$$

If one substitutes for the low-frequency flapping response, the hub forces are

$$-\begin{pmatrix} \frac{2C_H}{\sigma a} \\ \frac{2C_Y}{\sigma a} \end{pmatrix} = \frac{\begin{bmatrix} \frac{2C_T}{\sigma a} + H_{\dot{\beta}}^{*} - H_\theta K_P N_* & N_*\left(\frac{2C_T}{\sigma a} + H_{\dot{\beta}}^{*}\right) + H_\theta K_P \\ -N_*\left(\frac{2C_T}{\sigma a} + H_{\dot{\beta}}^{*}\right) - H_\theta K_P & \frac{2C_T}{\sigma a} + H_{\dot{\beta}}^{*} - H_\theta K_P N_* \end{bmatrix}}{1 + N_*^{2}} \begin{bmatrix} \frac{M_\theta}{-M_{\dot{\beta}}} \begin{pmatrix} -\theta_{1S} \\ \theta_{1C} \end{pmatrix} \end{bmatrix}$$

$$+ \frac{M_\mu}{-M_{\dot{\beta}}} \begin{pmatrix} \dot{x}_P - V\alpha_G + h\dot{\alpha}_y \\ \dot{y}_P + V\beta_G - h\dot{\alpha}_x \end{pmatrix} + \frac{2I_{\beta\alpha}^{*}}{-\gamma M_{\dot{\beta}}} \begin{pmatrix} \dot{\alpha}_y \\ -\dot{\alpha}_x \end{pmatrix} \Bigg] + \begin{bmatrix} H_\theta \begin{pmatrix} -\theta_{1S} \\ \theta_{1C} \end{pmatrix} + (H_\mu + R_\mu) \begin{pmatrix} \dot{x}_P - V\alpha_G + h\dot{\alpha}_y \\ \dot{y}_P + V\beta_G - h\dot{\alpha}_x \end{pmatrix} \end{bmatrix}$$

$$+ \frac{\begin{bmatrix} \frac{C_T}{\sigma a} - N_*(N_* H_{\dot{\beta}} + H_\theta K_P) & N_*\left(\frac{2C_T}{\sigma a} + H_{\dot{\beta}}^{*}\right) + H_\theta K_P \\ -N_*\left(\frac{2C_T}{\sigma a} + H_{\dot{\beta}}^{*}\right) - H_\theta K_P & \frac{C_T}{\sigma a} - N_*(N_* H_{\dot{\beta}} + H_\theta K_P) \end{bmatrix}}{1 + N_*^{2}} \begin{pmatrix} \dot{\alpha}_x \\ \dot{\alpha}_y \end{pmatrix} \tag{103}$$

Basically, the response for each input is a direct H force plus a contribution from the rotor flapping motion; the last term is the aerodynamic force produced by the flapping velocity due to shaft angular velocity, combining the direct and flapping terms. Note that the hub force response is considerably simplified if $N_{\dot{\beta}} = 0$; then the tip path plane tilt produces hub forces through only $2C_T/\sigma a + H_{\dot{\beta}}^*$, and the matrix in the last term reduces to simply $C_T/\sigma a$ (which may then be neglected for high inflow operation). The hub moment is simply a constant times the flap response.

Pivot moment - The total moment about the pivot a distance h aft of the hub is given by the hub moment plus the hub forces acting on the arm h:

$$\begin{pmatrix} -\dfrac{2C_{M_y}}{\sigma a} \\ \dfrac{2C_{M_x}}{\sigma a} \end{pmatrix}_{pivot} = \begin{bmatrix} -\left(\dfrac{2C_{M_y}}{\sigma a} + h\,\dfrac{2C_H}{\sigma a}\right) \\ \left(\dfrac{2C_{M_x}}{\sigma a} - h\,\dfrac{2C_Y}{\sigma a}\right) \end{bmatrix} \tag{104}$$

The hub moment is directly proportional to the tip path plane tilt, β_{1C} and β_{1S}; hub forces (eq. (101)) are also produced by the tip path plane tilt through $2C_T/\sigma a + H_{\dot{\beta}}^*$, the first term being the thrust vector tilt and the second, the negative H force contribution of high inflow. (The off-diagonal terms that result from pitch/flap coupling are not considered now, that is, it is assumed that $K_P = 0$.) The total moments about the pivot due to the tip path plane tilt are then (after the hub moment and hub force terms are combined):

$$\Delta \begin{pmatrix} -\dfrac{2C_{M_y}}{\sigma a} \\ \dfrac{2C_{M_x}}{\sigma a} \end{pmatrix} = \left[\frac{I_\beta^*(\nu_\beta^2 - 1)}{\gamma} + h\left(\frac{2C_T}{\sigma a} + H_{\dot{\beta}}^*\right)\right] \begin{pmatrix} \beta_{1C} \\ \beta_{1S} \end{pmatrix} \tag{105}$$

The combination of terms appearing on the right-hand side has already appeared in the equations of motion for the four-degree-of-freedom model (eq. (26)). With this result, a simple design criterion can be derived for optimum proprotor/pylon dynamic stability. If the total factor of β_{1C} and β_{1S} is set to zero, with a proper choice of the parameters, the moments due to the rotor flapping dynamics (at least the low-frequency response) will not be transmitted to the pylon. Then the pylon is effectively decoupled from the rotor and will not respond to rotor flapping motion: this is expected to improve the stability of the proprotor/pylon system. When the rotor lags the shaft in response to shaft angular velocity, that tip path plane tilt produces a hub force through $2C_T/\sigma a + H_{\dot{\beta}}^*$, which is dominated by the negative H force term $H_{\dot{\beta}}^*$ hence it results in negative damping of the shaft tilt motion. This effect, in particular, is nullified by setting the total tip path plane tilt

factor of equation (105) to zero. The thrust vector tilt term $2C_T/\sigma a$ contributes positive damping, but it is negligible compared to H_β^* for high inflow. Thus the criterion essentially is to use the positive damping available from the hub moment of a hingeless rotor to counter the negative aerodynamic damping of H_β^*, and the design rule becomes a specification of the flap frequency ν_β required to satisfy that criterion.

Setting the coefficient of β_{1C} and β_{1S} in equation (105) to zero gives the design choice for ν_β:

$$\begin{aligned} \nu_\beta^2 &= 1 - \frac{\gamma h}{I_\beta^*}\left(\frac{2C_T}{\sigma a} + H_\beta^*\right) \\ &\cong 1 + \gamma h \frac{\sin \phi}{6} \end{aligned} \tag{106}$$

For typical values of γ, h, and V for proprotor operation, equation (106) requires that $\nu_\beta \cong 1.1$ or so such a frequency is easily obtained with current hingeless rotor technology or even with an offset hinge on an articulated rotor. An obvious limitation is that H_β^* is a function of V while ν_β is not, so the design criterion can be met only at one design speed.

This result was first obtained by Young and Lytwyn (ref. 18). On the basis of optimum flutter stability with the pylon decoupled from the rotor, they obtained the above result for the optimum flap frequency ν_β. Numerical calculations of the flutter boundaries for a four-degree-of-freedom model (a flapping rotor on a pylon with pitch and yaw motion) show that the optimum flap stiffness is actually somewhat above this. They suggested that a value about 5 percent higher be used:

$$\nu_\beta^2 \cong 1.05\left[1 - \frac{\gamma h}{I_\beta^*}\left(\frac{2C_T}{\sigma a} + H_\beta^*\right)\right] \tag{107}$$

With this choice of ν_β, the remaining rotor force acting on the pylon is mainly a negative spring force due to the speed stability coefficient H_β^*; this force leads to a divergence criterion, which does not require very much pylon stiffness. They also point out that the only parameter of the pylon to enter this criterion on ν_β is the mast height h, because it is essentially a static decoupling criterion, so the pylon dynamics do not enter at all.

Unfortunately, the problem of proprotor dynamic stability is not so easily resolved. This criterion for ν_β is based on pylon pitch and yaw motion, while, for the rotor on the cantilever wing, the degrees of freedom produce much different shaft motion and respond differently to hub forces and moments. This criterion is based on only the low-frequency response of the rotor, and only the flap motion at that; the dynamics involved with high inflow proprotor instabilities is more complex. However, many other design considerations are involved in the choice of wing stiffnesses and blade frequencies; therefore,

while the proprotor dynamic stability must be verified, and perhaps the parameters modified somewhat to increase the margins, the actual choice of the rotor and wing configuration (including the placement of the fundamental frequencies) is not necessarily based on the criterion for optimum dynamic stability. The above result indicates that, for practical applications, a flapping frequency greater than 1/rev should be favorable for rotor and wing dynamic stability.

Whirl Flutter

This chapter examines the classical whirl flutter problem: a truly rigid propeller on a pylon with pitch and yaw degrees of freedom. With the infinite blade stiffness of a truly rigid propeller, there is no blade flapping motion. The theory developed here may accommodate the rigid propeller by letting the flap natural frequency ν_β go to infinity; in that limit, the four-degree-of-freedom model reduces to two degrees of freedom, pylon pitch α_y and yaw α_x, which is the usual whirl flutter formulation. Nomenclature particular to the whirl flutter analysis is given at the end of this section.

The whirl flutter model may exhibit instabilities at high forward speed or low pylon stiffness, primarily because of the high inflow aerodynamics. In fact, it has much different behavior than the flapping rotor case. The whirl flutter problem is considered here because it is a special limit of proprotor dynamics, often mentioned in the literature as an ancestor of the current proprotor analyses; and because, as a two-degree-of-freedom problem, exact expressions for the stability boundaries may be obtained. However, the dynamics and aerodynamics of the whirl flutter model are found to bear little relation to those of the flapping proprotor.

The whirl flutter equations can be derived from the four-degree-of-freedom equations of motion already given (eqs. (26)), with the limits $\nu_\beta \to \infty$ and $\beta_{1C}, \beta_{1S} \to 0$. However, $(\nu_\beta^2 - 1)\beta_{1C}$ and $(\nu_\beta^2 - 1)\beta_{1S}$ must remain finite in this limit because the propeller can still transmit a hub moment to the pylon; then the β_{1C} and β_{1S} equations become simple substitution relations for the pylon equations. A more direct approach is to first substitute for the hub moment $(\nu_\beta^2 - 1)\beta_{1C}$ and $(\nu_\beta^2 - 1)\beta_{1S}$ in the pylon equations of motion, and then take the limit of $\beta_{1C}, \beta_{1S} \to 0$. The pylon equations of motion for the four-degree-of freedom model (eq. (8)) are

$$\begin{bmatrix} I_y^* & 0 \\ 0 & I_x^* \end{bmatrix} \begin{pmatrix} \alpha_y \\ \alpha_x \end{pmatrix}'' + \begin{bmatrix} C_y^* & 0 \\ 0 & C_x^* \end{bmatrix} \begin{pmatrix} \alpha_y \\ \alpha_x \end{pmatrix}' + \begin{bmatrix} K_y^* & 0 \\ 0 & K_x^* \end{bmatrix} \begin{pmatrix} \alpha_y \\ \alpha_x \end{pmatrix}$$

$$= \gamma \begin{pmatrix} \dfrac{2C_{M_y}}{\sigma a} \\ \dfrac{C_{M_x}}{\sigma a} \end{pmatrix} + \gamma h \begin{pmatrix} \dfrac{2C_H}{\sigma a} \\ -\dfrac{2C_Y}{\sigma a} \end{pmatrix} \qquad (108)$$

which is simply a mass/spring/damper system for pylon pitch and yaw, forced by the rotor moments and inplane forces applied at the hub. The equations have been made dimensionless (using ρ, Ω, and R) and the inertias, damping coefficients, and spring constants have been normalized by dividing by $(N/2)I_b$. The hub moment is

$$\gamma\begin{pmatrix} \frac{2C_{M_y}}{\sigma a} \\ \frac{2C_{M_x}}{\sigma a} \end{pmatrix} = (\nu_\beta^2 - 1)\begin{pmatrix} -\beta_{1C} \\ \beta_{1S} \end{pmatrix} \tag{109}$$

The flapping equations of motion from the four-degree-of-freedom model (eq. (8) for $N \geq 3$) are rearranged as

$$(\nu_\beta^2 - 1)\begin{pmatrix} -\beta_{1C} \\ \beta_{1S} \end{pmatrix} = \begin{pmatrix} \beta_{1C} \\ -\beta_{1S} \end{pmatrix}'' + \begin{pmatrix} 0 & 2 \\ 2 & 0 \end{pmatrix}\begin{pmatrix} \beta_{1C} \\ \beta_{1S} \end{pmatrix}' - \begin{pmatrix} \alpha_y \\ \alpha_x \end{pmatrix}''$$
$$+ \begin{pmatrix} 0 & 2 \\ -2 & 0 \end{pmatrix}\begin{pmatrix} \alpha_y \\ \alpha_x \end{pmatrix}' + \gamma\begin{pmatrix} -\frac{M_{F_{1C}}}{\sigma a} \\ \frac{M_{F_{1S}}}{\sigma a} \end{pmatrix} \tag{110}$$

With this result, the hub moment in the pylon equations of motion may be replaced; then the indeterminant combination $(\nu_\beta^2 - 1)\beta$ no longer appears, and the limit $\beta_{1C}, \beta_{1S} \to 0$ may be taken properly. In other words, the β_{1C} and β_{1S} degrees of freedom may be dropped after substituting for the hub moment, thus the equations of motion are

$$\begin{bmatrix} I_y^* + 1 & 0 \\ 0 & I_x^* + 1 \end{bmatrix}\begin{pmatrix} \alpha_y \\ \alpha_x \end{pmatrix}'' + \begin{bmatrix} C_y^* & -2 \\ 2 & C_x^* \end{bmatrix}\begin{pmatrix} \alpha_y \\ \alpha_x \end{pmatrix}' + \begin{bmatrix} K_y^* & 0 \\ 0 & K_x^* \end{bmatrix}\begin{pmatrix} \alpha_y \\ \alpha_x \end{pmatrix}$$
$$= \gamma\begin{pmatrix} -\frac{M_{F_{1C}}}{ac} + h\frac{2C_H}{\sigma a} \\ \frac{M_{F_{1S}}}{ac} - h\frac{2C_Y}{\sigma a} \end{pmatrix} \tag{111}$$

The pylon is now forced directly by the flap moments on the disk $M_{F_{1C}}$ and $M_{F_{1S}}$, which are now transmitted directly to the hub rather than through the flapping response.

The aerodynamic forces follow directly from equations (23) for the four-degree-of-freedom mode, with the β_{1C} and β_{1S} terms dropped, of course. The hub moments and hub forces are then (hub moment is obtained by use of eqs. (109) and (110) with eqs. (23)):

$$\begin{pmatrix} \frac{2C_{M_y}}{\sigma a} \\ \frac{2C_{M_x}}{\sigma a} \end{pmatrix} = -\frac{1}{\gamma}\begin{pmatrix} \alpha_y \\ \alpha_x \end{pmatrix}^{\cdot\cdot} + \frac{1}{\gamma}\begin{bmatrix} 0 & 2 \\ -2 & 0 \end{bmatrix}\begin{pmatrix} \alpha_y \\ \alpha_x \end{pmatrix}^{\cdot} + \begin{bmatrix} M_{\dot\beta} & hM_\mu \\ -hM_\mu & M_{\dot\beta} \end{bmatrix}\begin{pmatrix} \alpha_y \\ \alpha_x \end{pmatrix}^{\cdot}$$

$$+ \begin{bmatrix} 0 & -(V+v)M_\mu \\ (V+v)M_\mu & 0 \end{bmatrix}\begin{pmatrix} \alpha_y \\ \alpha_x \end{pmatrix} + \begin{bmatrix} 0 & -M_\theta \\ M_\theta & 0 \end{bmatrix}\begin{pmatrix} \theta_{1S} \\ \theta_{1C} \end{pmatrix}$$

$$+ \begin{bmatrix} 0 & -VM_\mu \\ VM_\mu & 0 \end{bmatrix}\begin{pmatrix} \alpha_G \\ \beta_G \end{pmatrix} \tag{112}$$

$$\begin{pmatrix} \frac{2C_H}{\sigma a} \\ -\frac{2C_Y}{\sigma a} \end{pmatrix} = \begin{bmatrix} -h(H_\mu + R_\mu) & H_{\dot\beta} \\ -H_{\dot\beta} & -h(H_\mu + R_\mu) \end{bmatrix}\begin{pmatrix} \alpha_y \\ \alpha_x \end{pmatrix}^{\cdot} + (V+v)(H_\mu + R_\mu)\begin{pmatrix} \alpha_y \\ \alpha_x \end{pmatrix}$$

$$+ H_\theta\begin{pmatrix} \theta_{1S} \\ \theta_{1C} \end{pmatrix} + V(H_\mu + R_\mu)\begin{pmatrix} \alpha_G \\ \beta_G \end{pmatrix} \tag{113}$$

A comparison of these expressions with the results obtained for the flapping proprotor dynamics shows that the whirl flutter problem involves considerably different behavior. Comparing the hub forces with equations (101) indicates that the response to shaft tilt, cyclic control, and gusts is the same (except that eqs. (101) are in body axes, so the α_x and α_y terms are dropped). With the rigid propeller, however, there are no longer hub forces caused by flapping, acting through the thrust vector tilt and the negative H force due to inflow (the $2C_T/\sigma a + H_{\dot\beta}^*$ factor). Hub forces due to the tip path plane tilt are naturally not part of the whirl flutter problem since they arise only with the flapping rotor, and that difference is very significant.

Comparing the hub moment with equation (89) (the hub moment for the flapping rotor if it is multiplied by $(\nu_\beta^2 - 1)/\gamma$) shows that the role of the flap moments is altered. The rigid propeller limit of $\nu_\beta^2 \to \infty$ corresponds to

the limit $N_* \to \infty$ in equation (89), and with that the two results are identical (except that in eq. (89) the α_x and α_y terms were dropped again for body axes, and the inertia terms $\ddot{\alpha}_x$ and $\ddot{\alpha}_y$ were dropped for the low-frequency approximation). The more appropriate limit for studying the flapping rotor dynamics is $\nu_\beta^2 \to 1$, that is, $N_* \to 0$. Between $N_* \to \infty$ and $N_* \to 0$ there is a 90° azimuthal phase shift in the influence of all flap moments. For the rigid propeller, the flap moments on the disk are transmitted directly to the hub while, for the flapping rotor, there is a 90° azimuth lag (for $\nu_\beta = 1$) from the application of the flap moment to the achievement of maximum tip path plane tilt.

Hence the role of the rotor in the whirl flutter behavior changes greatly from that for the flapping rotor. The Coriolis flap moment and the speed stability moments on the disk (M_μ) now are off-diagonal terms (i.e., coupling terms), while the flap damping disk moment ($M_{\dot{\beta}}$) now contributes directly to the damping of the pylon motion. The hub inplane forces are given solely by the direct terms H_μ and $H_{\dot{\beta}}$, with no contributions from tip path plane tilt. The speed stability coefficients, M_μ and H_μ, have a dominant role in whirl flutter dynamics.

If one substitutes for the hub forces and moments, the equations of motion for the pitch and yaw motions of a pylon with a rigid propeller are

$$\begin{bmatrix} I_y^*+1 & 0 \\ 0 & I_x^*+1 \end{bmatrix} \begin{pmatrix} \alpha_y \\ \alpha_x \end{pmatrix}^{\cdot\cdot} + \begin{bmatrix} C_y^*+h^2\gamma(H_\mu+R_\mu)-\gamma M_{\dot{\beta}} & -(2+h\gamma H_{\dot{\beta}}+h\gamma M_\mu) \\ 2+h\gamma H_{\dot{\beta}}+h\gamma M_\mu & C_x^*+h^2\gamma(H_\mu+R_\mu)-\gamma M_{\dot{\beta}} \end{bmatrix} \begin{pmatrix} \alpha_y \\ \alpha_x \end{pmatrix}^{\cdot}$$

$$+ \begin{bmatrix} K_y^*-h\gamma(V+v)(H_\mu+R_\mu) & \gamma(V+v)M_\mu \\ -\gamma(V+v)M_\mu & K_x^*-h\gamma(V+v)(H_\mu+R_\mu) \end{bmatrix} \begin{pmatrix} \alpha_y \\ \alpha_x \end{pmatrix}$$

$$= \begin{bmatrix} h\gamma H_\theta & -\gamma M_\theta \\ \gamma M_\theta & h\gamma H_\theta \end{bmatrix} \begin{pmatrix} \theta_{1S} \\ \theta_{1C} \end{pmatrix} + \begin{bmatrix} h\gamma V(H_\mu+R_\mu) & -\gamma V M_\mu \\ \gamma V M_\mu & h\gamma V(H_\mu+R_\mu) \end{bmatrix} \begin{pmatrix} \alpha_G \\ \beta_G \end{pmatrix} \qquad (114)$$

These equations are valid for propellers with three or more blades. As usual, the notation of the aerodynamic coefficients indicates their source: H, for hub forces; M, for flap moments; subscript μ, for inplane velocities; and subscript $\dot{\beta}$, for flapwise velocities.

The inertia terms are the sum of the pylon and rotor inertias:

$$I_y^* + 1 = \frac{I_y}{(N/2)I_b} + 1 = \frac{I_y + (N/2)I_b}{(N/2)I_b}$$

where $I_Y + (N/2)I_b$ is the total moment of inertia of the pylon and rotor (for $N \geq 3$); I_y already includes the contribution $h^2 N M_b$ of the rotor mass to the moment of inertia about the pylon. The damping terms (diagonal) have contributions from the structural or mechanical damping of the pylon ($C_y{}^*$ or $C_x{}^*$ and from the aerodynamic forces on the rotor. All contributions to the diagonal damping terms are positive (H_μ and $-M_\beta^\cdot$ are positive) so the net damping is always positive. The aerodynamic contributions result from the flap damping of the rotation of the hub plane by $\dot{\alpha}_x$ or $\dot{\alpha}_y$, and from the inplane force due to the hub inplane velocity during pylon angular velocity. Based on the equivalent radius approximations, the aerodynamic damping terms are

$$\gamma[-M_\beta^\cdot + h^2(H_\mu + R_\mu)] \cong \gamma\left(\frac{\cos\phi}{8} + h^2\frac{V\sin\phi}{2}\right)$$

The first term decreases some with V, while the second term increases. The spring terms (diagonal) have contributions from the structural restraint of the pylon deflection ($K_y{}^*$ or $K_x{}^*$) and from the aerodynamic forces on the rotor. The aerodynamic term, a negative spring ($H_\mu > 0$) from the inplane force due to the inplane component of $(V + v)$ produced by pylon pitch or yaw, is approximately

$$-h\gamma(V + v)(H_\mu + R_\mu) \cong -h\gamma\frac{V^2\sin\phi}{2}$$

which increases with V. The coupling spring term (off-diagonal) is entirely aerodynamic, from the flap moment on the disk due to the inplane component of $V + v$ produced by pylon pitch or yaw; it is approximately

$$\gamma(V + v)M_\mu \cong \frac{V\sin\phi}{6}$$

which increases with V. The coupling damping terms (off-diagonal) have inertia and aerodynamic contributions. The inertia term ($-2\dot{\alpha}_x$ or $2\dot{\alpha}_y$) is the Coriolis acceleration produced by the pitch or yaw angular velocity of a rotating body. The aerodynamic terms are from the flap moment due to the inplane velocity produced by the pylon angular velocity, and from the inplane force due to the angular velocity of the hub plane. From equation (59), it follows that

$$h\gamma(M_\mu + H_\beta^\cdot) \cong h\gamma\frac{3C_T}{\sigma a} << 2$$

hence the aerodynamic contributions may be neglected compared with the gyroscopic coupling.

The whirl flutter model then consists of a mass/spring/damper system for pitch and yaw, with positive aerodynamic damping, a negative aerodynamic spring, gyroscopic coupling in the damping, and aerodynamic coupling in the springs.

Consider the single-degree-of-freedom problem: $K_x^* \to \infty$ so $\alpha_x \to 0$; the equation reduces to

$$(I_y^* + 1)\ddot{\alpha}_y + [C_y^* + h^2\gamma(H_\mu + R_\mu) - \gamma M_{\dot{\beta}}]\dot{\alpha}_y + [K_y^* - h\gamma(V + v)(H_\mu + R_\mu)]\alpha_y$$

$$= h\gamma H_\theta \theta_{1S} + h\gamma V(H_\mu + R_\mu)\alpha_G \qquad (115)$$

The damping is always positive, so the system is stable in this limit so long as the net spring constant (structural plus aerodynamic) is positive:

$$K_y^* > h\gamma(V + v)(H_\mu + R_\mu) \qquad (116)$$

This is simply a static stability boundary, that is, the divergence criterion (for $K_x^* \to \infty$). With one spring stiff enough, the system always has dynamic stability; the only stability criterion remaining is the divergence boundary for the other spring, due to the negative aerodynamic spring term.

Consider the case of no aerodynamics, but with gyroscopic (Coriolis) coupling included. For the isotropic case (same mass/spring/damping constants for both pitch and yaw), the characteristic equation is

$$[(I^* + 1)\lambda^2 + C^*\lambda + K^*]^2 + (2\lambda)^2 = 0 \qquad (117)$$

The four roots will have negative real parts so long as γ, K^*, and I^* are all positive. Therefore, the system is always stable, even with gyroscopic coupling, if there are no aerodynamic forces on the rotor.

It follows then that any dynamic whirl flutter instability can only be due to the aerodynamic cross-coupling of the pitch and yaw motion; there is only one such term, namely, the off-diagonal spring terms $\gamma V M_\mu$. Since this aerodynamic force increases with forward speed V, an instability is expected to occur eventually as the inflow is increased for a given pylon and rotor. Of course, there is the possibility of a static instability (divergence) due to the negative aerodynamic spring term. Whirl flutter instability is then the result of the high inflow rotor aerodynamics.

In Laplace form, the homogeneous equations of motion are

$$\begin{bmatrix} (I_y^*+1)s^2+[C_y^*+h^2\gamma(H_\mu+R_\mu)-\gamma M_{\dot{\beta}}]s & -2s+\gamma(V+v)M_\mu \\ +[K_y^*-h\gamma(V+v)(H_\mu+R_\mu)] & \\ 2s-\gamma(V+v)M_\mu & (I_x^*+1)s^2+[C_x^*+h^2\gamma(H_\mu+R_\mu)-\gamma M_{\dot{\beta}}]s \\ & +[K_x^*-h\gamma(V+v)(H_\mu+R_\mu)] \end{bmatrix} \begin{pmatrix} \alpha_y \\ \alpha_x \end{pmatrix} = 0 \qquad (118)$$

To simplify the notation, write V for $V + v$, H_μ for $H_\mu + R_\mu$, and I^* for $I^* + 1$:

$$\begin{bmatrix} I_y^* s^2 + (C_y^* + C_\mu)s + K_y^* - K_\mu & -sD_\mu + L_\mu \\ sD_\mu - L_\mu & I_x^* s^2 + (C_x^* + C_\mu)s + K_x^* - K_\mu \end{bmatrix} \begin{pmatrix} \alpha_y \\ \alpha_x \end{pmatrix} = 0 \tag{119}$$

where

$$C_\mu = h^2 \gamma H_\mu - \gamma M_\beta^\cdot$$

$$K_\mu = h\gamma V H_\mu$$

$$D_\mu = 2$$

$$L_\mu = \gamma V M_\mu$$

These are, respectively, the aerodynamic damping and negative spring, the gyroscopic coupling (which is given a symbol so that its influence can be identified in the results), and the aerodynamic cross spring. Combining the structural and aerodynamic terms in the spring and damping coefficients yields

$$\begin{bmatrix} I_y s^2 + C_y s + K_y & -sD + L \\ sD - L & I_x s^2 + C_x s + K_x \end{bmatrix} \begin{pmatrix} \alpha_y \\ \alpha_x \end{pmatrix} = 0 \tag{120}$$

This last and simplest expression is used for the derivations.

The characteristic equation for the whirl flutter eigenvalues λ is then:

$$(I_y \lambda^2 + C_y \lambda + K_y)(I_x \lambda^2 + C_x \lambda + K_x) + (-\lambda D + L)^2 = 0 \tag{121}$$

The stability of the system may be investigated by examination of the root loci, that is, the behavior of the eigenvalues with variations in V or some other parameters. For a two-degree-of-freedom problem, however, it is possible to solve explicitly for the stability boundaries. The stability boundaries on the K_x^*, K_y^* plane (i.e., as a function of the pylon stiffnesses) is the usual form for the presentation of the whirl flutter solution. The other major parameter is the inflow ratio V. Two kinds of instabilities are possible with a system that can be described by linear constant coefficient differential equations. The first is divergence, a static instability that, on the λ plane (root locus), takes the form of one root on the real axis that passes through the origin into the right half plane. The second type of instability is flutter, a dynamic instability that takes the form of a complex conjugate pair of roots that cross the imaginary axis (at finite frequency) into the right half plane. The stability boundaries for these two types of motion are examined.

Divergence- The divergence boundary is defined by the requirement that one of the roots of the characteristic equation be at the origin. For $\lambda = 0$, the characteristic equation gives

$$K_y K_x + L^2 = 0 \tag{122}$$

or

$$(K_y^* - K_\mu)(K_x^* - K_\mu) + L_\mu^2 = 0 \tag{123}$$

therefore,

$$(K_y^* - h\gamma VH_\mu)(K_x^* - h\gamma VH_\mu) + (\gamma VM_\mu)^2 = 0 \tag{124}$$

This sum must be greater than zero for divergence stability. An instability may be encountered if one of the spring constants, K_y^* or K_x^*, is too small, so the negative aerodynamic spring makes the first term and hence, perhaps, the sum negative. Sufficiently large structural spring restraint of pylon pitch and yaw motion guarantees divergence stability.

The equation for the divergence boundary is a hyperbola on the K_y^*, K_x^* plane; the divergence hyperbola is shown in figure 6. The asymptotes are the K_x, K_y axes, that is, K_x^* or $K_y^* = K_\mu = h\gamma VH$. The asymptotes give the divergence criterion when one of the springs is very stiff; for $K_x^* \to \infty$, equation (124) reduces to (for stability)

$$K_y > 0 \tag{125}$$

or

$$K_y^* > K_\mu = h\gamma VH_\mu \tag{126}$$

which, indeed, is the criterion obtained previously for the single-degree-of-freedom limit. This criterion is that the total spring constant - aerodynamic plus structural - be positive. For finite K_x^*, the cross spring $L_\mu = \gamma VM_\mu$ introduces coupling of the α_x and α_y motion, which eases the criterion on K_y^*. The hyperbola intersects the line $K_x = -K_y$ (the -45° line on the K_x, K_y plane) at points $K_y = \pm L_\mu = \pm\gamma VM_\mu$, where the closest approach of the two hyperbola branches occurs. The minimum width of the divergence-stable corridor is thus $2\sqrt{2}L_\mu = 2\sqrt{2}\gamma VM_\mu$. These points occur in the first quadrant of the K_x^*, K_y^* plane (fig. 6), only if $L_\mu/K_\mu < 1$ (which is, in fact, true only for rather large V). In any case, the cross spring L_μ is a good measure of the corridor width at low K_x^* and K_y^*.

In terms of the approximation based on the equivalent radius, the negative aerodynamic spring - which determines the asymptotes of the divergence boundaries - is

$$K_\mu = h\gamma VH_\mu \cong h\gamma \frac{V^2 \sin \phi}{2}$$

which increases with both V and h, so both decrease divergence stability. The minimum width of the divergence-free corridor at low K^* is

$$2\sqrt{2}L_\mu = 2\sqrt{2}\gamma VM_\mu \cong 2\sqrt{2}\gamma \frac{V \sin \phi}{6}$$

which increases with V.

The divergence boundary is then determined by two aerodynamic influences: the direct negative spring $K_\mu = h\gamma VH_\mu$, which gives the location of the asymptotes, and the cross spring coupling $L_\mu = \gamma VM_\mu$, which gives the width of the corridor at low K^* independent of K_μ. The first is the direct hub force due to the rotor and the second is the flap moment on the rotor - both react to the inplane hub velocity component of $V + v$ due to the shaft tilt by pylon pitch or yaw. Both spring terms increase with inflow ratio V; the effect of the direct negative spring also increases with h since it is a hub force.

The pylon and rotor will always be statically stable if both K_x^* and K_y^* are greater than the negative aerodynamic spring K_μ, which is usually not a very stringent criterion on the pylon stiffness. Static stability is also achieved always for the nearly isotropic case, $K_x^* \cong K_y^*$, even if the stiffnesses are smaller than K_μ. The cross spring $L_\mu = \gamma VM_\mu$ stabilizes the divergence motion if the springs are not too stiff, so that both degrees of freedom are active and the coupling of the aerodynamic spring may be effective. This effect produces the divergence-free corridor at low K^*. However, the low K_y^* and K_x^* region will be within the flutter instability region, so the presence of the divergence-free corridor has little practical application.

Flutter: Some preliminary considerations- Some general results for whirl flutter dynamic instability are presented here; they were originally obtained by Young and Lytwyn (ref. 18). The equations of motion are

$$\begin{bmatrix} I_y & 0 \\ 0 & I_x \end{bmatrix} \begin{pmatrix} \alpha_y \\ \alpha_x \end{pmatrix}'' + \begin{bmatrix} C_y & -D_\mu \\ D_\mu & C_x \end{bmatrix} \begin{pmatrix} \alpha_y \\ \alpha_x \end{pmatrix}' + \begin{bmatrix} K_y & L_\mu \\ -L_\mu & K_x \end{bmatrix} \begin{pmatrix} \alpha_y \\ \alpha_x \end{pmatrix} = 0 \qquad (127)$$

Forming the vector product with $[\dot{\alpha}_y \quad \dot{\alpha}_x]$ (i.e., the sum of $\dot{\alpha}_y$ times the first equation and $\dot{\alpha}_x$ times the second), one obtains

$$\frac{d}{d\psi}\left[\frac{1}{2} I_y \dot{\alpha}_y^2 + \frac{1}{2} I_x \dot{\alpha}_x^2 + \frac{1}{2} K_y \alpha_y^2 + \frac{1}{2} K_x \alpha_x^2\right]$$

$$= -[C_y \dot{\alpha}_y^2 + C_x \dot{\alpha}_x^2 + L_\mu(\alpha_x \dot{\alpha}_y - \alpha_y \dot{\alpha}_x)] \qquad (128)$$

This equation is an energy balance for the whirl flutter motion. The left-hand side is the time rate of change of the sum of the kinetic and potential energies of the system, which must always be positive (assuming that the divergence criterion is satisfied). If the right-hand side is negative, the total

energy is decreasing with time, hence the system is stable; if it is positive, the total energy is increasing with time, so the system is unstable. The damping contributions are always stabilizing and extracting energy from the system. An instability is possible only if $L_\mu(\alpha_x\dot{\alpha}_y - \alpha_y\dot{\alpha}_x)$ is sufficiently large and negative. Again, whirl flutter is a direct result of the aerodynamic spring coupling $L_\mu = \gamma V M_\mu \cong \gamma V(\sin\phi)/6$. Since this coupling increases with V, an increase in the forward speed eventually produces an instability (if the term is negative). The gyro coupling due to the rotor (D_μ) does not appear in this result, but it does influence the mode of motion of α_x and α_y and hence may influence the stability. Without L_μ, no instability is possible no matter what influence D_μ has on the motion.

Since the aerodynamic coefficient L_μ is positive, a necessary condition for an instability to occur is that $\alpha_x\dot{\alpha}_y - \alpha_y\dot{\alpha}_x < 0$. Writing $\alpha_y = q \sin\theta$ and $\alpha_x = q\cos\theta$, it follows that $\alpha_x\dot{\alpha}_y - \alpha_y\dot{\alpha}_x = q^2\dot{\theta}$. Hence the requirement is that $\dot{\theta} < 0$, which means a mode of motion in which the shaft whirls in the direction opposite the rotor rotation. This mode is called a backward whirl mode; the motion with the shaft whirling the same direction as the rotor is called forward whirl.

These considerations show that a whirl flutter dynamic instability for a rigid propeller on a pylon occurs only in a backward whirl mode, and that it is a high inflow instability due to the aerodynamic spring coupling M_μ.

Flutter- The flutter boundary is defined by the requirement that a complex conjugate pair of the roots of the characteristic equation be on the imaginary axis, that is, that roots with zero real part be a solution. For $\lambda = i\omega$, where ω is real ($\omega^2 > 0$), the characteristic equation becomes

$$(i\omega C_y + K_y - \omega^2 I_y)(i\omega C_x + K_x - \omega^2 I_x) + (-i\omega D + L)^2 = 0 \tag{129}$$

The real and imaginary parts of this equation are

$$\left.\begin{aligned}(K_y - \omega^2 I_y)(K_x - \omega^2 I_x) - \omega^2 C_x C_y + L^2 - D^2\omega^2 &= 0\\ i\omega[(K_y - \omega^2 I_y)C_x + (K_x - \omega^2 I_x)C_y - 2DL] &= 0\end{aligned}\right\} \tag{130}$$

If it is assumed that $\omega \neq 0$, the imaginary part may be solved for ω^2:

$$\omega^2 = \frac{K_y C_x + K_x C_y - 2DL}{I_y C_x + I_x C_y} \tag{131}$$

Substituting the solution for ω^2 from the imaginary part (eqs. (130)) into the real part produces

$$K_y^2 I_x^2 C_x C_y + K_x^2 I_y^2 C_x C_y - 2 I_x I_y C_y C_x K_x K_y + K_y [C_c (I_y C_x + I_x C_y)(C_y C_x + D^2)$$

$$+ 2DLI_x (C_x I_y - C_y I_x)] + K_x [C_y (I_y C_x + I_x C_y)(C_y C_x + D^2) - 2DLI_y (C_x I_y - C_y I_x)]$$

$$- [L^2 (I_y C_x + I_x C_y)^2 + 2DL (I_y C_x + I_x C_y)(C_y C_x + D^2) + I_x I_y 4D^2 L^2] = 0 \qquad (132)$$

This general second-order equation for K_x and K_y defines the flutter stability boundary; it is, in fact, the equation for a parabola. The equation is simplified by a transformation to a new axis system X and Y defined by

$$\left.\begin{aligned} X &= \frac{I_y}{I} K_y + \frac{I_x}{I} K_x \\ Y &= \frac{I_x}{I} K_y - \frac{I_y}{I} K_x \end{aligned}\right\} \qquad (133)$$

where $I^2 = I_x^2 + I_y^2$. This transformation is a rotation by the angle $\tan^{-1} I_y/I_x$ from the K_y and K_x axes; for isotropic inertias, $I_y = I_x$, the rotation angle is 45°. The X and Y axes remain orthonormal under this rotation. The relation of the X and Y axes to the original K_x and K_y axes is shown in figure 7; the K_x and K_y axes are, of course, already shifted by K_u (the negative aerodynamic spring) from the structural spring axes, K_x^* and K_y^*. With this rotation of the axes, the equation for the flutter boundary becomes

$$Y^2 + Y \left\{ \left[\frac{I_x I_y (C_x^2 - C_y^2) + (I_x^2 - I_y^2) C_x C_y}{I^2 C_x C_y} \right] \frac{C_x C_y + D^2}{I} + \frac{2DL (I_y C_x - I_x C_y)}{C_x C_y I} \right\}$$

$$+ X \left[\frac{(I_y C_x + I_x C_y)^2}{I^2 C_x C_y} \frac{C_x C_y + D^2}{I} \right] - \left[L^2 \frac{I_y C_x + I_x C_y}{I^2 C_x C_y} + \frac{2DL (I_y C_x + I_x C_y)}{I C_x C_y} \frac{C_x C_y + D^2}{I} \right.$$

$$\left. + \frac{I_x I_y 4D^2 L^2}{I^2 C_x C_y} \right] = 0 \qquad (134)$$

which is, indeed, the equation for a parabola.

This equation may be simplified further by expressing it in a form based on the isotropic case. Let ε_I and ε_C be measures of the anisotropy of the moments of inertia and damping coefficients that

$$\left.\begin{aligned} \tan \varepsilon_I &= \frac{I_x - I_y}{I_x + I_y} \\ \tan \varepsilon_C &= \frac{C_x - C_y}{C_x + C_y} \end{aligned}\right\} \qquad (135)$$

and, as representative inertia and damping, use

$$\left.\begin{aligned} I &= \sqrt{I_x^2 + I_y^2} \\ C &= \sqrt{C_x^2 + C_y^2} \end{aligned}\right\} \tag{136}$$

The angle ε_I is the rotation of the X axis from the 45° line on the K_x,K_y plane (fig. 7). With these definitions, the equation for the boundary becomes

$$Y^2 + Y\left[\frac{\sin 2(\varepsilon_I + \varepsilon_C)}{I \cos 2\varepsilon_C}\left(\frac{C^2}{2}\cos 2\varepsilon_C + D^2\right) + \frac{4DL}{C}\frac{\sin(\varepsilon_C - \varepsilon_I)}{\cos 2\varepsilon_C}\right]$$

$$+ X\left[\frac{2\cos^2(\varepsilon_I + \varepsilon_C)}{I \cos 2\varepsilon_C}\left(\frac{C^2}{2}\cos 2\varepsilon_C + D^2\right)\right]$$

$$= \left[2L^2\frac{\cos^2(\varepsilon_I + \varepsilon_C)}{\cos 2\varepsilon_C} + \frac{4DL}{IC}\frac{\cos(\varepsilon_I + \varepsilon_C)}{\cos 2\varepsilon_C}\left(\frac{C^2}{2}\cos 2\varepsilon_C + D^2\right) + \frac{4D^2L^2}{C^2}\frac{\cos 2\varepsilon_I}{\cos 2\varepsilon_C}\right] \tag{137}$$

The equation is now in the standard form for a parabola, namely,

$$(Y + \varepsilon_Y)^2 + 4dX = 4dh_v \tag{138}$$

The geometry of the parabola is described by the shape factor d and the vertex h_v (fig. 7). The axis of the parabola is parallel to the X axis, but shifted a distance ε_Y below it. The maximum value of X on the boundary occurs at the vertex, a distance h_v from the Y axis. The parameter d describes the shape of the parabola: at a distance d from the vertex, the parabola has a width of $4d$. Moreover, the isotropic inertias (so $\varepsilon_Y = 0$ and the parabola axis is parallel to the 45° line on the K_y^*,K_x^* plane), the shape factor points (points A in fig. 7) give the maximum values of K_y^* and K_x^* on the parabola.

To first order in ε_I and ε_C, that is, for small anisotropy, the parabola axis shift, vertex, and shape factor are given by:

$$\varepsilon_Y \cong \frac{C^2 + 2D^2}{2I}(\varepsilon_I + \varepsilon_C) + \frac{2DL}{C}(\varepsilon_C - \varepsilon_I) \tag{139}$$

$$h_v \cong \frac{2L}{C}\left(I\frac{L}{C} + D\right) \tag{140}$$

$$d \cong \frac{C^2 + 2D^2}{4I} \tag{141}$$

For small anisotropy, there is no first-order influence on h_v and d, which describe the parabola shape and position; there is only a small effect on the orientation of the parabola axis, which is rotated by ε_I and translated by ε_Y

from the 45° line on the K_y, K_x plane. In terms of the approximation based on the equivalent radius, the vertex is

$$h_v \cong \frac{2L}{C}\left(I\frac{L}{C} + D\right)$$

$$= \frac{2L_\mu}{\sqrt{2}\ (C^* + C_\mu)}\left(I^*\frac{L_\mu}{C^* + C_\mu} + D_\mu\right)$$

$$= \sqrt{2}\frac{\gamma VM_\mu}{C^* + h^2\gamma H_\mu - \gamma M_\beta^\cdot}\left(I^*\frac{\gamma VM_\mu}{C^* + h^2\gamma H_\mu - \gamma M_\beta^\cdot} + 2\right) \qquad (142)$$

where

$$\frac{L_\mu}{C^* + C_\mu} = \frac{\gamma VM_\mu}{C^* + h^2\gamma H_\mu - \gamma M_\beta^\cdot} \cong \frac{\gamma V(\sin\phi)/6}{C^* + \gamma[(\cos\phi)/8 + h^2(V\sin\phi)/2]} \qquad (143)$$

The farthest penetration of the parabola that defines the dynamic stability boundary is governed by the vertex h_v. The size of h_v is determined primarily by L/C, the ratio of the coupling aerodynamic spring to the total pylon damping. The damping of the pylon, with structural and aerodynamic contributions, decreases h_v. The aerodynamic damping probably does not change much with V, the larger term $(M_\beta^\cdot)$ decreasing somewhat while the other increases. An increase in mast height h is helpful for stability since it increases the aerodynamic damping. The major influence of V is on the coupling spring $L_\mu = \gamma VM_\mu \cong \gamma V(\sin\phi)/6$, which increases with V, and so h_v does also. The gyroscopic coupling D_μ contributes to the instability, but the primary source is the cross spring L_μ (the direct hub moment due to the inplane component of $V + v$ produced by the pylon tilt, $L_\mu = \gamma VM_\mu$). The shape factor is approximately

$$d \cong \frac{C^2 + 2D^2}{4I} = \frac{(C^* + C_\mu)^2 + D_\mu{}^2}{2\sqrt{2}\ I^*}$$

$$= \frac{(C^* + h^2\gamma H_\mu - \gamma M_\beta^\cdot)^2 + 4}{2\sqrt{2}\ I^*}$$

$$\cong \frac{\left\{C^* + \gamma[(\cos\phi)/8 + h^2(V\sin\phi)/2]\right\}^2 + 4}{2\sqrt{2}\ I^*} \qquad (144)$$

Small d means a flatter parabola; therefore, in this respect, damping $(C^* + C_\mu)$ is bad for stability and the inertia I^* is good, in contrast to their influence on h_v. The shape factor is relatively independent of V, however; hence the main influence of an increase in the inflow ratio is to increase h_v, which shifts the parabola outward without changing its shape much.

It may be concluded then that the whirl flutter dynamic instability is due to the aerodynamic spring coupling $L_\mu = \gamma V M_\mu$, as suggested by earlier discussions. The shape of the flutter parabola is relatively independent of V, while the vertex h_v increases greatly with V; forward speed therefore decreases the flutter stability by shifting the parabola outward. Since an increase in damping, either structural or aerodynamic, makes the parabola broader, but decreases the vertex size, the overall effect on stability is favorable. Conversely, an increase in the inertia is unfavorable. The mast height h only enters into the aerodynamic damping of the pylon, where its influence is favorable. The gyroscopic coupling participates in the instability, but cannot cause it if L_μ is small enough.

Construction of boundaries- From the previous solutions, the whirl flutter stability boundaries can be easily sketched on the K_x^*, K_y^* plane for a given V. The relevant axes for both flutter and divergence are the K_x, K_y axes on the K_x^*, K_y^* plane, which are offset from the K_x^*, K_y^* (structural spring) axes by the negative aerodynamic spring $K_\mu = h\gamma V H_\mu$. The lines $K_x^* = K_\mu$ and $K_y^* = K_\mu$ are constructed first.

The divergence hyperbola has as asymptotes the K_x and K_y axes, and a minimum width for small K_x^* and K_y^* of $2\sqrt{2}\, L_\mu = 2\sqrt{2}\, \gamma V M_\mu$. Since the portions of the divergence boundaries within the flutter boundary are not of practical interest, the divergence boundaries are defined primarily by the asymptotes.

The flutter boundary construction begins at the 45° line from the K_y and K_x axes. The X and Y axes are constructed, then rotated an angle ε_I from the 45° line; the parabola axis is then constructed a distance ε_γ below the X axis. The vertex of the parabola is given by the distance h_v from the Y axis; from the shape factor d, four more points on the parabola are easily found (on the Y axis, and points A as in fig. 7). The shape factor points (A in fig. 7) give the points of maximum K_y^* and K_x^*, at least for isotropic inertias ($\varepsilon_I = 0$).

It is almost as easy to construct the boundaries exactly as it is to sketch them. From the equations for the divergence hyperbola and the flutter parabola (eqs. (124) and (138)), a number of points on each boundary can be obtained quickly. Typical results are shown in figure 8, for $V/\Omega R = 1$, $h = 0.3$, $\gamma = 4$, $I_x^* = I_y^* = 2$, and $C_x^* = C_y^* = 0$ (high inflow, typical prop-rotor mast height and Lock number, isotropic inertia of the pylon, and no pylon structural damping). Also shown for the K_x^* axis is the equivalent pylon natural frequency, $\omega_x^2 = K_x^*/I_x^*$ (per rev), to aid in the interpretation of the results.

Whirl Flutter Nomenclature

$C_\mu = h^2 \gamma H_\mu - \gamma M_\beta^\cdot$	direct aerodynamic damping
$K_\mu = h\gamma V H_\mu$	direct aerodynamic spring
$D = D_\mu = 2$	Coriolis coupling
$L = L_\mu = \gamma V M_\mu$	cross aerodynamic spring

Whirl Flutter Nomenclature (Concl.)

$K_y = K_y^* - K_\mu$	total pitch spring
$K_x = K_x^* - K_\mu$	total yaw spring
$C_y = C_y^* + C_\mu$	total pitch damping
$C_x = C_x^* + C_\mu$	total yaw damping
$\varepsilon_I = \tan^{-1} \frac{I_x - I_y}{I_x + I_y}$	inertia anisotropy
$\varepsilon_C = \tan^{-1} \frac{C_x - C_y}{C_x + C_y}$	damping anisotropy
$I = \sqrt{I_x^2 + I_y^2}$	representative inertia
$C = \sqrt{C_x^2 + C_y^2}$	representative damping
X, Y	whirl flutter parabola axes
ε_Y	whirl flutter parabola axis offset
d	whirl flutter parabola shape factor
h_v	whirl flutter parabola vertex

Two-Bladed Rotor

A two-bladed rotor on a pylon is discussed briefly because early experiments (the XV-3) and analyses (ref. 8) have dealt with this case. The primary intention of this chapter is to indicate how special the $N = 2$ case is, because of the fact that this system is described by periodic coefficient differential equations.

Consider a two-bladed flapping rotor on a pylon with pitch and yaw degrees of freedom. The rotor flapping motion is composed of a teetering mode and a coning mode. As for $N > 3$, the coning mode does not transmit any net force or moment to the pylon to excite its pitch or yaw motion. Moreover, the usual case of a two-bladed rotor is the teetering rotor, which has both blades cantilevered to the hub, which is then attached to the shaft by a single flap hinge. For the teetering mode, the rotor acts as an articulated rotor, while, for the coning mode, it acts as a hingeless rotor with a very high natural frequency. Thus the coning mode may be neglected in this model, and the problem reduces to three degrees of freedom: rotor teetering and pylon pitch and yaw. (This differs from that for three or more blades, where the equivalent model has

four degrees of freedom.) For $N \geq 3$, the rotor motion in the fixed frame is described by tip path plane tilt degrees of freedom (plus N-2 other modes that do not couple with α_x and α_y). For $N = 2$, however, such a description overdescribes the transient motion since only one degree of freedom is involved - the teetering mode. For $N \geq 3$, the use of tip path plane coordinates results in constant coefficient differential equations, even though the equations of motion for the individual blades in the rotating frame involve a periodic variation of the inertia and aerodynamic forces. For $N = 2$, the periodic coefficients remain in the equations of motion since the teetering mode is really a rotating degree of freedom. The fundamental difference between the dynamics of the $N \geq 3$ and $N = 2$ cases, which makes the two-bladed rotor much more difficult to analyze, is that fact: for $N = 2$, the equations of motion for the coupled rotor and pylon system involve periodic coefficients even in purely axial equilibrium flow.

The equations of motion for the pylon and rotating blades are the same as for the four-degree-of-freedom development (eqs. (4)). If the coning mode is neglected, since it does not influence the coupled dynamics anyway, the flapping angle of the mth blade (m = 1, 2 here) is given by the teetering degree of freedom β: $\beta^{(2)} = \beta$ for the blade at azimuth position ψ, and $\beta^{(1)} = -\beta$ for the blade at azimuth position $\psi + \pi$. The equation of motion for the teetering mode is obtained by operating on the rotating equation with $1/2\sum_m (-1)^m(\ldots)$; this operation yields the total teetering moment on the rotor. With $\sin \psi_m = (-1)^m \sin \psi$ and $\cos \psi_m = (-1)^m \cos \psi$, the equation for β is

$$\ddot{\beta} + \nu_\beta^2\beta - (\ddot{\alpha}_y - 2\dot{\alpha}_x)\cos \psi + (\ddot{\alpha}_x + 2\dot{\alpha}_y)\sin \psi = \gamma \frac{M_{F_1}}{ac} \qquad (145)$$

where $M_{F_1} = 1/2 \sum_m (-1)^m M_{F_m}$ is the aerodynamic teetering moment. Already, periodic coefficients appear with the pylon inertia terms as seen by the rotating blade. The evaluation of the hub moment and force for the pylon equations and the flap moment for the rotor equation follows exactly that for the four-degree-of-freedom model, up to the point where the summation over the N blades is performed. At this point, the influence of $N = 2$ appears, usually the introduction of periodic coefficients.

The following equations of motion are obtained (for convenience, V is written for $V + v$, except in the gust terms, where it really is just V); and H_μ for $H_\mu + R_\mu$):

$$\begin{bmatrix} 1 & -\cos\psi & \sin\psi \\ 0 & I_y^* & 0 \\ 0 & 0 & I_x^* \end{bmatrix} \begin{pmatrix} \beta \\ \alpha_y \\ \alpha_x \end{pmatrix}^{\cdot\cdot}$$

$$+ \begin{bmatrix} -\gamma M_\beta^{\cdot} & (2+\gamma h M_\mu)\sin\psi + \gamma M_\beta^{\cdot}\cos\psi & (2+\gamma h M_\mu)\cos\psi - \gamma M_\beta^{\cdot}\sin\psi \\ -h\gamma H_\beta^{\cdot} 2\sin\psi & C_y^* + h^2\gamma H_\mu(1-\cos 2\psi) + h\gamma H_\beta^{\cdot}\sin 2\psi & h^2\gamma H_\mu \sin 2\psi - h\gamma H_\beta^{\cdot}(1-\cos 2\psi) \\ -h\gamma H_\beta^{\cdot} 2\cos\psi & h^2\gamma H_\mu \sin 2\psi + h\gamma H_\beta^{\cdot}(1+\cos 2\psi) & C_x^* + h^2\gamma H_\mu(1+\cos 2\psi) - h\gamma H_\beta^{\cdot}\sin 2\psi \end{bmatrix} \begin{pmatrix} \beta \\ \alpha_y \\ \alpha_x \end{pmatrix}^{\cdot}$$

$$+ \begin{bmatrix} \nu_\beta^2 + \gamma M_\theta K_P & -\gamma V M_\mu \sin\psi & -\gamma V M_\mu \cos\psi \\ \left(\nu_\beta^2 - 1 + \gamma h \frac{C_T}{\sigma a}\right) 2\cos\psi + h\gamma H_\theta K_P 2\sin\psi & K_y^* - h\gamma V H_\mu(1-\cos 2\psi) & -h\gamma V H_\mu \sin 2\psi \\ -\left(\nu_\beta^2 - 1 + \gamma h \frac{C_T}{\sigma a}\right) 2\sin\psi + h\gamma H_\theta K_P 2\cos\psi & -h\gamma V H_\mu \sin 2\psi & K_x^* - h\gamma V H_\mu(1+\cos 2\psi) \end{bmatrix} \begin{pmatrix} \beta \\ \alpha_y \\ \alpha_x \end{pmatrix}$$

$$= \begin{bmatrix} \gamma M_\theta \\ h\gamma H_\theta 2\sin\psi \\ h\gamma H_\theta 2\cos\psi \end{bmatrix} \theta_1 + \begin{bmatrix} \gamma V M_\mu \sin\psi & \gamma V M_\mu \cos 2\psi \\ h\gamma V H_\mu(1-\cos 2\psi) & h\gamma V H_\mu \sin 2\psi \\ h\gamma V H_\mu \sin 2\psi & h\gamma V H_\mu(1+\cos 2\psi) \end{bmatrix} \begin{pmatrix} \alpha_G \\ \beta_G \end{pmatrix} \tag{146}$$

This three-degree-of-freedom set of differential equations has periodic coefficients, with a period of 2π. These equations can be solved, by the techniques of Floquet theory, for the eigenvalues of the system, which indicate the stability (as described, e.g., in ref. 33). These equations agree with those derived by Hall (ref. 8) for the two-bladed rotor (that work involved the XV-3, which had teetering rotors). Hall did not obtain the linear differential equations, however; he solved the equations by numerical integration to find the transient motion, which allowed him to keep the equations in a more general form and even to include nonlinear aerodynamics.

The pitch input θ_1 is the differential blade pitch, a degree of freedom corresponding to the teetering mode; $\theta_1 = [\theta^{(2)} - \theta^{(1)}]/2$. If the blade pitch control is achieved by a conventional swashplate, then the input variables are really θ_{1C} and θ_{1S}, where $\theta_1 = \theta_{1C}\cos\psi + \theta_{1S}\sin\psi$.

The whirl flutter equations for $N = 2$ are obtained much as for $N \geq 3$: eliminate the combination $\nu_\beta^2\beta$ from the pylon equations of motion by use of the flapping equation, then drop the β degree of freedom in taking the limit to a truly rigid propeller. The result, for homogeneous equations, is

$$\begin{bmatrix} I_y^*+1+\cos 2\psi & -\sin 2\psi \\ -\sin 2\psi & I_x^*+1-\cos 2\psi \end{bmatrix}\begin{pmatrix}\alpha_y\\ \alpha_x\end{pmatrix}''$$

$$+\begin{bmatrix} C_y^*+h^2\gamma H_\mu(1-\cos 2\psi)-\gamma M_\beta^*(1+\cos 2\psi)-(2+2h\gamma M_\mu)\sin 2\psi & h^2\gamma H_\mu \sin 2\psi+\gamma M_\beta^* \sin 2\psi-2(1+\cos 2\psi)-2h\gamma M_\mu \cos 2\psi \\ h^2\gamma H_\mu \sin 2\psi+\gamma M_\beta^* \sin 2\psi+2(1-\cos 2\psi)-2h\gamma M_\mu \cos 2\psi & C_x^*+h^2\gamma H_\mu(1+\cos 2\psi)-\gamma M_\beta^*(1-\cos 2\psi)+(2+2h\gamma M_\mu)\sin 2\psi \end{bmatrix}\begin{pmatrix}\alpha_y\\ \alpha_x\end{pmatrix}'$$

$$+\begin{bmatrix} K_y^*-h\gamma VH_\mu(1-\cos 2\psi)+\gamma VM_\mu \sin 2\psi & -h\gamma VH_\mu \sin 2\psi+\gamma VM_\mu(1+\cos 2\psi) \\ -h\gamma VH_\mu \sin 2\psi-\gamma VM_\mu(1-\cos 2\psi) & K_x^*-h\gamma VH_\mu(1+\cos 2\psi)-\gamma VM_\mu \sin 2\psi \end{bmatrix}\begin{pmatrix}\alpha_y\\ \alpha_x\end{pmatrix} = 0 \tag{147}$$

This is a two-degree-of-freedom problem again, but now with periodic coefficients (of period π) because of the two-bladed rotor; the solution for the stability is obtained by Floquet theory techniques. Typical results for the stability boundaries on the K_x and K_y plane are shown in figure 9, for $V/\Omega R = 1$, $h = 0.3$, $\gamma = 4$, $I_x^*[= I_x/(N/2)I_b] = I_y^* = 2$, and $C_y^* = C_x^* = 0$. The divergence and flutter boundaries are much as for the $N \geq 3$ whirl flutter problem (fig. 8). The periodicity of the system also introduces the possibility of a divergence-like instability that occurs with a frequency 1/rev in addition to occurring on the real axis. (Such an instability may occur at any multiple of one-half the fundamental frequency of the system, which is 2/rev for the present case with a period of π.) Such instability regions appear in the solution presented in figure 9. One region occurs for low stiffness, where the natural frequencies of the pylon (ω_x and ω_y) are near zero; that region is buried in the classical flutter region though. A 1/rev divergence also appears where ω_x or ω_y is near 1/rev, since that is where one eigenvalue would be expected to be near 1/rev. This new kind of instability for the proprotor and pylon system, introduced by the periodic coefficients, illustrates how special the two-bladed rotor is.

AIRCRAFT STABILITY DERIVATIVES

This chapter examines the contributions of the proprotor to the aircraft stability derivatives, and hence the influence of the proprotor on the entire aircraft. The aircraft rigid-body motions are assumed to occur at low frequency, and are transmitted to the rotor shaft without modification by the wing motion. The expressions obtained previously for the response of the flapping rotor to low-frequency shaft motion are used to estimate the rotor contributions to the forces and moments on the aircraft. This means, of course, that the influence of the rotor lag and the wing motion is being neglected. The rotor contributions are compared with the usual airplane contributions to the stability derivatives, from the tail and wing in particular, to evaluate the relative importance of the rotor terms. Nomenclature particular to the aircraft stability derivative analysis is given at the end of the chapter.

While the assumption that the motion occurs at low frequencies for the aircraft rigid-body degrees of freedom is valid, it is not quite correct to

neglect the influence of the wing degrees of freedom and of the rotor lag motion in determining the low-frequency rotor response. Usually, there is not that much frequency separation between the aircraft rigid-body motions and the rotor flapping motions (β - 1) and the wing modes and rotor lag motion (ζ - 1) (i.e., between the motion included and the motion neglected in deriving the rotor low-frequency response). Although the results given here are thus no more than a qualitative assessment of the rotor influence, they are very useful as that.

The aircraft axis system and geometry considered are shown in figure 10. The forces and moments about the aircraft center of gravity are required. The wing span is ℓ_w, so the rotor at the wing tip acts a distance $\ell_w/2$ laterally from the aircraft center of gravity and a distance h forward. The forces and moments and the rigid-body motions of the aircraft are defined in the body axis system in figure 10; the corresponding rotor forces and shaft motion are shown in figure 3. It follows then that the rotor forces and moments acting at the center of gravity along the x, y, and z directions are

$$\left.\begin{aligned} F_x &= 2T \\ F_y &= 2Y \\ F_z &= -2H \\ N_x &= 2\left(-Q - \frac{\ell_w}{2} H \operatorname{sgn} \Omega\right) \\ N_y &= 2(M_y + hH) \\ N_z &= 2\left(-M_x + hY - \frac{\ell_w}{2} T \operatorname{sgn} \Omega\right) \end{aligned}\right\} \tag{148}$$

The factor of 2 accounts for the two contrarotating rotors. The rotor model in figure 3 assumes a specific direction of rotation (clockwise viewed from the rear) for the rotor placed on the right wing as in figure 10. The opposite direction of rotation is accounted for by use of the model in figure 3 for the rotor on the left wing. This feature is the source of the influence of the sign of Ω ($\operatorname{sgn} \Omega$) in N_x and N_z, and in x_P and z_P; Ω positive is taken to be the standard direction shown in figure 3, placed on the right wing. The rotor shaft motion due to the six rigid-body degrees of freedom of the center of gravity is then

$$\left.\begin{aligned} \dot{x}_P &= -V\alpha - \frac{\ell_w}{2} p \operatorname{sgn} \Omega \\ \dot{y}_P &= V\beta \\ \dot{z}_P &= Vu - \frac{\ell_w}{2} r \operatorname{sgn} \Omega \\ \dot{\alpha}_x &= -r \\ \dot{\alpha}_y &= q \\ \dot{\alpha}_z &= p \end{aligned}\right\} \tag{149}$$

where Vu, $V\beta$, $V\alpha$ are the velocity perturbations along the aircraft x, y, and z axes, respectively, and p, q, and r are the angular velocities about these axes.

Now examine some of the aircraft derivatives to which there are contributions from the proprotors. First, consider the pitch moment due to angle of attack, C_{m_α}; from its definition,

$$\Delta C_{m_\alpha} = \frac{\partial N_y / qS_w \bar{c}_w}{\partial \alpha} = -\frac{4}{VS_w \bar{c}_w} \frac{M_y + hH}{\dot{x}_P}$$

$$= -\frac{2\pi\sigma a}{VS_w \bar{c}_w} \left[\frac{2C_{M_y}/\sigma a + h(2C_H/\sigma a)}{\dot{x}_P} \right]$$

$$= -\frac{\sigma a}{V(S_w/2A)\bar{c}_w} \left[\frac{2C_{M_y}/\sigma a + h(2C_H/\sigma a)}{\dot{x}_P} \right] \tag{150}$$

where $S_w/2A$ is the ratio of the wing area to the total rotor disk area (two rotors), and $\bar{c}_w$ is the wing mean aerodynamic chord. This equation gives the rotor contribution in terms of the rotor coefficients times a factor that involves the ratio of the rotor and wing geometric parameters to account for the difference in the normalization of the rotor and airplane coefficients. Now the coefficient C_{m_α} is directly related to the aircraft static margin by $C_{m_\alpha} = C_{L_\alpha}(h_{CG} - h_n)$, where C_{L_α} is the aircraft lift curve slope and h_n is the position of the stick-fixed neutral point (as a fraction of $\bar{c}_w$). The change in the aircraft static margin due to the rotors is

$$\Delta h_n = \frac{\sigma a}{V(S_w/2A)\bar{c}_w C_{L_\alpha}} \left[\frac{2C_{M_y}/\sigma a + h(2C_H/\sigma a)}{\dot{x}_P} \right] \tag{151}$$

where $\Delta h_n < 0$ means a decrease in the static margin and h_n is moved forward by the rotors, which decreases the aircraft longitudinal stability.

The vertical force due to angle of attack, C_{z_α}, is

$$\Delta C_{z_\alpha} = \frac{\partial F_z / qS_w}{\partial \alpha} = \frac{4}{VS_w} \frac{H}{\dot{x}_P} = \frac{\sigma a}{V(S_w/2A)} \left(\frac{2C_H/\sigma a}{\dot{x}_P} \right) \tag{152}$$

The contribution from the rest of the aircraft, primarily from the wing, is $C_{z_\alpha} \cong -C_{L_\alpha}$; therefore,

$$\frac{\Delta C_{z_\alpha}}{C_{z_\alpha}} = \frac{-\sigma a}{V(S_w/2A)C_{L_\alpha}} \left(\frac{2C_H/\sigma a}{\dot{x}_P} \right) \tag{153}$$

A positive value means an increment in the same direction as the wing contribution.

The drag force due to the longitudinal velocity, C_{x_u}, is

$$\Delta C_{x_u} = \frac{\partial F_x / qS_w}{\partial u} = \frac{4}{VS_w} \frac{T}{\dot{z}_P} = \frac{2\sigma a}{V(S_w/2A)} \frac{C_T/\sigma a}{\dot{z}_P} = \frac{2\sigma a}{V(S_w/2A)} (T_\lambda) \qquad (154)$$

Because of the rest of the aircraft, $C_{x_u} = -2C_D = -2f/S_w$ and the influence of the rotors is

$$\frac{\Delta C_{x_u}}{C_{x_u}} = \frac{2\sigma a}{Vf/A} (-T_\lambda) \qquad (155)$$

where a positive value means a contribution in the same direction as the aircraft drag (a damping term). Using the approximation based on the equivalent radius for T_λ yields

$$\frac{\Delta C_{x_u}}{C_{x_u}} \cong \frac{2\sigma a}{Vf/A} \frac{\cos \phi}{4}$$

Since the rotor contribution remains fairly constant while the aircraft drag contribution increases with speed, the relative rotor contribution decreases with V. The rotor thrust due to inflow, T_λ, is always negative, so the rotor contribution is always in the same direction as the aircraft drag term.

The pitch moment due to pitching velocity, C_{m_q}, is

$$\Delta C_{m_q} = \frac{\partial N_y / qS_w \bar{c}_w}{\partial q \bar{c}_w / 2V} = - \frac{2\sigma a}{V(S_w/2A)\bar{c}_w^2} \left[\frac{2C_{M_y}/\sigma a + h(2C_H/\sigma a)}{\dot{\alpha}_y} \right] \qquad (156)$$

The contribution due to the horizontal tail is $C_{m_q} \cong -2a_t S_t \ell_t^2 / S_w c_w^2$, where a_t, S_t, and ℓ_t are, respectively, the horizontal tail lift curve slope, area, and arm. Then the increment required to counter the rotor contribution is

$$\Delta \frac{S_t \ell_t^2}{2A} = - \frac{\sigma a}{V a_t} \left[- \frac{2C_{M_y}/\sigma a + h(2C_H/\sigma a)}{\dot{\alpha}_y} \right] \qquad (157)$$

where a positive value means that more tail is required. This coefficient may also be expressed in terms of the maneuver margin change: $\Delta h_m = -(\rho S_w c_w / 4M) \Delta C_{m_q}$, where M is the aircraft mass. A positive ΔC_{m_q} due to the rotor then decreases the stick-fixed maneuver margin, moves h_m forward, or equivalently requires more horizontal tail to maintain the same margin as without the rotors.

The rolling moment due to roll rate, C_{ℓ_p}, is

$$\Delta C_{\ell_p} = \frac{\partial N_x / q S_w \ell_w}{\partial p \ell_w / 2V} = \frac{\sigma a}{2V(S_w/2A)} \left(\frac{2C_H/\sigma a}{\dot{x}_P} - \frac{8}{\ell_w^2} \frac{C_Q/\sigma a}{\dot{\alpha}_z} \right) \tag{158}$$

The contribution due to the wing is approximately $C_{\ell_p} = -C_{L_\alpha}/8$, and with $\partial(C_Q/\sigma a)/\partial \dot{\alpha}_z = Q_\zeta^{\cdot}$,

$$\frac{\Delta C_{\ell_p}}{C_{\ell_p}} = \frac{4\sigma a}{V(S_w/2A)C_{L_\alpha}} \left(- \frac{2C_H/\sigma a}{\dot{x}_P} + \frac{8}{\ell_w^2} Q_\zeta^{\cdot} \right) \tag{159}$$

The $Q_\zeta^{\cdot}$ term is due to the change in the rotor rotational velocity with respect to air, which is produced by the rolling rate of the aircraft; $Q_\zeta^{\cdot} \cong V(\sin \phi)/6$, so this contribution is always in the same direction as the wing term, and increases with V.

The yawing moment due to sideslip, C_{n_β}, is

$$\Delta C_{n_\beta} = \frac{\partial N_z / q S_w \ell_w}{\partial \beta} = - \frac{\sigma a}{V(S_w/2A)\ell_w} \left[\frac{2C_{M_x}/\sigma a - h(2C_Y/\sigma a)}{\dot{y}_P} \right] \tag{160}$$

The contribution of the vertical tail is $C_{n\beta} = a_v S_v \ell_v / S_w \ell_w$, so the tail required to counter the rotor contribution is

$$\Delta \frac{S_v \ell_v}{2A} = \frac{\sigma a}{V a_v} \left[\frac{2C_{M_x}/\sigma a - h(2C_Y/\sigma a)}{\dot{y}_P} \right] \tag{161}$$

where a positive value means that more tail is required.

The yaw moment due to yawing rate, C_{n_r}, is

$$\Delta C_{n_r} = \frac{\partial N_z / q S_w \ell_w}{\partial r \ell_w / 2V} = \frac{2\sigma a}{V(S_w/2A)\ell_w^2} \left[\frac{2C_{M_x}/\sigma a - h(2C_Y/\sigma a)}{\dot{\alpha}_x} + \frac{\ell_w^2}{2} \frac{C_T/\sigma a}{\dot{z}_P} \right] \tag{162}$$

The contribution of the vertical tail is $C_{n_r} \cong -2a_v S_v \ell_v^2 / S_w \ell_w^2$ and, with $\partial(C_T/\sigma a)/\partial \dot{z}_P = T_\lambda$,

$$\Delta \frac{S_v \ell_v^2}{2A} = - \frac{\sigma a}{V a_v} \left[- \frac{2C_{M_x} - h(2C_Y/\sigma a)}{\dot{\alpha}_x} - \frac{\ell_w^2}{2} T_\lambda \right] \tag{163}$$

where a positive value means that more tail is required to counter the rotor. The thrust coefficient T is negative, so at least that term requires less tail, that is, the rotor thrust damping contributes to the yaw damping of the aircraft.

The rolling moment due to sideslip, C_{ℓ_β}, is

$$\Delta C_{\ell_\beta} = \frac{\partial N_x/qS_w\ell_w}{\partial\beta} = \frac{\sigma a}{2V(S_w/2A)}\,(sgn\ \Omega)\left(-\frac{2C_H/\sigma a}{\dot{y}_P}\right) \tag{164}$$

The contribution due to wing dihedral is $C_{\ell_\beta} \cong -(C_{L_\alpha}/4)\Gamma$, where Γ is the wing dihedral angle (in radians, positive up). Then the equivalent dihedral due to the rotors is

$$\Delta\Gamma = \frac{2\sigma a}{V(S_w/2A)C_{L_\alpha}}\,(sgn\ \Omega)\left(-\frac{2C_H/\sigma a}{\dot{y}_P}\right) \tag{165}$$

where a positive value means that more wing dihedral is required to counter the rotor contributions.

The above coefficients are of primary interest for their influence on the aircraft dynamics; a few others to which the rotor contributes are also examined. The vertical force due to pitch rate, C_{z_q}, is

$$\Delta C_{z_q} = \frac{\partial F_z/qS_w}{\partial q\bar{c}_w/2V} = \frac{2}{V(S_w/2A)\bar{c}_w}\left(-\frac{2C_H/\sigma a}{\dot{\alpha}_y}\right) \tag{166}$$

The horizontal tail contribution is $C_{z_q} = -2a_t S_t \ell_t/S_w\bar{c}_w$, so

$$\Delta\frac{S_t\ell_t}{2A} = -\frac{4\sigma a}{Va_t}\left(-\frac{2C_Y/\sigma a}{\dot{y}_P}\right) \tag{167}$$

where a positive value means that more tail is required.

The side force due to sideslip, C_{y_β}, is

$$\Delta C_{y_\beta} = \frac{\partial F_z/qS_w}{\partial\beta} = -\frac{2\sigma a}{V(S_w/2A)}\left(-\frac{2C_Y/\sigma a}{\dot{y}_P}\right) \tag{168}$$

Because of the vertical tail, $C_{y_\beta} = -a_v S_v/S_w$; therefore,

$$\Delta \frac{S_v}{2A} = -\frac{4\sigma a}{V a_v}\left(-\frac{2C_Y/\sigma a}{\dot{y}_P}\right) \tag{169}$$

where a positive value means that more tail is required.

The yawing moment due to rolling rate, C_{n_p}, is

$$\Delta C_{n_p} = \frac{\partial N_z/qS_w\ell_w}{\partial p\ell_w/2V} = \frac{\sigma a(sgn\ \Omega)}{V(S_w/2A)\ell_w}\left[\frac{2C_{M_x}/\sigma a - h(2C_Y/\sigma a)}{\dot{x}_P} - 2\frac{C_T/\sigma a}{\dot{\alpha}_z}\right] \tag{170}$$

The contribution of the wing is approximately $C_{n_p} = -C_L/8$, and $\partial(C_T/\sigma a)/\partial\dot{\alpha}_z = T_\zeta$; therefore,

$$\frac{\Delta C_{n_p}}{C_{n_p}} = \frac{8\sigma a}{V(S_w/2A)\ell_w C_L}(sgn\ \Omega)\left[-\frac{2C_{M_x}/\sigma a - h(2C_Y/\sigma a)}{\dot{x}_P} + 2T_\zeta\right] \tag{171}$$

where a positive value means that the rotor contribution is in the same direction as that of the wing. Now $T_\zeta \cong (\sin\phi)/6$ is positive, so that contribution is at least the same as for the wing if $\Omega > 0$, and opposite if $\Omega < 0$.

The rolling moment due to yawing rate, C_{ℓ_r}, is

$$\Delta C_{\ell_r} = \frac{\partial N_x/qS_w\ell_w}{\partial r\ell_w/2V} = \frac{\sigma a(sgn\ \Omega)}{V(S_w/2A)\ell_w}\left(\frac{2C_H/\alpha a}{\dot{\alpha}_x} + \frac{2C_Q/\alpha a}{\dot{z}_P}\right) \tag{172}$$

The contribution of the wing is $C_{\ell_r} \cong C_L/4$, and $\partial(C_Q/\sigma a)/\partial z_P = Q_\lambda$; therefore,

$$\frac{\Delta C_{\ell_r}}{C_{\ell_r}} = \frac{4\sigma a}{V(S_w/2A)\ell_w C_L}(sgn\ \Omega)\left(\frac{2C_H/\sigma a}{\dot{\alpha}_x} + 2Q_\lambda\right) \tag{173}$$

where a positive value means a contribution in the same direction as from the wing. The torque due to inflow is $Q_\lambda \cong -(\sin\phi)/6$, which is always negative at least.

The influence of the proprotor forces and moments on the aircraft stability derivatives may be estimated with these expressions. Table 1 gives the values of the parameters required. Two types of rotors are considered: a gimballed rotor and a cantilever rotor. The gimballed rotor has a flap frequency of exactly 1/rev because of the hinge at the center of rotation; it also has positive pitch/flap coupling, $K_P < 0$ (negative δ_3 of about 15°), and the rotor rotates clockwise (from the rear) on the right wing. The cantilever rotor has a flap frequency above 1/rev, namely, $\nu_\beta = 1.35$; it has no pitch/flap

coupling, K_P = 0, and rotor rotation is counterclockwise on the right wing. The gimballed rotor has a somewhat larger mast height to account for the flapping clearance required. These parameters are representative of the two full-scale rotors discussed later. The other parameters in table 1 are typical of a proprotor aircraft. The rotor influence is evaluated at $V/\Omega R$ = 1, which is around V = 325 knots, approximately the maximum cruise speed of such an aircraft. Generally, the influence of the rotor increases with speed, hence the coefficients are evaluated at high velocity.

TABLE 1.- TYPICAL AIRCRAFT PARAMETERS USED TO EVALUATE THE INFLUENCE OF THE PROPROTOR ON AIRCRAFT STABILITY

	Cantilever rotor	Gimballed rotor
ν_β	1.35	1.0
K_P	0	-0.25
h/R	0.28	0.34
$sgn\ \Omega$	-1	1
σ	0.1	
a	5.7	
γ	4	
$S_w/2A$	0.19	
$\bar{c}_w/R$	0.44	
ℓ_w/R	2.65	
C_{L_α}	4.2	
a_t	3	
a_v	3	
$V_{max}/\Omega R$	1	
C_L at V_{max}	0.20	
f/A	0.013	
$S_t\ell_t/2AR$	0.09	
$S_v/2A$	0.05	
$S_v\ell_v/2AR$	0.07 to 0.09	
$S_v\ell_v^2/2AR$	0.10 to 0.16	

The rotor force and moment derivatives are given in table 2 for these two rotors; the first number is for the gimballed rotor; the second, for the

TABLE 2.- ROTOR FORCE AND MOMENT DERIVATIVES AT $V/\Omega R = 1$, FROM THE LOW-FREQUENCY RESULTS (EQS. (102) AND (103))

	$\dot{x}_P$	$\dot{y}_P$	$\dot{\alpha}_y$	$-\dot{\alpha}_x$	$-\theta_{1S}$	θ_{1C}
$-\frac{2C_H}{\sigma a}$	0.169/0.412*	-0.062/-0.077	-1.002/-0.041	-0.232/-0.427	0.143/0.527	-0.099/-0.122
$-\frac{2C_{M_y}}{\sigma a}$	0/0.044	0/0.115	0/0.246	0/0.442	0/0.063	0/0.165
$-\left(\frac{2C_{M_y}}{\sigma a} + h\frac{2C_H}{\sigma a}\right)$	0.057/0.157	-0.021/0.094	-0.340/0.258	-0.079/0.322	0.049/0.210	-0.034/0.131

*First value is for a gimballed rotor, the second for a cantilever rotor, with parameters given in table 1.

cantilever rotor. These low-frequency derivatives, obtained with equations (102) and (103), were evaluated using the parameters in table 1; only ν_β, K_P, h, γ, and V are required for the rotor derivatives, the others are aircraft parameters. The flap frequency is the primary parameter, responsible for the major differences between the derivatives for the gimballed and cantilever rotors; K_P is also important for the cross-derivatives of the gimballed rotor.

The rotor forces and moments due to the hub inplane velocity x_P or y_P are basically produced by the coefficients H_μ and M_μ. The derivative $-H/\dot{x}_P$, always positive and generally larger for the cantilever blade, gives positive damping then. The corresponding pivot moment derivative $-(M_y + hH)/\dot{x}_P$ is also always positive. The cross-derivative $-H/\dot{y}_P$ is always negative for the cantilever rotor, while it is proportional to K_P for the gimballed rotor and therefore has its sign. The pivot moment derivative $-(M_y + hH)/\dot{y}_P$ is also proportional to K_P for the gimballed rotor and has its sign; while, for the cantilever rotor, the hub moment dominates the hub force acting on the arm h, so the net pivot moment is always positive. The hub force due to the shaft angular velocity $-H/\dot{\alpha}_y$ is large and always negative for the gimballed rotor because of the flapping required to precess the rotor acting through the negative H force ($H_{\dot{\beta}}$) to give a hub force; the derivative is small for the cantilever rotor. The corresponding pivot moment $-(M_y + hH)/\dot{\alpha}_y$ is then also negative for the gimballed rotor (negative damping); for the cantilever rotor, it is always positive because of the hub moment. The cross-derivative $H/\dot{\alpha}_x$ is negative for the cantilever rotor, and has the sign of K_P for the gimballed rotor. The moment derivative $(M_y + hH)/\dot{\alpha}_x$ also has the sign of K_P for the gimballed rotor, and is positive for the cantilever rotor because of the hub moment. The longitudinal derivatives required ($-T_\lambda$, $-Q_\lambda$, $T_{\dot{\zeta}}$, and $Q_{\dot{\zeta}}$) are all positive and increases with V (all equal 0.133 at $V = 1$, based on just the c_{ℓ_α} terms as in eqs. (54)).

On the basis of the expressions above and the values given for the rotor derivatives, the following influence of the proprotor on the aircraft dynamics is found. The change in C_{m_α} due to the rotor always results in decreased static longitudinal stability, that is, a forward movement of the neutral point h_n. Typicaly, h_n moves forward 10 to 20 percent of the wing mean aerodynamic chord, with the larger value for the cantilever rotors. Like many of the rotor effects, this change is roughly proportional to H_μ/V, which, from the equivalent radius approximation, is proportional to $\sin \phi$; hence the rotor effect increases with V.

The rotor increases C_{z_α} somewhat over the wing contribution; that is, the rotor contributes to the total lift curve slope of the aircraft by about 10 to 30 percent (the higher value for cantilever rotors) of the wing contribution in the same direction, thereby increasing the total aircraft C_{L_α}. This effect is also proportional to H_μ/V, hence to $\sin \phi$ (roughly). The increase in the magnitude of C_{z_α} (the coefficient is negative) produces some increase in the damping of the aircraft longitudinal short period mode.

The rotor contributes to C_{x_u} in the same direction as the aircraft drag contribution (making C_{x_u} more negative). The rotor contribution is due to the

rotor thrust damping T_λ and hence is an order of magnitude larger than the aircraft drag contribution. The result is an increase in the phugoid mode damping and also in the sensitivity to longitudinal gusts. The great increase in C_{x_u} over the usual aircraft values also may change the motion involved in the longitudinal modes.

The rotor contribution to C_{m_q} moves the maneuver point h_m, typically 5 to 7 percent of the MAC. The maneuver margin is decreased for the gimballed rotor because of the negative H force and is increased for the cantilever rotor because of the hub moment capability. This indicates the need for about 40 percent more and less horizontal tail effectiveness, respectively. Equivalently, because of the rotor, the short period mode damping and frequency are decreased for the gimballed rotor and increased for the cantilever rotor. Note that, with the high wing configuration of the tilt rotor aircraft, pitching about the center of gravity also introduces a T_λ contribution to C_{m_q}, which always increases h_m (less horizontal tail effectiveness required).

The rotor contribution to C_{ℓ_p} is of the same order and sign as the wing contribution. Both the rotor H force and torque terms have the same sign, and both (H_μ/V and Q_ζ'/V) increase with V approximately as sin ϕ. The H force contribution is about the same as that of the torque for the gimballed rotor, but larger for the cantilever rotor. As a result, the aircraft roll damping is increased significantly, and hence the roll mode time control is decreased to typically half the value due to the wing alone.

The rotor contribution to C_{n_β} is always negative and, compared with the positive term from the vertical tail, the rotor term is small for the gimballed rotor but more significant for the cantilever rotor. An increase in vertical tail effectiveness is then required, especially for a cantilever rotor or, equivalently, the rotor decreases the aircraft Dutch roll mode frequency.

The rotor contributes to C_{n_r} by a T_λ term and a pivot moment term. To counter the rotor contribution (maintain the same net C_{n_r}), the T_λ term always requires less tail; the pivot moment term requires more tail for the gimballed rotor because of the negative H force, but less tail for a cantilever rotor because of the hub moment. The T_λ term dominates, though just barely for the gimballed rotor, so the net result is a requirement for less vertical tail to maintain the same value of C_{n_r}, especially for the cantilever rotor. Equivalently, the rotor influence means an increase in the Dutch roll damping.

The rotor contribution to C_{ℓ_β} is typically equivalent to about 5° of wing dihedral (by the present estimate). The rotor derivative involved is a cross term - a vertical force due to a lateral velocity - so it is proportional to N_* (K_P for the gimballed rotor), and the contribution to the aircraft derivative is proportional to the rotational direction of the rotor ($sgn\ \Omega$). The rotor contribution, in terms of the wing dihedral required to counter it, has the same sign as $-sgn\ \Omega$ for the cantilever rotor, and the same sign as $K_P\ sgn\ \Omega$ for the gimballed rotor. For the rotors considered here, more wing dihedral is required for the cantilever ($sgn\ \Omega = -1$) and less for the gimballed rotor ($K_P < 0$ and $sgn\ \Omega = 1$); or, equivalently, the rotor produces worse and

better spiral mode stability, respectively. Generally, the rotor contributes significantly to C_{ℓ_β}, the direction depending on the rotor rotation direction, whether a cantilever or articulated rotor is involved, and on pitch/flap coupling for the articulated rotor. Note that the large tip pylons usually associated with the tilt rotor configuration also contribute significantly to C_{ℓ_β}.

The rotor contribution to C_{y_β} is negative and several times the negative contribution of the vertical tail. Hence it requires less vertical tail or, equivalently, increases the Dutch roll damping. The influence of C_{y_β} is usually considered secondary to that of C_{n_r}, however.

The rotor contribution to C_{n_p} is an order of magnitude larger than the wing term; $C_{n_p} < 0$ is adverse yaw, which is the direction of the wing contribution. There is a thrust term and a pivot moment term from the rotor. In comparison to the wing term (so that positive ratio means adverse yaw), the T_ζ' term has the same sign as $sgn\ \Omega$; the pivot moment term has the same sign as $sgn\ \Omega$ for a cantilever rotor and the same sign as $K_P\ sgn\ \Omega$ for a gimballed rotor. The pivot moment contribution is small, however, especially for the gimballed rotor, and the T_ζ' term dominates. Hence the net contribution to $\Delta C_{\ell_p}/C_{\ell_p}$ has the same sign as $sgn\ \Omega$ and, with variations in V, it behaves as $V \sin \phi\ (T_\zeta'/VC_L)$. For the rotors used here, the rotor contribution for the gimballed rotor is adverse yaw and, for the cantilever rotor, it is favorable yaw. Since the rotor results in a coefficient larger by an order of magnitude than usual for aircraft, however, it is expected to significantly alter the lateral modes of the aircraft.

The rotor contribution to C_{ℓ_r}, like that to C_{n_p}, is an order of magnitude larger than the wing contribution. Relative to the wing term (i.e., $\Delta C_{\ell_r}/C_{\ell_r}$), the torque term has the same sign as $-sgn\ \Omega$, while the hub force term has the same sign as $-sgn\ \Omega$ for the cantilever rotor and the same sign as $K_P\ sgn\ \Omega$ for the gimballed rotor. The hub force and torque terms have approximately equal magnitudes; hence the sum would be small for an articulated rotor with $K_P > 0$. With the present examples then, the rotor contribution is in the same direction as the wing contribution for the cantilever rotor and opposite for the gimballed rotor. The increase in the magnitude of C_{ℓ_r} is expected to significantly alter the lateral modes of the aircraft.

In summary, the influence of the proprotor on the aircraft dynamics is as follows. The static longitudinal stability (static margin) is decreased (C_{m_α}); the phugoid damping is increased (C_{x_u}); the short period damping is increased somewhat by C_{z_α} (but influenced primarily by C_{m_q}); the roll damping is increased (C_{ℓ_p}); the Dutch roll frequency is decreased, especially for the cantilever rotor; and the Dutch roll damping is increased, especially for the cantilever rotor (C_{n_r}, and also C_{y_β}). Because of C_{m_q}, the short-period damping and frequency (i.e., maneuver margin) are decreased for the gimballed rotor (due to the negative H force damping) and are increased for the cantilever rotor (due to the hub moment capability). The rotor significantly influences the spiral mode stability (C_{ℓ_β}), the direction depending on the rotor rotation direction and also on ν_β and K_P. Three of the rotor contributions - C_{ℓ_β}, C_{n_p}, and C_{ℓ_r} - are lateral/vertical coupling rotor coefficients, hence they are proportional to $sgn\ \Omega$ and also depend on ν_β and K_P, the rotor coupling parameters (N_*). Three of the rotor contributions - C_{x_u}, C_{n_p}, and C_{ℓ_r} - are an

order of magnitude larger than the usual aircraft derivatives and therefore may be expected to significantly alter both the longitudinal and lateral modes of motion of the aircraft.

It is concluded that flapping rotors operating in high inflow contribute substantially to the aircraft derivatives. A numerical estimate of the rotor contributions to the aircraft stability derivatives, from the expressions given here, would probably not be adequate, primarily because rotor lag and wing motions were neglected.

Stability Derivative Nomenclature

F_x, F_y, F_z	aircraft longitudinal, lateral, and vertical forces (subscripts x, y, z for coefficients)
N_x, N_y, N_z	aircraft roll, pitch, and yaw moments (subscripts ℓ, m, n for coefficients)
u, β, α	aircraft longitudinal, lateral (sideslip), and vertical (angle of attack) velocity perturbations
p, q, r	aircraft roll, pitch, and yaw angular velocities
ℓ_w	wing span
h	mast height (aircraft center of gravity to rotor hub)
$\bar{c}_w$	wing chord
S_w	wing area
C_{L_α}	aircraft lift curve slope
C_L	aircraft lift coefficient
S_t	horizontal tail area
ℓ_t	horizontal tail arm
a_t	horizontal tail lift curve slope
S_v	vertical tail area
ℓ_v	vertical tail arm
a_v	vertical tail lift curve slope
$sgn\ \Omega$	rotor rotation direction
q	in coefficients, dynamic pressure $(1/2)\rho V^2$
h_n	neutral point

Stability Derivative Nomenclature (Concl.)

h_m maneuver point

Γ wing dihedral

The aircraft stability derivatives are defined as they are introduced.

SECTION 4: NINE-DEGREE-OF-FREEDOM MODEL FOR A PROPROTOR ON A CANTILEVER WING

Wing Equations of Motion

In this chapter, the equations of motion for a proprotor on a cantilever wing are derived. The equations of motion and the hub forces and moments were obtained previously for the six rotor degrees of freedom (blade collective and cyclic flap and lag motion), including the excitation by the six degrees of freedom of the shaft motion (eqs. (44) to (48)). The equations of motion for the wing elastic bending and torsion motion are now derived. The wing degrees of freedom are forced by the rotor hub forces and moments, and each mode of wing motion produces a corresponding shaft motion. Thus the two sets of equations, for the rotor and for the wing, are combined by substituting the wing degrees of freedom for the shaft motion in the rotor equations of motion and forces, and then substituting for the rotor forces in the wing equations of motion. The result is a coupled set of equations that describes the aeroelastic behavior of the proprotor and wing system.

The proprotor aircraft configuration consists of large diameter flapping rotors mounted on the wing tips. Usually, the engine and transmission are also mounted in the pylon at the wing tip; hence there is a large mass and inertia at the wing tip. The rotor hub forces are transmitted to the wing tip through a mast of height h (i.e., forward of the pylon pivot).

The dynamics specific to the proprotor configuration are of primary interest here, that is, the high inflow rotor dynamics coupled with the wing/pylon motion. Hence the model considered is restricted entirely to the airplane cruise mode configuration, with the shaft parallel to the free-stream velocity. The model is restricted also to the frequency range most important to the coupled wing and rotor motion. Only the lowest frequency wing modes are considered, and the elastic motion of the pylon with respect to the wing tip is neglected since it usually has a much higher natural frequency than the lowest wing modes. The motion considered then is the wing elastic motion with the pylon and the rotor shaft rigidly attached to the wing tip. The aircraft rigid-body motions are also neglected since they are degrees of freedom of low frequency and are not highly coupled with the motions to be examined. Neglecting the rigid-body motion places the primary emphasis on the basic rotor and wing dynamics, as is desired here, and so may be justified as an appropriate first step at least. Indeed this rotor and cantilever wing model is very useful in establishing the behavior of the proprotor aircraft. Hence a

cantilever wing model is used for the fixed system motion, with the understanding, of course, that eventually a more complete model including the aircraft motion must be used. In addition, the cantilever model corresponds to the configuration of many proprotor models that have been tested in wind tunnels, including the full-scale tests considered later.

The model considered consists of a wing and rotor in cruise flight configuration, operating in a free-stream velocity V with the shaft always parallel to V so that the rotor equilibrium flow is purely axial. The rotor operates in high inflow. The wing root is attached to an immovable support with cantilever root restraint. The wing motion consists of elastic bending, vertical and chordwise, and elastic torsion. A pylon with large mass and moment of inertia is rigidly attached to the wing tip. The rotor is mounted on the pylon with the hub forward of the wing elastic axis, with the rotor shaft horizontal (parallel to V). The rotor has three or more blades, with first mode flap and lag motion for each blade. The rotor hub forces and moments are transmitted through the pylon to the wing tip.

The wing is assumed to have a high aspect ratio so that strip theory can be used for the wing aerodynamics and engineering beam theory for the elastic bending; this assumption is well justified for the tilt rotor aircraft, which have, typically, an aspect ratio around 6. Wing sweep, dihedral, and angle of attack are considered, but the major effect is that of the wing sweep on the position of the effective elastic axis of the wing, hence on the effective mast height for the transmission of the rotor hub forces to the wing bending and torsion motion. Regardless of the wing sweep, dihedral, or angle of attack, the rotor shaft is assumed to be maintained parallel to the free-stream velocity in equilibrium trim flight. This assumption is required to avoid periodic coefficients in the rotor equations of motion due to an inplane component of the trim velocity.

Wing geometry and motion- The wing geometry is defined by a straight spar line that is the locus of the local elastic axis. The wing root is supported with cantilever restraint; the rotor shaft is attached rigidly to the wing tip. The wing geometry is shown in figure 11. The wing has a constant chord c_w and a length y_{T_w} from root to tip (semispan). The distance along the spar is y_w, measured from the root. The shaft has length h, the distance the rotor hub is forward of the wing tip elastic axis (mast height). The wing spar is basically perpendicular to the forward velocity V, but small wing sweep, dihedral, and angle of attack are considered. The wing root is attached to a plane defined by the forward velocity V and the vertical; then three rotation angles define the orientation of the spar with respect to the free-stream velocity: dihedral δ_{w_1} (positive for upward rotation of the wing tip), sweep δ_{w_3} (positive for sweep aft), and angle of attack δ_{w_2} (positive nose-up). All these angles are assumed to be small, an appropriate assumption for proprotor aircraft in cruise. The rotor shaft must then be rotated by the angles $-\delta_{w_1}$, $-\delta_{w_2}$, and $-\delta_{w_3}$ to keep the shaft parallel to the free-stream velocity.

The rotor (fig. 3) is placed on the tip of the wing (fig. 11) so that the wing tip motion is transmitted directly to the rotor shaft. It is also necessary to account for the rotational direction of the rotors. The aircraft has two counterrotating rotors, one on each wing tip, but the rotational direction

of the rotor on the right wing (fig. 11) may be either clockwise or counterclockwise. The equations of motion and hub forces for the rotor are derived for the rotor model in figure 3, that is, assuming clockwise rotation. This model is always used for the rotor, and then the rotational direction of the rotor is accounted for by placing the rotor on a right-hand wing (fig. 11) or on a left-hand wing as appropriate. The influence of the rotational direction is a number of sign changes in the equations of motion, which reflect how the hub forces and moments of the standard rotor (fig. 3) excite the right or left wing, and how the right or left wing produces motion of the rotor shaft.

The notation Ω indicates the influence of the rotational direction of the rotor. The clockwise rotating rotor on the right wing (figs. 3 and 11) is denoted by $\Omega = 1$; the clockwise rotor on the left wing (fig. 3 and the mirror image in fig. 11) is denoted by $\Omega = -1$:

$$\Omega = \left\{ \begin{array}{l} +1;\ \text{rotor rotation clockwise on right wing,} \\ \qquad \text{counterclockwise on left wing} \\ \\ -1;\ \text{rotor rotation counterclockwise on right wing,} \\ \qquad \text{clockwise on left wing} \end{array} \right\} \tag{174}$$

The wing motion is described by elastic bending and torsion of the wing spar; the wing displacement is shown in figure 11. The pylon (and with it the shaft) is rigidly attached to the wing tip. The existence of an elastic axis of the wing (assumed to be a straight line) means that the wing distortion may be described first by elastic torsion of the wing about the local elastic axis, without bending the wing; and then by elastic bending of the spar, which deflects the elastic axis from the undistorted position without changing the torsional deflection.

A modal description of the wing elastic deformation is used, and only the lowest frequency modes are retained. The elastic torsion of the wing results in a pitch change $\theta_w(t,y_w)$ of the local wing section (positive nose-up as shown in fig. 11). With a modal representation, this motion is written

$$\theta_w = \sum_i p_i(t)\,\xi_{w_i}(y_w)$$

which is an expansion of θ_w in a series of the mode shapes ξ_{w_i} of the elastic torsion motion. The generalized coordinates p_i are the degrees of freedom. The modal representation is useful because it separates the time and space dependence of θ_w. Associated with each degree of freedom p_i, there is an equation of motion with appropriate generalized mass and stiffness, hence a natural frequency of each mode. Only the lowest frequency degrees of freedom are retained in this study of the basic dynamics; it is sufficient, in fact, to consider only one wing torsion mode. Then,

$$\theta_w = p(t)\,\xi_w(y_w) \tag{175}$$

describes the motion. If the mode shape is normalized to unity at the tip, $\xi_w(y_{T_w}) = 1$, then p gives the nose-up torsion angle in radians at the tip.

The elastic bending of the wing results in the deflection of the wing spar with components both perpendicular to the wing surface (vertical or beamwise bending) and parallel to the wing surface (chordwise bending). The deflection of the spar line normal to the wing surface is $z_w(t, y_w)$, defined positive for upward deflection. The deflection in the plane of the wing is $x_w(t, y_w)$, defined positive for rearward deflection. The vertical and chordwise bending z_w and x_w are defined with respect to the direction of the local principle axes of the section. With no built-in wing twist, these axes are the same all along the wing spar, but they are not vertical or horizontal because of the wing sweep, dihedral, and angle of attack. A modal representation is used for the bending deflections, both vertical and chordwise, and only the lowest frequency modes are retained. For this analysis, it is sufficient to retain only one mode each for the z_w and x_w representations; hence

$$\left.\begin{aligned} z_w &= q_1(t)\eta_w(y_w) \\ x_w &= q_2(t)\eta_w(y_w) \end{aligned}\right\} \tag{176}$$

where η_w is the mode shape of elastic bending of the wing. For the present purposes, it is sufficient to use the same mode shape for both vertical and chordwise bending, but including different modes would be straightforward. The generalized coordinates q_1 and q_2 are the degrees of freedom that represent wing vertical and chordwise bending, respectively. If the mode shape is normalized to y_{T_w} at the tip, $\eta_w(y_{T_w}) = y_{T_w}$, then the degree of freedom q_1 represents the ratio of the tip deflection to the semispan and, similarly, for q_2.

The degrees of freedom that represent the wing motion are thus:

p, wing elastic torsion, positive nose-up ($p = \theta_w$ at the tip);

q_1, wing vertical or beamwise bending, positive upward ($q_1 = z_w/y_{T_w}$ at the tip);

q_2, wing chordwise bending, positive rearward ($q_2 = x_w/y_{T_w}$ at the tip)

Associated with these degrees of freedom are mode shape $\xi(y_w)$ for torsion and $\eta_w(y_w)$ for bending, which are normalized to ℓ and y_{T_w}, respectively, at the tip. The assumption of cantilever root restraint also gives the boundary conditions $\xi_w(0) = \eta_w(0) = \eta_w'(0) = 0$ at the root.

Consider the motion of the rotor shaft in terms of the wing degrees of freedom. The shaft displacement and rotation (x_P, y_P, z_P, α_x, α_y, α_z) at a point h aft of the hub are required because of the motion at the wing tip, which is specified by the wing degrees of freedom (q_1, q_2, and p). If one neglects for the moment the effects of the rotor rotation direction and wing sweep, dihedral, and angle of attack, the following shaft motion is produced. The wing torsion deflection p results in shaft pitch α_y. The wing vertical bending q_1 results in vertical displacement x_P of the shaft; and since bending also produces a slope of the elastic axis at the tip, it results in shaft roll

α_z. The wing chordwise bending q_2 results in longitudinal displacement z_P of the shaft and also shaft yaw angle α_x. With this model, there is no first-order source of shaft lateral displacement y_P. If the magnitude of the displacement and rotation at the tip due to the wing degrees of freedom (given by the mode shapes) are accounted for, the shaft motion is (for a clockwise rotating rotor on the right wing, figures 3 and 11, with $\delta_{w_1} = \delta_{w_2} = \delta_{w_3} = 0$)

$$\left.\begin{aligned} \alpha_x &= -q_2 \eta_w'(y_{T_w}) \\ \alpha_y &= p\xi_w(y_{T_w}) = p \\ \alpha_z &= -q_1 \eta_w'(y_{T_w}) \\ x_P &= q_1 \eta_w(y_{T_w}) = q_1 y_{T_w} \\ y_P &= 0 \\ z_P &= -q_2 \eta_w(y_{T_w}) = -q_2 y_{T_w} \end{aligned}\right\} \tag{177}$$

Note that the wing bending motion produces coupling of the longitudinal and the lateral/vertical groups of the rotor, q_1 and q_2, giving both longitudinal motion of the shaft (z_P and α_z) and lateral/vertical motion (x_P and α_x). The coupling is not strong, however, and it is found from the behavior of the system that wing chordwise bending q_2 is basically a longitudinal motion, and vertical bending and torsion (q_1 and p) belong with the lateral/vertical group.

Consider the clockwise rotating rotor on the left wing, that is, $\Omega = -1$: the only change is in the direction of the shaft angle due to the slope of the elastic axis at the tip during bending (consider the mirror image in fig. 11, including the definitions of the bending and torsion deflection). If this change in sign is incorporated by use of the Ω notation,

$$\left.\begin{aligned} \alpha_x &= -q_2 \Omega \eta_w'(y_{T_w}) \\ \alpha_y &= -q_1 \Omega \eta_w'(y_{T_w}) \end{aligned}\right\} \tag{178}$$

and the rest of the shaft motion in equations (177) is unchanged. If the wing motion produced a lateral shaft displacement y_P, that, too, would change sign with the direction of rotor rotation.

Consider the effect of wing sweep, dihedral, and angle of attack. The wing tip displacement and rotations, along with the wing motion, are defined with respect to the wing spar and the section principal axes - which are rotated by δ_{w_1}, δ_{w_2}, and δ_{w_3} with respect to the wind axes. Hence the wing tip motion will have a slightly different decomposition into the shaft motion, which remains in the wind axes. For example, vertical bending q_1 produces, in addition to vertical displacement x_P and shaft roll α_z as given previously, some shaft pitch α_y due to the wing sweep δ_{w_3}, some lateral displacement y_P due to the wing dihedral δ_{w_1}, and some shaft yaw α_x and axial displacement z_P due to angle of attack δ_{w_2}. After a consideration of the complete set of wing and shaft motions, the result is

$$
\left.
\begin{aligned}
\alpha_x &= -q_2 \Omega \eta_w'(y_{T_w}) + p\Omega\delta_{w_1} - q_1 \delta_{w_2} \Omega \eta_w'(y_{T_w}) \\
\alpha_y &= p + q_2 \Omega \delta_{w_1} \Omega \eta_w'(y_{T_w}) - q_1 \Omega \delta_{w_3} \Omega \eta_w'(y_{T_w}) \\
\alpha_z &= -q_1 \Omega \eta_w'(y_{T_w}) - p\Omega\delta_{w_3} + q_2 \delta_{w_2} \Omega \eta_w'(y_{T_w}) \\
x_P &= q_1 y_{T_w} - q_2 \delta_{w_2} y_{T_w} \\
y_P &= -q_1 \Omega \delta_{w_1} y_{T_w} - q_2 \Omega \delta_{w_3} y_{T_w} \\
z_P &= -q_2 y_{T_w} - q_1 \delta_{w_2} y_{T_w}
\end{aligned}
\right\} \qquad (179)
$$

Note that the effect of the rotational direction of the rotor, Ω, is only to change the signs of α_x, α_z, and y_P.

The influence of the wing sweep (and dihedral) requires more attention than given above. Consider the unswept wing, represented by a straight unswept elastic axis line with cantilever restraint at the root. This structure has these characteristics: elastic torsion at an inboard wing section results in pitch changes at outboard sections, but produces no vertical or chordwise displacement of the elastic axis from its undistorted position; and a force applied to the wing tip at the elastic axis results in bending of the wing, but produces no torsion motion since there is no torsion moment about any section due to this force. Thus, there is no elastic coupling of the wing bending and torsion motions.

If the wing is now swept, that behavior would be maintained if the root restraint were also swept. In that case, the description developed for the shaft motion produced by the wing torsion and bending would be correct, including the effects of sweep and dihedral. However, this is not the way swept wings (of the type used for proprotor aircraft) are built. The wings are usually built with a center box structure in the fuselage, where the spars are unswept, and only the wing structure outside the fuselage has swept spars. The wing is restrained at several points, where the wing box is tied to the fuselage. (The wing used in the full-scale, wind-tunnel tests considered later was also built this way.) One approach to treating such a structure is to use a good structural dynamics analysis to calculate the coupled bending and torsion modes of the wing and pylon, including the influence of the root restraint and sweep. Such an approach is useful if available and, in fact, it is probably necessary if an accurate representation of a specific design is required. Such an analysis is not desired here, however, rather the simplest representation that includes only the elements most fundamental to the behavior. Since this report is aimed at a general examination of proprotor dynamics rather than the design of a specific vehicle (with a swept wing), such a representation is adequate.

The model used to represent a swept wing has a straight elastic axis line except for a bend at span station $y_w = y_{B_w}$, where the wing sweep and dihedral

are entered. The root restraint and the wing inboard of y_{B_w} are unswept, while the outboard section is swept. The mast height h is measured from the wing tip elastic axis to the rotor hub. The following behavior is expected of such a model, typical of swept wing behavior: elastic torsion of the inboard sections produces a pitch change at y_{B_w}, which then rotates the entire outboard section about the extension of the inboard spar line, thereby producing displacements of the outboard elastic axis from its undistorted position; and a force (vertical for the sweep effect) at the tip elastic axis produces a torsional moment about the wing sections inboard of y_{B_w}, thereby producing torsion motion of the wing rather than just bending as for the unswept case. The torsion and bending motions of the wing are then elastically coupled. The first effect, in particular, means that torsion of the wing now results in the displacement of the wing spar, which is produced only by bending for the unswept wing. Specifically, the torsion motion produces now displacements at the tip - hence of the shaft - as well as rotation of the shaft. An advantage of this model is that the shaft motion due to the wing degrees of freedom can be obtained by simple geometric considerations, and the wing equations of motion can be obtained by a simple extension of the methods (based on section force and moment equilibrium) used for an unswept wing. Both are the result of retaining the representation of the wing by an elastic axis line. The wing motion is defined then by elastic torsion about the local elastic axis (producing local elastic pitch changes given by the mode shape ξ_w, and elastic axis deflections due to the sweep), followed by elastic bending of the spar (producing local spar displacement given by the mode shape η_w, from the displacement due to torsion). The effect of the bent elastic axis is to couple the influence of torsion and bending; with sweep, the tip is displaced due to torsion, and also the torsion mode is excited by forces at the tip elastic axis.

A swept wing is characterized by an effective elastic axis for the vertical bending of the tip: at some point on the shaft or its extension, the application of a vertical force results in purely vertical displacement of the shaft, with no rotation. Without sweep of the wing, this point would be at the wing tip elastic axis; but with sweep, a force there produces a nose-down pitch motion of the shaft also (for aft sweep). Hence the effective elastic axis is some distance forward of the wing tip elastic axis. This feature is included in the model used here. Generally, the effective elastic axis (for the tip) lies between the actual wing tip elastic axis and the extension of the inboard (unswept) spar line - the actual position depending on the degrees of root restraint and sweep and other structural details.

The model used here is, in fact, only conceptual. It is used because it allows an elementary derivation of the equations of motion, including the most important features of the swept wing behavior. The bend in the spar is not a feature that can be determined accurately from the geometry of the wing. Hence y_{B_w}, the spanwise location of the spar bend, is just a parameter that characterizes the influence of the wing sweep on the coupled bending and torsion motions of the wing, which is determined by the details of the wing structural construction, geometry, and root restraint. This parameter (it will be found that what is really required is $\xi_w(y_{B_w})$) can be identified by matching the behavior of the model to that known from a better model or from actual experiment. The most important feature of the swept wing is the effective elastic axis position at the wing tip. If that is known from a good structural

analysis of the wing, or measured experimentally, then the corresponding value of y_{B_w} which gives that effective elastic axis position for the model used here may be determined. Then that single parameter completely determines all the characteristics of the swept wing in this model.

The influence of the bent elastic axis model on the rotor shaft motion due to the wing degrees of freedom can now be determined from simple geometric considerations. Wing pitch deflection at y_{B_w} rotates the entire outboard portion of the wing about the inboard spar line, so torsion of the wing produces displacements at the wing tip - vertically due to sweep of the wing and longitudinally due to dihedral. The rotation angle is $\theta_w(y_{B_w}) = p\xi_w(y_{B_w})$ and the arm at the tip is $(y_{T_w} - y_{B_w})\delta_{w_3} \cong y_{T_w}\delta_{w_3}$ (to first order for small δ_{w_3} and y_{B_w}/y_{T_w}) for sweep, and $(y_{T_w} - y_{B_w})\delta_{w_1} \cong y_{T_w}\delta_{w_1}$ for dihedral. The increments in the shaft vertical and longitudinal displacement are then

$$\left.\begin{aligned} \Delta x_P &= -p\xi_w(y_{B_w})y_{T_w}\delta_{w_3} \\ \Delta z_P &= -p\xi_w(y_{B_w})y_{T_w}\delta_{w_3} \end{aligned}\right\} \tag{180}$$

The complete equations for the shaft motion due to the wing degrees of freedom are

$$\left.\begin{aligned} \begin{pmatrix} \alpha_x \\ \alpha_y \\ \alpha_z \end{pmatrix} &= \begin{bmatrix} -\Omega\eta_w'\delta_{w_2} & -\Omega\eta_w' & \Omega\delta_{w_1} \\ -\Omega\eta_w'\Omega\delta_{w_3} & \Omega\eta_w'\Omega\delta_{w_1} & 1 \\ -\Omega\eta_w' & \Omega\eta_w'\delta_{w_1} & -\Omega\delta_{w_3} \end{bmatrix} \begin{pmatrix} q_1 \\ q_2 \\ p \end{pmatrix} \\ \begin{pmatrix} x_P \\ y_P \\ z_P \end{pmatrix} &= \begin{bmatrix} y_{T_w} & -\delta_{w_2}y_{T_w} & h_{EA} - h \\ -\Omega\delta_{w_1}y_{T_w} & -\Omega\delta_{w_3}y_{T_w} & 0 \\ -\delta_{w_2}y_{T_w} & -y_{T_w} & z_{EA} \end{bmatrix} \begin{pmatrix} q_1 \\ q_2 \\ p \end{pmatrix} \end{aligned}\right\} \tag{181}$$

The length $h_{EA} = h - \xi_w\delta_{w_3}y_{T_w}$ is the distance from the effective tip elastic axis to the rotor hub and, similarly, for $z_{EA} = -\xi_w\delta_{w_1}y_{T_w}$, the vertical elastic axis displacement due to dihedral. For convenience, $\eta_w'^w$ is written for $\eta_w'(y_{T_w})$ and ξ_w, for $\xi_w(y_{B_w})$.

Wing Equations of Motion- The equations of motion for the wing degrees of freedom, lowest mode elastic bending and torsion, are

$$\left.\begin{aligned} (I_{q_w} + m_P y_{T_w}^2)\ddot{q}_1 + C_{q_1}\dot{q}_1 + K_{q_1}q_1 + S_w\ddot{p} &= M_{q_{1_{aero}}} + M_{q_{1_{rotor}}} \\ (I_{q_w} + I_{P_x}\eta_w'^2 + m_P y_{T_w}^2)\ddot{q}_2 + C_{q_2}\dot{q}_2 + K_{q_2}q_2 - S_w\delta_{w_2}\ddot{p} &= M_{q_{2_{aero}}} + M_{q_{2_{rotor}}} \\ (I_{P_w} + I_{P_y})\ddot{p} + C_p\dot{p} + K_P p + S_w\ddot{q}_1 - S_w\delta_{w_2}\ddot{q}_2 &= M_{P_{aero}} + M_{P_{rotor}} \end{aligned}\right\} \tag{182}$$

for the vertical bending, chordwise bending, and torsion motion, respectively. Each equation has inertia, structural damping, and structural spring terms, forced by wing aerodynamic forces and by the rotor hub forces and moments acting on the wing tip. The generalized inertia of the wing bending mode is $I_{q_w} = \int_0^{y_{T_w}} m_w \eta_w^2 \, dy_w$, and for the torsion mode, $I_{p_w} = \int_0^{y_{T_w}} I_{\theta_w} \xi_w^2 \, dy_w$, where m_w is the mass per unit length of the wing and I_{θ_w} is the wing section moment of inertial. To these wing inertias are added the pylon inertia terms: m_P is the pylon mass (without the rotor) and I_{P_x} and I_{P_y} are, respectively, the pylon yaw and pitch moments of inertia about the wing tip effective elastic axis. The inertia coupling of the bending and torsion of the wing is due to the offset of the pylon center of gravity: $S_w = m_P y_{T_w} z_{PEA}$, where z_{PEA} is the distance the pylon center of gravity (without the rotor) is ahead of the wing tip effective elastic axis. The structural spring terms are written

$$K_{q_1} = \int_0^{y_{T_w}} EI_{zz} \eta_w''^2 \, dy_w$$

$$K_{q_2} = \int_0^{y_{T_w}} EI_{xx} \eta_w'^2 \, dy_w$$

$$K_P = \int_0^{y_{T_w}} GJ_w \xi_w'^2 \, dy_w$$

where EI_{zz} is the section beamwise modulus/inertia product and, similarly, for the chordwise and torsion elastic restraint. These expressions are not used here, however, since a very accurate estimate of the bending and torsion mode shapes would be required to evaluate them.

The derivation of these modal equations follows the standard methods of aeroelastic analysis. For typical proprotor configurations, the pylon mass is so large that it dominates the wing inertias, that is, $I_{q_w} << m_P y_{T_w}^2$ and $I_{p_w} << I_{P_y}$. Hence the inertia is primarily that of the pylon and rotor, with the wing contributing only the elastic restraint of the motion. This is fortunate in that calculating the wing inertias requires an accurate estimate of the mode shapes, while the pylon mass and moments of inertia are well-defined characteristics that are easily determined. The wing structural spring constants (K_{q_1}, K_{q_2}, and K_p) are best determined by adjusting their values so that the predicted frequencies of the modes match the frequencies measured experimentally. By this procedure, the wing inertias and structural parameters are determined from the characteristics most well defined and easily measured: pylon inertia and natural frequencies of the modes. It is particularly important to match the measured frequencies well since they have the most important influence on the dynamic behavior of the system. This procedure is satisfactory here, but, for the preliminary design of an actual vehicle, a good structural analysis method for predicting the generalized masses and stiffnessess of the wing and pylon modes is necessary. It is evident that (for the lowest wing modes at least) the wing mode shapes have a secondary influence on

the equations of motion. A very rough approximation to η_w and ξ_w is satisfactory to estimate the wing contributions I_{q_w} and I_{p_w} to the inertias since they are dominated by the pylon contributions; the structural spring constants and other parameters such as $\eta_w'(y_{T_w})$ are determined by matching them to the measured characteristics of the wing (or those calculated by a more accurate method) rather than using their definitions in terms of the wing mode shapes (which are not really available).

The wing structural damping constants (C_{q_1}, C_{q_2}, and C_p) are determined, as the spring constants are, by matching the theoretical results to the measured characteristics. By definition, the damping constants are given by $\sqrt{K/I}\, g_s$ with the appropriate inertia and spring constant, where g_s is the measured structural damping coefficient of the wing (twice the fraction of critical damping). The wing structural damping is typically 1 or 2 percent of the critical damping.

The wing motion is excited by the rotor forces and moments acting at the hub. For the moment, if the effects of the rotor rotation direction and of the wing sweep, dihedral, and angle of attack are neglected, the rotor forcing terms are

$$\left.\begin{aligned} M_{q_1}{}_{rotor} &= \eta_w' Q + y_{T_w} H \\ M_{q_2}{}_{rotor} &= -\eta_w'(M_x - hY) - y_{T_w} T \\ M_{p}{}_{rotor} &= M_y + hH - C^*_{pq} y_{T_w} T q_1 \end{aligned}\right\} \qquad (183)$$

where $C^*_{pq} = \int_0^{y_{T_w}} \xi_w \eta_w'\, dy_w/y_{T_w} \cong 2/3$. The excitation of wing vertical bending q_1 is due to rotor torque and vertical force, with the effectiveness of the former determined by the slope of the mode shape at the tip $\eta_w'(y_{T_w})$ (written as η_w' in eqs. (183)) and for the latter, by its displacement $\eta_w(y_{T_w}) = y_{T_w}$. Similarly, the excitation of chordwise bending q_2 is due to the pivot yaw moment $(M_x - hY)$ and the thrust force. The wing torsion motion is excited by p, the pivot pitch moment $(M_y + hH)$, and by the trim thrust. The thrust term results because wing vertical bending q_1 elevates the rotor trim thrust above the inboard sections and so gives an arm about which the trim thrust produces a torsion moment; the constant involved, C^*_{pq}, was evaluated using the approximation $\xi_w = y_w/y_{T_w}$ and $\eta_w = y_w{}^2/y_{T_w}$ for the wing modes.

Introducing the influence of the rotor rotation direction, that is, putting the rotor in figure 3 on a left-hand wing, simply changes the signs of

the moment contributions to the wing bending excitation. If the convention for Ω (given previously) is used to indicate these sign changes, the result is

$$\left.\begin{aligned} M_{q_1}{}_{rotor} &= \Omega\eta_w' Q + y_{T_w} h \\ M_{q_2}{}_{rotor} &= -\Omega\eta_w' (M_x - hY) - y_{T_w} T \end{aligned}\right\} \tag{184}$$

and $M_{p_{rotor}}$ remains unchanged.

If wing sweep, dihedral, and angle of attack are considered, the first influence is a slightly different decomposition of the rotor forces, which are defined with respect to the shaft (wind) axes, into the wing tip axes for determining the excitation of the wing bending and torsion. With the appropriate coordinate rotations, the result is

$$\left.\begin{aligned} M_{q_1}{}_{rotor} &= \Omega\eta_w' [Q - \Omega\delta_{w_3}(M_y + hH) - \delta_{w_2}(M_x - hY)] \\ &\quad + y_{T_w}(H - \Omega\delta_{w_1} Y - \delta_{w_2} T') \\ M_{q_2}{}_{rotor} &= \Omega\eta_w' [-M_x + hY + \Omega\delta_{w_1}(M_y + hH) - \delta_{w_2} Q] \\ &\quad + y_{T_w}(-T - \Omega\delta_{w_3} Y - \delta_{w_2} H) \\ M_{p}{}_{rotor} &= M_y + hH + \Omega\delta_{w_3} Q + \Omega\delta_{w_1}(M_x - hY) \\ &\quad + C^*_{pq} y_{T_w} T(-q_1 + \delta_{w_2} q_2) \end{aligned}\right\} \tag{185}$$

However, these expressions are for a wing that is swept along its entire length, including the root restraint. The model considered here has the inboard portion unswept, and only the wing outboard of $y_{t_w} = y_{B_w}$ has sweep and dihedral. With this model, there are also the additional terms:

$$
\left.
\begin{aligned}
\Delta M_{q_{1_{rotor}}} &= \delta_{w_3}\eta_w'(y_{B_w})(M_y + hH) + \Omega\delta_{w_1}\eta_w(y_{B_w})Y \\
\Delta M_{q_{2_{rotor}}} &= -\delta_{w_1}\eta_w'(y_{B_w})(M_y + hH) + \Omega\delta_{w_3}\eta_w(y_{B_w})Y \\
\Delta M_{p_{rotor}} &= \xi_w(y_{B_w})[-\Omega\delta_{w_3}Q - \Omega\delta_{w_1}(M_x - hY) \\
&\quad - \delta_{w_3}y_{T_w}H - \delta_{w_1}y_{T_w}T]
\end{aligned}
\right\} \qquad (186)
$$

The terms in equations (186) (except for last two in the torsion moment) simply account for the decrease in the effect of the δ_{w_1} and δ_{w_3} components of the rotor forces and moments in exciting the wing when not all of the wing has sweep and dihedral. These terms combine with the similar terms in equations (185) to produce a reduced net influence. For example, sweep of the wing produces a component $\delta_{w_3}M_y$ of the rotor pitch moment that tends to produce vertical bending motion, that is, it contributes to $M_{q_{1_{rotor}}}$. The corresponding terms in equations (185) and (186) combine to give

$$
-\Omega\eta_w'(y_{T_w})(\Omega\delta_{w3}M_y) + \delta_{w_3}\eta_w'(y_{B_w})M_y = -\delta_{w_3}[\eta_w'(y_{T_w}) - \eta_w'(y_{B_w})]
$$

which illustrates the decrease in effectiveness due to y_{B_w}. The other terms are similar, a straightforward decrease in the effectiveness of the effect of the sweep and dihedral because they occur only on the outboard portion of the wing.

The remaining terms in equations (186), the torsion moment due to H and T, are the effective elastic axis influence. The torsion moments due to the hub vertical force H (from eqs. (185) and (186)) combine to give $\Delta M_{p_{rotor}} = [h - \xi_w(y_{B_w})\delta_{w_3}y_{T_w}]H$. From this, it follows that a vertical force on the shaft at $h = \xi_w(y_{B_w})\delta_{w_3}y_{T_w}$ produces no torsion, and so, by definition, that is the location of the effective elastic axis at the wing tip. Now $\delta_{w_3}y_{T_w}$ is the distance of the wing tip behind (for aft sweep) the root elastic axis, and $\xi_w(y_{B_w})$ is a constant less than 1 (of order y_{B_w}/y_{T_w}); thus the effective elastic axis is moved forward of the wing tip elastic axis, a fraction $\xi_w(y_{B_w})$ toward the root spar line. The distance from the wing tip effective elastic axis to the rotor hub is then

$$
h_{EA} = h - \xi_w(y_{B_w})\delta_{w_3}y_{T_w} \qquad (187)
$$

where h is the actual distance from the wing tip spar to the hub. The corresponding vertical displacement of the effective elastic axis, due to the dihedral, is

$$z_{EA} = -\xi_w(y_{B_w})\delta_{w_1} y_{T_w} \tag{188}$$

(Zero geometric vertical displacement of the shaft from the wing tip has been assumed.)

The parameter $\xi_w(y_{B_w})$ can be evaluated from a knowledge of the effective elastic axis position. If Δh is the distance the effective elastic axis is ahead of the wing tip spar ($\Delta h = h - h_{EA}$), then

$$\xi_w(y_{B_w}) = \frac{\Delta h}{\delta_{w_3} y_{T_w}} \tag{189}$$

The other parameters required can be estimated in terms of $\xi_w(y_{B_w})$ as

$$\left.\begin{aligned} \eta_w(y_{B_w}) &\cong \eta_w(y_{T_w})\xi_w{}^2(y_{B_w}) = y_{T_w}\xi_w{}^2(y_{B_w}) \\ \eta_w'(y_{B_w}) &\cong \eta_w'(y_{T_w})\xi_w(y_{B_w}) \end{aligned}\right\} \tag{190}$$

Only a single parameter remains to be determined for this model, $\xi_w(y_{B_w})$. It is determined by matching to the correct effective elastic axis position, hence the most important feature is correct and this model should provide an adequate estimate for the other influences of sweep and dihedral.

The complete expressions for the rotor forcing terms in the wing equations of motion are then:

$$\left.\begin{aligned} M_{q_1}{}_{rotor} &= \Omega\eta_w'[Q - \Omega\delta_{w_3}(1 - \xi_w)(M_y + hH) - \delta_{w_2}(M_x - hY)] \\ &\quad + y_{T_w}[H - \Omega\delta_{w_1}(1 - \xi_w{}^2)Y - \delta_{w_2}T] \\ M_{q_2}{}_{rotor} &= \Omega\eta_w'[-M_x + hY + \Omega\delta_{w_1}(1 - \xi_w)(M_y + hH) - \delta_{w_2}Q] \\ &\quad + y_{T_w}[-T - \Omega\delta_{w_3}(1 - \xi_w{}^2)Y - \delta_{w_2}H] \\ M_p{}_{rotor} &= M_y + h_{EA}H + z_{EA}T + \Omega\delta_{w_3}(1 - \xi_w)Q \\ &\quad + \Omega\delta_{w_1}(1 - \xi_w)(M_x - hY) + C^*_{pq}y_{T_w}T(-q_1 + \delta_{w_2}q_2) \end{aligned}\right\} \tag{191}$$

where η_w' is written for $\eta_w'(y_{T_w})$ and ξ_w for $\xi_w(y_{B_w})$.

The wing equations of motion are normalized by dividing by $(N/2)I_b$; this normalization is denoted by superscript $*$, as in $I_{q_w}/(N/2)I_b = I^*_{q_w}$ and similarly for the other inertia, damping, and spring constants. The rotor forcing terms then take the usual rotor coefficient form. The wing aerodynamic terms (presented in the next section) are normalized by dividing by $\gamma(N/2)I_b = (\pi/2)\sigma a$, which is also denoted by superscript $*$. This introduces a factor γ for the wing aerodynamic terms, as for the rotor aerodynamics. The equations of motion for the wing vertical bending, chordwise bending, and torsion modes are then:

$$\begin{bmatrix} I^*_{q_w} + m_P^* & 0 & S_w^* \\ 0 & I^*_{q_w} + I^*_{P_x}\eta_w'^2 + m_P^* & -S_w^*\delta_{w_2} \\ S_w^* & -S_w^*\delta_{w_2} & I^*_{P_w} + I^*_{P_y} \end{bmatrix} \begin{pmatrix} q_1 \\ q_2 \\ p \end{pmatrix}^{\cdot\cdot}$$

$$+ \begin{bmatrix} C^*_{q_1} & 0 & 0 \\ 0 & C^*_{q_2} & 0 \\ 0 & 0 & C_P^* \end{bmatrix} \begin{pmatrix} q_1 \\ q_2 \\ p \end{pmatrix}^{\cdot} + \begin{bmatrix} K^*_{q_1} & 0 & 0 \\ 0 & K^*_{q_2} & 0 \\ C^*_{pq} y_{T_w}(\gamma 2C_T/\sigma a) & -C^*_{pq} y_{T_w}(\gamma 2C_T/\sigma a)\delta_{w_2} & K_P^* \end{bmatrix} \begin{pmatrix} q_1 \\ q_2 \\ p \end{pmatrix}$$

$$= \begin{pmatrix} M^*_{q_1 aero} \\ M^*_{q_2 aero} \\ M^*_{p\,aero} \end{pmatrix} + \gamma \begin{bmatrix} \Omega\eta_w'\Omega\delta_{w_3}(1-\xi_w) & -\Omega\eta_w'\delta_{w_2} \\ -\Omega\eta_w'\Omega\delta_{w_1}(1-\xi_w) & -\Omega\eta_w' \\ -1 & -\Omega\delta_{w_1}(1-\xi_w) \end{bmatrix} \begin{pmatrix} -2C_{M_y}/\sigma a \\ 2C_{M_x}/\sigma a \end{pmatrix}$$

$$+ \gamma \begin{bmatrix} y_{T_w} - \Omega\eta_w'\Omega\delta_{w_3} h(1-\xi_w) & -\Omega\eta_w'\delta_{w_2} h + y_{T_w}\Omega\delta_{w_1}(1-\xi_w^2) \\ -\delta_{w_2} y_{T_w} + \Omega\eta_w'\Omega\delta_{w_3} h(1-\xi_w) & -\Omega\eta_w' h + y_{T_w}\Omega\delta_{w_3}(1-\xi_w^2) \\ h_{EA} & \Omega\delta_{w_1}(1-\xi_w)h \end{bmatrix} \begin{pmatrix} 2C_H/\sigma a \\ -2C_Y/\sigma a \end{pmatrix}$$

$$+ \gamma \begin{bmatrix} 2\Omega\eta_w' \\ -2\Omega\eta_w'\delta_{w_2} \\ 2\Omega\delta_{w_3}(1-\xi_w) \end{bmatrix} C_Q/\sigma a + \gamma \begin{bmatrix} -2y_{T_w}\delta_{w_2} \\ -2y_{T_w} \\ 2z_{EA} \end{bmatrix} C_T/\sigma a \qquad (192)$$

An exception to the normalization is the definition of m_P^*:

$$m_P^* = m_P y_T^2/(N/2)I_b$$

It also follows that $S_w^* = S_w/(N/2)I_b = m_P^* z_{P_{EA}}/y_{T_w}$. The Lock number γ appears as a factor of all the aerodynamic terms (the rotor forces and moments have inertia terms, too, but always with a factor γ^{-1}). This single parameter accounts for the relative influence of the aerodynamic and inertia forces; specifically, it is the only parameter that varies with air density ρ, all other constants being the ratio of inertias (that is, of course, the reason for the normalization by $(N/2)I_b$). The spring and damping constants are $K_{q_1}^* = K_{q_1}/(N/2)I_b$ and $C_{q_1}^* = C_{q_1}/(N/2)I_b$ (and similarly for chordwise bending and torsion). Since these constants have already been made dimensionless, in terms of the dimensional values the normalized spring and damping rates are $K_{q_1}^* = K_{q_1}/(N/2)I_b\Omega^2$ and $C_{q_1}^* = C_{q_1}/(N/2)I_b|\Omega|$. The effect of a variation in rotor rotational speed is to change the relative spring and damping rates of the wing, because the wing natural frequencies are really constant dimensional values (cycles/sec). The wing frequencies then change with Ω when expressed as dimensionless quantities (per rev). This is, in fact, the only influence of Ω on the equations of motion, besides a possible change in the rotor natural frequencies ν_β and ν_ζ with Ω. In the inertias, as in the spring and damping constants, it is not necessary to introduce the intermediate steps of making the quantities dimensionless (using ρ, Ω, and R); for example, $I_{P_y}^* = I_{P_y}/(N/2)I_b$ is correct with dimensional quantities on the right-hand side. The rotor radius R enters only in normalizing lengths, such as y_{T_w} and h_{EA} and, of course, the air density ρ appears only in γ.

Wing aerodynamics- The wing aerodynamic forces that excite the bending and torsion motions of the wing are defined by

$$\left.\begin{aligned} M_{q_{1_{aero}}} &= \int_0^{y_{T_w}} F_{z_w}\eta_w \, dy_w \\ M_{q_{2_{aero}}} &= \int_0^{y_{T_w}} F_{x_w}\eta_w \, dy_w \\ M_{p_{aero}} &= \int_0^{y_{T_w}} M_w\xi_w \, dy_w \end{aligned}\right\} \qquad (193)$$

where F_{z_w} is the vertical aerodynamic force on the wing section (lift); F_{x_w}, the chordwise force (profile and induced drag); and M_w, the aerodynamic moment about the local elastic axis. The section forces F_{z_w} and F_{x_w} are defined with respect to the section principle axes, not with respect to the free stream. The integrals of these section forces over the span, weighted by the appropriate mode shape, give the net forces that excite the wing degrees of freedom. The velocity seen by the section has perturbations that result from the wing

degrees of freedom and from aerodynamic gusts; any interference with the rotor is neglected. From the velocity perturbation, the perturbations of the section forces are found (following a procedure similar to that used for the rotor aerodynamics), and hence the wing aerodynamic coefficients (the trim terms are dropped):

$$\begin{pmatrix} M^*_{q_1 aero} \\ M^*_{q_2 aero} \\ M^*_{p aero} \end{pmatrix} = \begin{bmatrix} C^*_{q_1\dot{q}_1} & C^*_{q_1\dot{q}_2} & C^*_{q_1\dot{p}} \\ C^*_{q_2\dot{q}_1} & C^*_{q_2\dot{q}_2} & C^*_{q_2\dot{p}} \\ C^*_{p\dot{q}_1} & C^*_{p\dot{q}_2} & C^*_{p\dot{p}} \end{bmatrix} \begin{pmatrix} q_1 \\ q_2 \\ p \end{pmatrix} \cdot$$

$$+ \begin{bmatrix} C^*_{q_1 q_1} & C^*_{q_1 q_2} & C^*_{q_1 p} \\ C^*_{q_2 q_1} & C^*_{q_2 q_2} & C^*_{q_2 p} \\ C^*_{p q_1} & C^*_{p q_2} & C^*_{pp} \end{bmatrix} \begin{pmatrix} q_1 \\ q_2 \\ p \end{pmatrix}$$

$$+ \begin{bmatrix} C^*_{q_1 u} & C^*_{q_1 \beta} & C^*_{q_1 \alpha} \\ C^*_{q_2 u} & C^*_{q_2 \beta} & C^*_{q_2 \alpha} \\ C^*_{pu} & C^*_{p\beta} & C^*_{p\alpha} \end{bmatrix} \begin{pmatrix} u_G \\ \beta_G \\ \alpha_G \end{pmatrix} \qquad (194)$$

The coefficients are

$$\left.\begin{aligned} C^*_{q_1 u} &= d_{12} V^2 2 C_{L_o} e_1 \\ C^*_{q_1 \alpha} &= d_{12} V^2 C_{L_\alpha} e_1 \\ C^*_{q_1 \beta} &= \delta_{w_1} C^*_{q_1 \alpha} + \delta_{w_3} C^*_{q_1 u} \\ C^*_{q_1 \dot{q}_1} &= -d_{13} V C_{L_\alpha} e_2 \\ C^*_{q_1 \dot{q}_2} &= -d_{13} V C_{L_o} e_2 \\ C^*_{q_1 q_1} &= -d_{12} V^2 \delta_{w_3} C_{L_\alpha} e_3 \\ C^*_{q_1 q_2} &= -d_{12} V^2 \delta_{w_3} C_{L_o} e_3 \\ C^*_{q_1 \dot{p}} &= d_{22} (1/2) V [3/4 + (x_{A_w}/c_w)] C_{L_\alpha} e_4 \\ C^*_{q_1 p} &= d_{12} V^2 C_{L_\alpha} e_4 \end{aligned}\right\} \qquad (195)$$

(Eqs. (195) continued on next page.)

$$
\left.
\begin{aligned}
C^*_{q_2 u} &= d_{12} V^2 2 (C_{D_o} - \delta_{\omega_2} C_{L_o}) e_1 \\
C^*_{q_2 \alpha} &= d_{12} V^2 (C_{D_\alpha} - 2C_{L_o}) e_1 \\
C^*_{q_2 \beta} &= \delta_{\omega_1} C^*_{q_2 \alpha} + \delta_{\omega_3} C^*_{q_2 u} \\
C^*_{q_2 \dot{q}_1} &= -d_{13} V (C_{D_\alpha} - 2C_{L_o}) e_2 \\
C^*_{q_2 \dot{q}_2} &= -d_{13} V (2C_{D_o} - \delta_{\omega_2} C_{D_\alpha}) e_2 \\
C^*_{q_2 q_1} &= -d_{12} V^2 \delta_{\omega_3} (C_{D_\alpha} - 2C_{L_o}) e_3 \\
C^*_{q_2 q_2} &= -d_{12} V^2 \delta_{\omega_3} (2C_{D_o} - \delta_{\omega_2} C_{D_\alpha}) e_2 \\
C^*_{q_2 \dot{p}} &= d_{22} (1/2) V \left\{ [1/2 + (x_{A_w}/c_w)] (C_{D_\alpha} - 2C_{L_o}) - (1/4) C_{L_o} \right\} e_4 \\
C^*_{q_2 p} &= d_{12} V^2 (C_{D_\alpha} - C_{L_o}) e_4
\end{aligned}
\right\} \qquad (195)
$$

$$
\left.
\begin{aligned}
C^*_{pu} &= d_{21} V^2 2 C_{m_{ac}} f_1 \\
C^*_{p\alpha} &= -d_{21} V^2 (x_{A_w}/c_w) f_1 C_{L_\alpha} \\
C^*_{p\beta} &= \delta_{\omega_1} C^*_{p\alpha} + \delta_{\omega_3} C^*_{pu} \\
C^*_{p\dot{q}_1} &= d_{22} V (x_{A_w}/c_w) e_4 C_{L_\alpha} \\
C^*_{p\dot{q}_2} &= -d_{22} V 2 C_{m_{ac}} e_4 \\
C^*_{p q_1} &= d_{12} V^2 C_{m_{ac}} f_2 \\
C^*_{p q_2} &= -d_{12} V^2 C_{L_o} f_2 \\
C^*_{p\dot{p}} &= -d_{31} (1/2) V [1/4 + (1/2)(x_{A_w}/c_w)] C_{L_\alpha} f_3 \\
C^*_{pp} &= -d_{21} V^2 (x_{A_w}/c_w) f_3 C_{L_\alpha}
\end{aligned}
\right\}
$$

where C_{L_o} and C_{D_o} are the aircraft trim lift and drag (profile and induced) coefficients; C_{L_α} and C_{D_α} are their derivatives with respect to angle of attack. The section moment characteristics are given by x_{A_w}, the distance the aerodynamic center is behind the elastic axis, and $c_{m_{ac}}$, the nose-up moment coefficient about the aerodynamic center. The coefficients can be corrected for unsteady airfoil effects (by use of a lift deficiency function) and for the increased dynamic pressure in the rotor slipstream; such corrections would be small, however, and probably would not be consistent with the accuracy of the methods used to derive the coefficients. The constant $d_{nm} = c_w^n y_{T_w}^m / (\pi \sigma a)$ accounts for the difference in the normalization of the wing and rotor

coefficients. The dependence on forward velocity V is shown explicitly, except that for a fixed gross weight; C_{L_O} and C_{D_α} are proportional to V^{-2} while C_{L_α} and C_{D_O} are constant (at high speed at least, where the induced drag is small). The constants e_n and f_n are integrals of the wing mode shapes, which account for the way the motion produces forces on the wing:

$$e_1 = \int_0^{y_{T_w}} \eta_w \, dy_w / y_{T_w}^2 \cong 1/3$$

$$e_2 = \int_0^{y_{T_w}} \eta_w{}^2 \, dy_w / y_{T_w}^3 \cong 1/5$$

$$e_3 = \int_0^{y_{T_w}} \eta_w \eta_w{}' \, dy_w / y_{T_w}^2 \cong 1/2$$

$$e_4 = \int_0^{y_{T_w}} \eta_w \xi_w \, dy_w / y_{T_w} \cong 1/4$$

$$f_1 = \int_0^{y_{T_w}} \xi_w \, dy_w / y_{T_w} \cong 1/2$$

$$f_2 = \int_0^{y_{T_w}} \xi_w \eta_w{}'' [(y_w - y_{T_w})^2/2] dy_w / y_{T_w}^2 \cong 1/12$$

$$f_3 = \int_0^{y_{T_w}} \xi_w{}^2 \, dy_w / y_{T_w} \cong 1/3$$

The constants were evaluated using the approximate mode shapes $\eta_w \cong y_w{}^2/y_{T_w}$ and $\xi_w \cong y_w/y_{T_w}$ (which are reasonably close with the large mass on the wing tip).

The derivation of the coefficients follows the standard techniques of strip theory in aeroelasticity, similar, for example, to the derivation of the contributions of the wing to the aircraft stability derivatives. The most important wing aerodynamic coefficients are the vertical bending forces due to direct angle-of-attack changes: $C_{q_1\dot{q}_1}$, $C_{q_1 p}$, and $C_{q_1\alpha}$. The change in angle of attack due to wing vertical bending, torsion, and vertical gusts is

$$\delta\alpha = - \frac{\eta_w \dot{q}_1}{V} + \xi_w p + \alpha_G$$

The lift perturbation is $\delta F_{z_w} \cong \delta L = (1/2)V^2 c_w C_{L_\alpha} \delta\alpha$, and the moment exciting vertical bending is

$$\delta M_{q_1 aero} = \int_0^{y_{T_w}} \delta F_{z_w} \eta_w \, dy_w$$

$$= \int_0^{y_{T_w}} \frac{1}{2} V^2 c_w C_{L_\alpha} \eta_w \left[- \frac{\dot{q}_1 \eta_w}{V} + p\xi_w + \alpha_G \right] dy_w$$

$$= \frac{c_w y_{T_w}^2 V}{2} \left[\alpha_G (C_{L_\alpha} e_1) + \frac{y_{T_w}}{V} \dot{q}_1 (-C_{L_\alpha} e_2) + p(C_{L_\alpha} e_4) \right]$$

If one normalizes by dividing by $(\pi/2)\sigma a$, coefficients $C^*_{q_1\alpha}$, $C^*_{q_1\dot{q}_1}$, anc $C^*_{q_1 p}$ are identified (as given in eqs. (195)). The remaining coefficients are derived in a similar fashion.

Equations of motion for proprotor and wing- All the elements are now available to construct the equations of motion for the proprotor and cantilever wing system: the rotor equations of motion (eqs. (44) and (47)), the rotor hub forces and moments (eqs. (45), (46), and (48)), the shaft motion due to the wing degrees of freedom (eqs. (181)), and the wing equations of motion (eqs. (192)). It is only necessary to perform the matrix multiplications required because of the substitutions. The result is a set of linear ordinary differential equations for the nine degrees of freedom:

β_{1C} cyclic flap (longitudinal tip path plane tilt)

β_{1S} cyclic flap (lateral tip path plane tilt)

ζ_{1C} cyclic lag (lateral rotor center-of-gravity offset)

ζ_{1S} cyclic lag (longitudinal rotor center-of-gravity offset)

β_0 collective flap (coning)

ζ_0 collective lag (or rotor speed perturbation)

q_1 wing vertical (or beamwise) bending

q_2 wing chordwise bending

p wing torsion

with the inputs

θ_{1C} cyclic pitch (lateral control plane tilt)

θ_{1S} cyclic pitch (longitudinal control plane tilt)

θ_0 collective pitch

u_G longitudinal gust

β_G lateral gust

α_G vertical gust

The matrix multiplications could be left to the machine, but it is better done by hand since there is considerable cancellation of terms in the coefficients of the equations of motion. The final expressions for the coefficients remain rather complex, however, because of the many (small) terms that involve the wing sweep, dihedral, and incidence angles.

For the autorotation case, the collective lag degree of freedom $\dot{\zeta}_0$ becomes the rotor speed perturbation in the rotor model used here by setting $I^*_{\zeta_0} = I^*_{\zeta_{0\alpha}} = 1$ and $\nu_{\zeta_0} = 0$ (as discussed earlier). Setting the collective lag natural frequency to zero assures that no torque is transmitted to the wing, but it is probably better to directly drop the $C_Q/\sigma a$ forcing of the wing motion from equations (192) (primarily forcing of q_1).

Structural damping of the rotor blades is also added to this model; however, since the blade flap and lag damping are high already because of the high inflow aerodynamic forces, the low structural damping of the rotors considered here is not very important to the dynamics. A term $I_\zeta{}^* g_{s_\zeta} \nu_\zeta$ is added to the rotating lag equation of motion, and $I_\beta{}^* g_{s_\beta} (\nu_\beta{}^2 - 1)^{1/2}$ is added to the rotating flap equation (the structural damping does not act on the centrifugal spring term in ν_β). The transformation to the nonrotating degrees of freedom and equations of motion follows as usual. Different damping coefficients are allowed for the rotor cyclic and collective modes of the rotor, specifically to account for the collective lag mode in autorotation (which must have zero structural damping as well as zero spring) and the coning mode of the gimballed rotor. The structural damping parameter g_s is twice the fraction of critical damping, which is typically 0.5 to 1 percent for the cantilever rotor blades considered here.

Simplified equations- The coefficients of the nine equations of motion for this proprotor model are simplified considerably if all the effects of sweep, dihedral, and angle of attack are neglected. Since these angles are always small for the model considered here, they generally contribute only small corrections to the coefficients. An exception, however, is the effective elastic axis shaft at the wing tip due to the sweep, which is an important aspect of the wing structural dynamics; this may be included by use of, for the mast height h, the distance from the hub to the effective elastic axis rather than to the actual wing tip spar. The simplified version of the equations of motion then is obtained by neglecting all effects of δ_{w_1}, δ_{w_2}, and δ_{w_3}

except that the effect of the effective elastic axis is included if h_{EA} is used for h wherever it appears. In addition, the calculation of the rotor coefficients is simplified by considering only the c_{ℓ_α} terms (i.e., eqs. (54)); this primarily limits the results to below the critical tip Mach number and is, in fact, the form used almost exclusively for the rotor aerodynamics in the results presented here. Similarly, only the wing aerodynamic forces due to C_{L_α} are retained. This simplified model is not usually used here, and for the design and analysis of actual vehicles these simplifications of the structural and aerodynamic features would probably not be satisfactory. It will be shown, however, that the simplified model incorporates the essential features of the high inflow proprotor dynamics and so may be useful in further studies.

Dropping the δ_{ω_1}, δ_{ω_2}, and δ_{ω_3} terms from the shaft motion expressions (eqs. (181)) yields

$$\left.\begin{aligned}\begin{pmatrix}\alpha_x\\ \alpha_y\\ \alpha_x\end{pmatrix} &= \begin{bmatrix}0 & -\Omega\eta_w' & 0\\ 0 & 0 & 1\\ -\Omega\eta_w' & 0 & 0\end{bmatrix}\begin{pmatrix}q_1\\ q_2\\ p\end{pmatrix}, \quad \begin{pmatrix}x_P\\ y_P\\ z_P\end{pmatrix} = \begin{bmatrix}y_{T_w} & 0 & 0\\ 0 & 0 & 0\\ 0 & -y_{T_w} & 0\end{bmatrix}\begin{pmatrix}q_1\\ q_2\\ p\end{pmatrix}\end{aligned}\right\} \tag{196}$$

and the wing equations of motion (eqs. (192)) reduce to

$$\begin{bmatrix}I^*_{q_w} + m_p^* & 0 & S_w^*\\ 0 & I^*_{q_w} + I^*_{P_x}\eta_w'^2 + m_p^* & 0\\ S_w^* & 0 & I^*_{p_w} + I^*_{P_y}\end{bmatrix}\begin{pmatrix}q_1\\ q_2\\ p\end{pmatrix}^{\cdot\cdot}$$

$$+\begin{bmatrix}C^*_{q_1} - \gamma C^*_{q_1\dot{q}_1} & 0 & -\gamma C^*_{q_1\dot{p}}\\ 0 & C^*_{q_2} & 0\\ 0 & 0 & C_p^* - \gamma C^*_{p\dot{p}}\end{bmatrix}\begin{pmatrix}q_1\\ q_2\\ p\end{pmatrix}^{\cdot} + \begin{bmatrix}K^*_{q_1} & 0 & -\gamma C^*_{q_1 p}\\ 0 & K^*_{q_2} & 0\\ C^*_{pq} y_{T_w}(\gamma 2C_T/\sigma a) & 0 & K_p^*\end{bmatrix}\begin{pmatrix}q_1\\ q_2\\ p\end{pmatrix}$$

$$= \begin{bmatrix}0 & 0 & \gamma C^*_{q_1\alpha}\\ 0 & 0 & 0\\ 0 & 0 & 0\end{bmatrix}\begin{pmatrix}u_G\\ \beta_G\\ \alpha_G\end{pmatrix} + \gamma\begin{bmatrix}0 & 0\\ 0 & -\Omega\eta_w'\\ -1 & 0\end{bmatrix}\begin{pmatrix}-\dfrac{2C_{M_y}}{\sigma a}\\ \dfrac{2C_{M_x}}{\sigma a}\end{pmatrix} + \gamma\begin{bmatrix}y_{T_w} & 0\\ 0 & -\Omega\eta_w' h_{EA}\\ h_{EA} & 0\end{bmatrix}\begin{pmatrix}\dfrac{2C_H}{\sigma a}\\ -\dfrac{2C_Y}{\sigma a}\end{pmatrix}$$

$$+ \gamma\begin{bmatrix}2\Omega\eta_w'\\ 0\\ 0\end{bmatrix}\frac{C_Q}{\sigma a} + \gamma\begin{bmatrix}0\\ -2y_{T_w}\\ 0\end{bmatrix}\frac{C_T}{\sigma a} \tag{197}$$

The simplification is quite substantial. If one substitutes for the shaft motion into the rotor equations and forces, and then for the rotor forces into the wing equations, the matrix multiplications are easily carried out. The result is a set of nine equations of motion of the form:

$$A_2\ddot{\vec{x}} + A_1\dot{\vec{x}} + A_0\vec{x} = B\vec{v} \tag{198}$$

where the degree-of-freedom vector is

$$\vec{x} = \begin{bmatrix} \beta_{1C} \\ \beta_{1S} \\ \zeta_{1C} \\ \zeta_{1S} \\ \beta_0 \\ \zeta_0 \\ q_1 \\ q_2 \\ p \end{bmatrix}$$

and the control vector is

$$\vec{v} = \begin{bmatrix} \theta_{1C} \\ \theta_{1S} \\ \theta_0 \\ u_G \\ \beta_G \\ \alpha_G \end{bmatrix}$$

The coefficient matrices are given below for the simplified equations. For convenience, in these matrices, η is written for $\Omega\eta_w'(y_{T_w})$, y for y_{T_w}, h for h_{EA}, and V for $V + v$; all C_T and C_Q terms are dropped and the structural damping of the blade is neglected; superscripts $*$ on the inertias and spring constants are dropped.

$$
A_2 = \begin{bmatrix}
I_\beta & & & & & & & & -I_{\beta\alpha} \\
& I_\beta & & & & & & -\eta I_{\beta\alpha} & \\
& & I_\zeta & & & & & -S_\zeta h\eta & \\
& & & I_\zeta & & & S_\zeta y & & S_\zeta h \\
& & & & I_{\beta_0} & & & -S_{\beta_0} y & \\
& & & & & I_{\zeta_0} & \eta I_{\zeta_0\alpha} & & \\
& & & S_\zeta y & & 2\eta I_{\zeta_0\alpha} & I_{q_w}+m_P \\ & & & & & & +y^2 2M_b \\ & & & & & & +2\eta^2 I_0 & & S_w \\ & & & & & & & & +2hyM_b \\
& & -S_\zeta h\eta & & -2yS_{\beta_0} & & & I_{q_w}+m_P \\ & & & & & & & +I_{P_x}\eta^2 \\ & & & & & & & +h^2\eta^2 2M_b \\ & & & & & & & +y^2 2M_b & \\
& & & S_\zeta h & & & S_w & & I_{p_w}+I_{P_y} \\ & & & & & & +2hyM_b & & +2h^2 M_b
\end{bmatrix}
$$

$$
A_1 = \left[\begin{array}{c|c|c|c|c|c|c|c|c}
-\gamma M_\beta^{\cdot} & 2I_\beta & \gamma M_\zeta^{\cdot} & & & & & -2I_{\beta\alpha}\eta \; -\gamma M_\mu h\eta & \gamma M_\beta^{\cdot} \\
\hline
-2I_\beta & -\gamma M_\beta^{\cdot} & & \gamma M_\zeta^{\cdot} & & & \gamma M_\mu y & \gamma M_\beta^{\cdot}\eta & 2I_{\beta\alpha} \; +\gamma M_\mu h \\
\hline
-\gamma Q_\beta^{\cdot} & & \gamma Q_\zeta^{\cdot} & 2I_\zeta & & & & -\gamma Q_\mu h\eta & \gamma Q_\beta^{\cdot} \\
\hline
 & -\gamma Q_\beta^{\cdot} & -2I_\zeta & \gamma Q_\zeta^{\cdot} & & & \gamma Q_\mu y & \gamma Q_\beta^{\cdot}\eta & \gamma Q_\mu h \\
\hline
 & & & & -\gamma M_\beta^{\cdot} & \gamma M_\zeta^{\cdot} & \gamma M_\zeta^{\cdot}\eta & \gamma M_\lambda y & \\
\hline
 & & & & -\gamma Q_\beta^{\cdot} & \gamma Q_\zeta^{\cdot} & \gamma Q_\zeta^{\cdot}\eta & \gamma Q_\lambda y & \\
\hline
 & -\gamma H_\beta^{\cdot} y & & \gamma H_\zeta^{\cdot} y & -\gamma Q_\beta^{\cdot} 2\eta & \gamma Q_\zeta^{\cdot} 2\eta & C_{q_1} \; +2\eta^2\gamma Q_\zeta^{\cdot} \; +y^2\gamma H_\mu \; -\gamma C_{q_1}\dot{q}_1 & 2\eta y\gamma Q_\lambda \; +y\eta\gamma H_\beta^{\cdot} & yh\gamma H_\mu \; -\gamma C_{q_1}\dot{p} \\
\hline
\gamma H_\beta^{\cdot} h\eta & & -\gamma H_\zeta^{\cdot} h\eta & & \gamma T_\beta^{\cdot} 2y & -\gamma T_\zeta^{\cdot} 2y & -2y\eta\gamma T_\zeta^{\cdot} & C_{q_2} \; +h^2\eta^2\gamma H_\mu \; -2y^2\gamma T_\lambda & -h\eta\gamma H_\beta^{\cdot} \\
\hline
 & -\gamma H_\beta h & & \gamma H_\zeta^{\cdot} h & & & \gamma H_\mu hy & h\eta\gamma H_\beta^{\cdot} & C_{P_\omega} \; +h^2\gamma H_\mu \; -\gamma C_p\dot{p}
\end{array}\right]
$$

$$
A_0 = \left[\begin{array}{c|c|c|c|c|c|c|c|c}
I_\beta(\nu_\beta^2-1) + K_P\gamma M_\theta & -\gamma M_\beta^{\cdot} & & \gamma M_\zeta^{\cdot} & & & & \gamma V M_\mu \eta & \\
\hline
\gamma M_\beta^{\cdot} & I_\beta(\nu_\beta^2-1) + K_P\gamma M_\theta & -\gamma M_\zeta^{\cdot} & & & & & & -\gamma V M_\mu \\
\hline
\gamma Q_\theta K_P & -\gamma Q_\beta^{\cdot} & I_\zeta(\nu_\zeta^2-1) & \gamma Q_\zeta^{\cdot} & & & & \gamma V Q_\mu \eta & \\
\hline
\gamma Q_\beta^{\cdot} & \gamma Q_\theta K_P & -\gamma Q_\zeta^{\cdot} & I_\zeta(\nu_\zeta^2-1) & & & & & -\gamma V Q_\mu \\
\hline
 & & & & I_{\beta_0}\nu_{\beta_0}^2 + \gamma M_\theta K_P & & & & \\
\hline
 & & & & \gamma Q_\theta K_P & I_{\zeta_0}\nu_{\zeta_0}^2 & & & \\
\hline
y\gamma H_\beta^{\cdot} & yK_P\gamma H_\theta & -y\gamma H_\zeta^{\cdot} & & 2\eta K_P\gamma Q_\theta & & K_{q_1} & & -y\gamma V H_\mu - \gamma C_{q_1} p \\
\hline
-h\eta K_P\gamma H_\theta & \eta I_\beta(\nu_\beta^2-1) + h\eta\gamma H_\beta^{\cdot} & & -h\eta\gamma H_\zeta^{\cdot} & -2yK_P\gamma T_\theta & & & K_{q_2} - h\eta^2\gamma V H_\mu & \\
\hline
I_\beta(\nu_\beta^2-1) + h\gamma H_\beta^{\cdot} & hK_P\gamma H_\theta & -h\gamma H_\zeta^{\cdot} & & & & & & K_P - h\gamma V H_\mu
\end{array}\right]
$$

$$
B = \left[\begin{array}{c|c|c|c|c|c}
\gamma^{M}{}_{\theta} & & & & \gamma^{VM}{}_{\mu} & \\
\hline
 & \gamma^{M}{}_{\theta} & & & & \gamma^{VM}{}_{\mu} \\
\hline
\gamma^{Q}{}_{\theta} & & & & \gamma^{VQ}{}_{\mu} & \\
\hline
 & \gamma^{Q}{}_{\theta} & & & & \gamma^{VQ}{}_{\mu} \\
\hline
 & & \gamma^{M}{}_{\theta} & \gamma^{VM}{}_{\lambda} & & \\
\hline
 & & \gamma^{Q}{}_{\theta} & \gamma^{VQ}{}_{\lambda} & & \\
\hline
 & y\gamma^{H}{}_{\theta} & 2n\gamma^{Q}{}_{\theta} & 2n\gamma^{VQ}{}_{\lambda} & & y\gamma^{VH}{}_{\mu} + \gamma^{C}{}_{q_1\alpha} \\
\hline
-hn\gamma^{H}{}_{\theta} & & -2y\gamma^{T}{}_{\theta} & -2y\gamma^{VT}{}_{\lambda} & -hn\gamma^{VH}{}_{\mu} & \\
\hline
 & h\gamma^{H}{}_{\theta} & & & & h\gamma^{VH}{}_{\mu}
\end{array}\right]
$$

The incorporation of the wing vertical bending motion into the model introduces the possibility of a mechanical instability involving that degree of freedom and the rotor blade inplane motion. Since instability involves the elastic bending of the airframe, it may occur in flight; hence it is termed air resonance. The basic mechanism involved, however, is identical with that in classical helicopter ground resonance (involving inplane hub motion, typically due to vibration of the helicopter on its landing gear while on the ground). The analysis and conclusions from ground resonance are thus directly applicable to air resonance also.

Certain conclusions immediately follow then from the ground resonance analysis (ref. 34). Air resonance involves a coincidence of the wing vertical bending frequency (for the proprotor configuration) and the frequency (in the fixed system) of the lower lag mode ζ - 1. Any resonance with the upper lag mode (ζ + 1) are always stable. Furthermore, the resonances with the lower lag mode are also stable if the rotor is stiff inplane, that is, if $\nu_\zeta > 1/\text{rev}$. Air resonance instability is possible only with a soft inplane rotor, that is, with $\nu_\zeta < 1/\text{rev}$.

Air resonance instability then occurs at a resonance of the frequencies ω_{q_1} and 1 - ν_ζ of the wing and rotor modes, with $\nu_\rho < 1/\text{rev}$. Such conditions must be avoided, for example, by use of a wing that is stiff enough so that any resonance occurs at a rotor speed Ω much higher than the normal operating rotational speed. Alternatively, it is possible to stabilize any resonances that occur by including sufficient damping - structural or aerodynamic - in the wing and rotor motions.

High inflow operation of the rotor results in an aerodynamic damping of the lag motion, Q_ζ^*, which is of order 1 in high inflow, compared to the order of the inflow squared in low inflow. Thus increasing forward speed in the airplane configuration greatly increases the lag damping and eventually will stabilize the air resonance motion. Forward speed also contributes to stability by increasing the wing aerodynamic damping. Therefore, above a certain speed, no instability occurs even at a coincidence of the wing and lag frequencies; it is desirable, of course, that this speed be as low as possible, at least below the aircraft stall speed.

A simple model will yield an estimate of the damping required, so of the forward speed required, to stabilize the air resonance motion. Consider the rotor lag and wing vertical bending degrees of freedom (ζ_{1C}, ζ_{1S}, and q_1) retain only the direct damping of the wing and lag motion as the only aerodynamic influence. The homogeneous equation of motion, in Laplace form, reduces, for this set of degrees of freedom, to

$$\begin{bmatrix} I_\zeta^*(s^2+C_\zeta s+\nu_\zeta^2-1) & I_\zeta^*(2s+C_\zeta) & 0 \\ -I_\zeta^*(2s+C_\zeta) & I_\zeta^*(s^2+C_\zeta s+\nu_\zeta^2-1) & S_\zeta^* y_{T_w} s^2 \\ 0 & S_\zeta^* y_{T_w} s^2 & M_{q_1}^*(s^2+C_{q_1} s+\omega_{q_1}^2) \end{bmatrix} \begin{pmatrix} \zeta_{1C} \\ \zeta_{1S} \\ q_1 \end{pmatrix} = 0 \qquad (199)$$

where the definitions of the coefficients follow by a comparison with the complete set (eqs. (198)). In particular, $I_\zeta^* C_\zeta$ has been introduced for the total lag damping, $M_{q_1}^* C_{q_1}$ for the total wing vertical bending damping, and ω_{q_1} for the natural frequency (per rev) of the wing vertical bending motion. The characteristic equation is then

$$I_\zeta^{*2}[(s^2 + C_\zeta s + \nu_\zeta^2 - 1)^2 + (2s + C_\zeta)^2]M_{q_1}^*(s^2 + C_{q_1} s + \omega_{q_1}^2)$$

$$- I_\zeta^*(s^2 + C_\zeta s + \nu_\zeta^2 - 1)S_\zeta^{*2} y_{T_w}^2 s^4 = 0 \qquad (200)$$

The only coupling of the rotor and wing degrees of freedom is the inertia coupling that results from S_ζ^{*2}; it follows then, as in ground resonance, that the damping required must also be of order S_ζ^{*2}. Examine the resonant case, where $\omega_{q_1} = 1 - \nu_\zeta$ ($\nu_\zeta < 1$). Assume that the system is exactly on the stability boundary, so that $s = i\omega$ is a solution of the characteristic equation, with ω real. Let ω^2 be an order S_ζ^{*2} distance from $\omega_{q_1}^2$. Then, to the lowest order in S_ζ^{*2}, the characteristic equation is

$$I_\zeta^{*2} 2C_\zeta i\omega_{q_1}(\nu_\zeta^2 + 1 - \omega_{q_1}^2)M_{q_1}^* C_{q_1} i\omega_{q_1}$$

$$- I_\zeta^*(\nu_\zeta^2 - 1 - \omega_{q_1}^2)S_\zeta^{*2} y_{T_w}^2 \omega_{q_1}^4 = 0 \qquad (201)$$

Since the resonant case is being considered, for $\omega_{q_1} = 1 - \nu_\zeta$, then

$$\nu_\zeta^2 - 1 - \omega_{q_1}^2 = 2(\nu_\zeta - 1) = -2\omega_{q_1}$$

$$\nu_\zeta^2 + 1 - \omega_{q_1}^2 = 2\nu_\zeta$$

and equation (201) becomes

$$I_\zeta^* C_\zeta M_{q_1}^* C_{q_1} 2\omega_{q_1}^2 2\nu_\zeta - 2\omega_{q_1} S_\zeta^{*2} y_{T_w}^2 \omega_{q_1}^4 = 0$$

For dynamic stability, it is required then that

$$I_\zeta^* C_\zeta M_{q_1}^* C_{q_1} > \frac{S_\zeta^{*2} y_{T_w}^2 \omega_{q_1}^3}{2\nu_\zeta} \qquad (202)$$

that is, that the product of the wing and rotor damping be above a certain critical value.

To estimate the damping available, consider the aerodynamic damping of the wing:

$$M^*_{\dot{q}_1} C_{q_1} = -\gamma C^*_{q_1 \dot{q}_1} = \gamma C_{L_\alpha} \frac{1}{5} \frac{c_w y^3_{T_w} V}{\pi \sigma a}$$

and the aerodynamic lag damping:

$$I_\zeta{}^* C_\zeta = \gamma Q^{\cdot}_\zeta \cong \gamma \frac{V \sin \phi}{6}$$

The contributions of the structural damping of the wing and blade are negligible at the forward speeds involved. The boundary is usually at a low enough V that the small V approximation to $Q^{\cdot}_\zeta$ is accurate still; therefore,

$$I_\zeta{}^* C_\zeta = \gamma Q^{\cdot}_\zeta \cong \gamma \frac{V^2}{4}$$

The requirement on forward speed V for air resonance stability is then:

$$V^3 > \frac{S^{*2}_\zeta \omega^3_{q_1} / 2\nu_\zeta}{\gamma^2 (1/20) C_{L_\alpha} c_w y_{T_w} / a \pi \sigma} \tag{203}$$

which gives a critical V only a few percent below that for $Q^{\cdot}_\zeta \cong (V \sin \phi)/6$, and so the low inflow approximation for $Q^{\cdot}_\zeta$ is within the general accuracy of the result. This result is, of course, in dimensionless form, so the velocity is really the inflow ratio $V/\Omega R$ and the frequencies are all dimensionless values (per rev).

For the type of soft inplane rotor considered here, ν_ζ (per rev) does not vary much with Ω, at least near and above the normal operating rotational speed. Consequently, the value of ω_{q_1} (per rev) at resonance with $1 - \nu_\zeta$ is also independent of Ω. Then the entire right-hand side of equation (203) for the critical V is a constant; it depends on the rotor (ν_ζ) and on some geometric properties of the rotor and wing. It does not, however, depend on Ω or on ω_{q_1} (dimensional) because it is in dimensionless form.

The criterion for stabilizing the air resonance motion is then a requirement for a fixed value of the ratio $V/\Omega R$ for a given rotor (soft inplane, with ν_ζ (per rev) independent of Ω). The rotor rotational speed for the instability is given by the criterion of resonance of the q_1 and $\zeta - 1$ modes; therefore,

$$\Omega = \frac{\omega_{q_1}}{\omega_{q_1}/\Omega} = \frac{\omega_{q_1}}{1 - \nu_\zeta} \tag{204}$$

where in equation (204) ω_{q_1} is dimensional and ν_ζ, per rev. Thus the rotor rotational speed (RPM) for resonance is directly proprotional to the wing vertical bending frequency (Hz). The forward speed required for stability at the resonance is given in terms of a critical inflow ratio:

$$V = \Omega R\left(\frac{V}{\Omega R}\right)_{critical} \tag{205}$$

Thus the aircraft velocity (knots) required for stability is directly proportional to the rotor rotational speed (rpm). Then increasing the wing vertical bending stiffness increases the Ω at which air resonance occurs, but it also increases the V required for stability. Both effects are linear with ω_{q_1} (Hz) or $(K_{q_1})^{1/2}$ for a fixed ν_ζ (per rev); on the V - Ω plane, the locus of the highest air resonance instability speed is a constant $V/\Omega R$ line, that is, a straight line through the origin. The increase in Ω is favorable for air resonance occurring above the normal operating range, but the corresponding increase in V is unfavorable.

SECTION 5: RESULTS OF THE THEORY AND COMPARISON WITH FULL-SCALE TESTS

Proprotor Dynamic Characteristics

In this chapter (and the following two chapters), the dynamic characteristics of a proprotor operating at high inflow on the tip of a cantilever wing are examined. The investigation uses the results of the theory developed previously. The cases examined are based on actual proprotor designs - two full-scale proprotors that were tested recently in the Ames 40- by 80-Foot Wind Tunnel on a dynamic test stand consisting of a cantilever wing simulating the full-scale aircraft wing stiffnesses. One rotor was designed and constructed by the Bell Helicopter Company, and the other by the Boeing Vertol Company. The Bell and Boeing rotors are shown in the configuration for the dynamic tests in the 40- by 80-Foot Wind Tunnel in figures 12 and 13, respectively. The two rotors differ primarily, so far as their dynamic characteristics are concerned, in the placement of the rotating natural frequencies of the blade flap and lag motions. The Bell rotor has a gimballed hub and stiff inplane cantilever blade attachment to the hub, hence $\nu_\beta = 1$ (nearly, for it does have a weak hub spring) and $\nu_\zeta > 1$; it also incorporates positive pitch/flap coupling, $K_P < 0$ or $\delta_3 < 0$, to increase the blade flap/lag stability. The Boeing rotor has a cantilever or hingeless hub with soft inplane blade attachment, hence $\nu_\beta > 1$ and $\nu_\zeta < 1$. The flap frequency is large even for a hingeless rotor because of the operation at lower rotor speed in airplane mode (the hover value of ν_β is more typical of a hingeless rotor helicopter). The different placement of the blade frequencies, at opposing extremes of the range of choices, results in quite different dynamic characteristics for the two aircraft. A description of the rotors and the full-scale test results are given in references 25 to 28. For convenience, in the following discussion,

the gimballed, stiff-inplane rotor is referred to as the Bell rotor; the hingeless, soft-inplane rotor is referred to as the Boeing rotor.

The dynamic characteristics of the rotors are examined in the following two chapters. Of primary interest are the eigenvalues - the frequency and damping of the roots of the coupled wing/rotor modes of motion. The basic parameters for this investigation are forward speed V, rotor rotational speed Ω, and inflow ratio $V/\Omega R$. A velocity sweep, varying V (and so $V/\Omega R$) at constant Ω is of interest since it is the way the rotor actually operates in airplane mode. The rotor speed Ω determines the relative values (i.e., dimensionless, per rev) of the wing natural frequencies, and so has a fundamental influence on the dynamics. Varying Ω also changes the blade natural frequencies, especially for the cantilever rotors considered here. A rotor speed sweep at constant V also varies the inflow ratio $V/\Omega R$. The inflow ratio $V/\Omega R$ is the primary parameter for the rotor aerodynamics and the wing aerodynamics as well. Varying $V/\Omega R$ may also change the blade frequencies because of the change in the rotor collective pitch angle with the inflow ratio.

Several elements in the theoretical model are examined to determine their influence on the proprotor dynamics: blade lag degrees of freedom, wing aerodynamics, rotor speed perturbation degree of freedom, the complete expressions for the rotor aerodynamics, and a simplified theoretical model. The influence of the rotor lag motion can be examined by studying the effect of dropping the ζ_{1C} and ζ_{1S} degrees of freedom from the complete nine-degree-of-freedom model. The influence of the wing aerodynamics can be examined by setting all wing aerodynamic coefficients to zero and by comparing the results with those from the model that includes the wing aerodynamic forces.

The rotor is usually considered to be operating in autorotation for the theoretical results presented here because this state is found to be least stable and also it is the configuration in which the full-scale dynamic tests were conducted. In autorotation, $\dot{\zeta}_0$ is the rotor speed perturbation degree of freedom, which is achieved by setting $\nu_{\zeta_0} = 0$ (as discussed previously); also, no rotor torque is delivered to the wing tip. The other extreme examined, considered the powered operation case, is when the hub operates at constant angular velocity (Ω) with no perturbation; then ζ_0 is the collective lag degree of freedom, which is achieved by setting $\nu_{\zeta_0} = \nu_\zeta$, and the rotor torque perturbations are transmitted to the wing. This representation of the powered case is, of course, the limit of a perfect governor, but it provides an indication of the real powered state dynamics of the proprotor.

The rotor aerodynamic coefficients are usually calculated for the present results using only the c_{ℓ_α} terms (eqs. (54)). This approximation simplifies the calculations considerably since then the coefficients depend only on $V/\Omega R$, and it provides an adequate representation of the rotor aerodynamics for the range of inflow considered here, at least so long as the critical tip Mach number is not exceeded. The validity of the approximation can be assessed by comparisons with the dynamics that result when the complete expressions for the rotor aerodynamic coefficients are used (eqs. (50)). Since only a check on the influence of the complete expressions is desired here, representative

analytical expressions are used for the airfoil characteristics rather than the characteristics of the actual rotor blade sections (as described in eqs. (55) and (56)). To evaluate the complete coefficients, the angle-of-attack distribution over the blade span in the trim operating state is required, hence the rotor collective pitch is required. The determination of the collective pitch requires a performance analysis to find $\theta_{0.75}$ for a given C_T or C_Q; a simpler procedure - the use of an approximate collective pitch angle based on the inflow angle at 75 percent radius (plus about 1° to account for the mean operating section angle of attack) - is also evaluated. The evaluation of the complete rotor aerodynamic coefficients is also the only time the blade twist is required in the calculations (with the exception that when only the c_{ℓ_α} terms are used, the blade is assumed to have the twist required to maintain unstalled flow over the entire span).

The effects of the wing sweep, dihedral, and angle of attack considerably complicate the coefficients of the equations of motion. Therefore, a simpler theory is evaluated in which all the δ_{ω_1}, δ_{ω_2}, and δ_{ω_3} terms are dropped. The shift of the effective elastic axis at the wing tip is included by use of h_{EA} (the distance from the hub to the effective elastic axis at the wing tip) for the mast height h (the physical shaft length in the unswept wing model). The simplified theory also uses only the c_{ℓ_α} terms for the rotor and wing aerodynamic coefficients. Of course, that is the usual approximation used here for the rotor coefficients, and it includes the primary effects of the wing coefficients. When the option of using the complete expressions for the rotor coefficieints is not included, the calculations are simplified considerably.

The two full-scale rotors were also tested on a quarter stiffness wing, which had natural frequencies half those of the full stiffness wing. Therefore, by operating at half normal rotor rotational speed, the dimensionless wing frequencies (per rev) could be maintained and a given $V/\Omega R$ achieved with half the normal forward velocity V. With the quarter stiffness wing, it was possible to simulate operation at forward speeds twice the maximum capability of the wind tunnel, at least so far as the wing natural frequencies (maintained at the same per rev values) and the rotor aerodynamics (primarily a function of $V/\Omega R$) were concerned. The rotor stiffness was, however, not correspondingly scaled down; therefore, the increase (per rev) in the blade flap and lag natural frequencies where the rotor was slowed down to half normal Ω violated the simulation. For the gimballed rotor, at least the flapping mode (which has only centrifugal stiffening, except for the weak hub spring) was simulated on the quarter stiffness wing; but the lag frequency and both the flap and lag frequencies for the cantilever rotor were considerably different. Consequently, the results of the quarter stiffness wing tests are not presented here as simulating operation at twice the actual speed; the results are studied since they do provide additional data for investigating the dynamic characteristics of the proprotor.

The theoretical studies concentrate on the eigenvalues as primary indicators of the dynamic behavior. However, the eigenvectors and also the frequency response of the system are examined at a typical operating condition ($V/\Omega R$ = 0.7). Finally, the results of the theory developed here are compared

with experimental data from the full-scale tests and also with results from other theories.

With the nine-degree-of-freedom model of the present theory, there are eighteen roots or eigenvalues. The eigenvalues for each mode are usually a complex conjugate pair, which are then described by a frequency ω and damping ratio ζ:

$$\omega = Im\lambda$$

$$\zeta = -Re\lambda/|\lambda|$$

The damping ratio ζ is the fraction of critical damping for the mode. The coincidence of the notation for the damping ratio and the rotor lag angle is unfortunate, but both are well established and the context should always clarify which is meant.

Nine eigenvectors or modes correspond to the eigenvalues. The modes are identifiable by their frequency (which is near the uncoupled frequency, approximately the appropriate natural frequency as indicated in parentheses below) and by the participation of the degrees of freedom in the eigenvector. The modes are labelled here as follows:

q_1	wing vertical bending (ω_{q_1})
q_2	wing chordwise bending (ω_{q_2})
p	wing torsion (ω_p)
$\beta - 1$	low-frequency flap ($\nu_\beta - 1$)
$\zeta - 1$	low-frequency lag ($\nu_\zeta - 1$)
β	coning (ν_{β_0})
$\beta + 1$	high-frequency flap ($\nu_\beta + 1$)
$\zeta + 1$	high-frequency lag ($\nu_\zeta + 1$)
ζ	collective lag (ν_{ζ_0})

Each mode involves motion of all nine degrees of freedom, of course (q_1, q_2, p, β_{1C}, β_{1S}, β_0, ζ_{1C}, ζ_{1S}, and ζ_0). The low- and high-frequency modes were discussed earlier.

Description of the full-scale proprotors.- The parameters that describe the two full-scale proprotors are given in table 3 and in figures 14 to 17. The wing described in table 3 is for the configuration tested in the 40- by 80-Foot Wind Tunnel. The rotors are flight-worthy designs. (For further descriptions of the full-scale rotors and aircraft, see references 25 to 28.) The parameters given in table 3 are those required for the present theory.

TABLE 3.- DESCRIPTION OF THE BELL AND BOEING FULL-SCALE PROPROTORS AS TESTED IN THE AMES 40- BY 80-FOOT WIND TUNNEL

	Bell	Boeing
Rotor		
Type	Gimballed, stiff inplane	Cantilever, soft inplane
Number of blades, N	3	3
Radius, R	3.82 m (12.5 ft)	3.97 m (13 ft)
Lock number, γ	3.83	4.04
Solidity, σ	0.089	0.115
Pitch/flap feedback, K_P	-0.268	0
Lift curve slope, a	5.7	5.7
Rotor rotation direction, $sgn\ \Omega$	+1	-1
Tip speed, ΩR	183 m/sec (600 ft/sec)	160 m/sec (525 ft/sec)
Rotational speed, Ω	458 RPM 7.63 Hz 48.0 rad/sec	386 RPM 6.43 Hz 40.4 rad/sec
Blade frequencies (per rev)		
ν_β	$\left[1 + 0.0355\left(\frac{600}{\Omega R}\right)^2\right]^{1/2}$ (fig. 16(a))	figure 17(a)
ν_{β_0}	1.85	ν_β
ν_ζ	figure 16(b)	figure 17(b)
ν_{ζ_0}	0 for autorotation, ν_ζ for powered	
Blade inertias		
I_b	142 kg-m^2 (105 slug-ft^2)	203 kg-m^2 (150 slug-ft^2)
$I_\beta{}^*$	1.000	0.922
$I^*_{\beta_0}$	.779	.922
$I_\zeta{}^*$	.670	.860
$I^*_{\zeta_0}$	.670	.860
$I_0{}^*$	1.0	1.0
$I^*_{\beta\alpha}$	1.0	.955
$I^*_{\zeta_0\alpha}$	.787	.917

TABLE 3.- DESCRIPTION OF THE BELL AND BOEING FULL-SCALE PROPROTOR AS TESTED IN THE AMES 40- BY 80-FOOT WIND TUNNEL - Continued

		Bell	Boeing
Blade inertias	$S_\zeta{}^*$	1.035	1.092
	$S^*_{\beta_0}$	1.212	1.286
	$M_b{}^*$	6.160	4.344
Except in autorotation where			
	$I^*_{\zeta_0}$	1	
	$I^*_{\zeta_{0\alpha}}$	1	
	ν_{ζ_0}	0	
Blade structural damping			
	g_{s_β}	0.1 percent	0.5 percent
	$g_{s_{\beta_0}}$	.5 percent	.5 percent
	g_{s_ζ}	.5 percent	.5 percent
	$g_{s_{\zeta_0}}$	.5 percent	.5 percent
Wing			
Semispan, y_{T_w}		1.333	1.281
Chord, c_w		.413	.398
Mast height,			
	h	.261	.276
	h_{EA}	.342	.354
Pylon center of gravity, $z_{P_{EA}}$		.050	.145
Inertias			
	$m_P{}^*$	76.9	110.93
	$I^*_{P_x}$	1.086	1.323
	$I^*_{P_y}$	1.206	2.926
	$I^*_{q_w}$	4.03	2.822
	$I^*_{p_w}$	.0141	.0099
	C^*_{pq}	.667	.667
	$S_w{}^*$	2.88	12.56

TABLE 3.- DESCRIPTION OF THE BELL AND BOEING FULL-SCALE PROPROTOR AS TESTED IN THE AMES 40- BY 80-FOOT WIND TUNNEL - Continued

	Bell		Boeing	
Mode shape				
$\zeta_w(y_{B_w})$	0.535			
$\eta_w'(y_{T_w})$	1.74			
Sweep, δ_{w_3}	-6.5°			
Dihedral, δ_{w_1}	0			
Thickness ratio, t_w/c_w	13.5 percent			
Aspect ratio	6.6			
Aerodynamic center, x_{A_w}/c_w	-.01			
Moment coefficient, $c_{m_{ac}}$	-.005			
Full stiffness wing				
Dimensional stiffness				
K_{q_1}	9.20×10^6 kg m^2/sec^2 (6.793×10^6 slug ft^2/sec^2)			
K_{q_2}	2.50×10^7 (1.840×10^7)			
K_p	1.77×10^6 (1.305×10^6)			
Dimensional structural damping				
C_{q_1}	9030 kg m^2/sec (6653 slug ft^2/sec, ζ = 1 percent)			
C_{q_2}	27,300 (20,185, 1.8 percent)			
C_p	955 (703, 1.5 percent)			
Dimensionaless stiffness				
$K^*_{q_1}$	18.72		18.51	
$K^*_{q_2}$	50.70		50.14	
$K_p{}^*$	3.595		3.555	
Dimensionless damping				
$C^*_{q_1}$	.880		.732	
$C^*_{q_2}$	2.67		2.22	
$C_p{}^*$	.093		.077	
Typical resulting frequencies				
q_1	3.2 Hz	0.42/rev	2.3 Hz	0.36/rev
q_2	5.35	.70	4.0	.62
p	9.95	1.30	9.2	1.43

TABLE 3.- DESCRIPTION OF THE BELL AND BOEING FULL-SCALE PROPROTOR AS TESTED IN THE AMES 40- BY 80-FOOT WIND TUNNEL - Concluded

	Bell	Boeing
Quarter stiffness wing		
Dimensional stiffness		
K_{q_1}	2.28×10^6 kg m^2/sec^2 (1.687×10^6 slug ft^2/sec^2)	
K_{q_2}	6.60×10^6 (4.863×10^6)	
K_p	5.30×10^5 (3.908×10^5)	
Dimensional damping		
C_{q_1}	3590 kg m^2/sec (2646 slug ft^2/sec, ζ = 0.8 percent)	
C_{q_2}	4700 (3462, 0.6 percent)	
C_p	441 (325, 1.0 percent)	
Dimensionless stiffness		
$K^*_{q_1}$	4.65	4.60
$K^*_{q_2}$	13.40	13.25
$K_p{}^*$	1.077	1.065
Dimensionless damping		
$C^*_{q_1}$	.35	.29
$C^*_{q_2}$	.458	.381
$C_p{}^*$	.043	.036
Typical resulting frequencies		
q_1	1.5 Hz 0.40/rev	1.1 Hz 0.35/rev
q_2	2.6 .68	1.85 .58
p	5.65 1.48	5.55 1.73
Full-scale aircraft wing		
Typical frequencies		
q_1	0.45/rev	0.49/rev
q_2	.78	.95
p	1.15	1.22

The Bell rotor is of gimballed, stiff inplane construction; the Boeing rotor is of cantilever, soft inplane construction. The Lock number γ is based on the representative inertia I_b, which is also given in table 3. The Bell rotor has -15° of δ_3, from which $K_P = \tan \delta_3 = -0.268$. The two rotors rotate in opposite directions; with $sgn\ \Omega = 1$, the Bell rotor rotates clockwise on the right wing, and with sgn $\Omega = -1$, the Boeing rotor rotates counterclockwise on the right wing. The blade twist and thickness distributions are given in figure 14 for the two rotors. The structural properties of the blades are given in figure 15. The rotor rotational speed Ω and the corresponding tip speed ΩR, given in table 3, are the design operating speeds for airplane configuration. All theoretical results for frequencies are presented dimensionless, that is, as a fraction of Ω (per rev); table 3 gives the dimensional values of Ω for reference and to orientate the dimensionless results.

The blade rotating natural frequencies are given in table 3 and in figures 16 and 17 for the Bell and Boeing rotors, respectively. Figure 16(a) shows the variation of the Bell flap frequency with rotor speed Ω, from the expression given in table 3. Since the Bell hub is gimballed, ν_β is independent of $V/\Omega R$ (collective pitch); the variation shown results from the hub spring restraint, which is rather weak at the normal Ω. The coning mode natural frequency (for which the Bell rotor acts as a cantilever rotor) given in table 3 is only approximate, for it should vary with Ω and with the inflow ratio (with collective) as the lag frequency does. The coning mode, especially with this high frequency, does not participate significantly in the proprotor and wing dynamics. The lag frequency for the Bell rotor (fig. 16(b)) is greater than 1/rev for the stiff inplane blade; the variation with $V/\Omega R$ is actually the effect of the collective pitch variation. For normal Ω, the Bell blade has a lag frequency from about 1.6 to 1.2 over the usual range of inflow ratio; for reference, the forward speed is about 250 knots at $V/\Omega R = 0.7$ and normal Ω. The flap and lag frequencies for the Boeing blade are shown in figures 17(a) and 17(b) for this cantilever, soft inplane blade, $\nu_\beta > 1/\text{rev}$ and $\nu_\zeta < 1/\text{rev}$ (for the normal operating Ω at least). The frequencies of the Boeing rotor do not vary much with inflow ratio (i.e., with collective) because the blade has a nearly isotropic shank construction to achieve the soft inplane lag frequencies; in fact, a soft inplane rotor for which the lag frequency did vary with collective would not be a useful design for the proprotor because of the restraints of blade loads and blade stability. For reference, the forward speed for the Boeing rotor is about 218 knots at $V/\Omega R = 0.7$ and normal Ω. The Bell and Boeing rotors both have a hover rotational speed of about 550 rpm; the blade frequencies up to this Ω value are given in figures 16 and 17. The blade frequencies at half normal operating Ω (229 and 193 rpm, respectively, for the Bell and Boeing rotors) required for operating on the quarter stiffness wing, are also given in figures 16 and 17.

The blade inertia constants are normalized by the I_b values given. The blade structural damping values are only approximate; the structural damping of the blade is in any case negligible compared with the aerodynamic damping in high inflow.

The same wing is used for both rotors. The wing semispan is 5.1 m (16.67 ft) from the tunnel floor to the rotor shaft; the difference in the

dimensionless values results from the use of different rotor radii in the normalization. The mast height h is from the wing tip spar to the rotor hub, and h_{EA} is from the effective elastic axis to the hub. The wing has a forward sweep ($\delta_{w_3} < 0$) of 6.5° which shifts the effective elastic axis at the wing tip a distance $h_{EA} - h = 0.31$ m aft of the wing tip spar. The elastic axis shift results in the value of $\xi_w(y_{B_w})$ given. The pylon center-of-gravity location is the distance forward of the wing tip effective elastic axis; it is used only to find $S_w^* = mP^* z_{P_{EA}}/y_{T_w}$. The value of $\eta_w'(y_{T_w})$ given was obtained from a structural dynamics analysis of the wing modes; note that the approximate mode shape $\eta_w = y_w^2/y_{T_w}$ gives $\eta_w'(y_{T_w}) = 2$.

The inertia parameters of the wing were obtained from measurements; the wing stiffnesses were then obtained by finding the values required to match the experimental frequencies. This procedure makes use of the most accurately known wing properties (mass and frequencies) and ensures that the most important parameters of the wing dynamic characteristics - the frequencies - are accurately represented. The result was the dimensional stiffnesses given in table 3 for the full stiffness wing and the quarter stiffness wing; the dimensional stiffnesses are the same for both rotors since the same wing was used. The dimensionless stiffnesses are obtained by dividing by $(N/2)I_b\Omega^2$. The values given are based on the normal operating rotor speed, and so must, in general, be multiplied by $(\Omega R_o/\Omega R)^2$ where $\Omega R_o = 183$ and 160 m/sec (600 and 525 ft/sec), respectively, for the Bell and Boeing rotors. To indicate the meaning of the stiffnesses, table 3 includes typical values of the resulting wing frequencies; since these values are for the coupled motion - at 100 knots and normal Ω (one-half normal Ω for the quarter stiffness wing) - they include the rotor inertia and aerodynamic influences, but the latter are small at this low speed. The results for the predicted and measured frequencies are always given here in dimensionless form (per rev); for reference, the corresponding dimensional values of the wing natural frequencies are given in table 3.

The wing structural damping coefficients were determined from the stiffness and the measured values of the damping ratio (with the rotor off and no forward speed, so they include no aerodynamic influences). The wing structural damping is not well known, which means there is some uncertainty in the predictions of the wing mode damping levels. The values given in table 3 are based on the measurements with and without the rotor and wing aerodynamic influences, and are found to produce reasonable correlation with the data. The dimensionless damping values given are based on the normal rotor operating speed, so, in general, they must be multiplied by $(\Omega R_o/\Omega R)$.

The wing used, while having properties representative of the full-scale aircraft, actually was somewhat thinner ($t_w/c_w = 13.5$ percent as compared with the more likely 20-23 percent) and of quite different construction. Wing frequencies characteristic of the full-scale aircraft (for airplane cruise configuration and rotor speed) conclude table 3 to indicate the appropriateness of the wing used for the full-scale tests.

Other theories- The results of the theory developed here compared with the results of other theories, as well as with the experimental data from the full-scale tests. The reports of the full-scale tests of the Bell and Boeing rotors (refs. 25 and 26) include predictions of the dynamic characteristics, using theories developed by the companies for their rotors.

The Bell Helicopter Company uses two theories, a linear model and a nonlinear model. The Bell linear theory (refs. 15 and 25) consists of a closed-form analysis for calculating eigenvalues and eigenvectors. The model has linear blade aerodynamics, but no wing aerodynamics. The degrees of freedom consist of flap and lag for each rotor blade and, for the wing and pylon, there are five modes: vertical bending, chordwise bending, torsion, pylon yaw, and pylon pitch. The Bell nonlinear theory (refs. 25 and 29) consists of an open-form analysis for calculating the time history of the motion by numerical integration of the equations of motion. The model uses better blade aerodynamics than does the linear theory, and incorporates wing aerodynamics (including rotor/wing interference effects). For this application at least, the same degrees of freedom are used as for the linear theory. The nonlinear theory uses normal modes for the airframe (wing and pylon here) degrees of freedom, obtained from a NASTRAN calculations.

The Boeing Vertol Company uses a linear theory (refs. 26, 28, and 30) that consists of a closed-form analysis for calculating the eigenvalues and eigenvectors. The degrees of freedom consist of flap and lag motion for each blade and normal modes for the wing.

The Gimballed, Stiff-Inplane Rotor

A 25-ft-diam flight-worthy gimballed, stiff-inplane proprotor, designed and constructed by the Bell Helicopter Company, was tested in the 40- by 80-Foot Wind Tunnel in July 1970. The configuration for the dynamics test (fig. 12) consisted of the windmilling rotor mounted on the tip of a cantilever wing. The rotor was operated in high inflow axial flow. The rotor and wing were described previously. The test results, and also theoretical results from the Bell theories, are given in reference 25. Only the data for the case with the yaw link in are used here; that configuration had the pylon yaw stiffness at the airplane mode value. The theoretical dynamic characteristics of this rotor and wing are discussed, followed by a comparison with the full-scale test results and the Bell theoretical results. The aspects of the theory to be examined were discussed in the previous section.

The predicted variation of the eigenvalues of the system with forward speed, at the normal airplane mode rotor speed (Ω = 458 rpm), is shown in figure 18: the frequency and damping ratio and the root locus. The wing mode frequencies show a slight decrease with V. The decrease in the lag frequency ν_ζ with $V/\Omega R$ (really the effect of collective pitch) is apparent in the $\zeta \pm 1$ mode frequencies. The $\beta \pm 1$ modes show the influence of the negative δ_3, which drops the effective flap frequency below 1/rev. For the rotor operating in autorotation, the rotor speed perturbation degree of freedom ζ is a first-order motion (a balance of the inertia and the aerodynamic lag damping) so its

eigenvalue is on the negative real axis (not shown in fig. 18). The time constant of the ζ mode increased greatly from low inflow, where the lag damping comes from the c_{ℓ_α} terms (Q_ζ). The damping of the wing chordwise bending mode q_2 decreases with V, the damping of the torsion mode p increases. The damping of the wing vertical bending mode first increases with V, then it decreases. The peak occurs where the frequencies of the ζ - 1 and q_1 modes cross; hence it is an effect of the coupling of the rotor lag and wing bending modes. A similar effect is apparent in the q_2 damping where the ζ - 1 and q_2 frequencies cross, but it occurs at very low inflow so the effect is small. The q_1 mode becomes unstable at 495 knots ($V/\Omega R$ = 1.39); and the q_2 mode, at 600 knots ($V/\Omega R$ = 1.69); these are the characteristic high inflow instabilities of the proprotor and wing configuration. Of course, the helical tip Mach number ($M_{max} = M_{tip}[1 + (V/\Omega R)^2]^{1/2}$) is unity at about 550 knots ($V/\Omega R$ = 1.55), certainly an upper limit on the validity of the theory.

The influence of the rotor lag motion on the system stability is shown in figure 19, which compares the damping of the wing modes with and without the ζ_{1C} and ζ_{1S} degrees of freedom in the theory (ζ_0 is the rotor speed perturbation for this autorotation case, so it must be retained); figure 19(c) shows the complete root locus without ζ_{1C} and ζ_{1S} in comparison with figure 18(c). The rotor lag motion has a very important influence on the wing modes, especially the q_1 damping. Without the resonance of the lower-frequency lag mode with wing vertical bending, the damping does not show a peak at the resonance, rather it continues to increase with V until the high inflow effects appear at about 450 knots ($V/\Omega R$ = 1.27); then the damping drops off very quickly. So the rotor lag motion has the following influence on the stability: when the ζ - 1 frequency is greater than the q_1 frequency (roughly, when $\nu_\zeta > \omega_{q_1}$ + 1/rev), the resonance increases the q_1 mode damping, while, when the ζ -1 frequency is less than the q_1 frequency, it decreases the damping. The result is that the rotor lag motion significantly reduces the wing vertical bending mode damping at the higher speeds. The speed at which the q_1 mode becomes unstable is not changed much, however, which indicates that the high inflow instability mechanism is not greatly influenced by the lag motion. The reduction in damping at high speed is then more importantly accompanied by a great reduction in the rate at which the damping decreases, which is very beneficial. The rotor lag motion thus makes the high inflow instability less severe. The flap and lag modes in high inflow are highly coupled by the aerodynamics. Eliminating the ζ_{1C} and ζ_{1S} motions therefore greatly influences the behavior of the $\beta \pm 1$ mode, as shown in the root loci of figures 18 and 19. The rotor flap motion is expected to be important to the proprotor and wing dynamics. The above comparison shows that the rotor lag motion can be equally important. The influence of the lag motion is a combination of the high inflow aerodynamic forces and inertia coupling with the shaft motion.

The influence of the rotor speed perturbation degree of freedom and the wing aerodynamics on the system stability is shown in figure 20. The basic case is autorotation operation, including the wing aerodynamics. Eliminating the wing aerodynamic forces decreases the q_1 and p mode damping, but has only a small influence on the q_2 damping, which indicates that the C_{L_α} wing damping is the most important effect. Powered operation (including the wing

aerodynamics again) is considerably stabilizing for all the wing modes, over the autorotation case. The powered model considers the hub rotating at a constant speed, so the ζ mode becomes the elastic motion of the blades about the hub, with spring restraint ν_ζ. The powered operation has little influence on the $\beta \pm 1$ and $\zeta \pm 1$ modes, or on the wing mode frequencies.

The influence of the complete expressions for the rotor aerodynamic coefficients, that is, including the c_ℓ, c_d, c_{d_α}, c_{ℓ_M}, and c_{d_M} terms as well as the c_{ℓ_α} terms, is shown in figure 21. The better rotor aerodynamic model reduces the predicted stability of the wing modes, for both autorotation and powered cases. The details of the coupling of the high-frequency rotor modes $\beta + 1$ and $\zeta + 1$ are also changed somewhat. The complete rotor aerodynamic coefficients were calculated both by use of the correct collective pitch from a performance analysis (the collective pitch required for $C_Q = 0$ for autorotation, or for the C_T needed in equilibrium cruise for powered flight), and by use of an approximate collective value based on the inflow at 75 percent radius ($\theta_{0.75} = \tan^{-1}(V/\Omega R)/(3/4) + 1.25°$). The performance calculation is very sensitive to the collective pitch used, but figure 21 shows that the dynamics behavior is not; the approximate collective used is, in fact, within 1 or 2° of the correct value for both autorotation and powered flight at high speed, and so evidently is an adequate representation of angle-of-attack distribution. The complete expressions for the aerodynamic coefficients give somewhat different numerical values compared with those obtained when only the c_{ℓ_α} terms are used (fig. 5), but the general behavior remains the same. An exception is when the drag divergence critical Mach number is exceeded. The helical tip Mach number exceeds the critical Mach number for the blade section characteristics used ($M_{crit} = 0.9$) at about 475 knots ($V/\Omega R = 1.33$); it exceeds the sonic value ($M = 1$) at about 550 knots ($V/\Omega R = 1.55$). These points (fig. 21) are limits to the validity of the theory, but the main effects of the better blade aerodynamic model occur below these limits. It is concluded that using only the c_{ℓ_α} terms in the rotor aerodynamic coefficients is satisfactory for studying the basic behavior, and, in fact, is quite accurate so long as V is neither too small (low inflow) nor too large (stall and compressibility). For this example, the range in which the c_{ℓ_α} expressions are adequate is approximately V = 25 to 350 or 400 knots ($V/\Omega R$ = 0.1 to 1.0 or 1.1). When one predicts the characteristics of an actual aircraft, however, especially the high-speed stability, the best available rotor blade aerodynamic model should be used, which probably means tabular data for the lift and drag coefficients as a function of angle of attack and Mach number for the blade sections used.

Figure 22 shows the influence of using the simplified theoretical model on the predicted system stability. The effect is that of eliminating the wing sweep terms (except for the effective elastic axis shift, which is retained through h_{EA}); the basic model already uses only the c_{ℓ_α} terms in the rotor aerodynamics and has no angle of attack or dihedral. The effect of the better blade aerodynamics was discussed previously; the effect of dihedral is expected to be similar to that for sweep; and there is little influence of angle of attack generally (either experimentally or theoretically, for small angles at least). Therefore, the simpler theoretical model is quite

satisfactory for studying basic proprotor dynamics, giving the same general characteristics as the more involved model. For the design of an actual aircraft, however, a good structural analysis of the wing and pylon motion should be used.

Figure 23 shows the behavior of the system dynamics during a rotor rotational speed sweep at 185 knots. The decrease in the wing mode frequencies is almost exactly proportional to Ω^{-1}, that is, the dimensional frequencies are nearly constant during the Ω variation. The lag frequency decreases with Ω faster than the (per rev) wing frequencies do. The ζ - 1 mode again shows a frequency resonance with the q_1 mode with increased damping when the ζ - 1 frequency is higher, and decreased damping when it is lower than the q_1 frequency. Some of the damping variation probably results from the high inflow influence. At low Ω, a resonance of the β + 1 and p modes occur, which is apparent in both the frequency and damping of these two eigenvalues.

The dynamic characteristics of the Bell rotor on the quarter stiffness wing, at half normal operating rotor speed (Ω = 229 rpm), are shown in figure 24, including a comparison with the full stiffness wing results (plotted vs. $V/\Omega R$). The frequencies of the modes are given in figure 24(a) (except for the β, β + 1, and ζ + 1 modes), and the great increase in the lag frequency that results from slowing the rotor is evident (see also fig. 16(b)). The wing frequencies are fairly well matched between the quarter- and full-stiffness wings. However, because of the difference in lag frequencies, the damping for the wing modes is not well simulated on the quarter-stiffness wing (figs. 24(b) and (c)), especially for the q_1 mode, which, for the full-stiffness wing, encounters a resonance with the ζ - 1 mode. The influence of the rotor lag motion may be removed from the full-stiffness wing theory by eliminating the ζ_{1C} and ζ_{1S} degrees of freedom and, indeed, the q_1 damping on the quarter-stiffness wing correlates well with that case. With the increased lag frequency on the quarter-stiffness wing, the p mode (instead of the q_1 mode) encounters a ζ - 1 mode resonance, with a corresponding influence on the torsion damping.

Figure 25 shows the eigenvalues and eigenvectors for the Bell rotor at the typical cruise condition $V/\Omega R$ = 0.7, Ω = 458 rpm, V = 249 knots. This figure is a time vector representation of the modes, so the eigenvector set for a given mode rotates counterclockwise at $\omega = Im\lambda$ and decreases exponentially at a rate given by $Re\lambda$. The projection of each vector on the real axis gives the participation of the degrees of freedom in the motion during the damped oscillation of the system in that mode. The degrees of freedom not shown for a given mode have a magnitude negligible on the scale used (i.e., less than about 5 percent of the maximum). The autorotation and powered cases show little difference except for the ζ_0 motion, of course, and in the wing mode eigenvalues. The rotor degrees of freedom participate significantly in the wing modes. The $\beta \pm 1$ and $\zeta \pm 1$ modes show the coupling of the flap and lag motions due to the high inflow aerodynamics, but little coupling with the wing motion or with the collective rotor degrees of freedom. If β_{1C} leads β_{1S} in the time vector representation, the flap mode is progressive (the tip path plane wobbles in the same direction as the rotor rotation) and, similarly, for the lag modes. With the stiff-inplane rotor ($\nu_\zeta > 1$) and negative δ_3 (so the

effective $\nu_\beta < 1$), then the $\beta - 1$, $\beta + 1$, and $\zeta + 1$ modes are progressive and the $\zeta - 1$ mode is regressive, as expected.

The frequency response of the Bell rotor to each of the six input quantities is shown in figures 26 and 27 for autorotation and powered flight, respectively. The magnitude of the response of each degree of freedom to the input is shown; the rotor is operating at $V/\Omega R = 0.7$, $\Omega = 458$ rpm, and $V = 249$ knots (the same as for the eigenvectors in fig. 25). The frequency response of the system is a good indicator of the dynamics involved, particularly the peaks in the response that occur at the resonant frequencies if the degree of freedom can be excited by that input. The frequencies of the eigenvalues are also shown (lower right) to identify the resonances. The wing vertical bending resonance (q_1) is most important for the cyclic inputs (α_G, β_G, θ_{1C}, and θ_{1S}), and the chordwise bending resonance (q_2), for the collective inputs (u_G and θ_0). There are also significant resonances with the upper-frequency rotor modes ($\beta + 1$, $\zeta + 1$). The degrees of freedom usually show significant excitation at the higher frequencies, especially near resonance with the wing modes, even if there is small or negligible steady-state response. The major differences between the powered and autorotation cases are the steady-state response (especially for the collective inputs), which carries into the low frequencies, too, and the response of the ζ_0 motion.

The response shown at very low frequencies in figures 26 and 27 indicates the static response of the system to the six inputs. The system generally separates into a longitudinal or collective group (variables β_0 and ζ_0 and inputs u_G and θ_0) and a lateral/vertical or cyclic group (variables β_{1C}, β_{1S}, ζ_{1C}, and ζ_{1S} and inputs α_G, β_G, θ_{1C}, and θ_{1S}). The wing variables (q_1, q_2, p) couple the two groups, but are excited most by the cyclic group. In autorotation, the static response of the cyclic rotor variables to the cyclic inputs is of order 1 for the flap motion and of order 0.1 for the lag motion; their response to the collective inputs is negligible. The static response of the collective rotor variables to the cyclic inputs is negligible; the response of β_0 to θ_0 is small, and to u_G, it is negligible. The response of $\dot{\zeta}_0$ to the collective inputs is of order 1; $\dot{\zeta}_0/u_G = -1$, of course, as discussed earlier (eq. (86)). The static response of the wing variables to the collective inputs is negligible; the response of q_1 and p to the cyclic inputs is of order 0.05 and the response of q_2 is of order 0.005. For powered flight, there is negligible effect on the response to the cyclic inputs compared to autorotation, but the response to collective inputs (θ_0, u_G) increases significantly. The static response of the cyclic flap motion to the collective inputs is then of order 0.05, the response of the cyclic lag motion is of order 0.005, the response of q_1 is of order 0.1, the response of q_2 is of order 0.05, and the response of p is of order 0.01. The static response of the collective variables (β_0 and ζ_0) to the collective inputs in powered flight is of order 0.2.

Consider a comparison of the predicted dynamic characteristics for the Bell rotor with experimental results from the full-scale tests in the 40- by 80-Foot Wind Tunnel and with the results of the Bell theories. Full-scale experimental data are available for the frequency and damping ratio of the wing modes. The data are limited by the tunnel maximum speed (about 200 knots) and by the use of an experimental technique that gave primarily only the damping ratio for the wing vertical bending mode. The data were obtained by use

of an aerodynamic shaker vane on the wing tip (evident in fig. 12; the same technique was used for the Boeing rotor, fig. 13). The vane was oscillated to excite the wing motion desired; when sufficient amplitude was obtained, the vane was stopped and the system frequency and damping were determined from the subsequent decaying transient motion. This configuration is best suited for excitation of the wing vertical bending mode (q_1).

Figure 28 shows the variation of the system stability with velocity at the normal operating rotor speed (Ω = 458 rpm), in terms of the frequency and damping ratio for the wing modes. The results of the present theory are compared with the experimental data from the full-scale test, and with the results of the Bell linear and nonlinear theories. Reasonable correlation with both experiment and the Bell theories is shown. The good correlation of the frequencies predicted by use of the present theory with the experimental data (fig. 28(a)) follows because the wing stiffnesses were chosen specifically to match the measured frequencies (at around 100 knots). The difference between the predicted damping levels of the Bell linear and nonlinear theories is largely due to the neglect of the wing aerodynamic forces in the former.

Figure 29 shows the variation with rotor speed Ω of the wing vertical bending mode damping for the Bell rotor at V = 185, 162, and 150 knots. Reasonable correlation is shown with both the experiment and the Bell theories. For V = 162 and 150 knots, the predictions from the Bell theories are available only at normal operating rotor speed (Ω = 458 rpm, from fig. 28(b)).

Figure 30 shows the variation of the system stability with forward speed for the Bell rotor on the quarter-stiffness wing, at half normal operating rotor speed (Ω = 229 rpm). During the full-scale test of this configuration, the available collective pitch was limited to the value reached at about 155 knots (at Ω = 229 rpm). Since the rotor was operated in autorotation, the collective pitch and inflow ratio $V/\Omega R$ were directly correlated. The maximum value of the inflow ratio was reached at 155 knots, where $V/\Omega R$ = 0.875. Above this speed, the collective was constant, and the inflow ratio was fixed at about $V/\Omega R$ = 0.840. The increase in velocity above 155 knots was accompanied by an increase in the rotor speed Ω to keep the inflow ratio at the constant value demanded by the collective limit. The theoretical predictions include the actual rotor speed. The predicted frequency and damping with the rotor speed maintained at a constant value (Ω = 229 rpm) are also shown in figure 30. The true values of the inflow ratio $V/\Omega R$ for the experimental points above 155 knots are shown in figure 30. Reasonable correlation is shown with both the experiment and the Bell theories. The decrease in the frequencies at high speed is produced mainly by the increasing Ω. The increasing Ω at high speed due to the collective limit significantly reduces the wing vertical bending and torsion damping, primarily because of the decrease in the effective (i.e., per rev) wing frequencies.

The variation with rotor speed of the wing vertical bending and torsion damping for the Bell rotor on the quarter stiffness wing is shown in figure 31 for V = 150 and 170 knots. Reasonable correlation is shown with experiment and the Bell theories.

Figure 32 shows the rotor flapping due to shaft angle of attack. The correlation of experiment and theory is shown in figure 32(a). The present theory predicts fairly well the magnitude of the flapping due to shaft angle of attack and also the longitudinal flapping β_{1C}. However, the theory underestimates the lateral flapping β_{1S} by about a factor of 1/2. The results of the Bell linear theory are almost identical with the results of the present theory. The Bell nonlinear theory, however, predicts well the lateral flapping β_{1S} also, as shown in figure 32(a). As discussed in reference 25, the better prediction of β_{1S} with the nonlinear theory is probably due to the inclusion of the influence of the wing-induced velocity on the rotor motion. Further evidence for that conclusion is the single point in figure 32(a) for which the present theory adequately predicts the lateral flapping β_{1S}. That point is from the powered test, which was not conducted on a wing. The lateral flapping β_{1S} is small compared to the longitudinal flapping β_{1C}, so the present theory does predict the magnitude of the flapping well. The azimuthal phase prediction has the same order of error as does β_{1S}, however. Figure 32(b) shows the predicted and experimental variation of the flapping with inflow ratio $V/\Omega R$. The theoretical results are for a velocity sweep at normal rotor speed (Ω = 458 rpm), while the experimental results include limited variation of Ω as well as V, and the flagged points are even for the quarter-stiffness wing. Yet the flapping correlates well with the single parameter $V/\Omega R$, indicating that the primary influence is the rotor aerodynamic forces. The underprediction of β_{1S} is again observed; the single point that agrees with the theory is the powered test point.

Figure 33 shows the variation of the wing vertical bending (q_1) damping with $V/\Omega R$, during velocity sweeps for the Bell rotor on the full-stiffness and quarter-stiffness wings. The full-scale experimental data show a definite trend to higher damping levels with the full-stiffness wing than with the quarter-stiffness wing, and this trend correlates well with the present theory. The difference in damping at the same inflow ratio results from the lag motion. Figure 33(b) shows the frequencies of the ζ - 1, q_1, and p modes for the full-stiffness and quarter-stiffness wings. The full-stiffness wing has a resonance of the ζ - 1 and q_1 modes that increases the q_1 damping below the resonance and decreases it above, and produces the peak in the damping observed in figure 33(a). Slowing the rotor on the quarter-stiffness wing greatly increases the lag frequency and removes it from resonance with q_1 (instead there is a resonance with the p mode, as shown in figure 33(b) and discussed earlier). Another way to remove the influence of the rotor lag motion - in the theory - is to simply drop the ζ_{1C} and ζ_{1S} degrees of freedom from the full-stiffness wing case. Then the predicted wing vertical bending damping is almost identical to that for the quarter-stiffness wing (fig. 33(a)).

The Hingeless, Soft-Inplane Rotor

A 26-ft-diam, flight-worthy, hingeless, soft-inplane proprotor, designed and constructed by the Boeing Vertol Company, was tested in the 40- by 80-Foot Wind Tunnel in August 1972. The configuration for the dynamics test (fig. 13) consisted of the windmilling rotor mounted on the tip of a cantilever wing,

with the rotor operating in high inflow axial flow. The rotor and wing were described previously. The full-scale test data for the quarter-stiffness wing runs, and the theoretical results from the Boeing theory are from reference 26. The theoretical dynamic characteristics of this rotor and wing are discussed, followed by a comparison with the full-scale test results and the Boeing theoretical results.

The major changes in the dynamic behavior compared with that of the Bell rotor are due to the different placement of the blade frequencies. The Boeing rotor has 1 - ν_ζ of the same order as the wing vertical bending frequency (as did the Bell rotor), but the soft-inplane rotor with $\nu_\zeta < 1$ introduces the possibility of an air resonance instability, that is, a mechanical instability that results from the resonance of the ζ - 1 and q_1 modes. This instability will occur at a definite Ω (for resonance) which, in this case, is above the normal operating rotor speed and at low forward speed. At high enough $V/\Omega R$, the lag damping Q_ζ becomes large enough to stabilize the resonance. An analytical discussion of the air resonance instability was given earlier. Besides introducing the possibility of an instability, at high Ω and low V, the lag motion of the soft-inplane rotor generally decreases the wing vertical bending mode stability.

The Boeing rotor has cantilever blades with ν_β sufficiently above 1/rev so that ν_β - 1 is very close to the wing vertical bending mode frequency. Hence the β - 1 mode takes on many of the characteristics of the q_1 mode, especially at high $V/\Omega R$. In fact, it is usually the β - 1 mode that becomes unstable at high inflow rather than the q_1 mode. By the time the β - 1 root enters the right half plane, the mode has however assumed the character of a wing vertical bending mode (this behavior is discussed further in terms of the eigenvectors of the two modes). Thus the high inflow instability mechanism is the same as observed already for the Bell rotor.

The predicted variation of the eigenvalues of the system with forward speed, at the normal airplane mode rotor speed (Ω = 386 rpm), is shown in figure 34: frequency and damping ratio and root locus. The flap frequency is greater than 1/rev and the coupled frequency of the β ± 1 modes increases somewhat with the inflow ratio. The lag frequency is less than 1/rev and the coupled frequency decreases with the inflow ratio. Since $\nu_\zeta < 1$, the ζ - 1 mode frequency increases. The proximity of the β - 1 and ζ - 1 mode frequencies to the q_1, and even the q_2, frequencies is apparent in figure 34(a). The q_1 damping is quite low at low speeds and has a minimum around 200 knots because of the influence of the ζ - 1 mode, that is, the air resonance behavior. The q_1 damping increases at high V, but there is considerable coupling of the β - 1 and q_1 modes (as indicated by the frequencies and the eigenvectors). The β - 1 mode damping decreases very quickly at high speed and, by the time the root crosses into the right half plane at V = 480 knots ($V/\Omega R$ = 1.54), the mode is really a wing vertical bending instability, that is, the high inflow inflow proprotor and wing instability. This change in the character of the β - 1 and q_1 modes is shown in figure 34(d), which presents the eigenvectors at V = 250, 400, and 500 knots. At low speed, the eigenvector on the left is clearly identifiable as the q_1 mode, and the eigenvector on the right as the β - 1 mode, based both on the frequency of the root and on the participation of the degrees of freedom in the eigenvector. As forward speed increases, the

wing vertical bending motion decreases in one mode and increases in the other. The mode that is originally the rotor low-frequency flap mode (β - 1) becomes unstable just before 500 knots, and by that time this mode has assumed the character of the primary wing vertical bending mode. Note that the wing vertical bending motion is characterized not simply by the q_1 degree of freedom, but also by the motion of ζ_{1C}, ζ_{1S}, ζ_0, and p associated with the mode.

The wing chord (q_2) mode damping decreases with speed until an instability is encountered at V = 510 knots ($V/\Omega R$ = 1.64). This is an air resonance instability, as indicated by the coincidence of the ζ - 1 and q_2 mode frequencies at this speed (fig. 34(a)). Wing chord bending produces a lateral motion at the rotor hub forward of the wing tip, which couples with the rotor lag motion. An air resonance instability can occur at even high speed with the wing chord mode because the wing aerodynamic damping of that mode remains small. The q_2 instability occurs at a slightly higher speed than the β - $1/q_1$ instability, so, in some cases, it may be the critical boundary.

The wing torsion (p) mode couples with the rotor coning (β) mode in this case, mainly due to simply a coincidence of the damping and frequencies of the two modes. These modes have fundamentally different character (β_0 is in the longitudinal group of variables and p, in the lateral/vertical group) and do not really want to couple. The roots try to cross on the root locus plane (fig. 34(c)) and instead exchange roles; the coupling is significant only in a narrow region near 300 knots; elsewhere, the roots are clearly distinguishable. While this coupling does not have great physical significance, it is discussed because a slight change in the parameters or in the model may eliminate the coupling. For comparison with such cases, it is most convenient to plot the damping (fig. 34(b)) as if the root loci really did cross, that is, by joining the corresponding p and β pieces. This practice is followed in the comparisons that follow.

The influence of the rotor lag motion on the system stability is shown in figure 35, which compares the damping of the wing modes with and without the ζ_{1C} and ζ_{1S} degrees of freedom in the theory. The rotor lag motion has a large and important influence on the wing modes. The rotor lag motion substantially decreases the stability of the q_1 and β - 1 modes. The β - 1 mode behavior remains the same when the lag degrees of freedom are eliminated, but the sharp damping decrease (and instability) occurs at a speed about 250 to 300 knots higher, beyond the scale used in figure 35(a). The low damping of the q_1 mode around 200 knots is shown to be due to coupling with the ζ - 1 mode, that is, air resonance behavior. The rotor lag motion also decreases the q_2 mode stability at high V, another air resonance effect. The lag motion stabilizes the p mode, but that is not really needed. The complete root locus is shown in figure 35(c), which is to be compared with the root locus that includes the lag motion (fig. 34(c)).

The influence of the rotor speed perturbation degree of freedom and the wing aerodynamics on the system stability is shown in figure 36. The basic case is autorotation operation, including the wing aerodynamics. The rotor speed perturbation degree of freedom generally decreases the stability, that is, powered operation is more stable, especially for the q_1 mode where the air

resonance behavior is much less noticeable. The wing aerodynamic forces generally increase the stability.

The influence of the complete expressions for the rotor aerodynamic coefficients is shown in figure 37(a) (for clarity, only the autorotation case is shown for the β - 1 and p modes). Generally, the use of the better blade section aerodynamics decreases the predicted stability of the wing modes. The correct collective was obtained from a performance analysis for powered and autorotation operation of the Boeing rotor. The approximate collective used, based on the inflow angle at 75 percent radius, was $\theta_{0.75} = \tan^{-1}(V/\Omega R)/(3/4) + 1.0°$. The helical tip Mach number reaches the blade critical Mach number ($M = 0.9$) at about 500 knots ($V/\Omega R = 1.61$) and reaches the sonic value at about 580 knots ($V/\Omega R = 1.86$). The conclusions are the same as for the Bell rotor: the basic behavior of the system is described well with only the c_{ℓ_α} terms in the rotor aerodynamic coefficients, but the complete expressions should be used to obtain correct predictions for actual vehicles, particularly for the high-speed stability boundaries. The use of the approximate collective does not influence the dynamics much, although it is, of course, not satisfactory for performance calculations.

Figure 38 shows the influence of the use of the simplified theoretical model on the predicted system stability. As for the Bell rotor, it is concluded that the simpler model is satisfactory for studying the basic behavior, but for the design of a particular vehicle, the best available model should be used.

Figure 39 shows the variation of the system eigenvalues with rotor speed Ω for the Boeing rotor at 50 knots. At this low speed, the ζ - 1 and q_1 frequency resonance around 530 rpm (fig. 39(a)) results in an air resonance instability in the q_1 mode (fig. 39(b)). At resonance, there is a corresponding increase in the ζ - 1 damping. The resonance and corresponding instability occur above the normal rotor operating speed (Ω = 386 rpm) even with the wing used for the wind-tunnel test, which was softer in bending than the full-scale design. The general decrease in the $\zeta \pm 1$ mode damping with Ω results from the low lag damping at low inflow. Figure 40 shows the variation of the eigenvalues with Ω for the Boeing rotor at 192 knots. The ζ - 1 and q_1 resonance again occurs at about Ω = 500 rpm, but this speed is sufficient to stabilize the air resonance motion. Figure 41 summarizes the Boeing rotor air resonance behavior: the wing vertical bending mode (q_1) damping variation with rotor speed Ω for V = 50 to 192 knots. The stabilizing influence of the forward speed is shown. An earlier section derived an estimate for the V value required to stabilize the air resonance motion. In this case, resonance occurs with the wing vertical bending frequency of about 0.28/rev, and ν_ζ of about 0.8/rev; with the other parameters required from table 3, equation (203) gives $V/\Omega R > 0.268$ for the stability requirement. At this speed, resonance occurs at Ω = 500 rpm, so the velocity requirement is $V > 108$ knots. The use of the equivalent radius approximation for the rotor lag damping $Q_\zeta^\cdot$ gives instead $V/\Omega R > 0.285$ or $V > 114$ knots, which is only about 6 percent higher. The estimate compares well with the calculated boundary of about 120 knots (fig. 41), better, in fact, than is reasonable to expect from the simple model used for the air resonance estimate.

The dynamic characteristics of the Boeing rotor on the quarter-stiffness wing, at half normal operating rotor speed (Ω = 193 rpm) are shown in figure 42. The frequencies of some of the corresponding modes on the full-stiffness wing are also shown in figure 42(a) (plotted vs. $V/\Omega R$; the β + 1, ζ + 1, and β frequencies are not shown for the full-stiffness wing). The wing mode frequencies are well matched to the full stiffness wing values (per rev), but slowing the rotor increases both the flap and lag frequencies of the blade considerably, the flap frequency to near 2/rev and the lag frequency to near 1/rev, as compared with about ν_β = 1.35 and ν_ζ = 0.75 at normal Ω (see also fig. 17). The lag frequency moves nearer 1/rev and thus the ζ - 1 mode frequency is lower for the quarter-stiffness wing (besides the influence on the dynamics, the lag frequency near 1/rev also means large vibration and blade loads). With the rotor frequencies so different, the system damping shown in figure 42(b) has much different behavior than for the full-stiffness wing (compare with fig. 34(b)), especially for the q_1 and β - 1 modes. Figure 43 shows the variation of the system stability with rotor speed Ω, for the Boeing rotor on the quarter-stiffness wing at 80 knots. Air resonance effects are evident in q_1 at about 400 rpm and in q_2, at about 500 rpm. The peak in the q_2 damping at 225 rpm is due to the coupling with the β - 1 mode.

Figure 44 shows the eigenvalues and eigenvectors for the Boeing rotor at the typical cruise condition of $V/\Omega R$ = 0.7, Ω = 386 rpm, V = 218 knots. With this soft-inplane ($\nu_\zeta < 1$) and cantilever ($\nu_\beta > 1$) rotor, the ζ - 1, β + 1, and ζ + 1 modes are progressive and the β - 1 mode is regressive as expected.

The frequency response of the Boeing rotor to each of the six input quantities is shown in figures 45 and 46 for autorotation and powered flights, respectively. The magnitude of the response of each degree of freedom to the input is shown; the rotor is operating at $V/\Omega R$ = 0.7, Ω = 386 rpm, and V = 218 knots (the same as for the eigenvectors in fig. 44). The steady-state (low-frequency) response, compared with that of the Bell rotor, shows only the following differences: with the hub moment capability of the cantilever rotor ($\nu_\beta < 1$), the flap motion with respect to the shaft is reduced, and the wing motion is increased. There is increased lag motion because of the softer blade inplane restraint (lower ν_ζ) and there is a change in the azimuthal phasing of the cyclic rotor response (e.g., β_{1C} and β_{1S}) to the cyclic inputs (e.g., θ_{1C} and θ_{1S}) because of the change in rotor frequencies.

Consider a comparison of the predicted dynamic characteristics for the Boeing rotor with experimental results from the full-scale tests in the 40- by 80-Foot Wind Tunnel and with the results of the Boeing theory. Full-scale experimental data are available for the frequency and damping of the wing vertical bending mode, obtained by the same shaker vane excitation technique as used with the Bell rotor.

Figure 47 shows the variation of the system stability with velocity at the normal operating rotor speed (Ω = 386 rpm) in terms of the frequency and damping ratio for the wing modes. Reasonable correlation of the present theory with both experiment and the Boeing theory is shown. However, data are available only for wing vertical bending mode damping.

Figure 48 shows the variation of the wing vertical bending mode damping for the Boeing rotor with rotor speed Ω at V = 50 to 192 knots. These runs were conducted to investigate the air resonance behavior of this proprotor and wing configuration. Reasonable correlation is shown with both experiment and the Boeing theory, except at the higher tunnel speeds. There the data show considerable scatter because the tunnel turbulence made analysis of the transient motion difficult.

Figure 49 shows the variation of the system stability with forward speed for the Boeing rotor on the quarter-stiffness wing, at half normal operating rotor speed (Ω = 193 rpm). Figure 50 shows the variation with rotor speed Ω for the Boeing rotor on the quarter-stiffness wing at V = 80 knots. Reasonable correlation is shown with both experiment and the Boeing theory. The Ω sweep also shows the air resonance behavior in both theory and experimental data.

SECTION 6: COMPARISONS WITH OTHER INVESTIGATIONS

In this chapter, the present theory and the results obtained are compared with the published work of other authors; of primary interest here are the theoretical models developed in the literature.

Hall (ref. 8) discussed the role of the negative H force damping on the high inflow proprotor behavior, reviewed the problems found in the XV-3 flight tests, and reviewed the results of the 1962 test of the XV-3 in the 40- by 80-Foot Wind Tunnel. He presented an investigation of the influence of various parameters on the stability of the rotor and pylon, particularly forward speed, pylon pitch and yaw spring rate, and pitch/flap coupling (δ_3); this investigation used the full-scale XV-3 test results, model tests that simulated the XV-3 configuration, and analysis results from a theory presented in the paper. Hall derived the equations of motion for a two-bladed rotor on a pylon; N = 2 was chosen because the analysis was to support the XV-3 investigation. His model then had three degrees of freedom: flap angle β (teetering), pylon pitch ϕ_x, and pylon yaw ϕ_y. The present results (eqs. (146) for N = 2) agree with Hall's equations, with the following correspondence of notation:

Present Notation	Hall
$-\alpha_y$	ϕ_x
α_x	ϕ_y
M_{F_1}	$(1/2)M_\beta$
H	$H \sin \psi$
Y	$H \cos \psi$

Hall considered only the case of ν_β = 1, that is, no hub spring restraint of the teetering blade; therefore, no hub moment due to flapping is transmitted to the pylon motion in his model. The aerodynamic forces M_β and H were expressed in terms of integrals of the blade section forces F_z and F_x over the

span, which agree with the present results except that the radial drag force was neglected. Hall did not, however, expand the rotor aerodynamic forces in terms of the perturbed rotor and pylon motion because he did not derive a set of linear differential equations. Hall solved for the dynamic behavior by numerically integrating the equations of motion; hence he found the transient motion rather than eigenvalues because of the periodic coefficients for $N = 2$. With this method, the exact, nonlinear aerodynamic forces could be included rather than the linearized expansion.

Gaffey, Yen, and Kvaternik (ref. 11) discussed the proprotor aircraft behavior and design considerations in relation to the wing frequencies, gust response, and ride quality. The influence of the blade frequencies and pitch/flap coupling on the rotor and the rotor/wing stability were discussed. It was shown that a cantilever rotor, that is, $\nu_\beta > 1$, has greater stability, and that $\nu_\beta > 1$ reduces flapping significantly but also increases blade loads. Expressions were given for the low-frequency response of flapping to shaft angle of attack ($\dot{x}_P/V$ here) and shaft angular velocity ($\dot{\alpha}_y$ here) in terms of the equivalent radius approximations; the present results (eqs. (96) to (100)) agree with their expressions. Experimental and theoretical data were given for proprotor/wing stability, flapping, loads, vibration, and gust response.

Tiller and Nicholson (ref. 13) discussed the stability and control considerations involved with proprotor aircraft. They found the following influences on the aircraft stability. The proprotors with positive pitch/flap coupling and clockwise rotation on the right wing produce, through the negative H force, an increased effective dihedral in C_{ℓ_β}, the effect increasing with forward speed. The proprotor negative damping requires a larger horizontal tail for the short-period mode frequency and damping; the rotor contribution found was on the order of 30 to 40 percent of the stabilizer contribution. Similar results were found for the vertical tail requirements (C_{n_β}). The rotor thrust damping in yaw (T_λ) contributes significantly to C_{n_r}. The rotor torque (Q_ζ) and hub force during rolling increase C_{ℓ_p} by about 30 to 50 percent of the wing value. The thrust due to rolling (T_ζ) produces adverse yaw ($\Delta C_{n_p} < 0$, for this rotor rotational direction) that appreciably alters the Dutch roll damping and mode shape. The rotor influence on the aircraft stability derivatives found here agrees with the results of Tiller and Nicholson. They also discussed other features of the proprotor configuration that influence the aircraft stability and control: the thick wing, the high roll inertia, the nacelle contribution to C_{ℓ_α}, the important influence of the interconnect shaft stiffness on the lateral derivatives (particularly, C_{n_r} and C_{n_p}), and the control features in helicopter and cruise mode. They point out that the influence of the rotors on the lateral dynamics is more complex than that on the longitudinal dynamics, but that meeting the requirements is largely a matter of enough vertical tail effectiveness.

Young and Lytwyn (ref. 18) developed a four-degree-of-freedom theoretical model (β_{1C}, β_{1S}, α_y, and α_x) for studying proprotor dynamics. They found an optimum value for the flap stiffness for pylon/rotor stability at about

$\nu_\beta = 1.1$. An approximation to this result was obtained by setting to zero the term that couples the rotor with the pylon; that is, in the present notation,

$$\frac{I_\beta^*(\nu_\beta^2 - 1)}{\gamma} + h\left(\frac{2C_T}{\sigma a} + H_\beta^{\dot{}*}\right) = 0$$

There is then no moment about the pivot due to tip path plane tilt, which greatly increases the rotor/pylon stability. This optimum was discussed in a previous section and was also the subject of the discussion of reference 18 by Wernicke and Gaffey. Young and Lytwyn presented several results for the whirl flutter case (a truly rigid propeller on the pylon), which were also discussed previously. Young and Lytwyn found the power-on case to be less stable than the windmilling case; they were considering, however, the case of $\bar{\alpha} \neq 0$, that is, the influence of the e_ℓ terms in the rotor aerodynamic coefficients. The present results confirm that the use of the better calculation of the aerodynamic coefficients decreases the predicted stability. The really important factor in windmill operation (autorotation) is the rotor speed perturbation degree of freedom, which makes the windmilling case much less stable than the power-on case. The theoretical model considered by Young and Lytwyn was an N-bladed rotor ($N \geq 3$) on an elastically restrained pylon with pitch and yaw degrees of freedom. The blade motion allowed was rigid flapping ($\eta_\beta = r$), but elastic blade restraint was included so that $\nu_\beta > 1$ was possible. Only the rotor tip path plane tilt couples with the pylon motion, so the system reduces to four degrees of freedom. The same four-degree-of-freedom model was considered here (fig. 1), with the corresponding notation:

Present Notation	Young and Lytwyn
β_{1C}	β_C
β_{1S}	β_S
$-\alpha_y$	ϕ_x
α_x	ϕ_y

Although the derivation of the rotor aerodynamic coefficients in the linear equations was considerably different from that used here, the final form is essentially equivalent to the present result. The corresponding notation for the rotor aerodynamic coefficients is

Present Notation	Young and Lytwyn
$2C_T/\sigma a$	M_{TO}
$2C_Q/\sigma a$	M_{HO}
$2H_\mu$	M_{HT}
$2H_\beta^{\dot{}}$	M_{HP}
$2M_\mu$	M_{TT}
$-2M_\beta^{\dot{}}$	M_{TP}

Young and Lytwyn evaluate these coefficients assuming constant $\bar{a}$ and c_d over the blade span. The set of four equations of motion obtained correspond to equations (26).

Descriptions of analyses typical of the most sophisticated currently used for calculating the dynamic characteristics of tilting proprotor aircraft may be found in references 29 and 30. These are, in fact, the most complete descriptions available in the literature for the proprotor aircraft analyses. Their use lies primarily in the development and support of the design of specific aircraft. More elementary models remain valuable for general and exploratory investigations of proprotor dynamics.

Descriptions of the tilting proprotor aircraft, and the design considerations involved, may be found in references 10, 15, 22, 27, and 28. The XV-3 flight test results are described in references 2 and 3, and the XV-3 tests in the 40- by 80-Foot Wind Tunnel are described in references 1, 8, and 9. Recent tests of full-scale proprotors in the 40- by 80-Foot Wind Tunnel are described in references 14, 15, 25, and 26. Some experimental data from small-scale model tests are also available (refs. 11, 15, 16, and 24, for example).

CONCLUDING REMARKS

A theoretical model has been developed for a proprotor on a cantilever wing, operating in high inflow axial flight, for use in investigations of the dynamic characteristics of tilting proprotor aircraft in the cruise configuration. The equations of motion and hub forces of the rotor were found including the response to general shaft motion. This rotor model was combined with the equations of motion for a cantilever wing. In further studies, however, the rotor model could easily be combined with a more general vehicle or support model, including, for example, the rigid-body degrees of freedom of the aircraft. The general behavior of the high inflow rotor has been investigated and, in particular, the stability of the proprotor and cantilever wing configuration. The effects of various elements of the theoretical model were examined, and the predictions were compared with experimental data from wind-tunnel tests of two full-scale proprotors.

From the theoretical results for the two full-scale rotors, and comparisons with the full-scale, wind-tunnel test data, it is concluded that the nine-degree-of-freedom model developed here is a satisfactory representation of the fundamental proprotor dynamic behavior. The model consists of first mode flap and lag blade motions of a rotor with three or more blades, and the lowest frequency wing modes. The limitations of the present theory are primarily the structural dynamics models of the rotor blades and the wing and the neglected degrees of freedom of the proprotor aircraft system. For the rotor, it was assumed that the blade flap and lag motions are not coupled, that is, are pure out-of-plane and pure inplane motions, respectively. The model neglected the higher bending modes of the blades, and the blade elastic torsion degrees of freedom were neglected entirely. For the support, the model used only an elementary representation of the structural modes of the

wing. The model was limited to the cantilever wing configuration, neglecting the aircraft rigid-body degrees of freedom as well as the higher frequency modes of the wing and pylon. The present model does incorporate the fundamental features of the proprotor aeroelastic system. Hence these limitations of the model are primarily areas where future work would be profitable, rather than restirctions on its current use.

From a comparison of the behavior of the gimballed, stiff-inplane rotor and the hingeless, soft-inplane rotor, it is concluded that the placement of the rotor blade natural frequencies of first mode bending - the flap frequency ν_β and the lag frequency ν_ζ - greatly influences the dynamics of the proprotor and wing. Moreover, the rotor lag degrees of freedom was found to have a very important role in the proprotor dynamics, for both the soft-inplane (ν_ζ < 1/rev) and the stiff-inplane (ν_ζ > 1/rev) configurations.

The theoretical model developed here has been established as an adequate representation of the basic proprotor and wing dynamics. It will then be a useful tool for further studies of the dynamics of tilting proprotor aircraft, including more sophisticated topics such as the design of automatic stability and control systems for the vehicle.

Ames Research Center
National Aeronautics and Space Administration
Moffett Field, Calif., 94035, Dec. 26, 1973

REFERENCES

1. Koenig, D. G.; Grief, R. H.; and Kelly, M. W.: Full Scale Wind Tunnel Investigation of the Longitudinal Characteristics of a Tilting-Rotor Convertiplane. NASA TN D-35, 1959.

2. Deckert, W. H.; and Ferry, R. C.: Limited Flight Evaluation of the XV-3 Aircraft. Air Force Flight Test Center,TR-60-4, May 1960.

3. Quigley, H. C.; and Koenig, D. C.: A Flight Study of the Dynamic Stability of a Tilting-Rotor Convertiplane. NASA TN D-778, 1961.

4. Reed, W. H. III; and Bland, S. R.: An Analytical Treatment of Aircraft Propeller Precession Instability. NASA TN D-659, 1961.

5. Houbolt, John C.; and Reed, Wilmer H. III: Propeller-Nacelle Whirl Flutter. J. Aerospace Sci., vol. 29, no. 3, March 1962, pp. 333-346.

6. Reed, Wilmer H. III: Propeller-Rotor Whirl Flutter: A State of the Art Review. J. Sound Vibration, vol. 4, no. 3, Nov. 1966, pp. 526-544.

7. Reed, Wilmer H. III: Review of Propeller-Rotor Whirl Flutter. NASA TR R-264, 1967.

8. Hall, W. Earl, Jr.: Prop-Rotor Stability at High Advance Ratios. J. Am. Helicopter Soc., vol. 11, no. 2, April 1966, pp. 11-26.

9. Edenborough, H. Kipling: Investigation of Tilt-Rotor VTOL Aircraft Rotor-Pylon Stability. J. Aircraft, vol. 5, no. 2, March-April 1968, pp. 97-105.

10. Wernicke, K. G.: Tilt Proprotor Composite Aircraft, Design State of the Art. J. Am. Helicopter Soc., vol. 14, no. 2, April 1969, pp. 10-25.

11. Gaffey, T. M.; Yen, J. G.; and Kvaternik, R. G.: Analysis and Model Tests of the Proprotor Dynamics of a Tilt-Proprotor VTOL Aircraft. U.S. Air Force V/STOL Technology and Planning Conference, Las Vegas, Nevada, Sept. 1969.

12. DeTore, J. A.; and Gaffey, T. M.: The Stopped-Rotor Variant of the Prop-rotor VTOL Aircraft. J. Am. Helicopter Soc., vol. 15, no. 3, July 1970, pp. 45-56.

13. Tiller, F. E., Jr.; and Nicholson, Robert: Stability and Control Considerations for a Tilt-Fold-Proprotor Aircraft. J. Am. Helicopter Soc., vol. 16, no. 3, July 1971, pp. 23-33.

14. Wernicke, Kenneth G.; and Edenborough, H. Kipling: Full-Scale Proprotor Development. J. Am. Helicopter Soc., vol. 17, no. 1, Jan. 1970, pp. 31-40.

15. Edenborough, H. Kipling; Gaffey, Troy M.; and Weiberg, James A.: Analysis and Tests Confirm Design of Proprotor Aircraft. AIAA Paper 72-803, 1972.

16. Marr, Robert L.; and Neal, Gordon T.: Assessment of Model Testing of a Tilt-Proprotor VTOL Aircraft. Mideast Region Symposium, American Helicopter Society, Philadelphia, Pennsylvania, Oct. 26-27, 1972.

17. Sambell, Kenneth W.: Proprotor Short-Haul Aircraft - STOL and VTOL. J. Aircraft, vol. 9, no. 10, Oct. 1972, pp. 744-750.

18. Young, Maurice I.; and Lytwyn, Roman T.: The Influence of Blade Flapping Restraint on the Dynamic Stability of Low Disk Loading Propeller-Rotors. J. Am. Helicopter Soc., vol. 12, no. 4, Oct. 1967, pp. 38-54; see also Wernicke, Kenneth G.; and Gaffey, Troy M.: Review and Discussion. J. Am. Helicopter Soc., vol. 12, no. 4, Oct. 1967, pp. 55-60.

19. Magee, John P.; Maisel, Martin D.; and Davenport, Frank J.: The Design and Performance Prediction of Propeller/Rotors for VTOL Applications. Paper No. 325, 25th Annual Forum of the American Helicopter Society, Washington, D. C., May 14-16, 1969.

20. DeLarm, Leon N.: Whirl Flutter and Divergence Aspects of Tilt-Wing and Tilt-Rotor Aircraft. U.S. Air Force V/STOL Technology and Planning Conference, Las Vegas, Nevada, Sept. 1969.

21. Magee, John P.; and Pruyn, Richard R.: Prediction of the Stability Derivatives of Large Flexible Prop/Rotors by a Simplified Analysis. Preprint No. 443, 26th Annual Forum of the American Helicopter Society, Washington, D. C., June 1970.

22. Richardson, David A.: The Application of Hingeless Rotors to Tilting Proprotor Aircraft. J. Am. Helicopter Soc., vol. 16, no. 3, July 1971, pp. 34-38.

23. Johnston, Robert A.: Parametric Studies of Instabilities Associated With Large Flexible Rotor Propellers. Preprint No. 615, 28th Annual Forum of the American Helicopter Society, Washington, D. C., May 1972.

24. Baird, Eugene F.; Bauer, Elmer M.; and Kohn, Jerome S.: Model Tests and Analyses of Prop-Rotor Dynamics for Tilt-Rotor Aircraft. Mideast Region Symposium of the American Helicopter Society, Philadelphia, Pennsylvania, Oct. 1972.

25. Anon.: Advancement of Proprotor Technology Task II - Wind Tunnel Test Results. NASA CR-114363, Bell Helicopter Co., Sept. 1971.

26. Magee, John P.; and Alexander, H. R.: Wind Tunnel Tests of a Full Scale Hingeless Prop/Rotor Designed for the Boeing Model 222 Tilt Rotor Aircraft. NASA CR 114664, Boeing Vertol Co., Oct. 1973.

27. Anon.: V/STOL Tilt-Rotor Study Task II - Research Aircraft Design. NASA CR-114442, Bell Helicopter Co., March 1972.

28. Anon.: V/STOL Tilt-Rotor Aircraft Study Volume II - Preliminary Design of Research Aircraft. NASA CR-114438, Boeing Vertol Co., March 1972.

29. Yen, J. C.; Weber, Gottfried E.; and Gaffey, Troy M.: A Study of Folding Proprotor VTOL Aircraft Dynamics. AFFDL-TR-71-7, vol. 1, Bell Helicopter Co., Sept. 1971.

30. Alexander, H. R.; Amos, A. K.; Tarzanin, F. J.; and Taylor, R. B.: V/STOL Dynamics and Aeroelastic Rotor-Airframe Technology. AFFDL-TR-72-40, vol. 2, Sept. 1972, Boeing Co.

31. Bailey, F. J., Jr.: A Simplified Theoretical Method of Determining the Characteristics of a Lifting Rotor in Forward Flight. NACA Rep. 716, 1941.

32. Gessow, Alfred; and Myers, Garry C., Jr.: Aerodynamics of the Helicopter, Frederick Ungar Publishing Co., New York, 1952.

33. Peters, David A.; and Hohenemser, Kurt H.: Application of the Floquet Transition Matrix to Problems of Lifting Rotor Stability. J. Am. Helicopter Soc., vol. 16, no. 2, April 1971, pp. 25-33.

34. Coleman, Robert P.; and Feingold, Arnold M.: Theory of Self-Excited Mechanical Oscillations of Helicopter Rotors With Hinged Blades. NACA Rep. 1351, 1958.

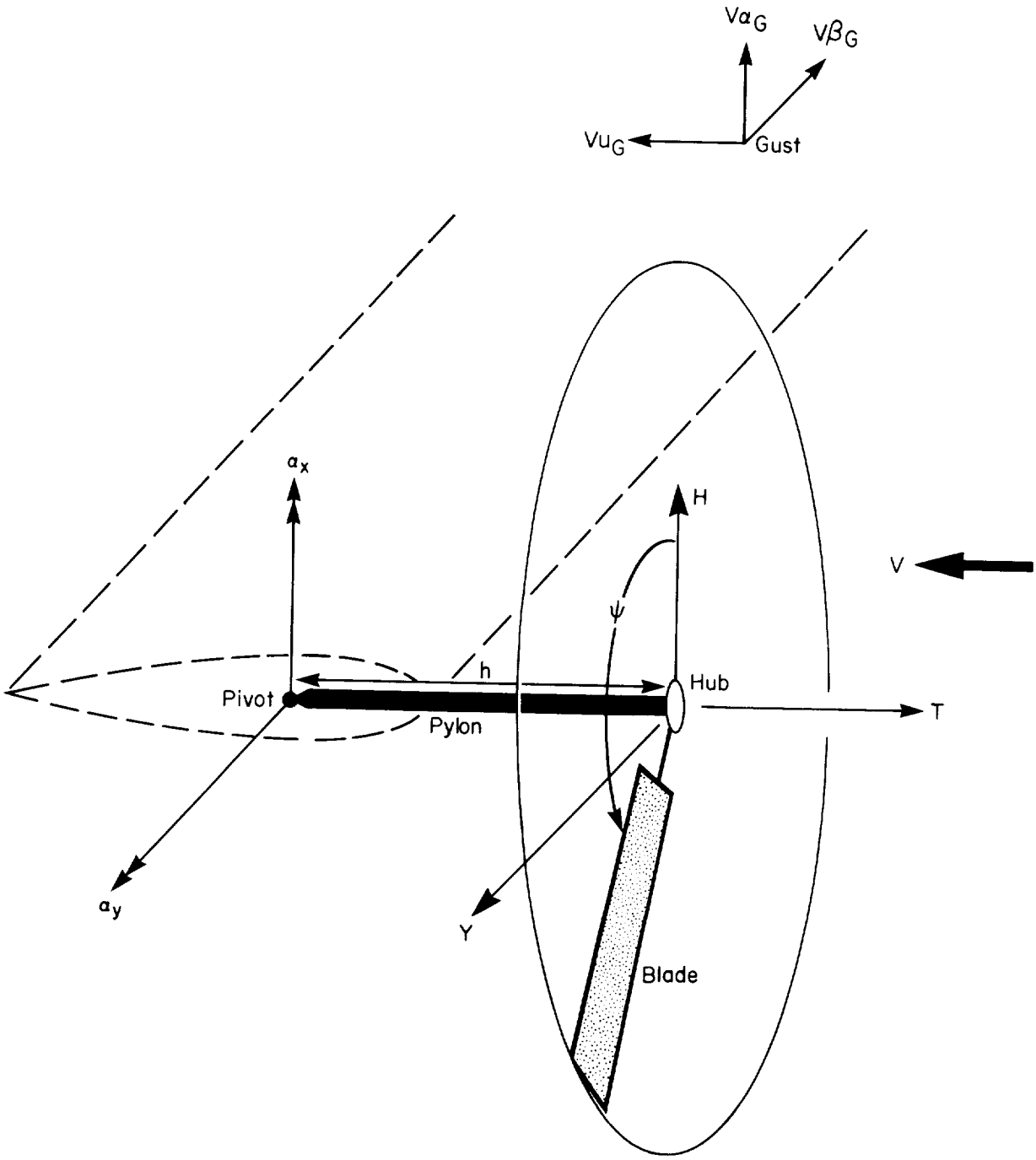

Figure 1.- Four-degree-of-freedom model for proprotor dynamics with conventions for hub forces, pylon motion, and gust velocity; only one of the N rotor blades is shown.

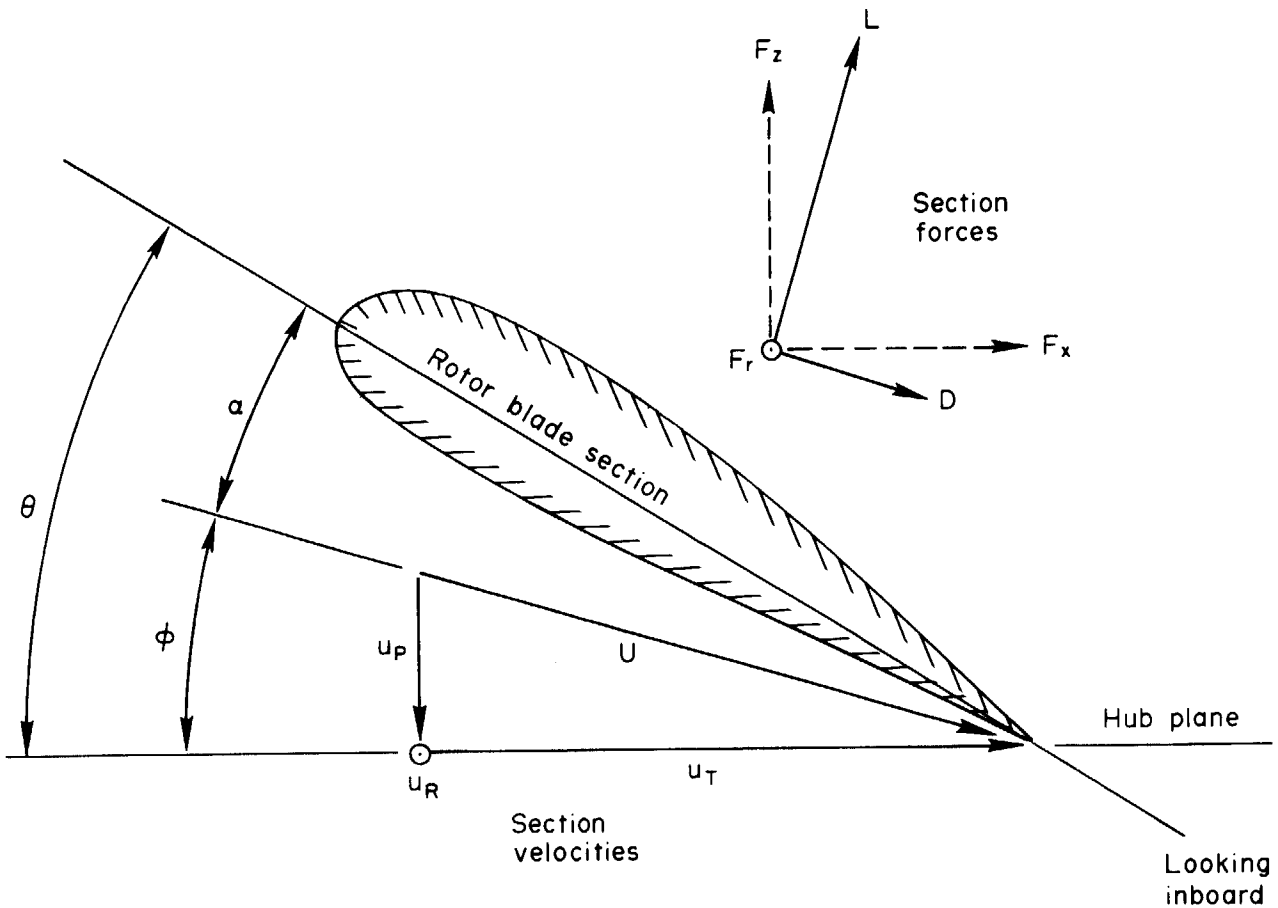

Figure 2.- Velocities seen by rotor blade section and resulting aerodynamic forces on the section.

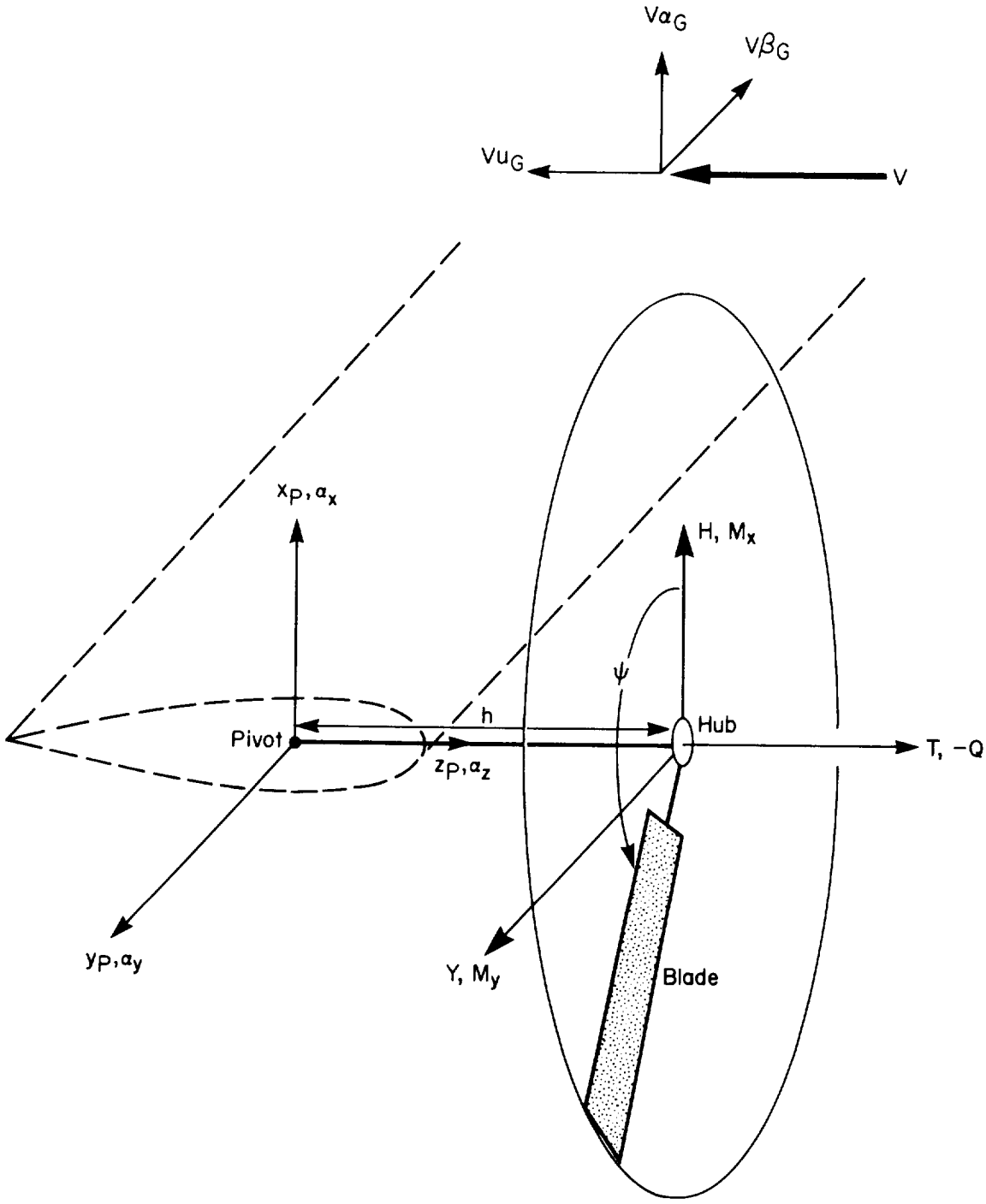

Figure 3.- Rotor model for proprotor dynamics: hub forces and moments, pylon linear and angular motion, and gust velocities; only one of the N rotor blades is shown.

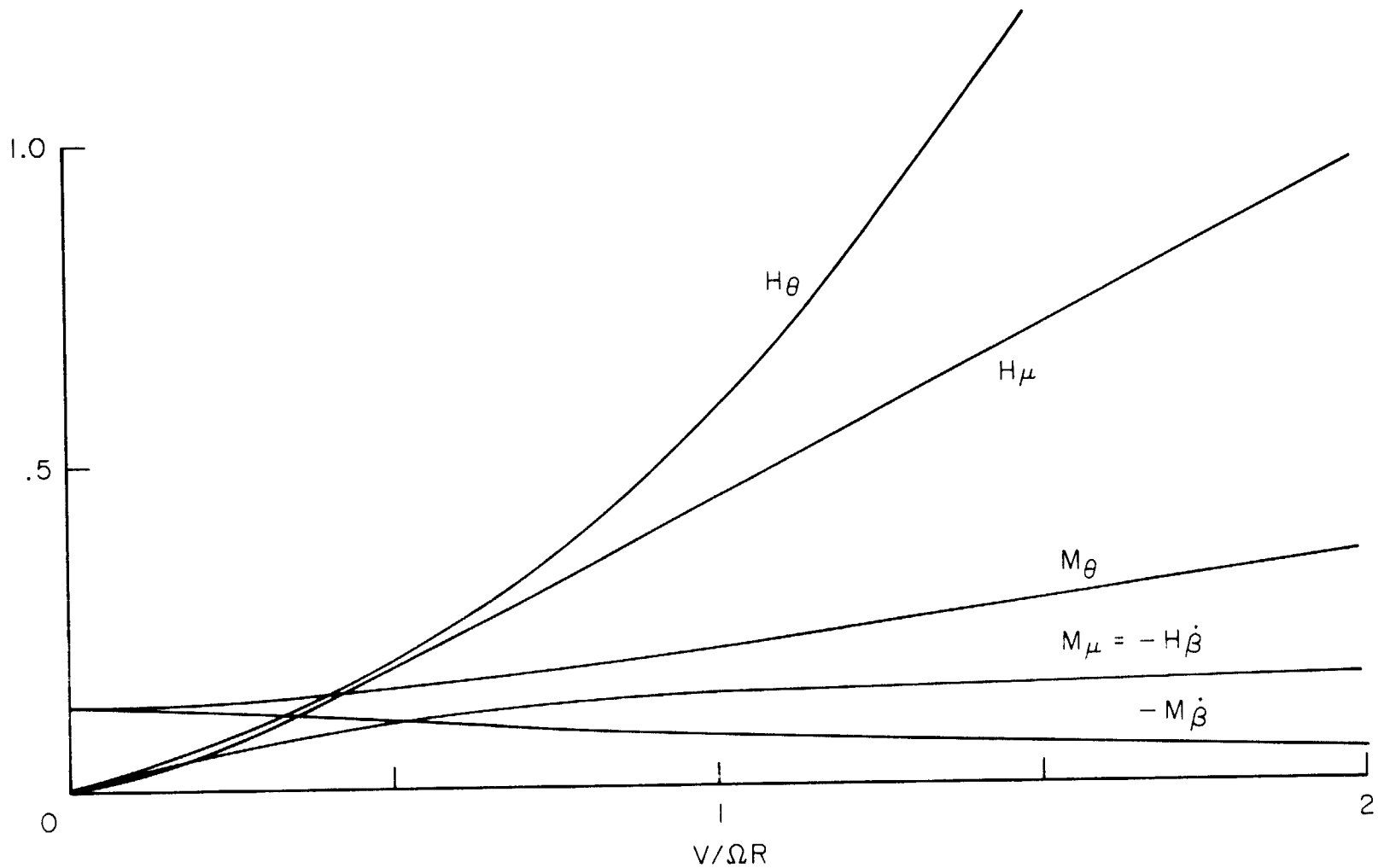

Figure 4.- Variation of the aerodynamic coefficients with forward speed, based on only the c_{ℓ_α} terms in the coefficients.

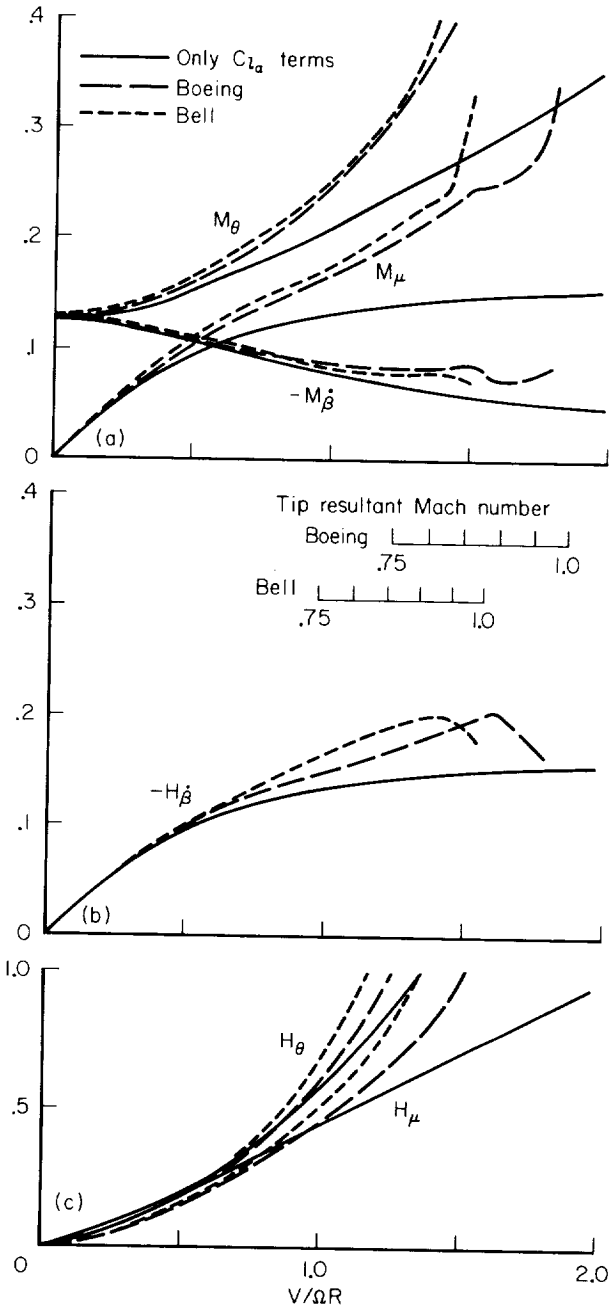

(a) M_θ, M_μ, $M_{\dot\beta}$
(b) $H_{\dot\beta}$
(c) H_θ, H_μ

Figure 5.- Influence of blade section aerodynamics on rotor coefficients for the Bell and Boeing rotors, compared with coefficients based on only the c_{ℓ_α} terms.

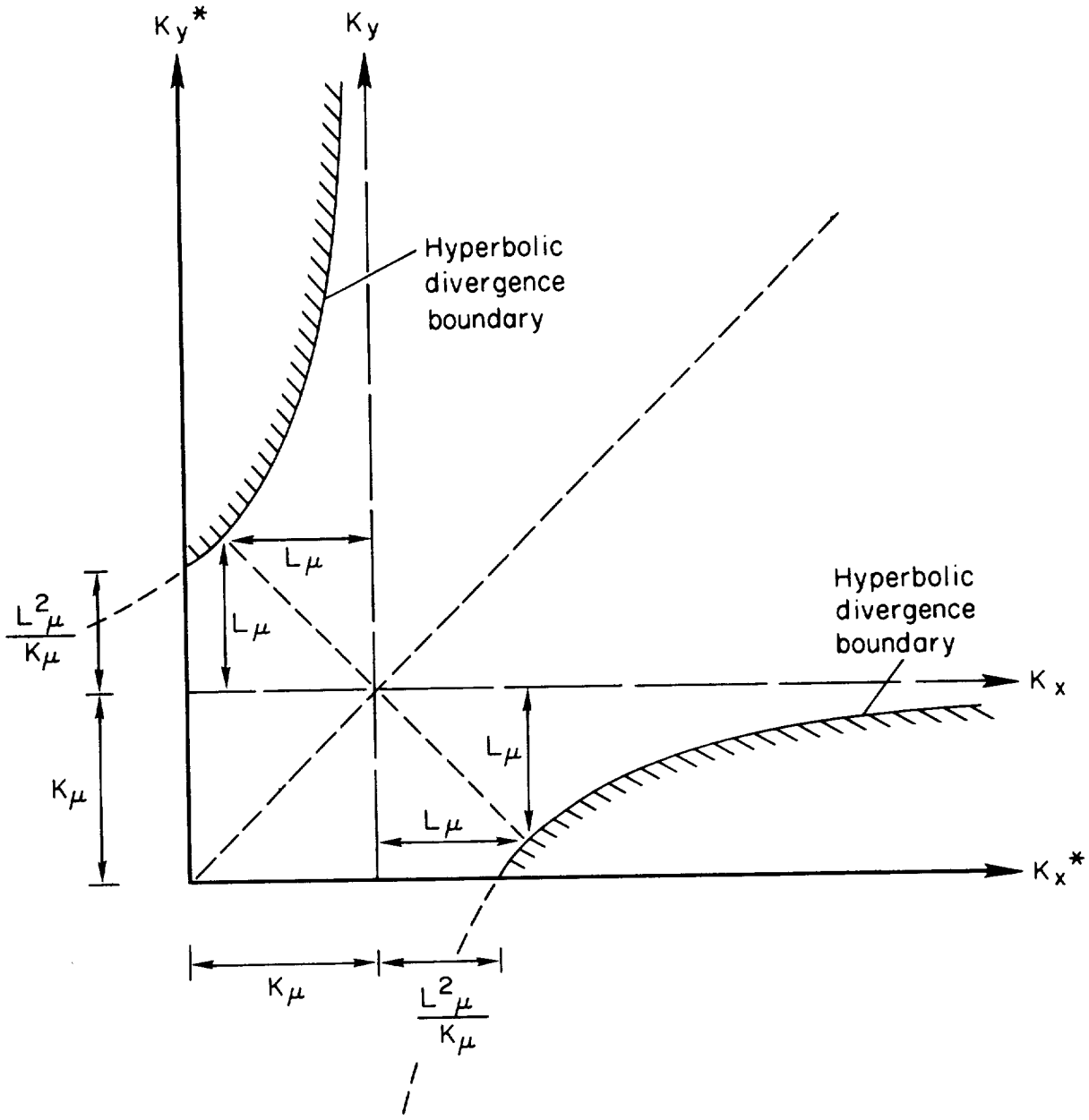

Figure 6.- Whirl flutter (two-degree-of-freedom) divergence instability boundary.

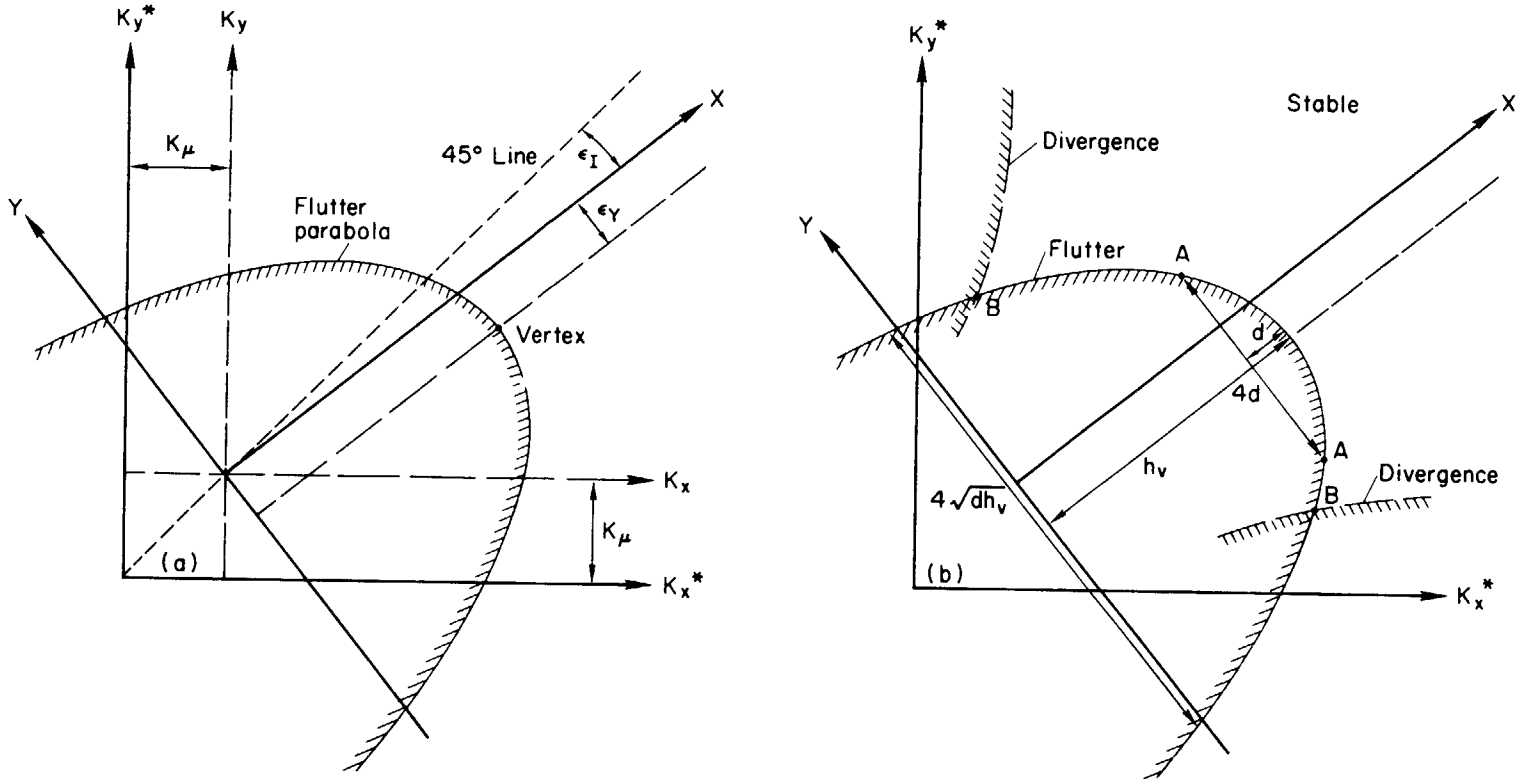

(a) Positioning the parabola axes.
(b) Location and size of the flutter parabola.

Figure 7.- Whirl flutter (two-degree-of-freedom) flutter instability boundaries.

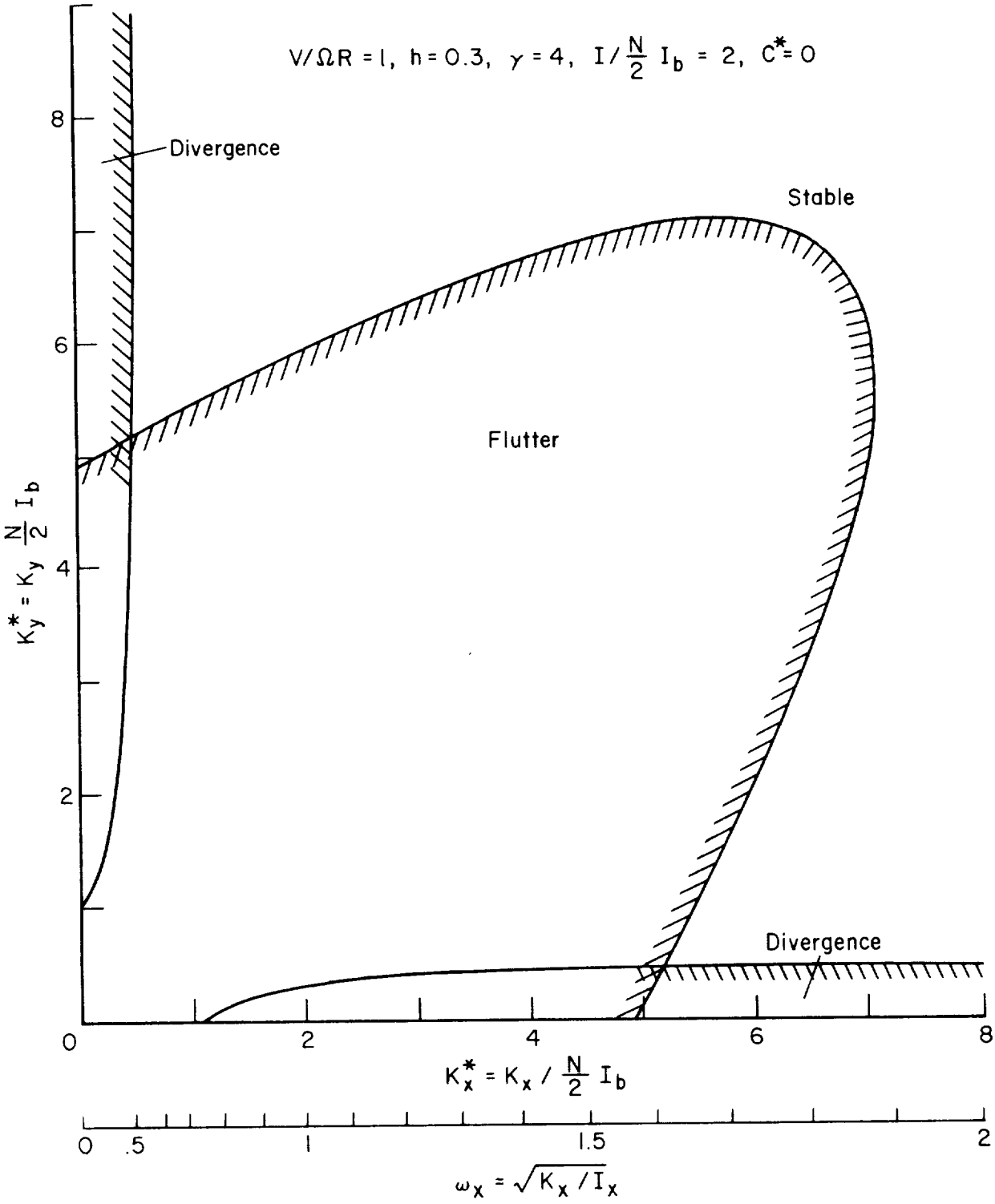

Figure 8.- Typical whirl flutter stability boundaries.

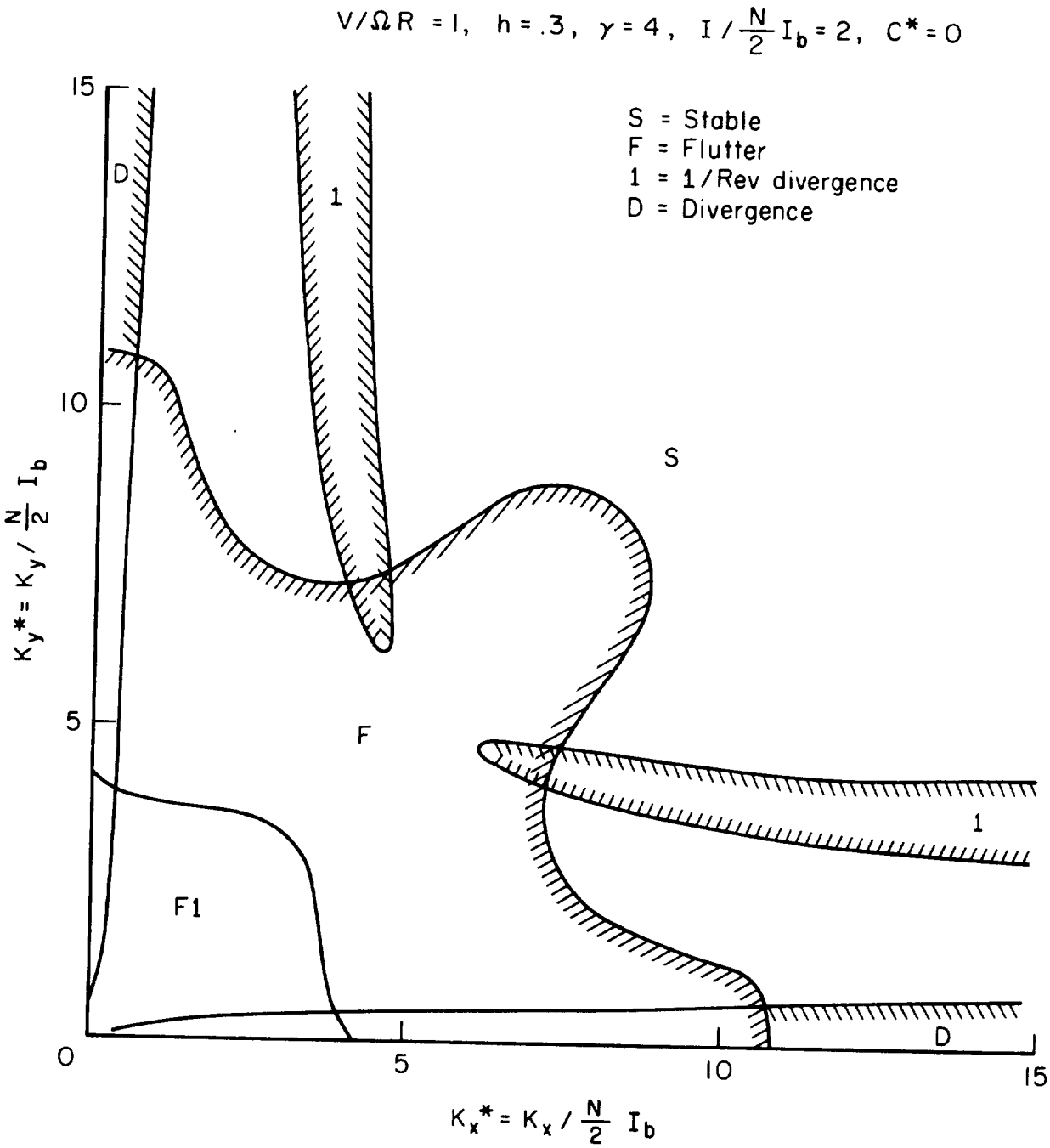

Figure 9.- Whirl flutter stability boundaries for a two-bladed rotor.

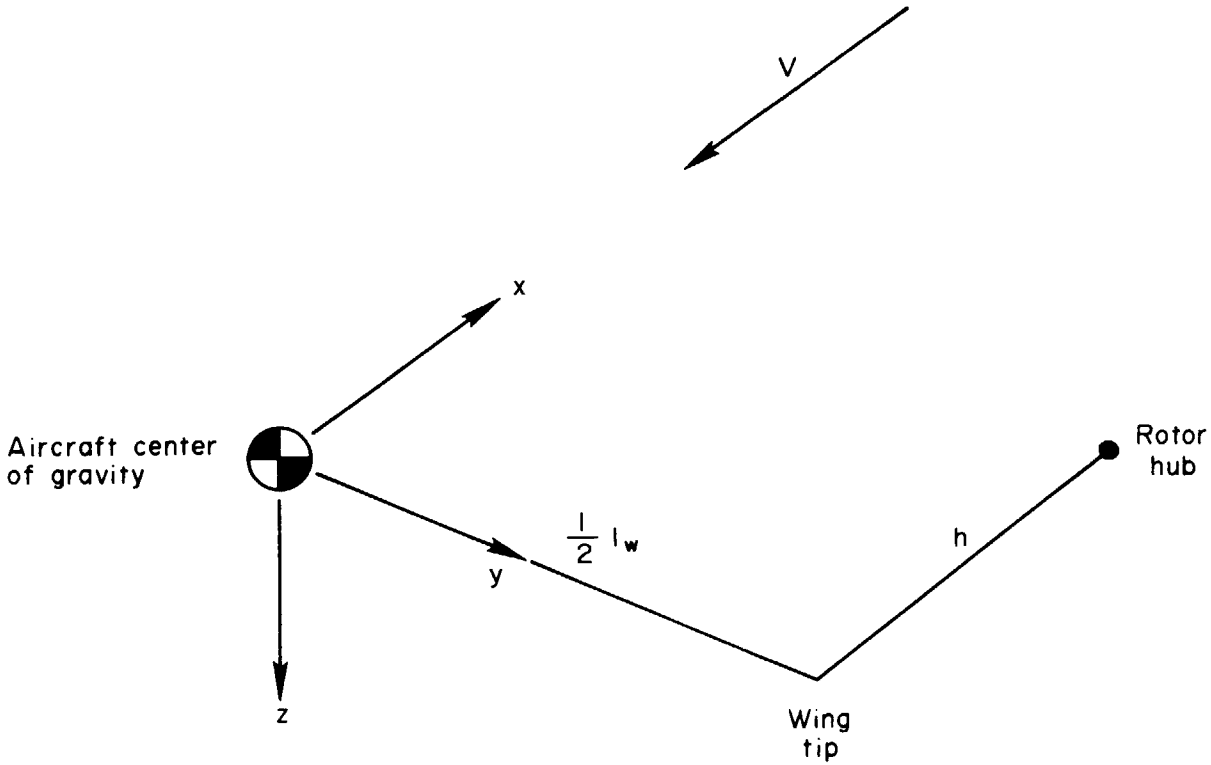

Figure 10.- Axis system and geometry for evaluating proprotor influence on aircraft stability derivatives.

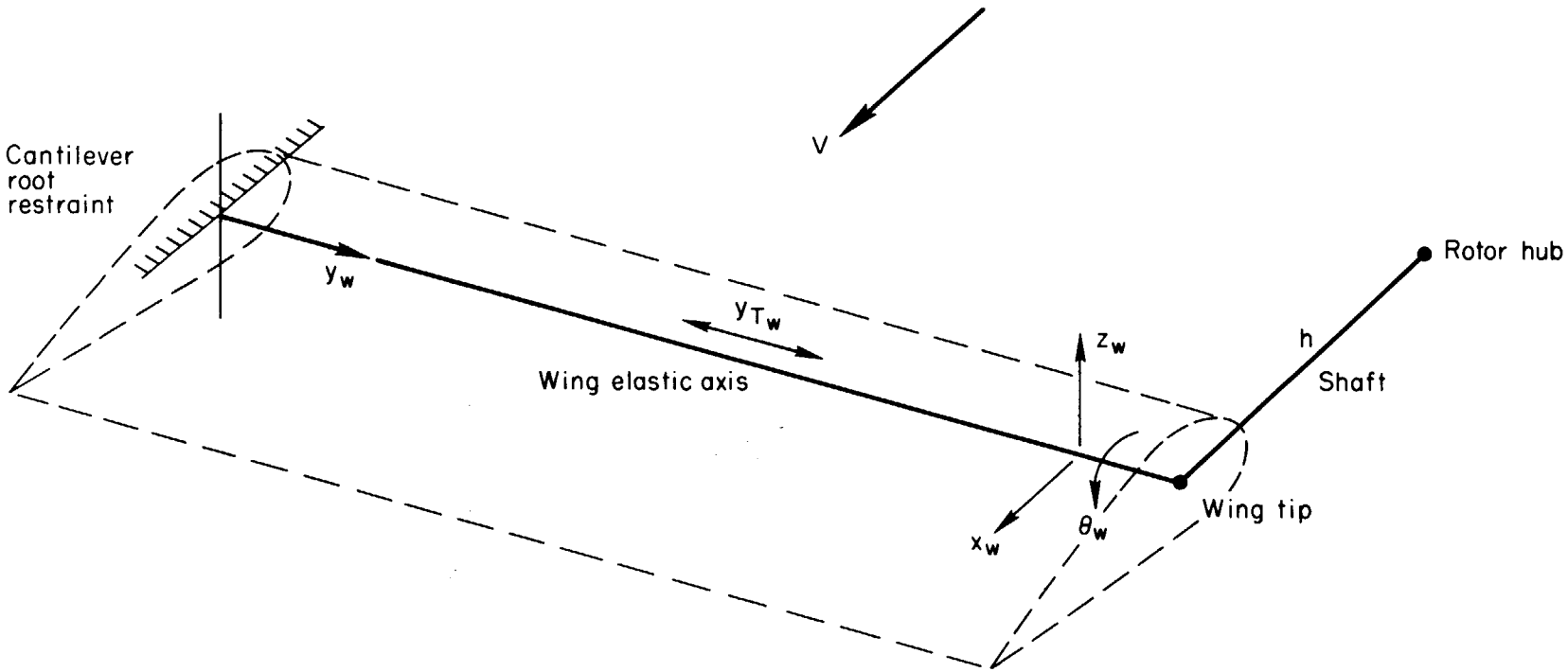

Figure 11.- Cantilever wing geometry and motion.

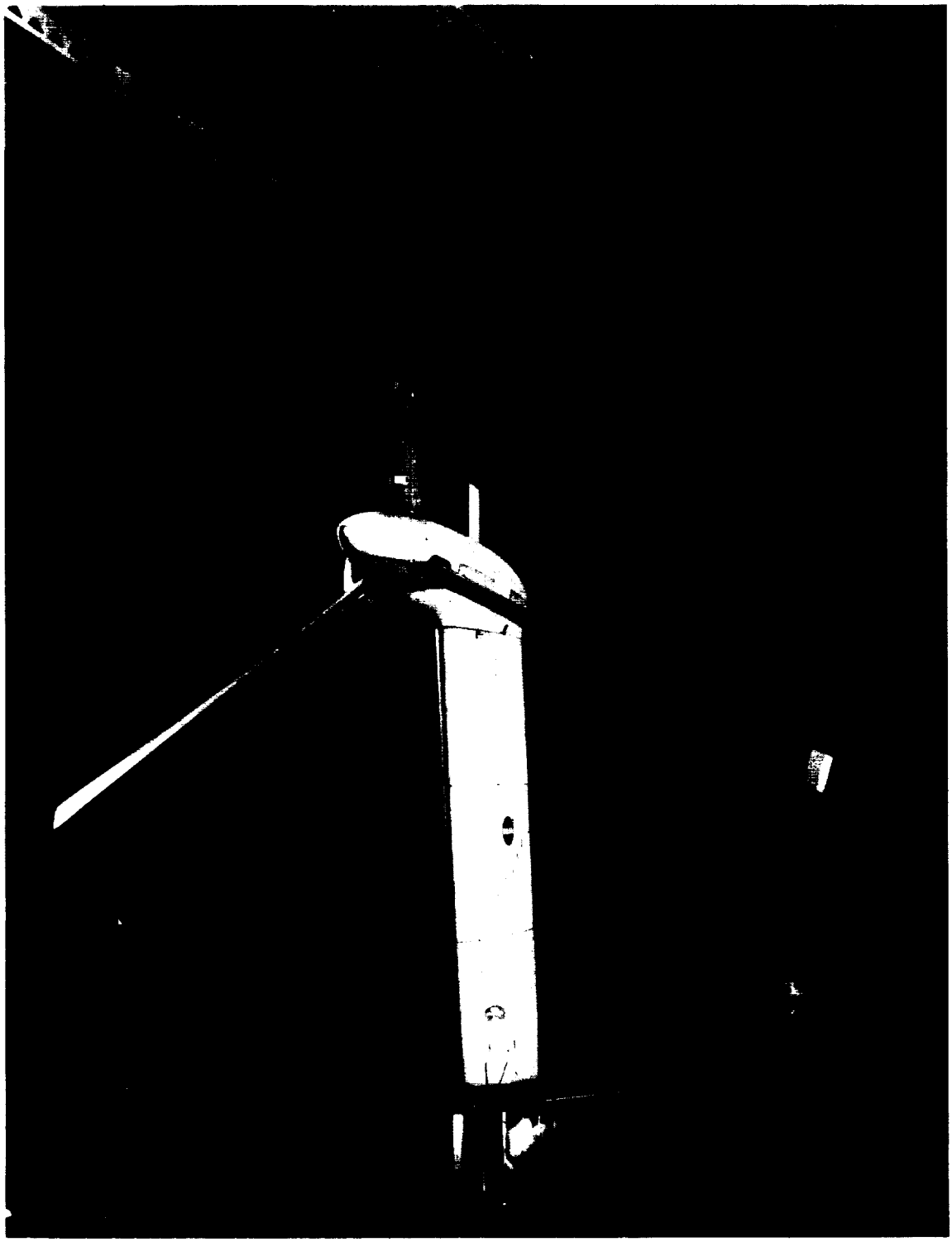

Figure 12.- Bell Helicopter Company full-scale, 25-ft-diam proprotor on cantilever wing for dynamic tests in the Ames 40- by 80-Foot Wind Tunnel.

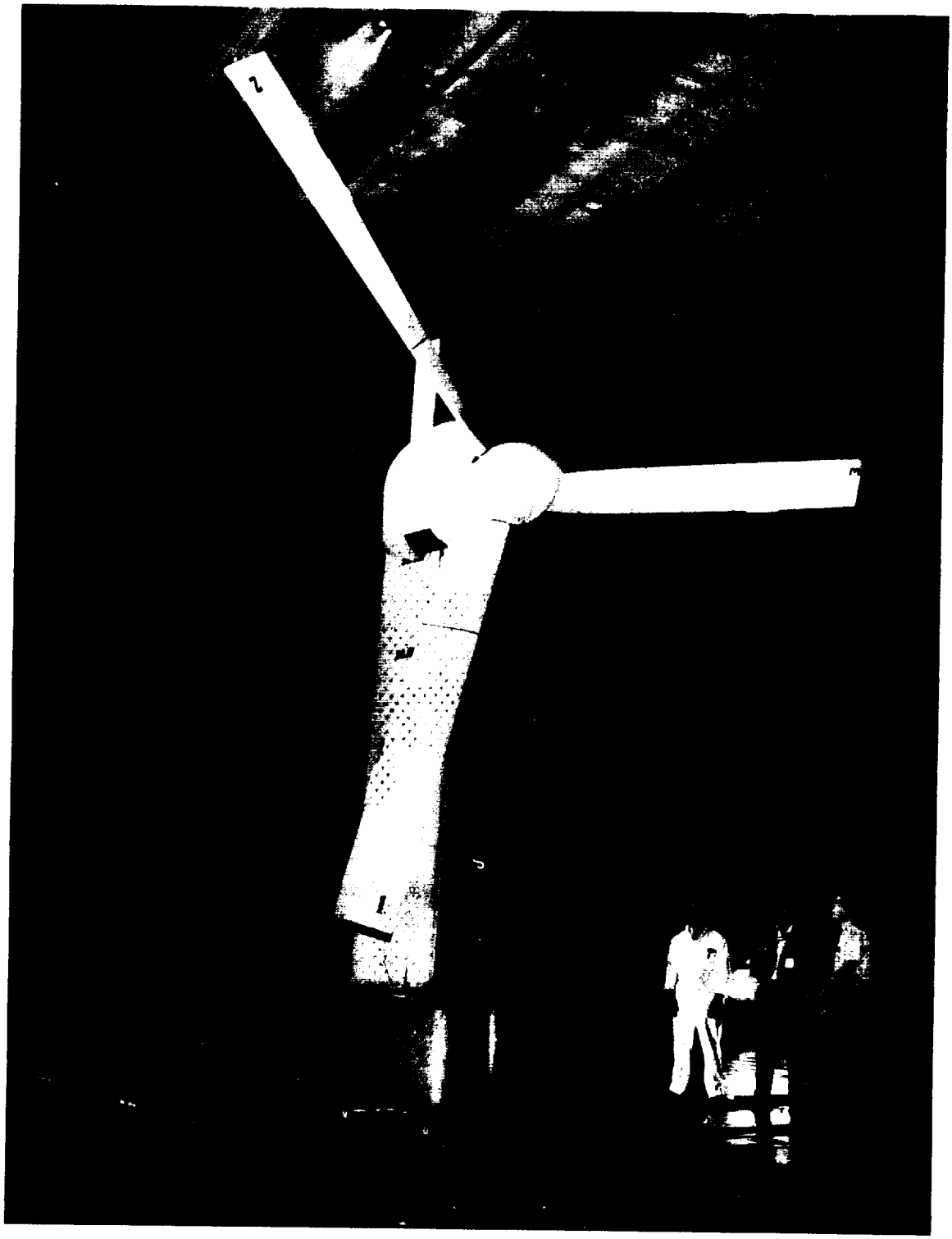

Figure 13.- Boeing Vertol Company full-scale, 26-ft-diam proprotor on cantilever wing for dynamic tests in the Ames 40- by 80-Foot Wind Tunnel.

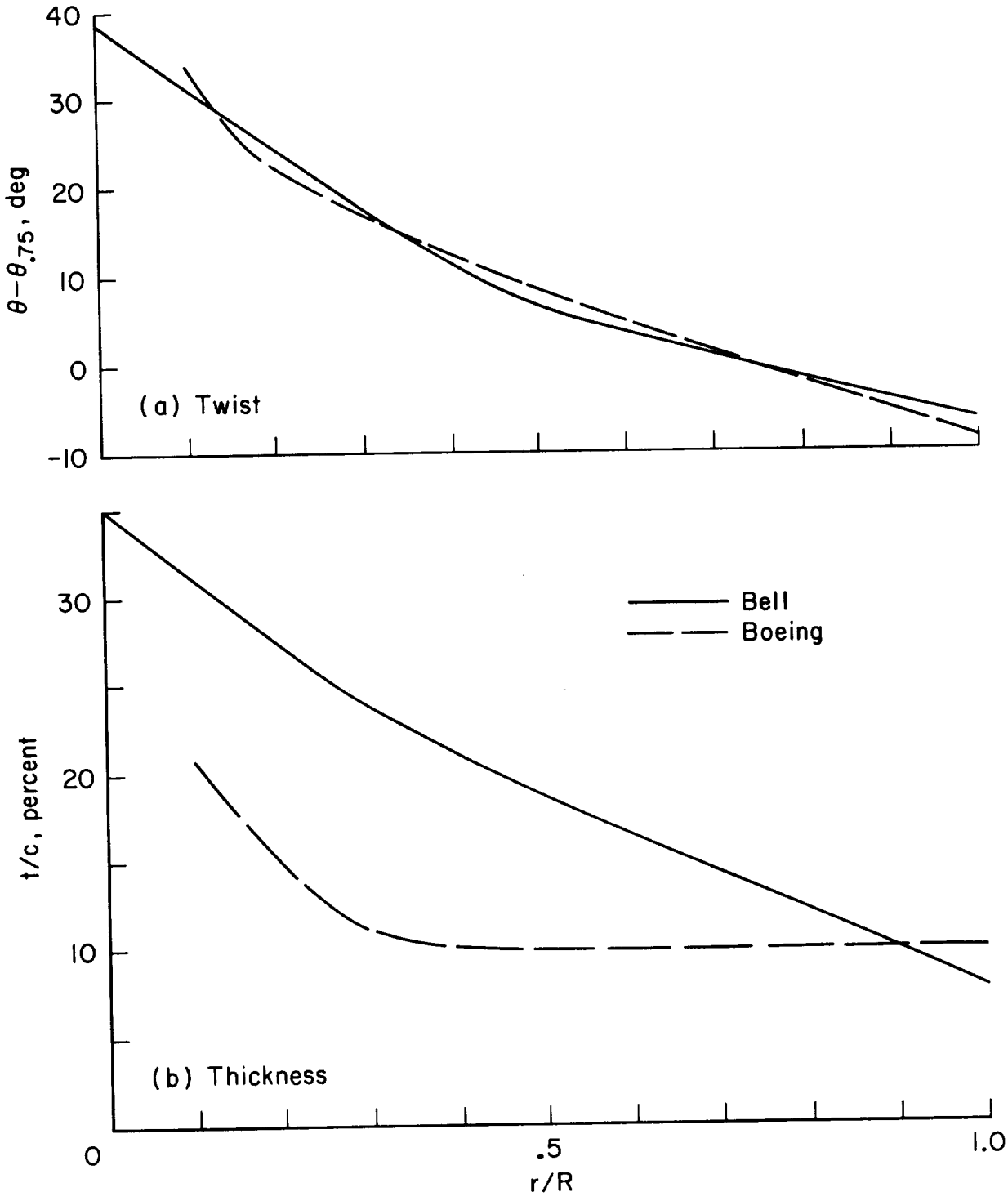

(a) Twist.
(b) Thickness ratio.

Figure 14.- Geometric characteristics of two full-scale proprotor blades.

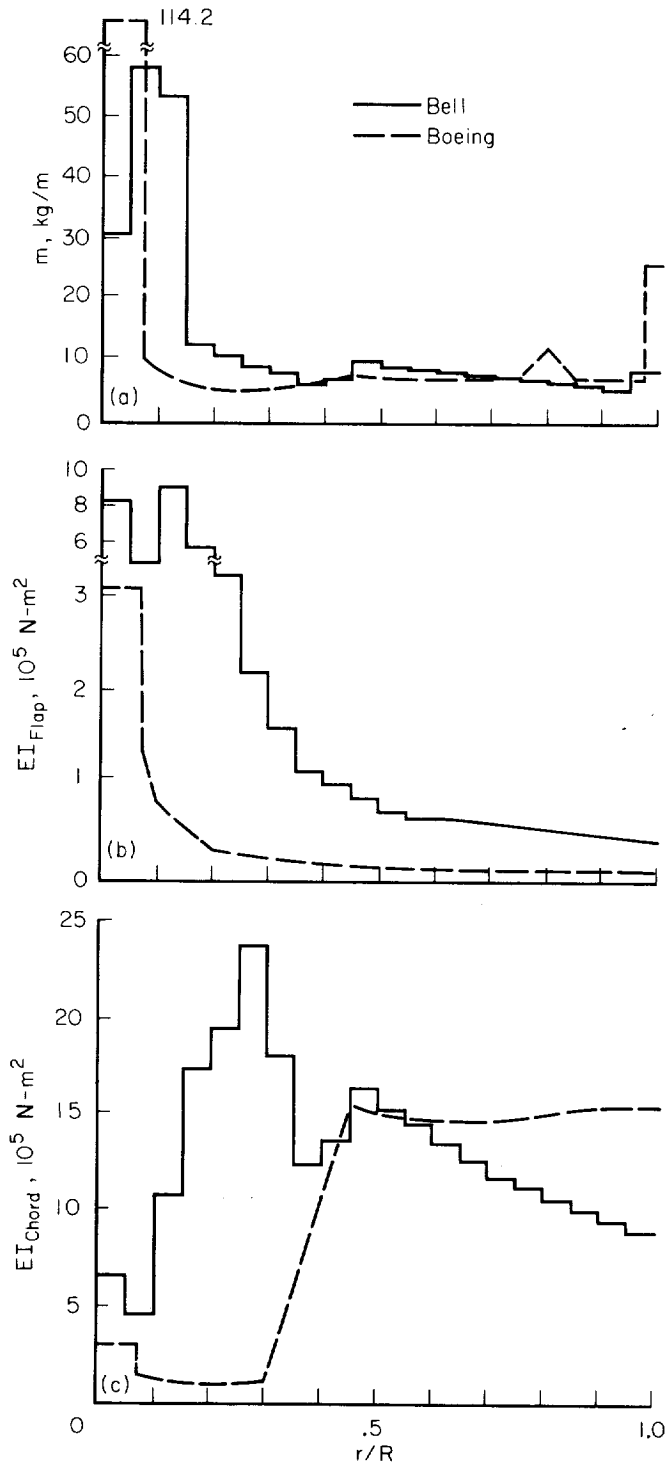

(a) Section mass.
(b) Section flapwise modulus/moment product.
(c) Section chordwise modulus/moment product.

Figure 15.- Structural characteristics of two full-scale proprotor blades.

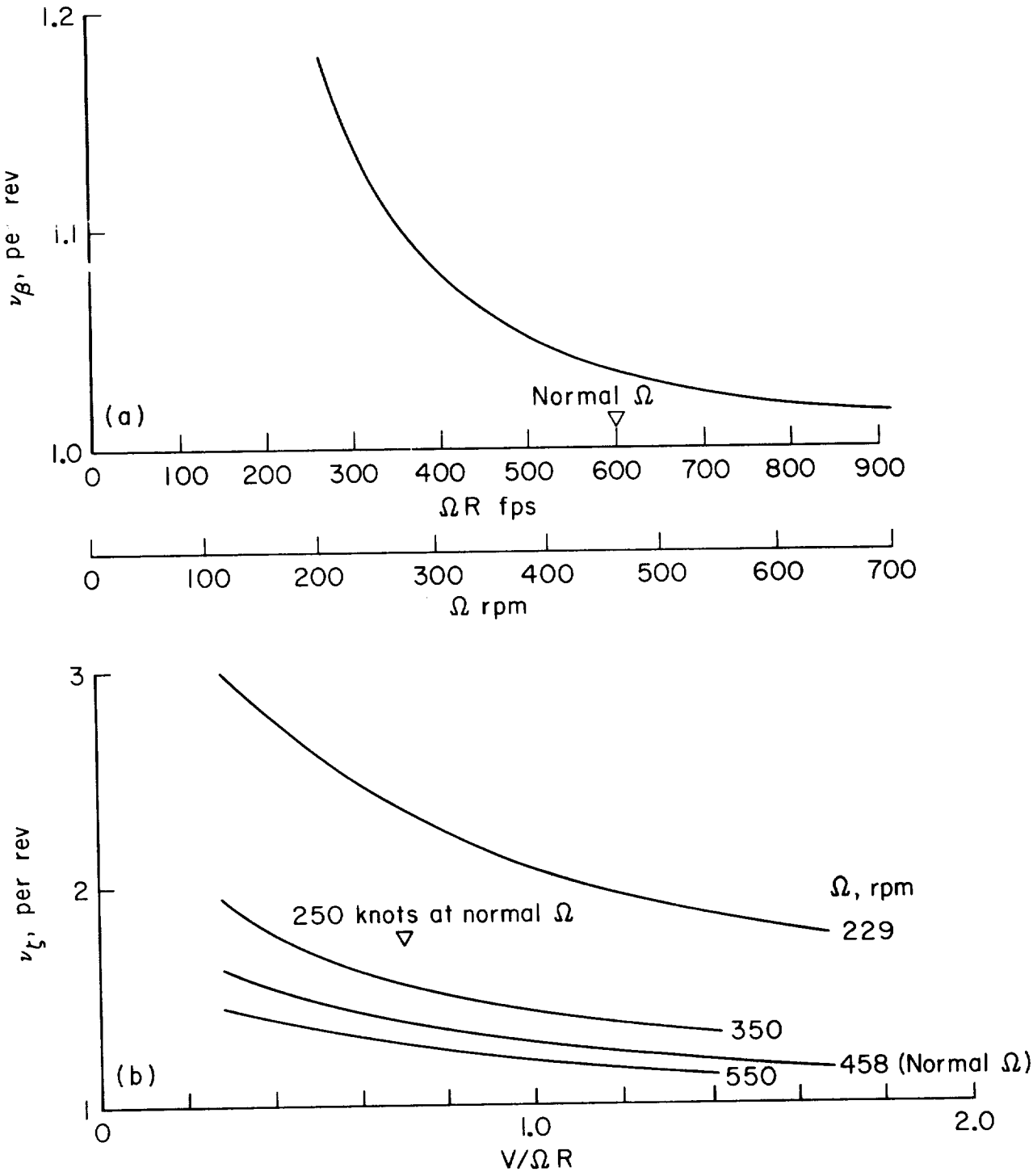

(a) Flap frequency ν_β.
(b) Lag frequency ν_ζ.

Figure 16.- Blade rotating natural frequencies for Bell rotor.

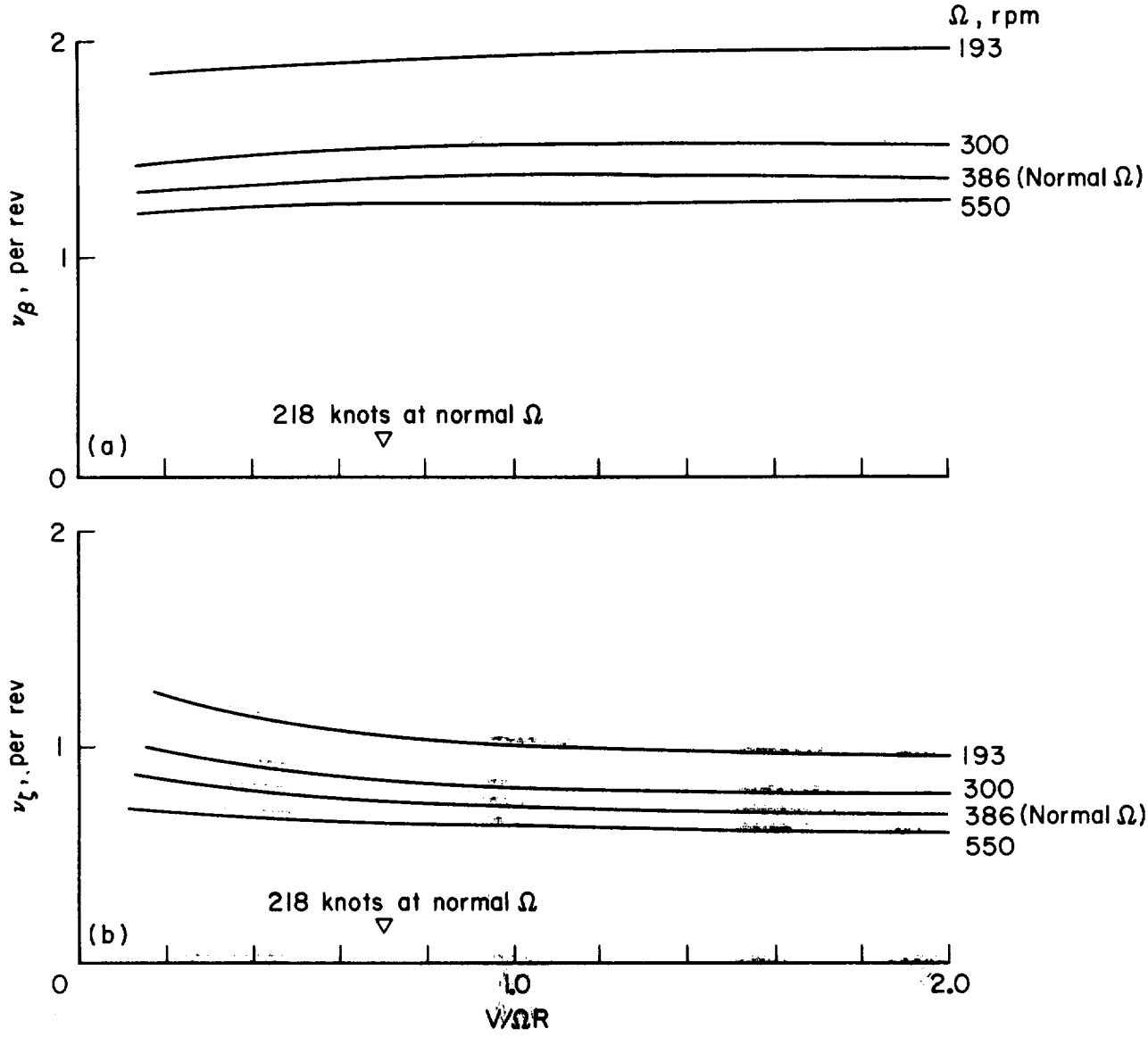

(a) Flap frequency ν_β.
(b) Lag frequency ν_ζ.

Figure 17.- Blade rotating natural frequencies for Boeing rotor.

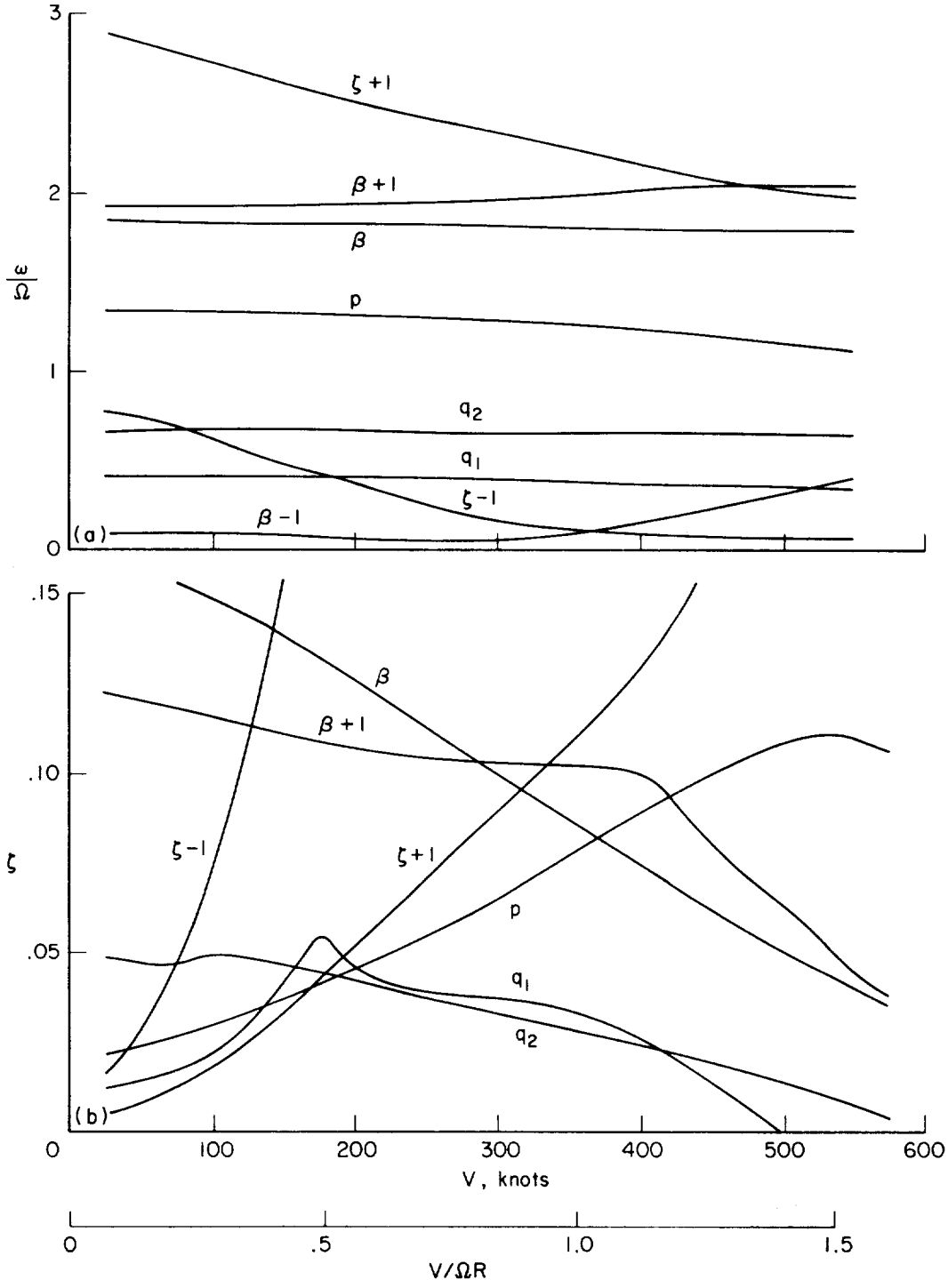

(a) Frequency of modes.
(b) Damping ratio of the modes.

Figure 18.- Bell rotor velocity sweep, Ω = 458 rpm; predicted eigenvalues.

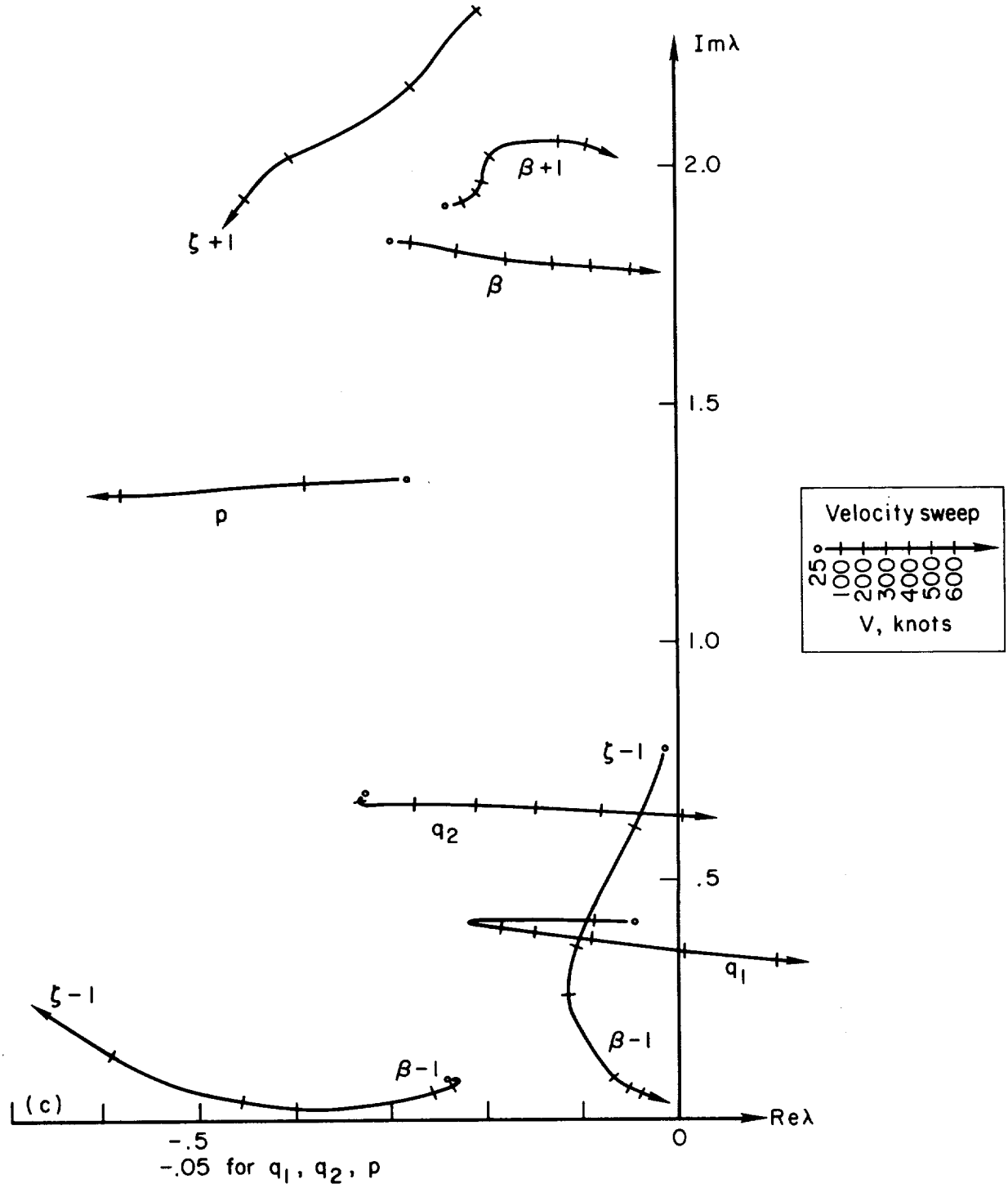

(c) Root locus.

Figure 18.- Concluded.

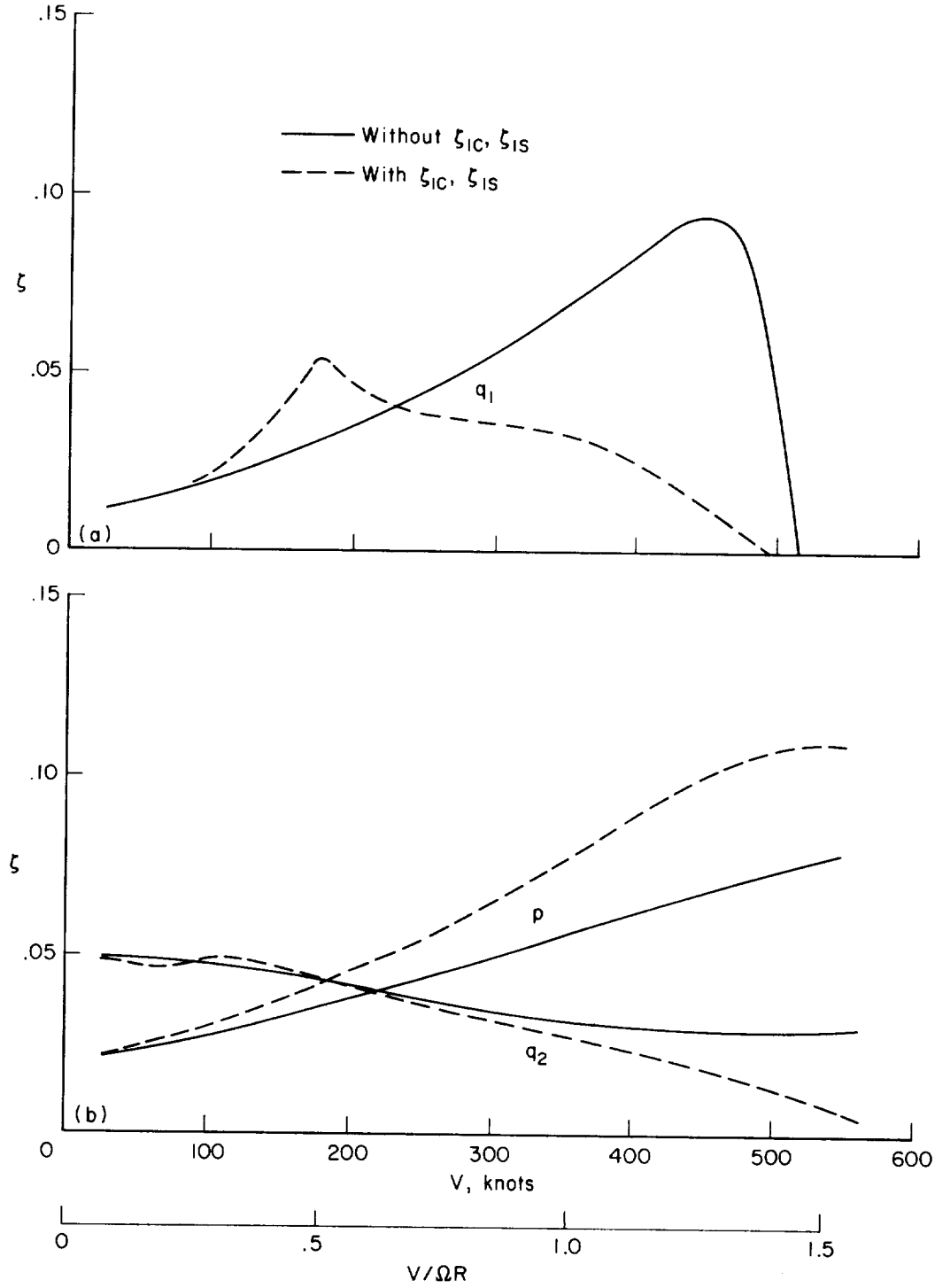

(a) Wing vertical bending (q_1) damping.
(b) Wing chordwise bending (q_2) and torsion (p) damping.

Figure 19.- Bell rotor velocity sweep, Ω = 458 rpm; with and without ζ_{1C} and ζ_{1S} rotor lag motion.

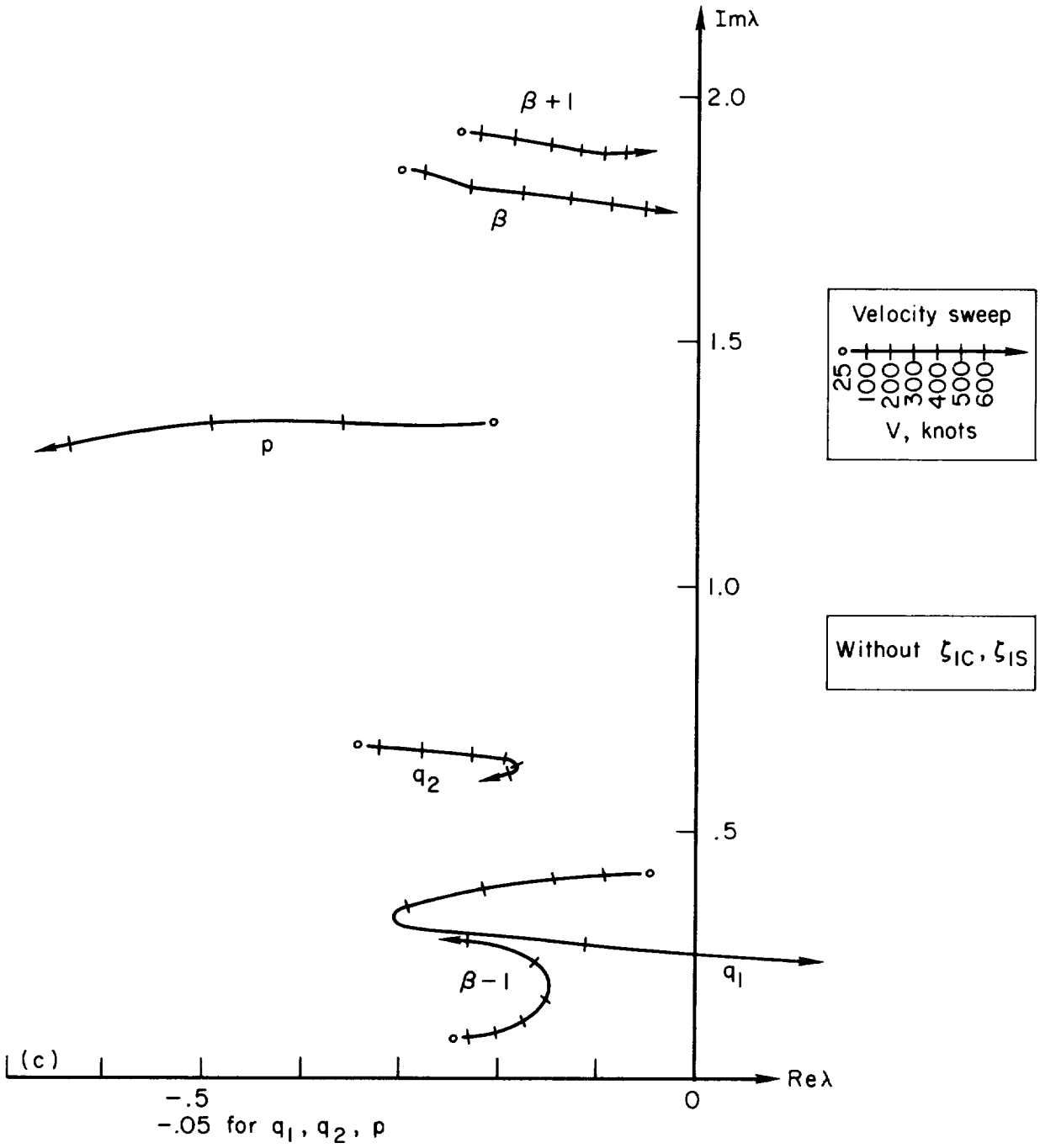

(c) Root locus.

Figure 19.- Concluded.

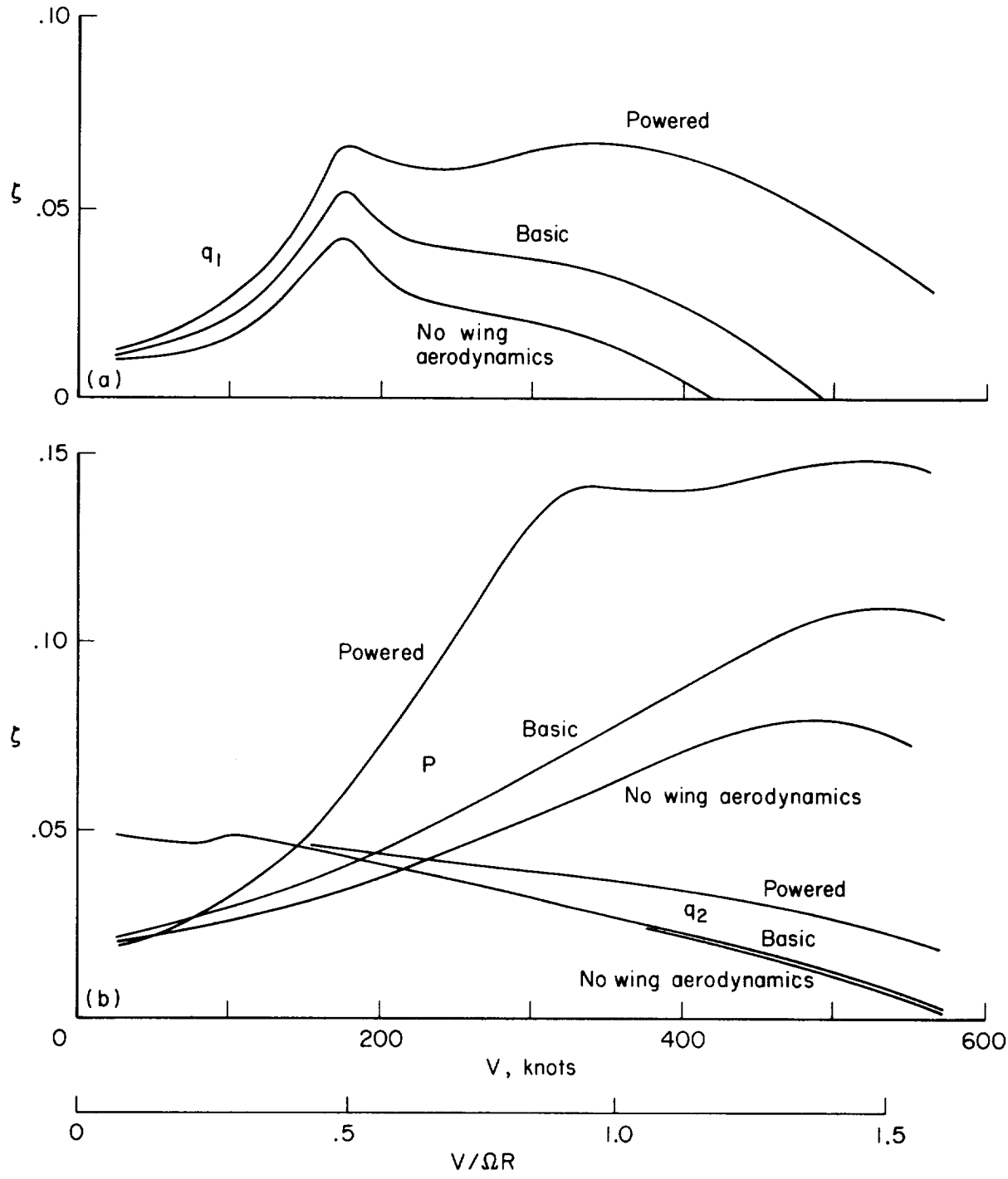

(a) Wing vertical bending (q_1) damping.
(b) Wing chordwise bending (q_2) and torsion (p) damping.

Figure 20.- Bell rotor velocity sweep, Ω = 458 rpm; comparison of basic (autorotation and wing aerodynamics), powered, and no wing aerodynamics cases.

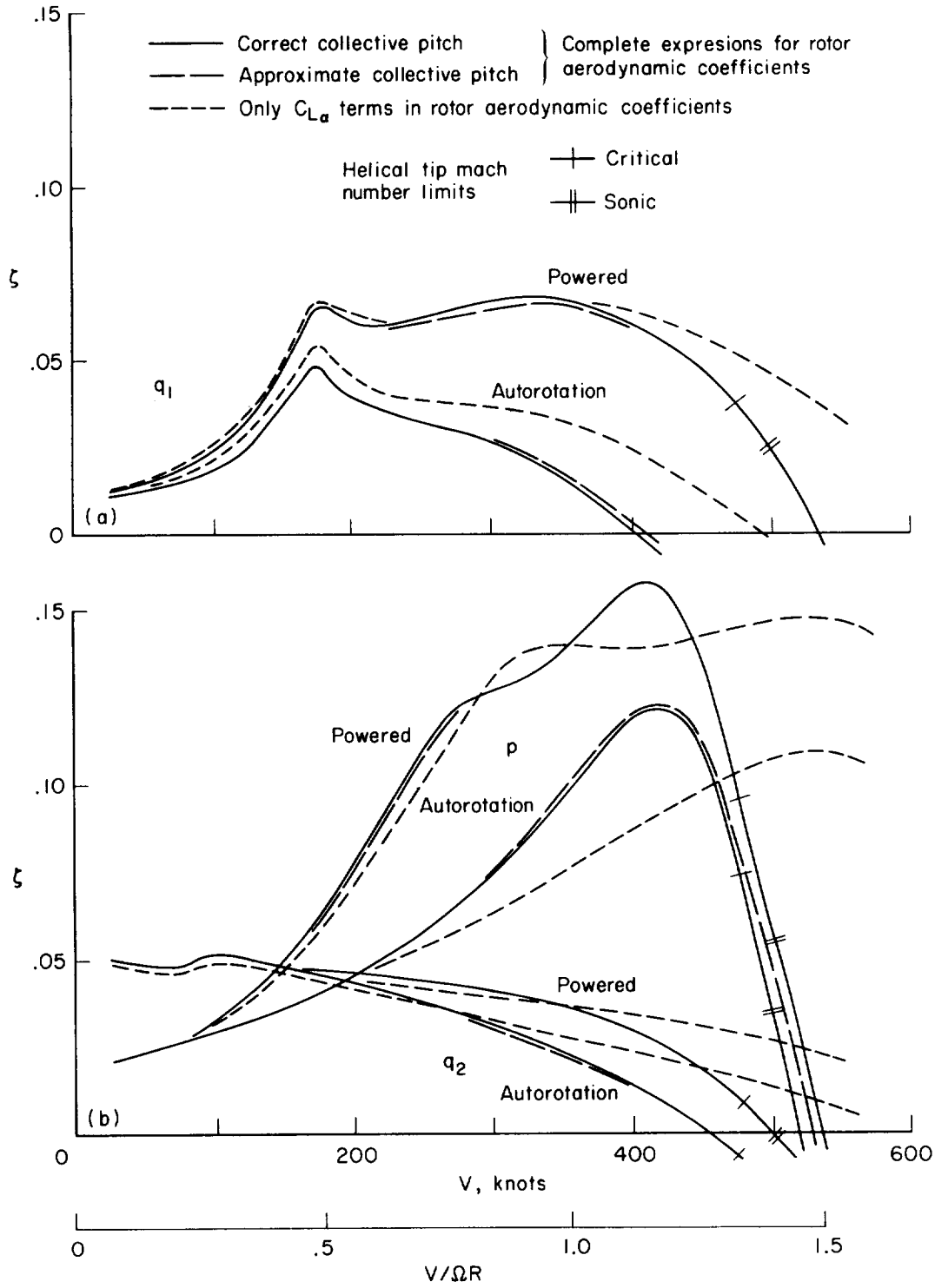

(a) Wing vertical bending (q_1) damping.
(b) Wing chordwise bending (q_2) and torsion (p) damping.

Figure 21.- Bell rotor velocity sweep, Ω = 458 rpm; influence of the complete expressions for the rotor aerodynamic coefficients.

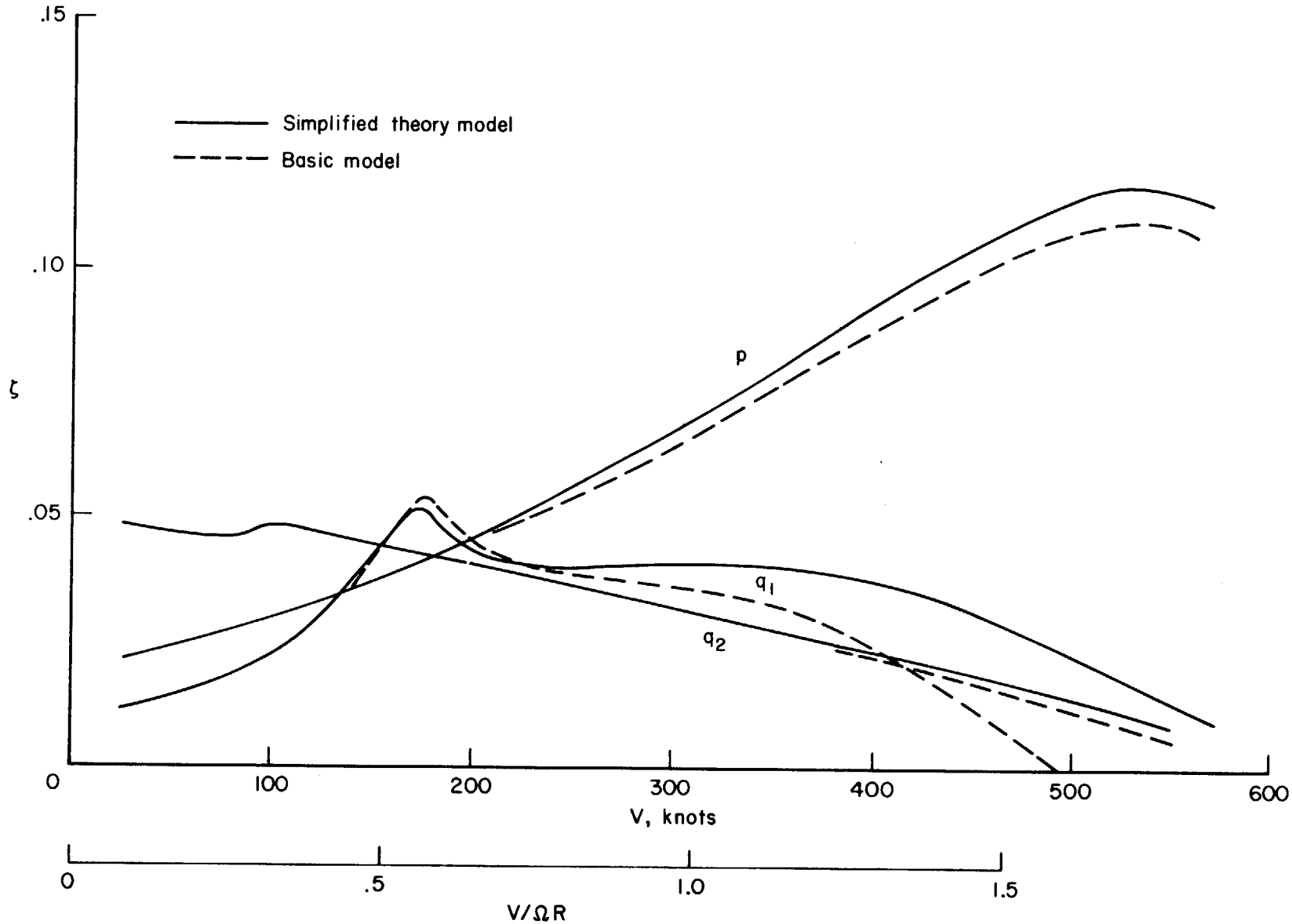

Figure 22.- Bell rotor velocity sweep, Ω = 450 rpm; comparison of simplified and basic theoretical models; damping ratio for wing vertical bending (q_1), chordwise bending (q_2), and torsion (p).

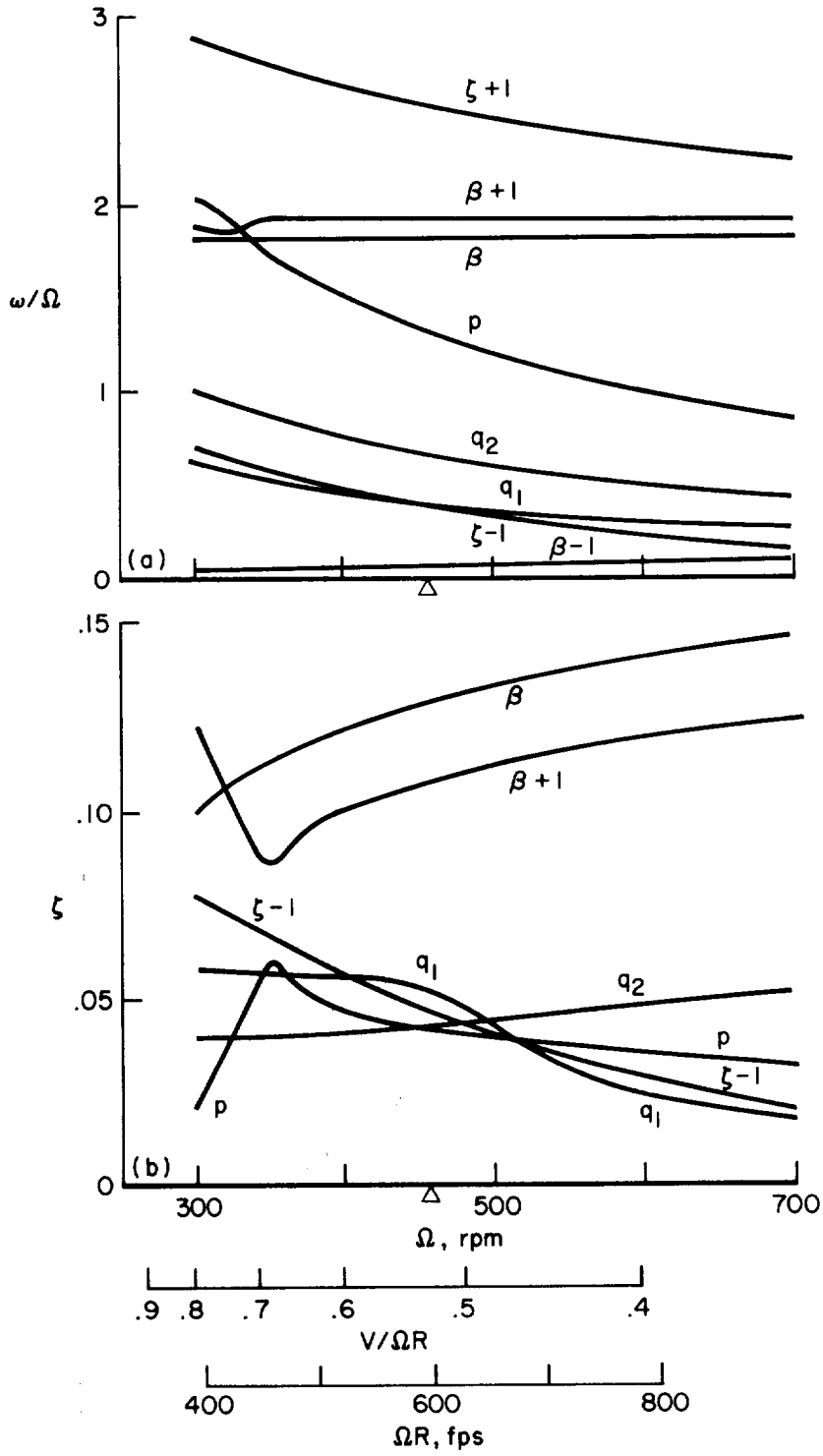

(a) Frequency of the modes.
(b) Damping ratio of the modes.

Figure 23.- Bell rotor rpm sweep, V = 185 knots.

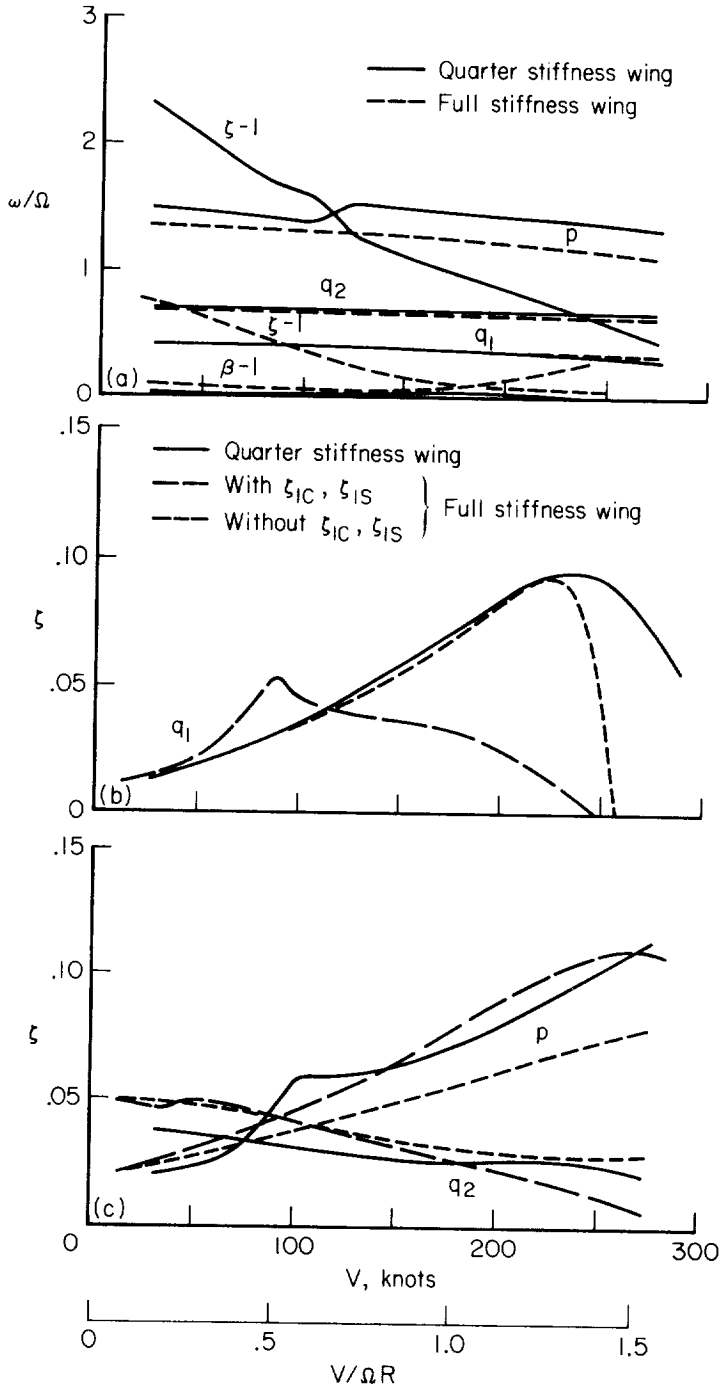

(a) Frequency of the modes.
(b) Wing vertical bending (q_1) damping.
(c) Wing chordwise bending (q_2) and torsion (p) damping.

Figure 24.- Bell rotor velocity sweep, quarter-stiffness wing, Ω = 229 rpm; compared with the full-stiffness wing results with and without ζ_{1C} and ζ_{1S} degrees of freedom.

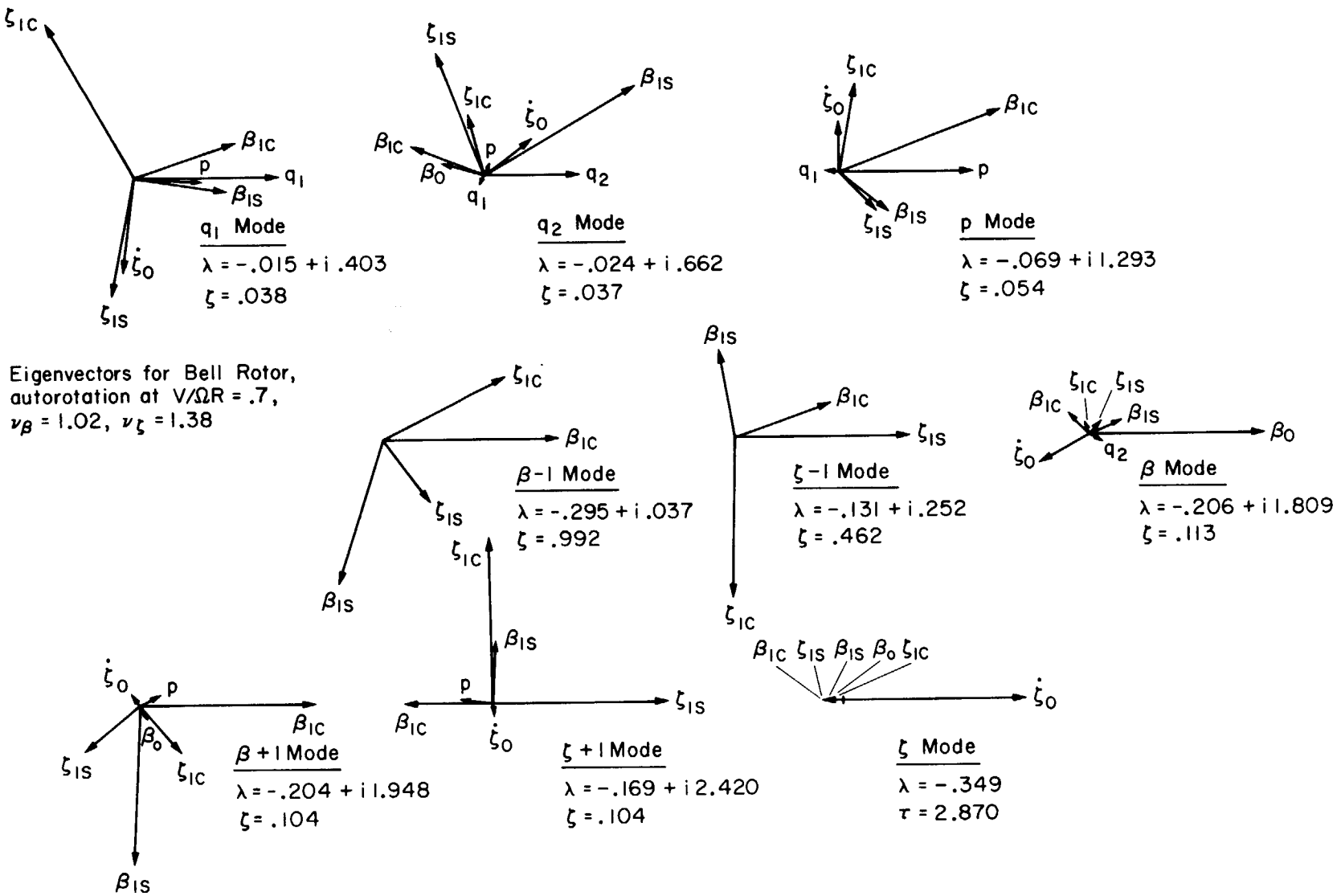

(a) Autorotation.

Figure 25.- Bell rotor roots and modes at $V/\Omega R$ = 0.7, Ω = 458 rpm, V = 249 knots.

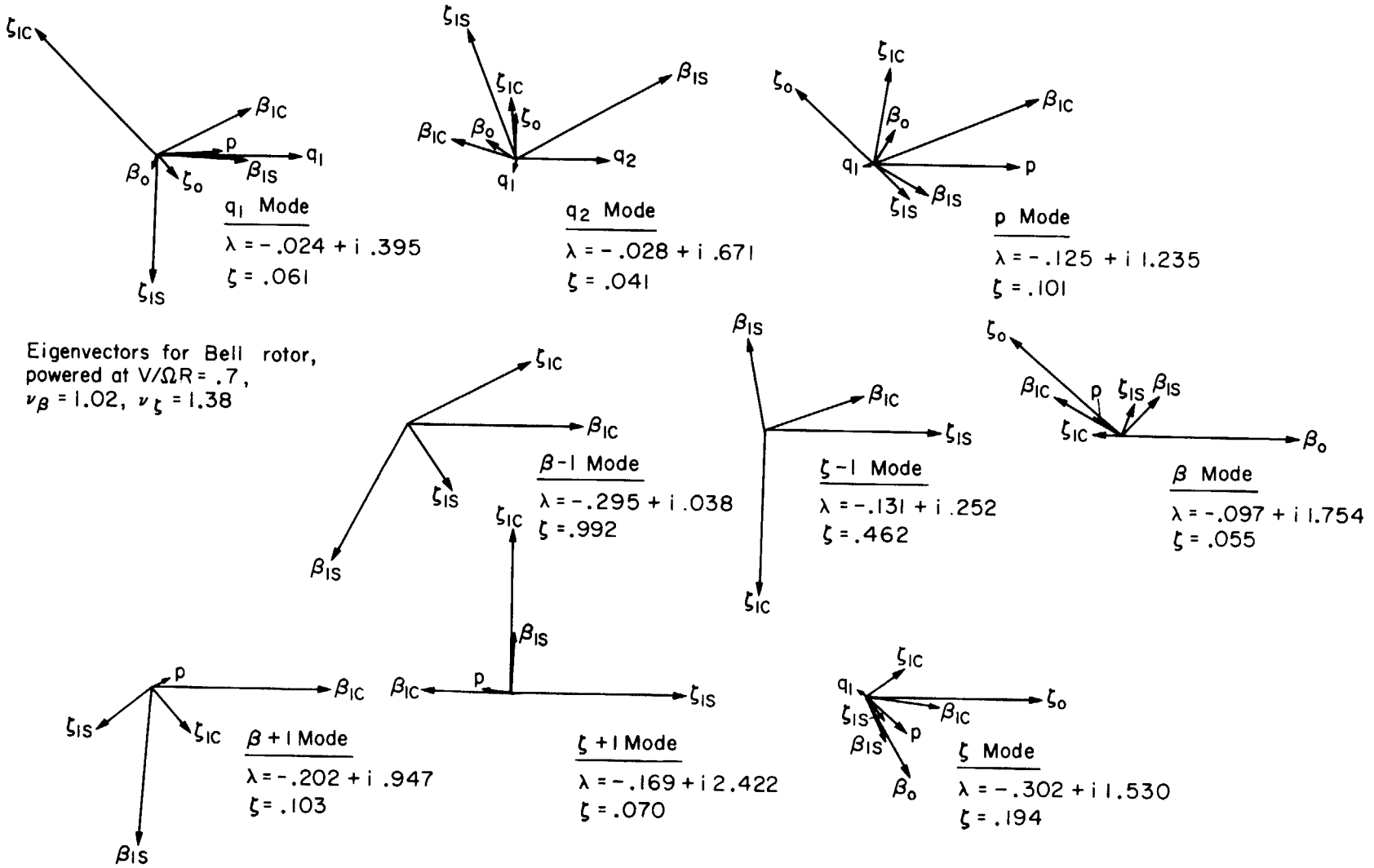

(b) Powered flight.

Figure 25.- Concluded.

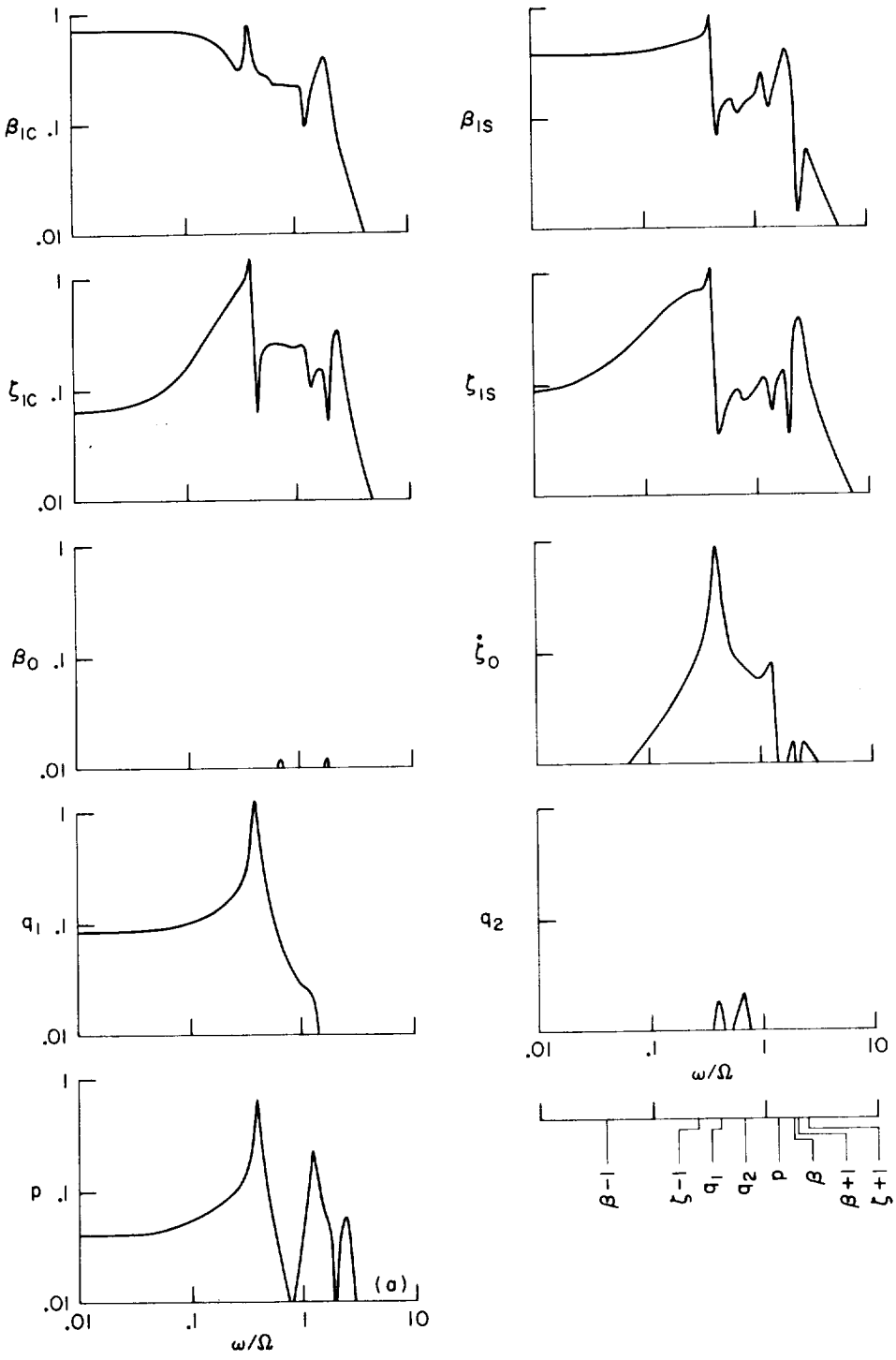

(a) Vertical gust α_G input.

Figure 26.- Bell rotor in autorotation at $V/\Omega R$ = 0.7 (Ω = 458 rpm, V = 249 knots), magnitude of response of each degree of freedom to input at frequency ω.

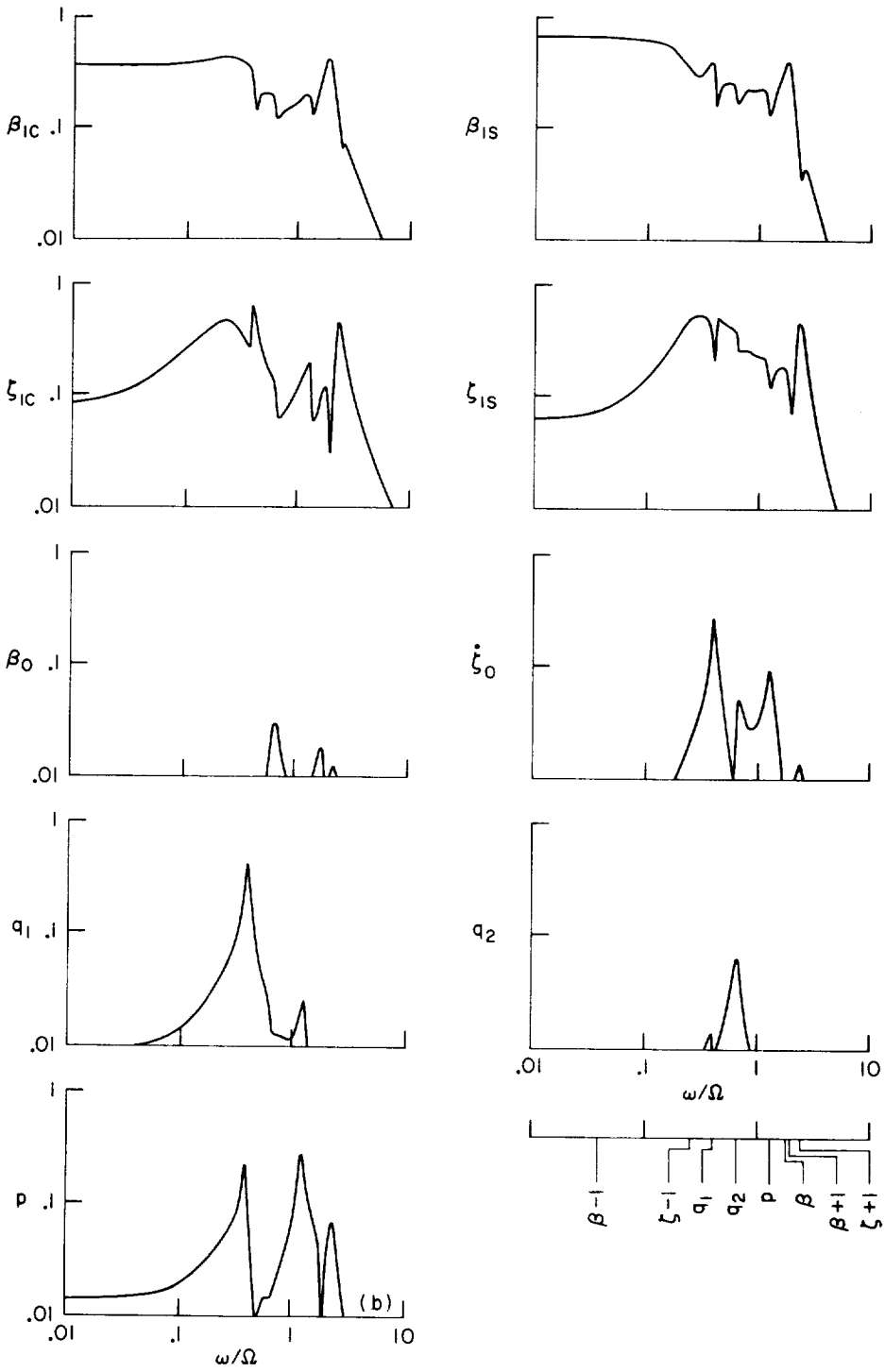

(b) Lateral gust β_G input.

Figure 26.- Continued.

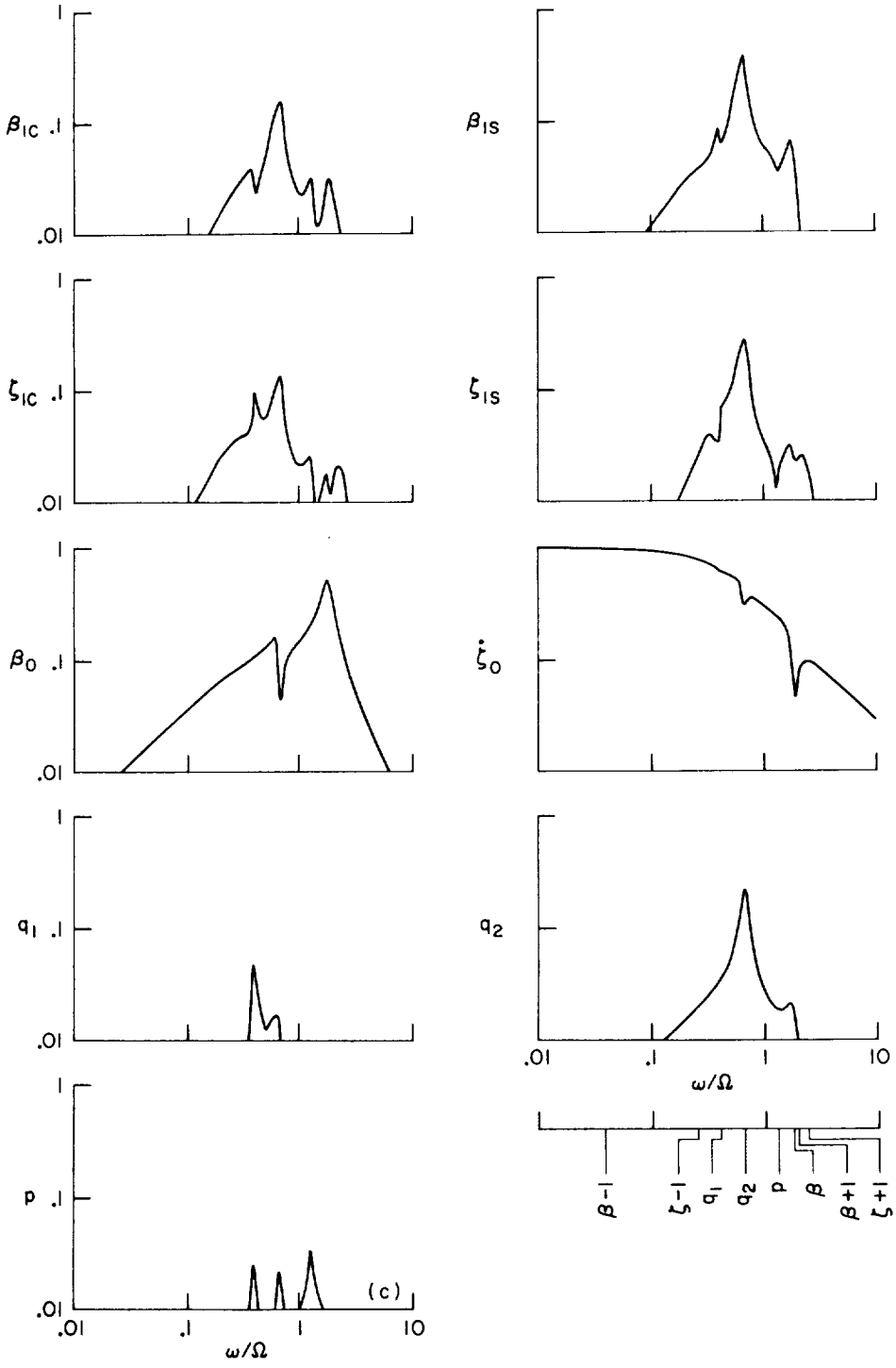

(c) Longitudinal gust u_G input.

Figure 26.- Continued.

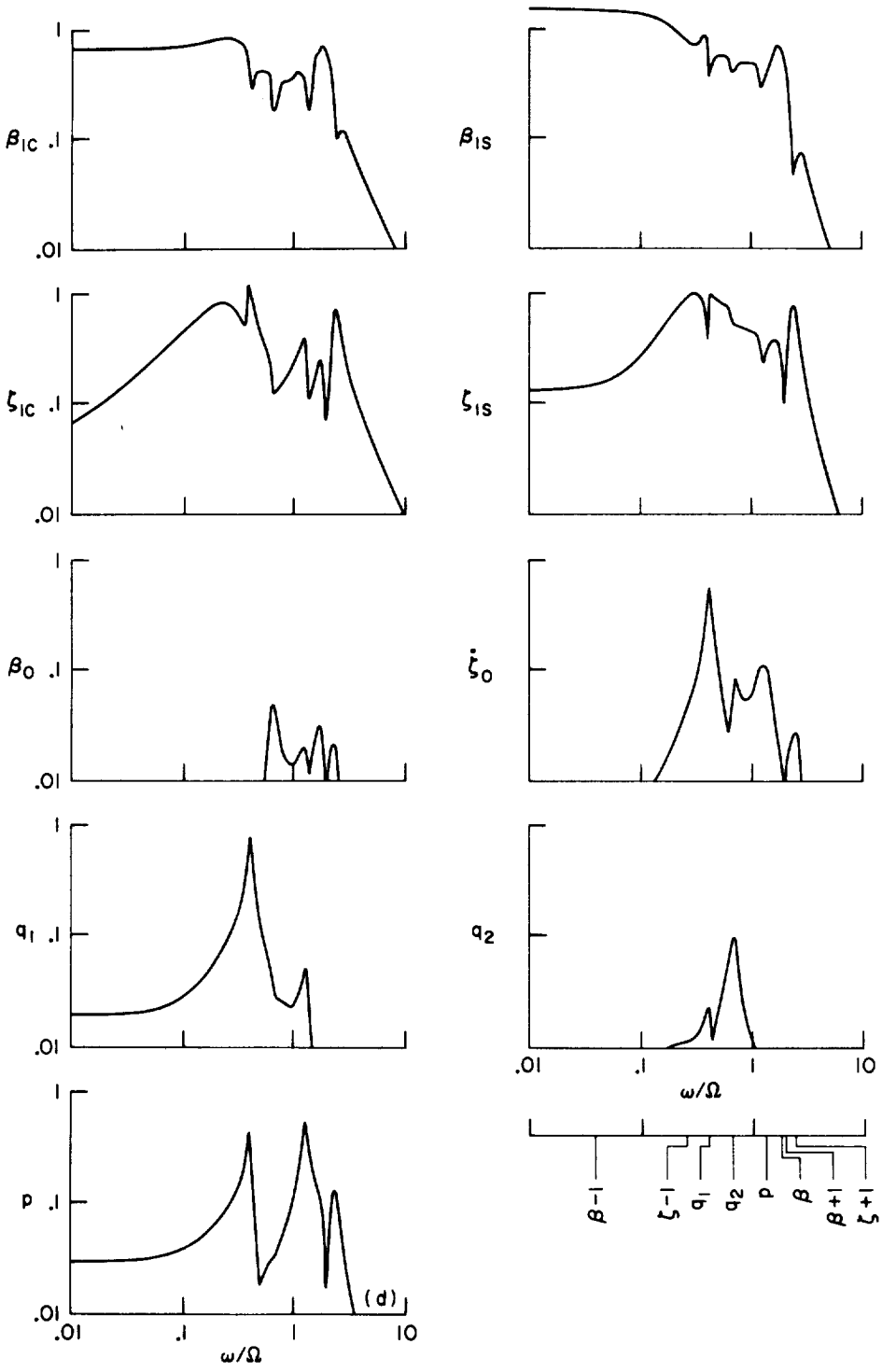

(d) Lateral cyclic pitch θ_{1C} input.

Figure 26.- Continued.

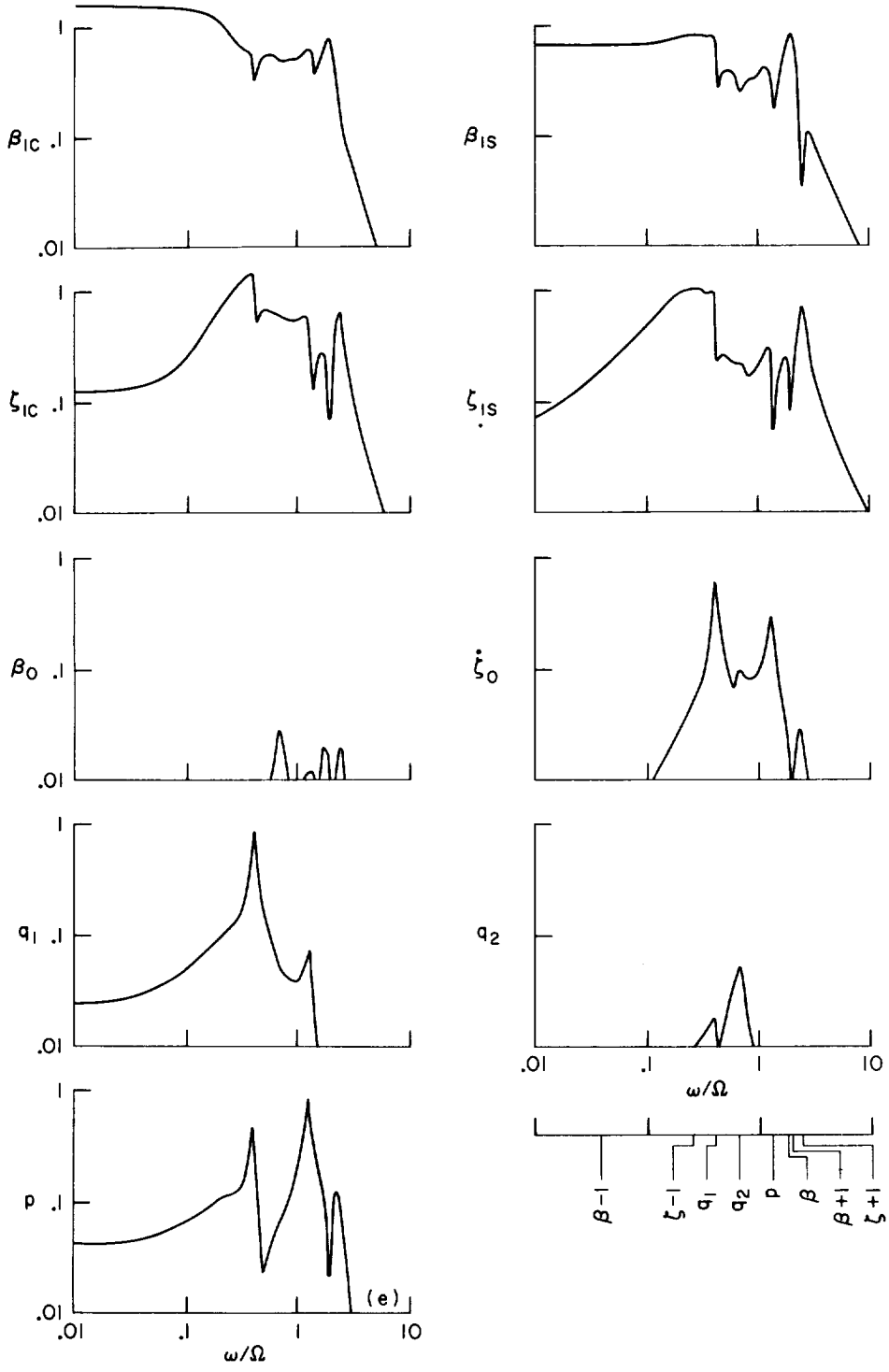

(e) Longitudinal cyclic pitch θ_{1S} input.

Figure 26.- Continued.

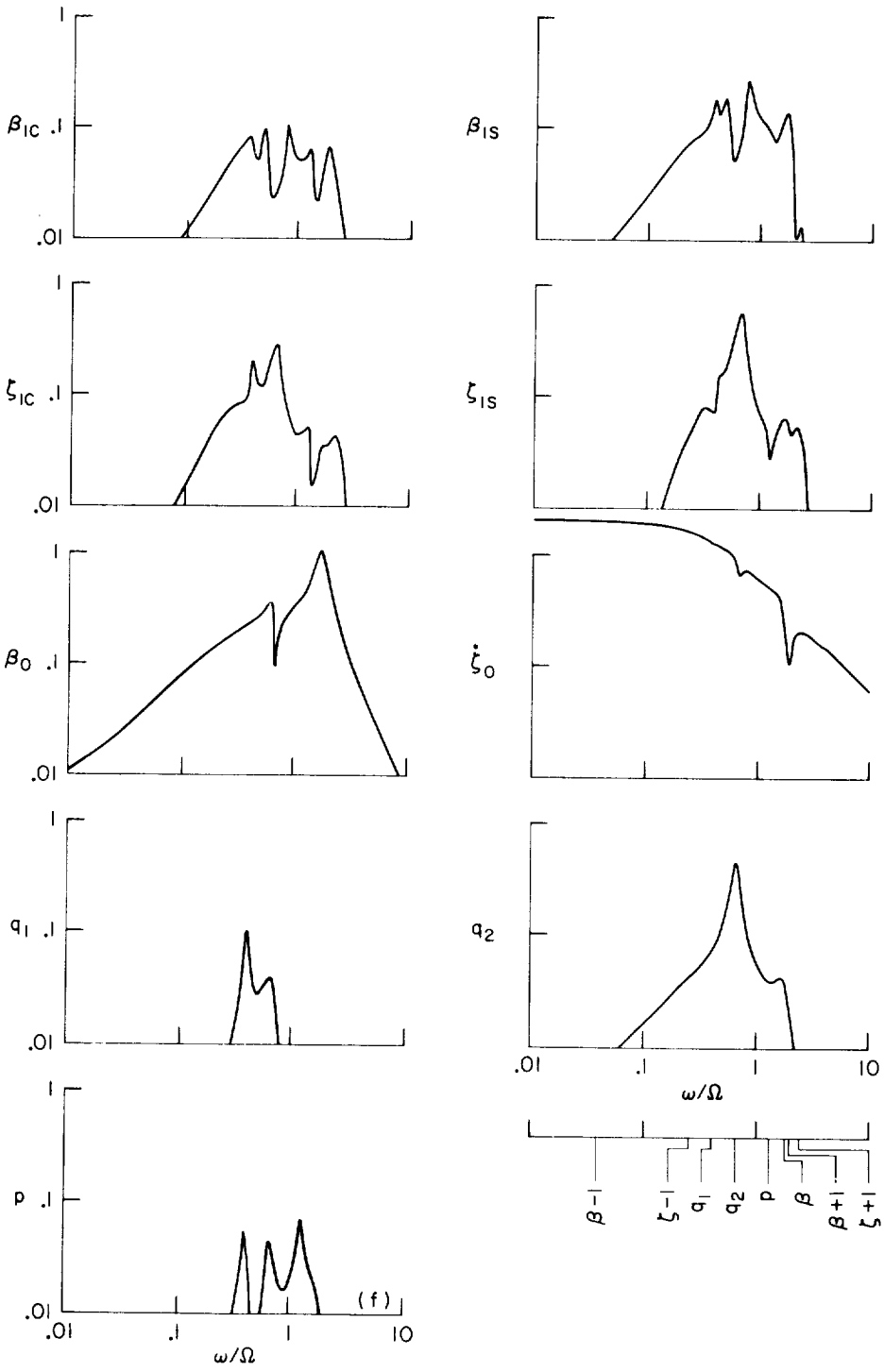

(f) Collective pitch θ_o input.

Figure 26.- Concluded.

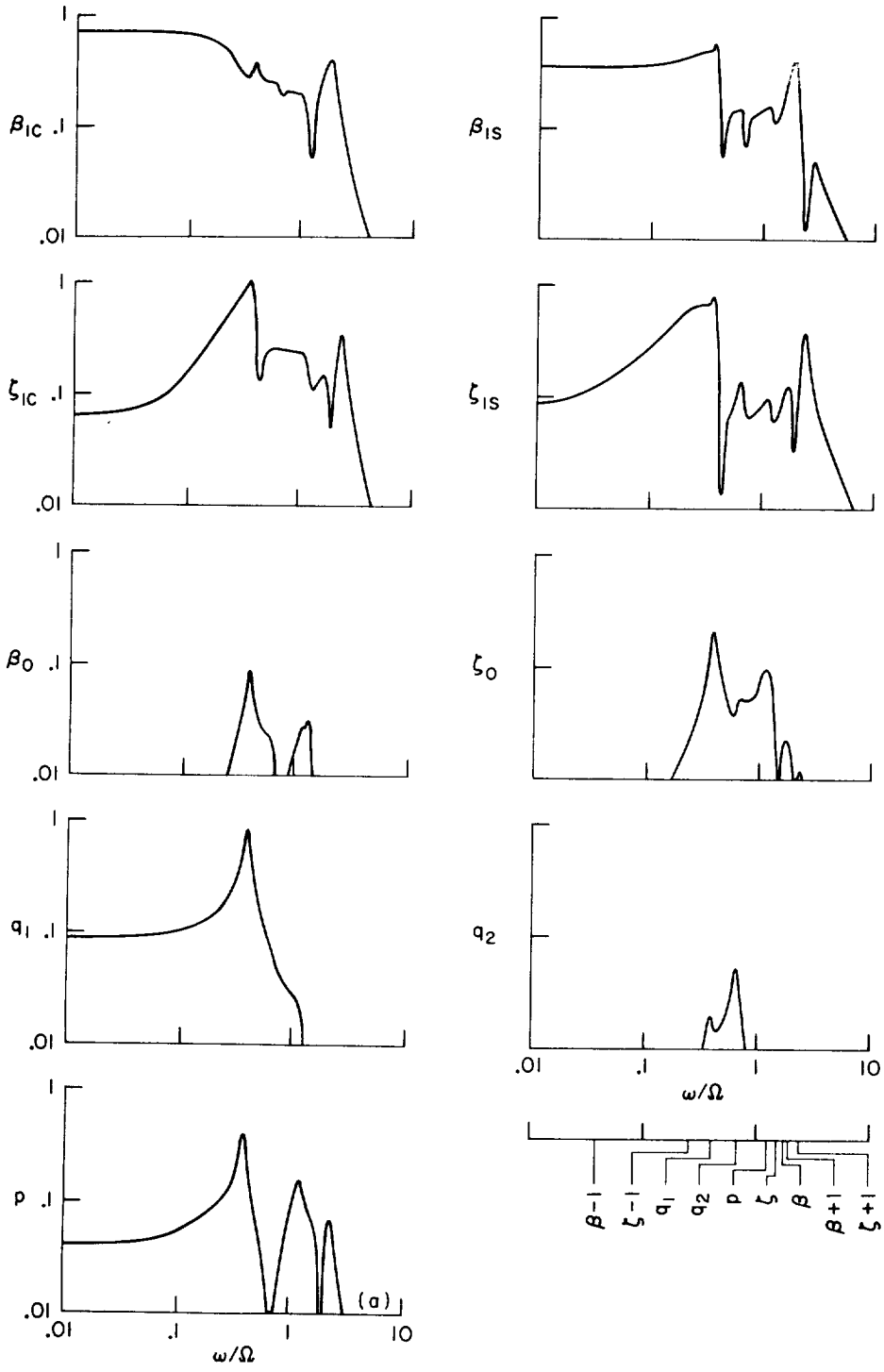

(a) Vertical gust α_G input.

Figure 27.- Bell rotor in powered operation at $V/\Omega R$ = 0.7 (Ω = 458 rpm, V = 249 knots), magnitude of response of each degree of freedom to input at frequency ω.

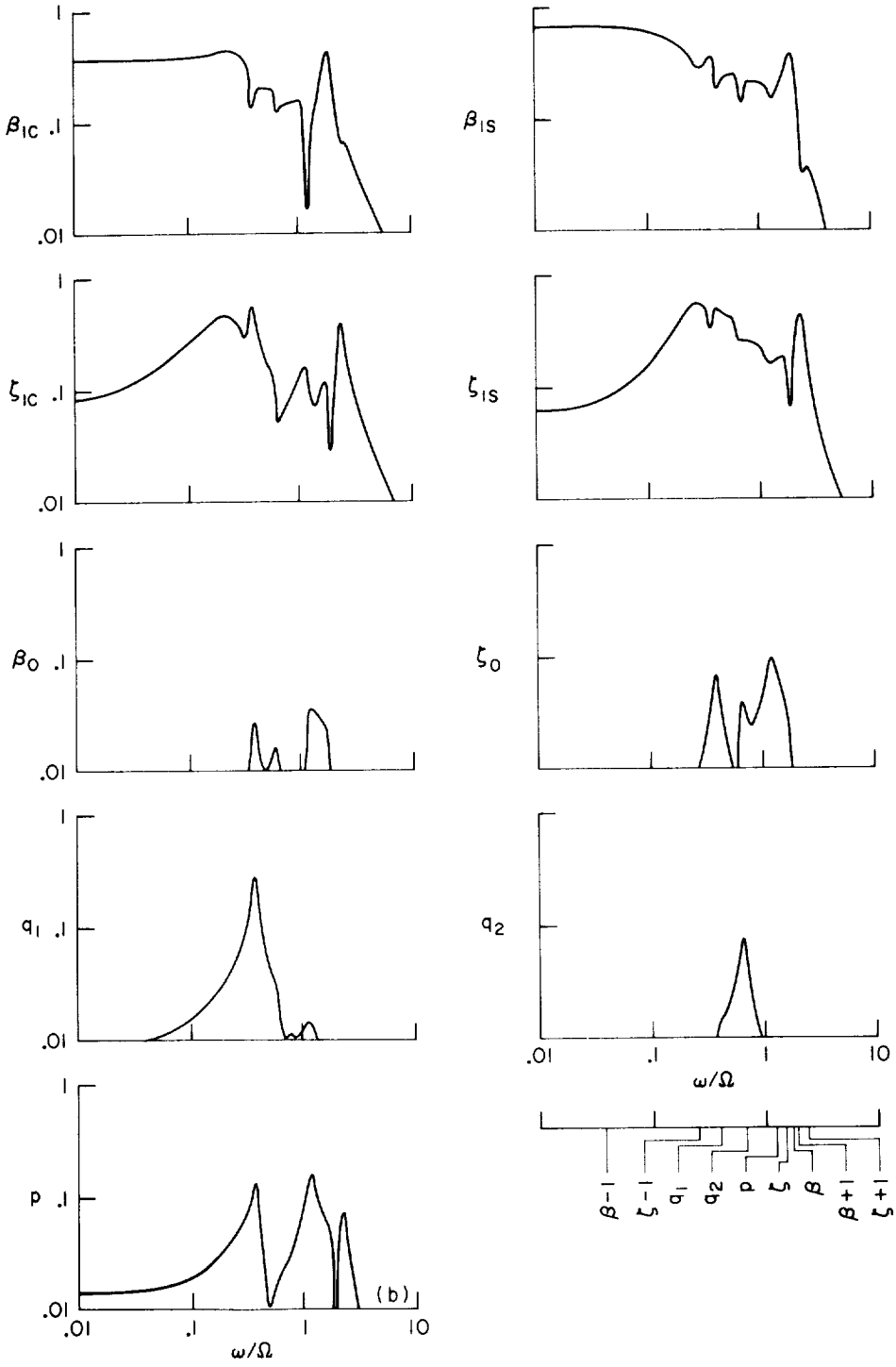

(b) Lateral gust β_G input.

Figure 27.- Continued.

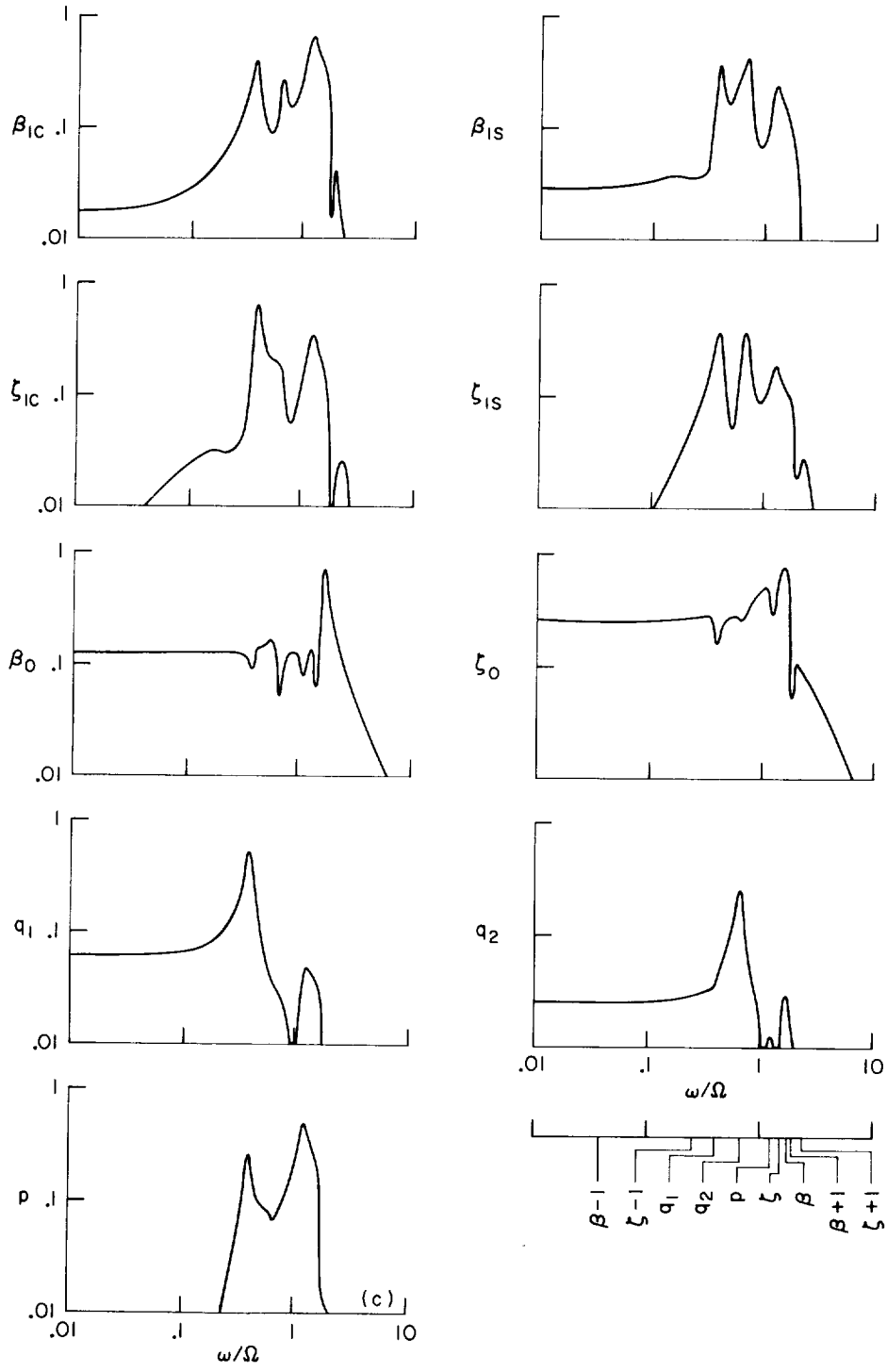

(c) Longitudinal gust u_G input.

Figure 27.- Continued.

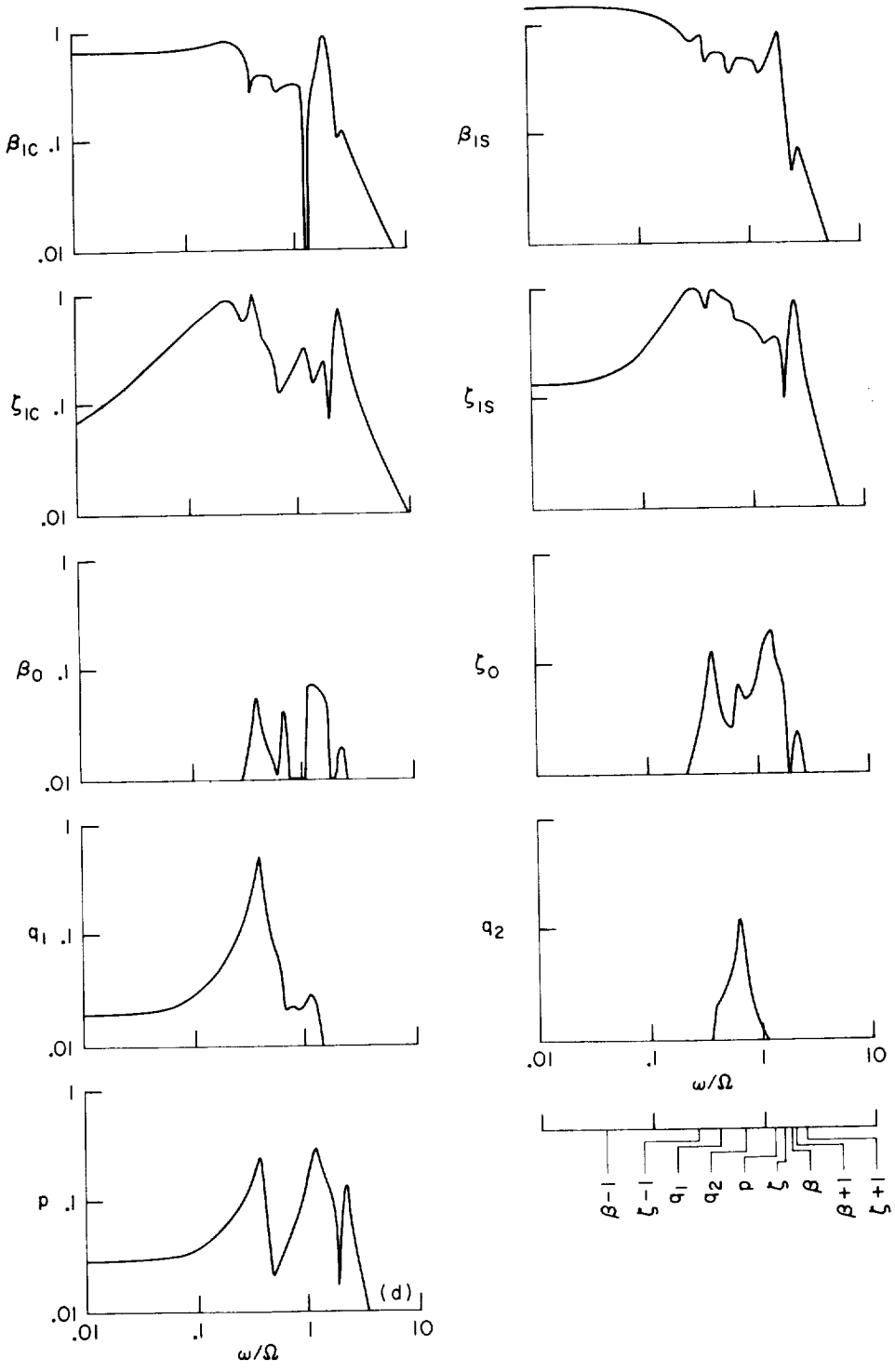

(d) Lateral cyclic pitch θ_{1C} input.

Figure 27.- Continued.

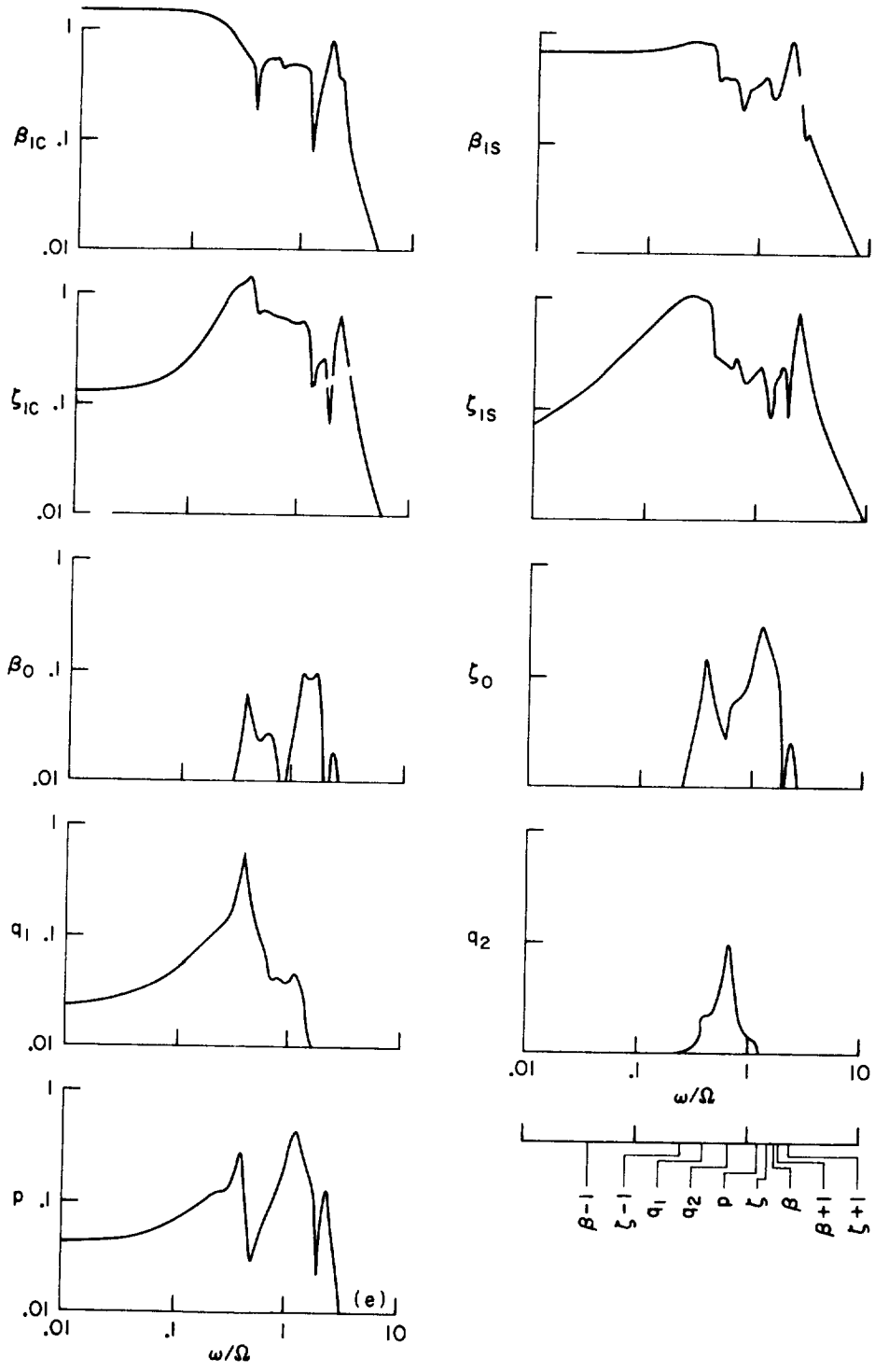

(e) Longitudinal cyclic pitch θ_{1S} input.

Figure 27.- Continued.

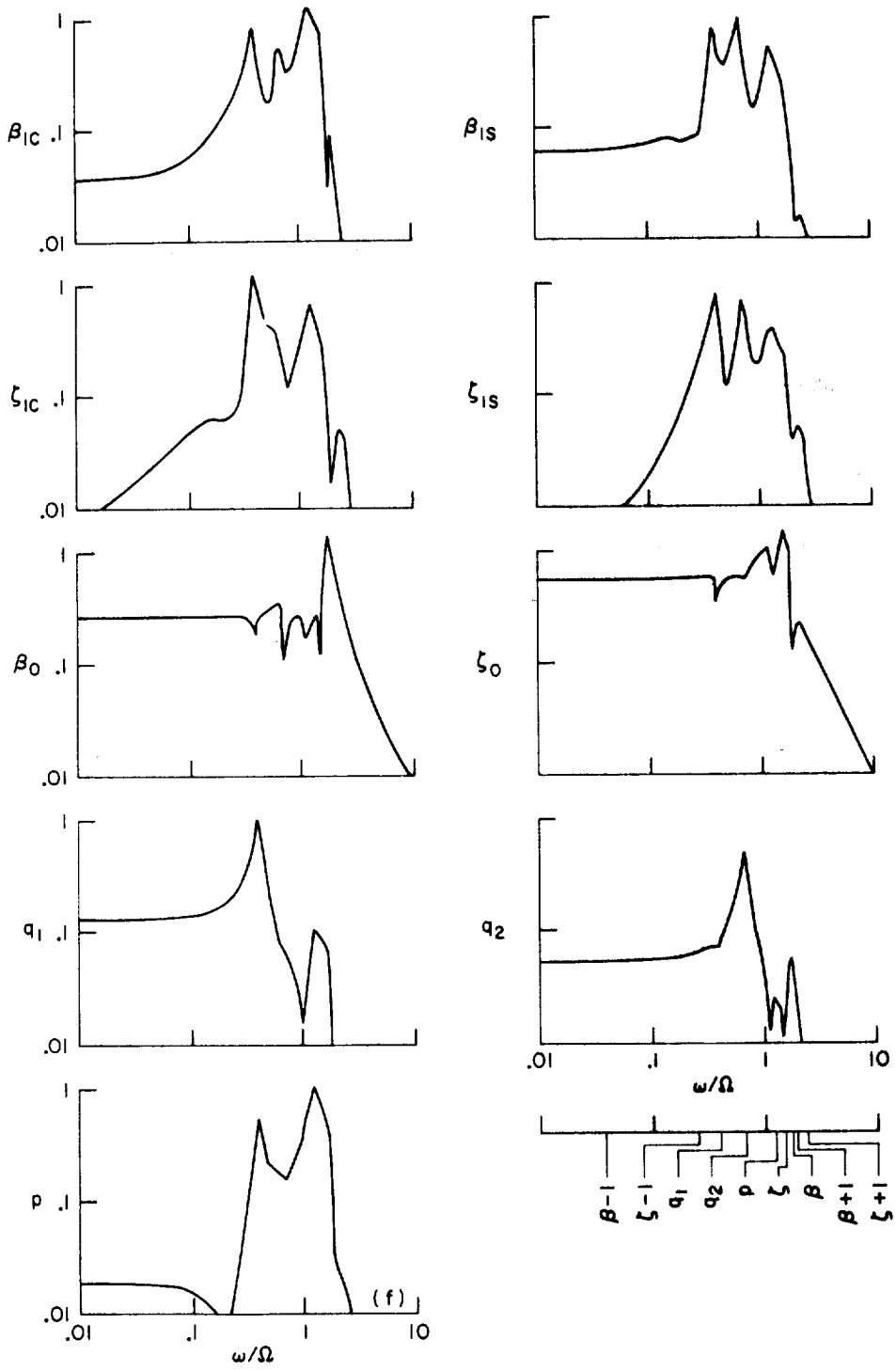

(f) Collective pitch θ_0 input.

Figure 27.- Concluded.

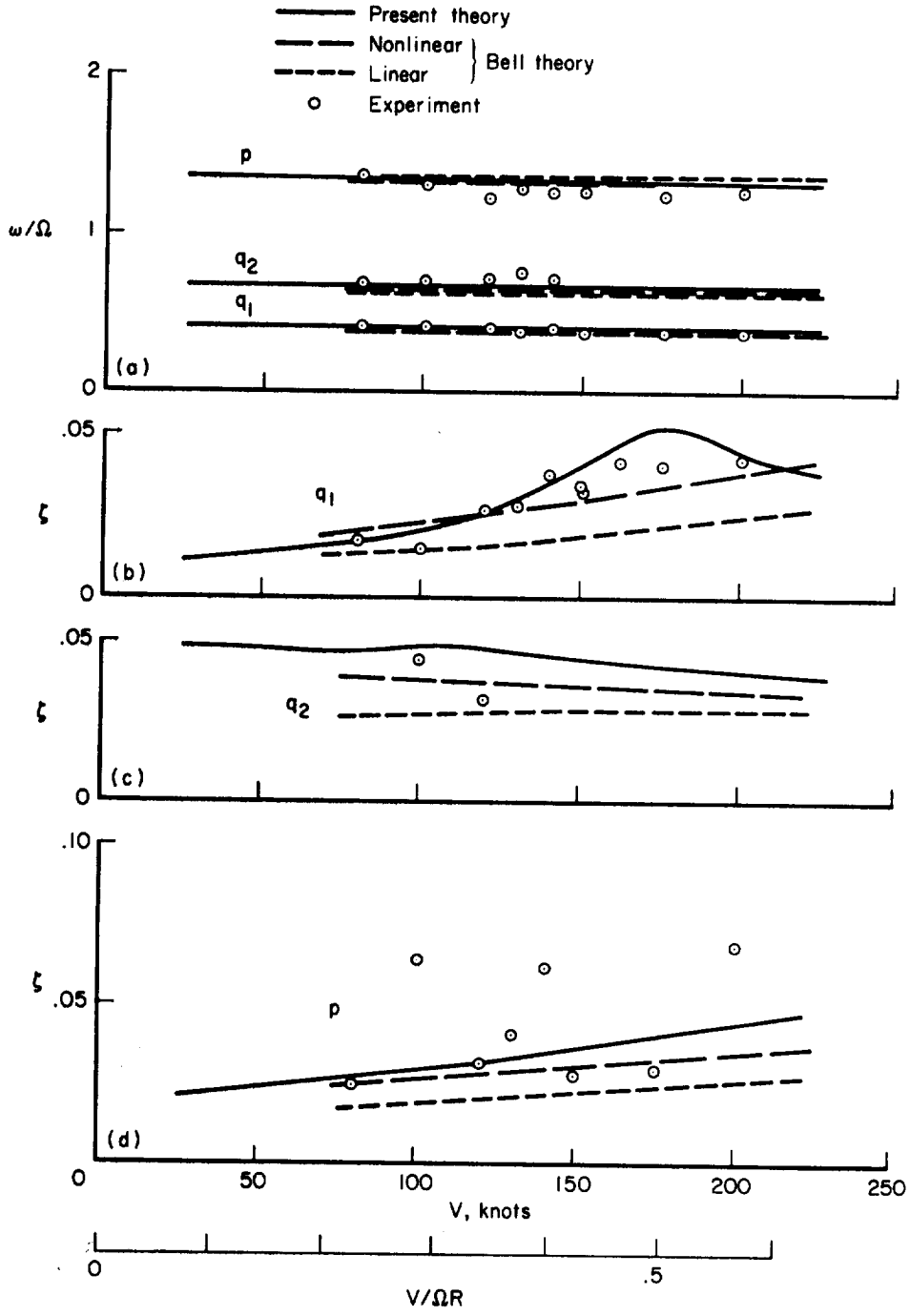

(a) Frequency of the modes.
(b) Wing vertical bending damping (q_1).
(c) Wing chordwise bending damping (q_2).
(d) Wing torsion damping (p).

Figure 28.- Bell rotor velocity sweep at Ω = 458 rpm, comparison with full-scale experimental data and the Bell theories.

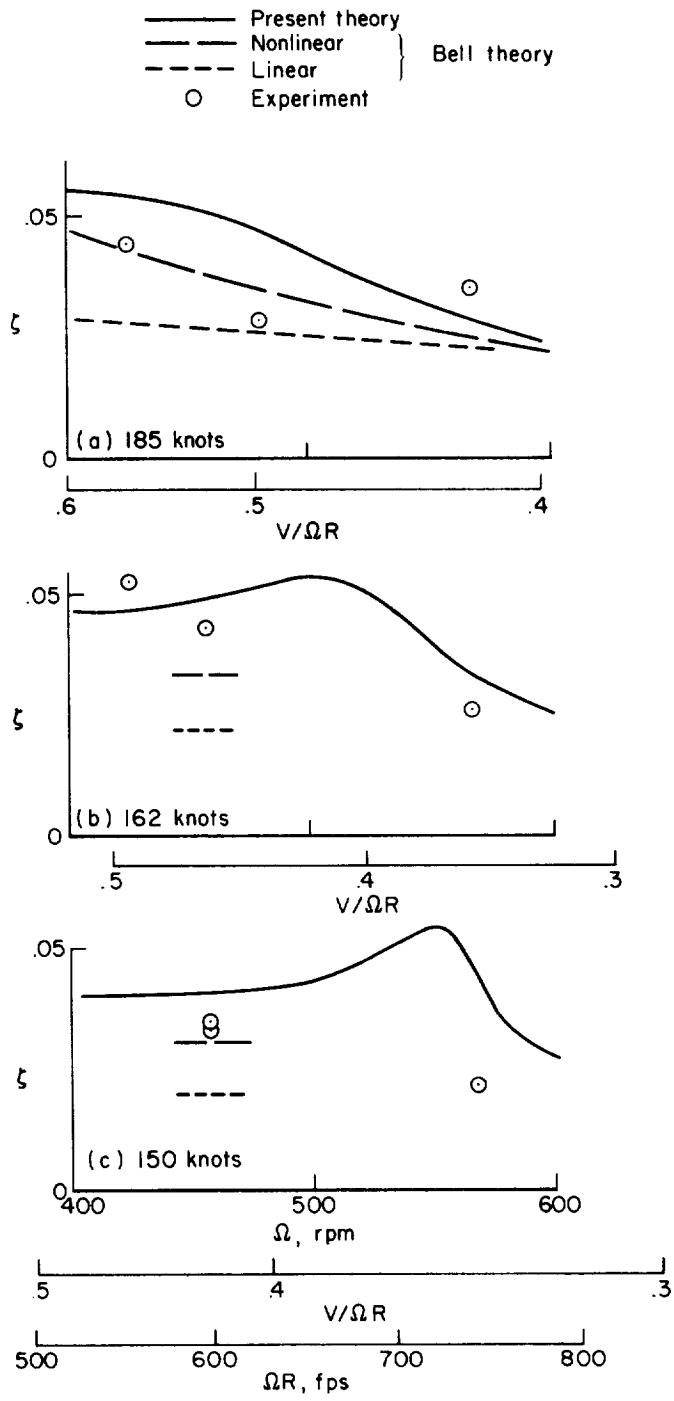

(a) Wing vertical bending damping (q_1) at 185 knots.
(b) Wing vertical bending damping (q_1) at 162 knots.
(c) Wing vertical bending damping (q_1) at 150 knots.

Figure 29.- Bell rotor rpm sweep, comparison with full-scale experimental data and Bell theories.

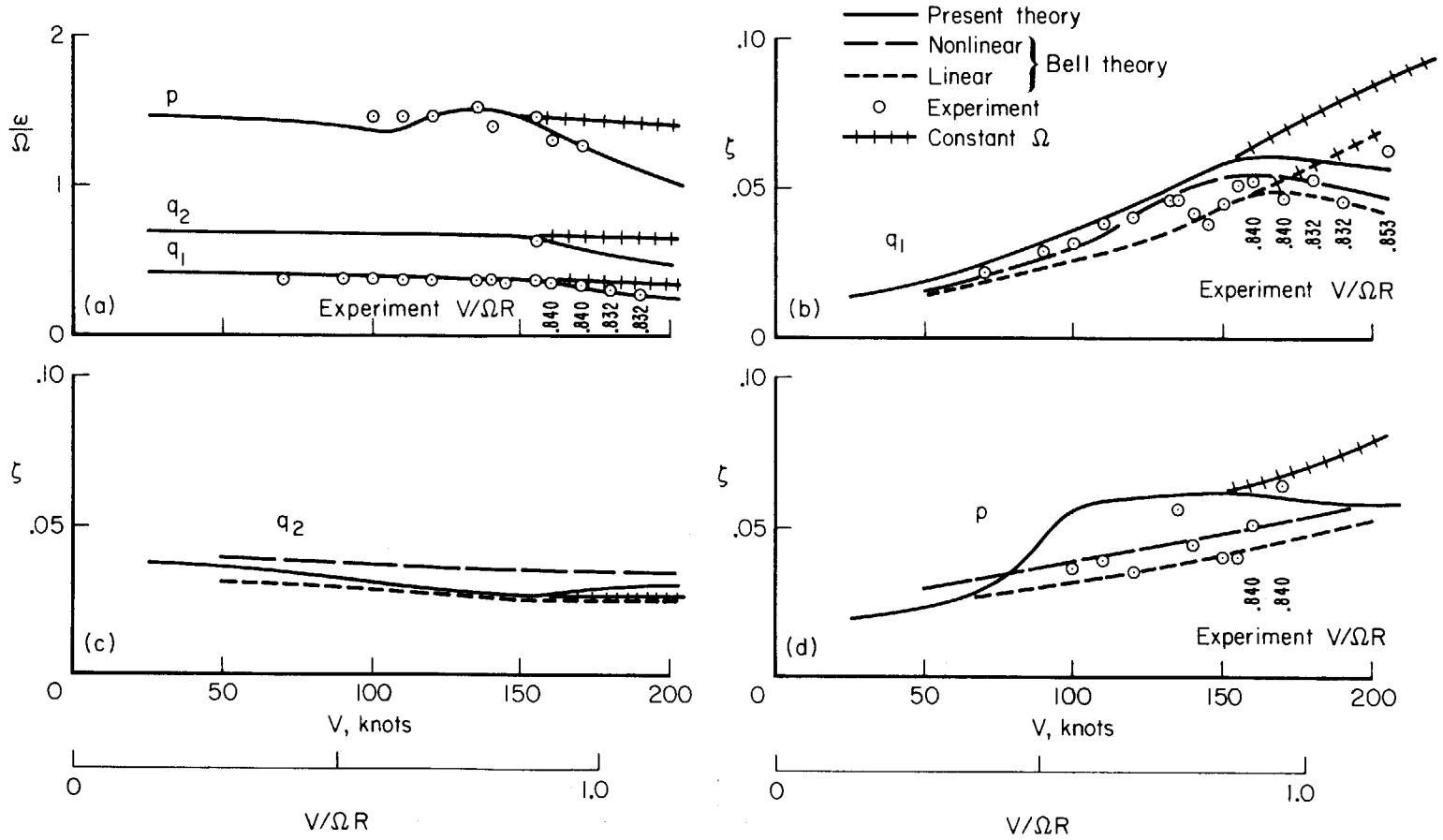

(a) Frequency of the modes.
(b) Wing vertical bending damping (q_1).
(c) Wing chordwise bending damping (q_2).
(d) Wing torsion damping (p).

Figure 30.- Bell rotor on quarter-stiffness wing, velocity sweep at Ω = 229 rpm; comparison with full-scale experimental data and Bell theories.

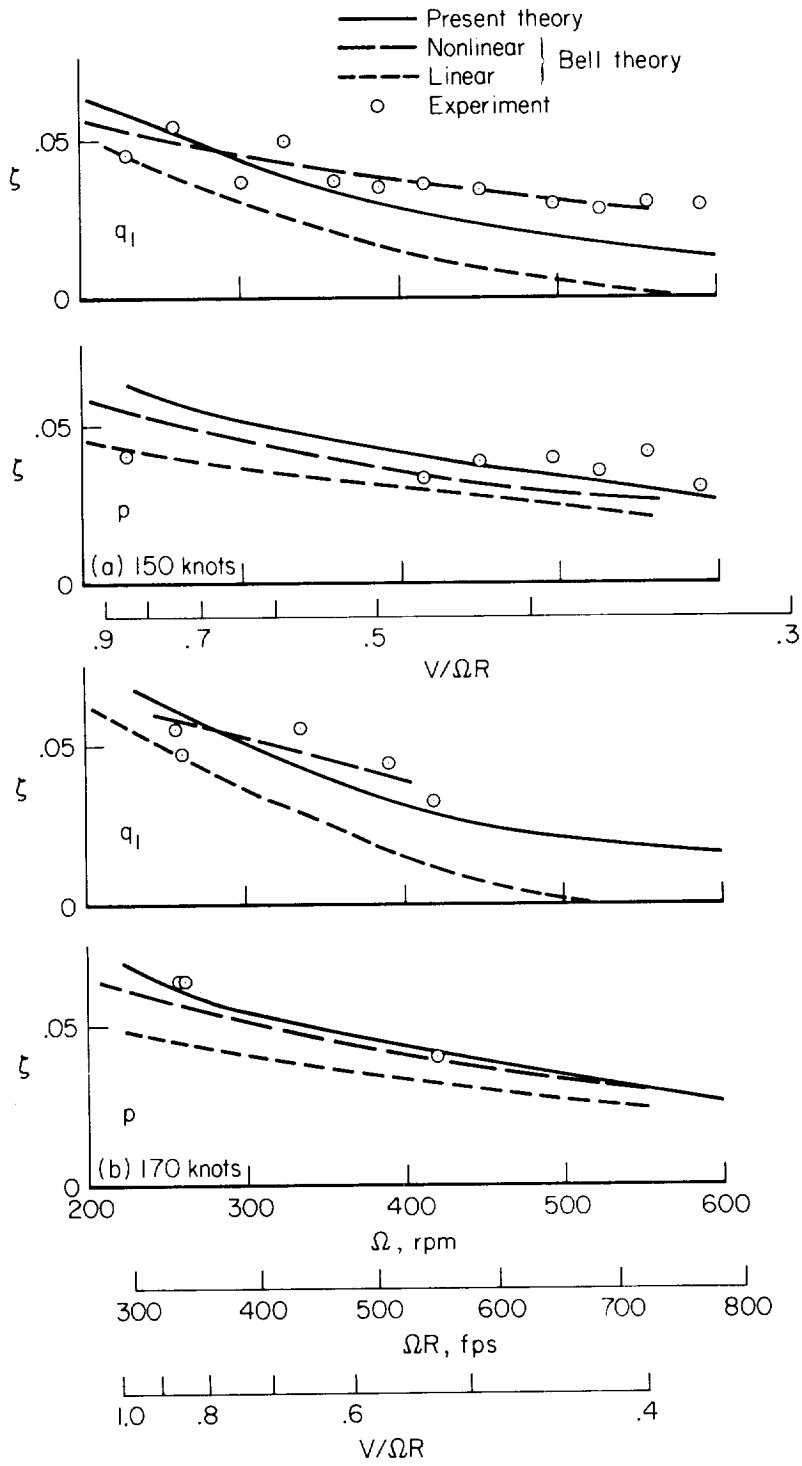

(a) Wing vertical bending (q_1) and torsion (p) damping at 150 knots.
(b) Wing vertical bending (q_1) and torsion (p) damping at 170 knots.

Figure 31.- Bell rotor on quarter-stiffness wing, rpm sweeps; comparison with full-scale experimental data and with Bell theories.

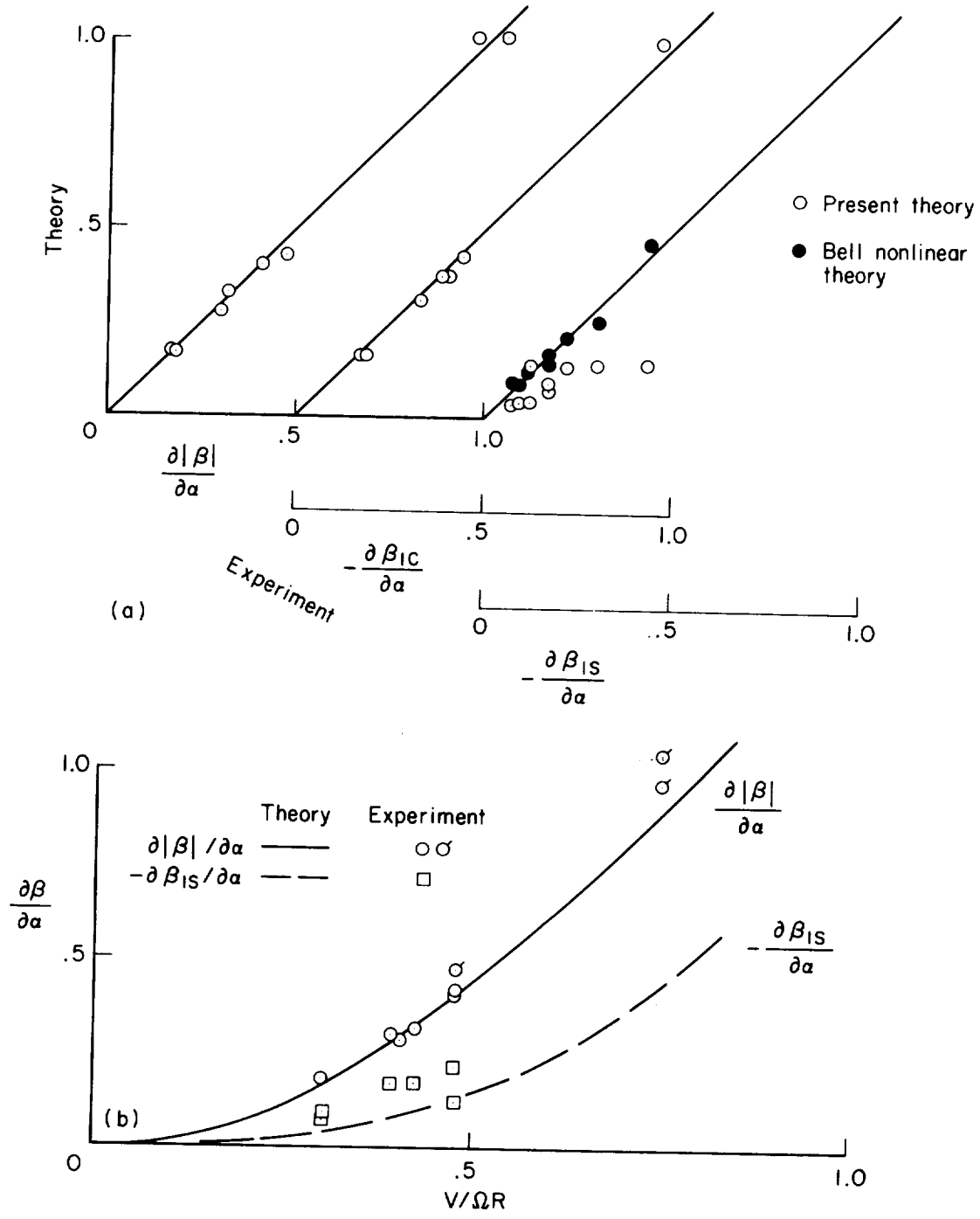

(a) Correlation between theory and experiment.
(b) Variation with inflow ratio $V/\Omega R$ (flagged symbols are for quarter-stiffness wing at Ω = 229 rpm).

Figure 32.- Bell rotor flapping due to shaft angle of attack; comparison with full-scale experimental data and Bell theories.

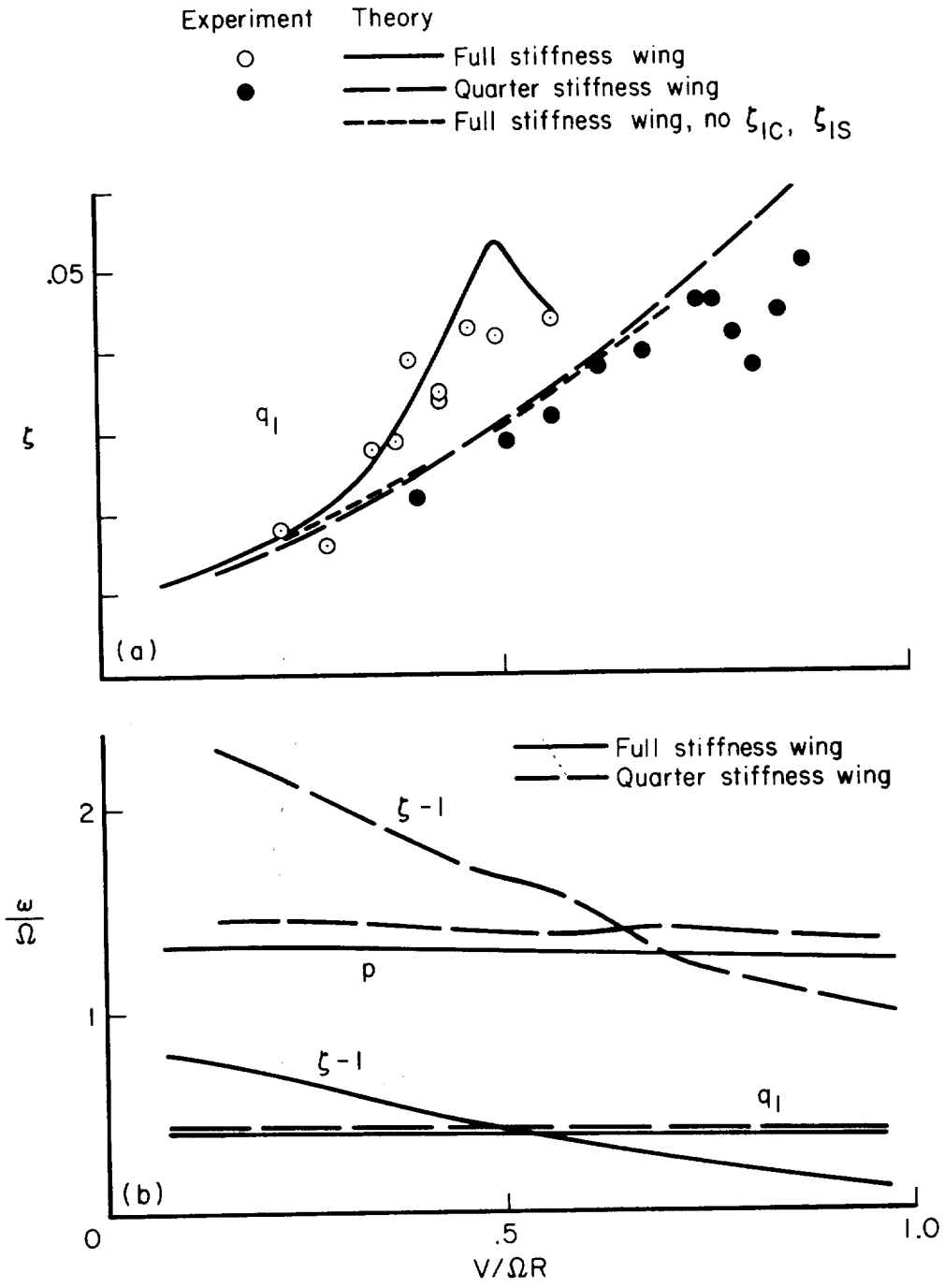

(a) Comparison with full-scale experimental data.
(b) Frequency of the modes.

Figure 33.- Bell rotor wing vertical bending (q_1) damping, velocity sweeps on full-stiffness and quarter-stiffness wings.

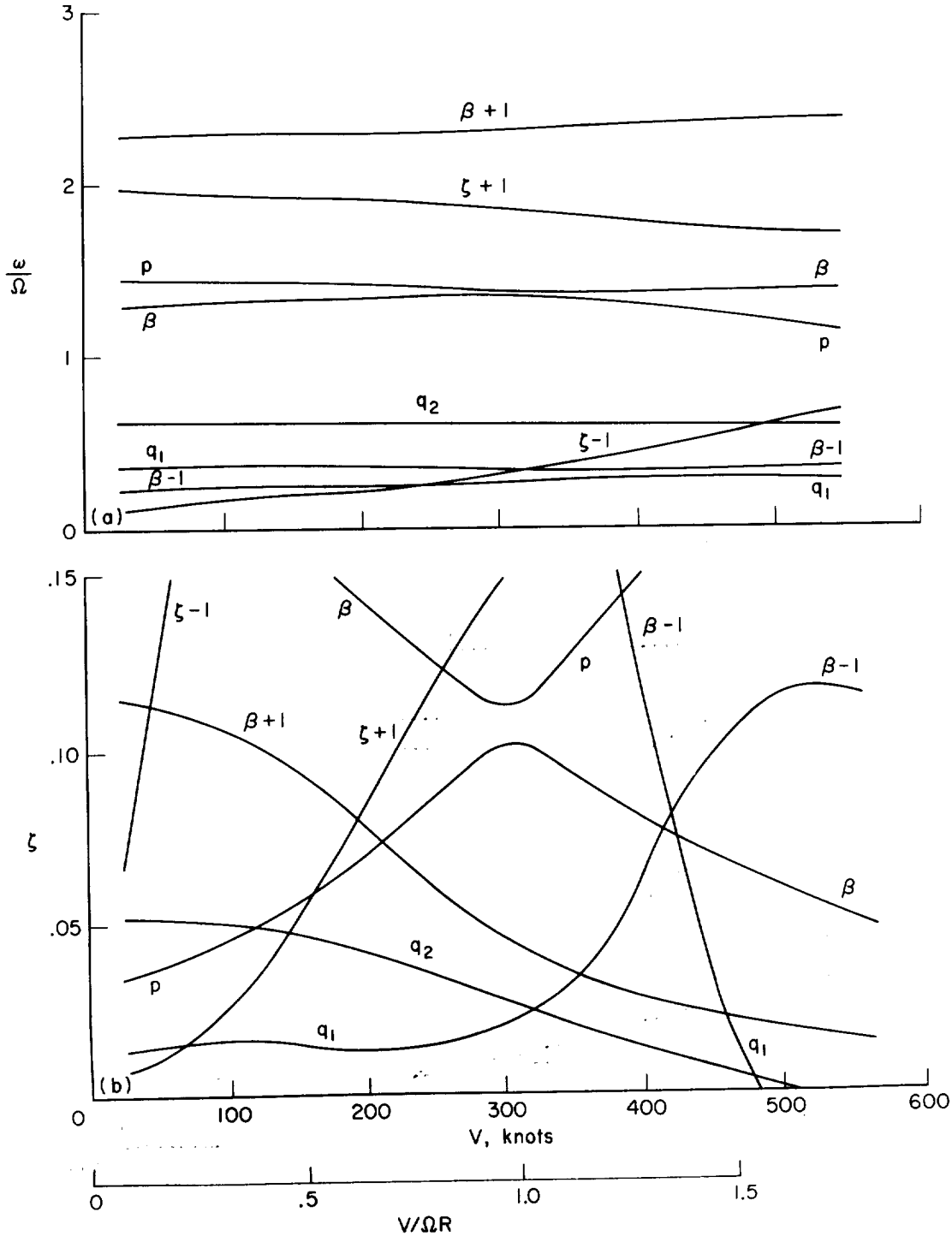

(a) Frequency of the modes.
(b) Damping ratio of the modes.

Figure 34.- Boeing rotor velocity sweep, Ω = 386 rpm; predicted eigenvalues.

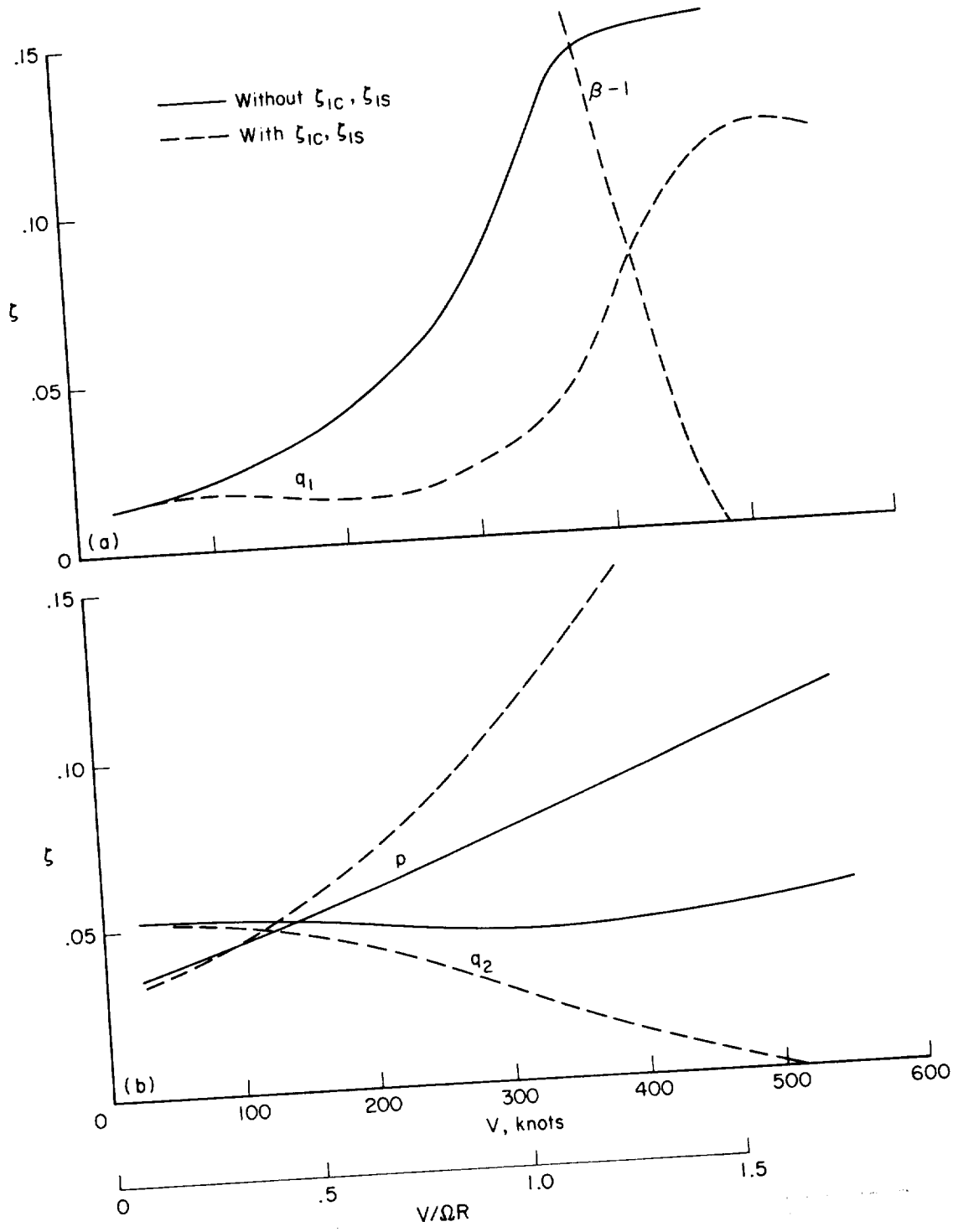

(a) Wing vertical bending (q_1) and rotor flap (β - 1) damping.
(b) Wing chordwise bending (q_2) and torsion (p) damping.

Figure 35.- Boeing rotor velocity sweep, Ω = 386 rpm; with and without ζ_{1C} and ζ_{1S} rotor lag motion.

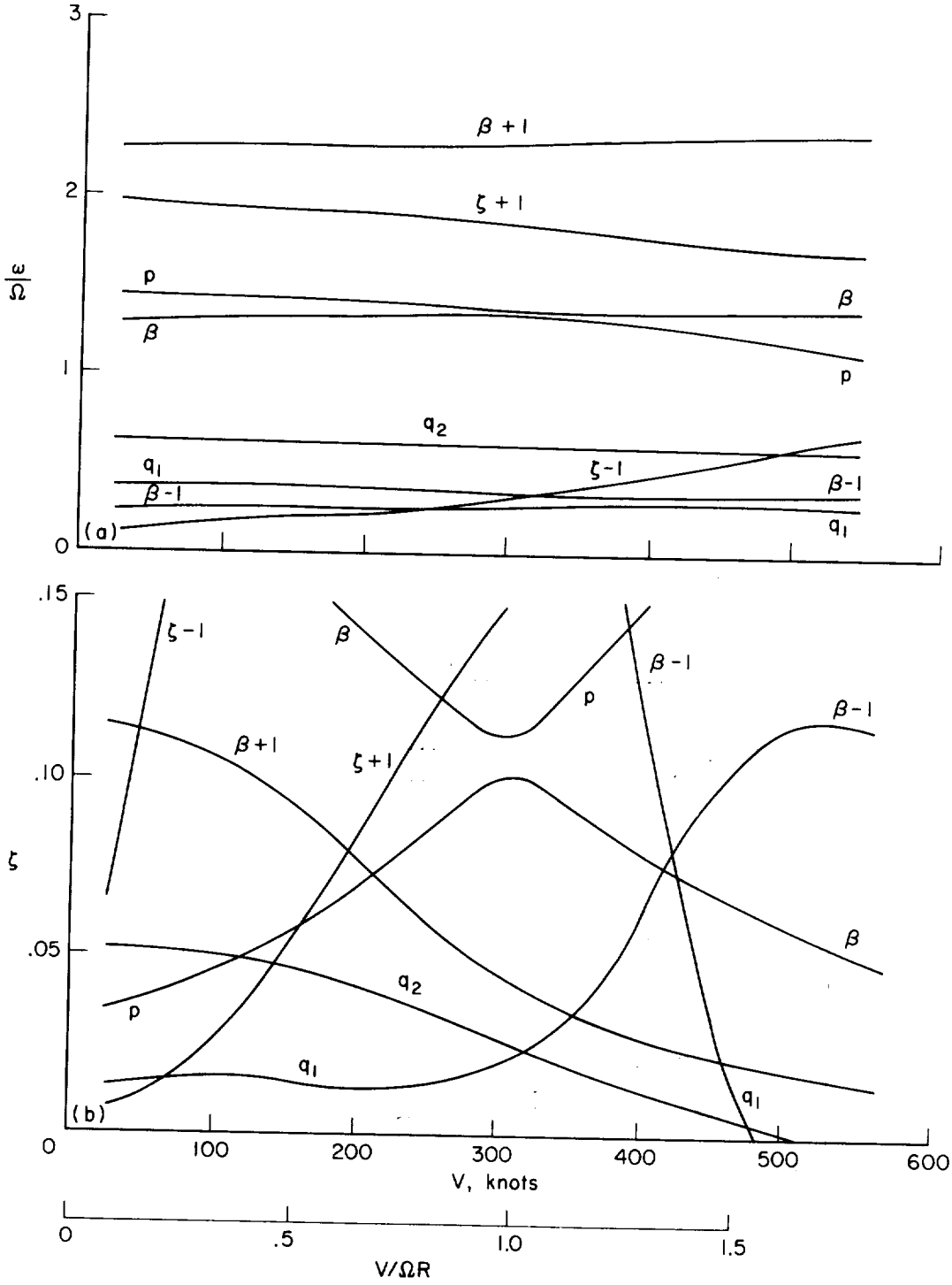

(a) Frequency of the modes.
(b) Damping ratio of the modes.

Figure 34.- Boeing rotor velocity sweep, Ω = 386 rpm; predicted eigenvalues.

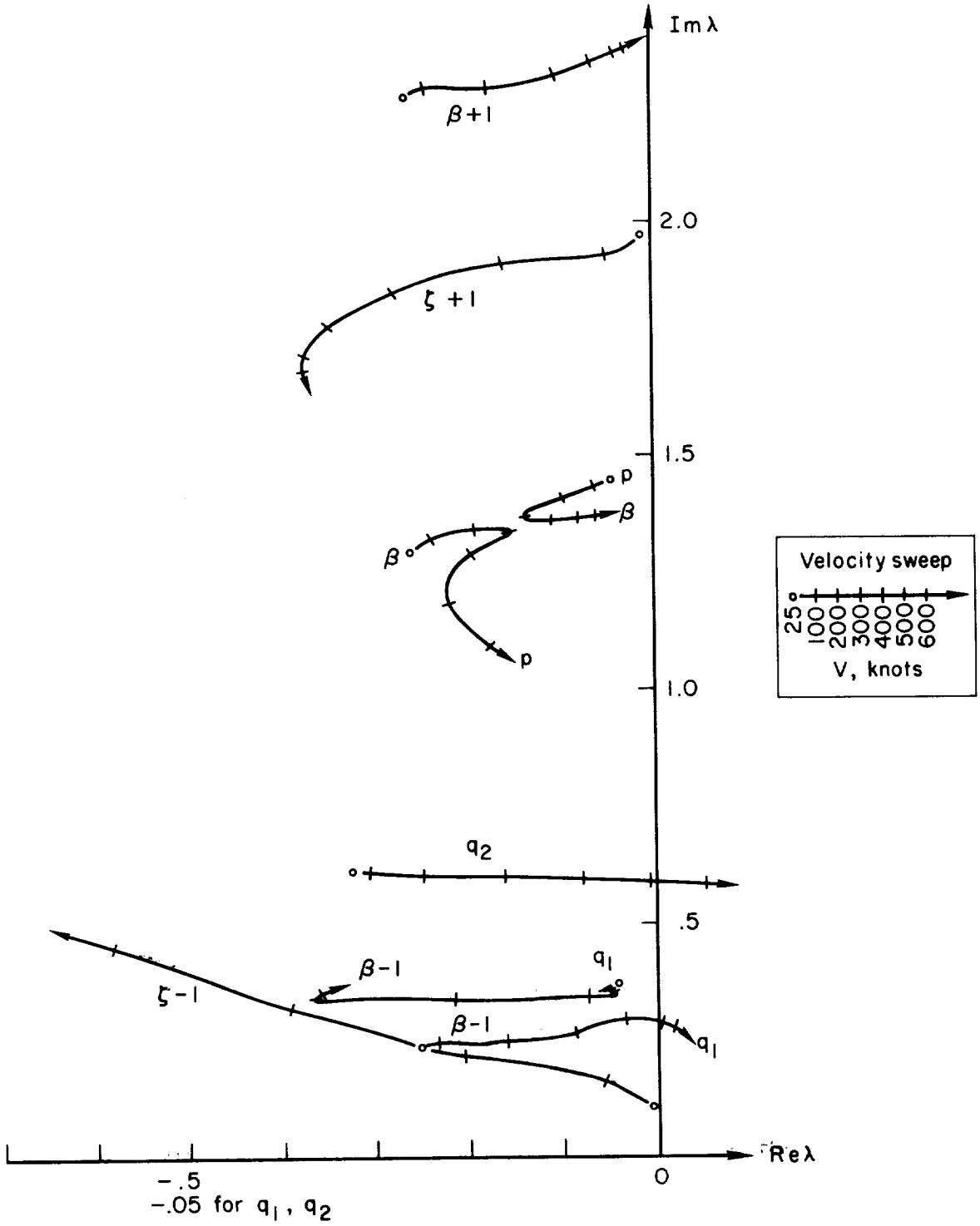

(c) Root locus.

Figure 34.- Continued.

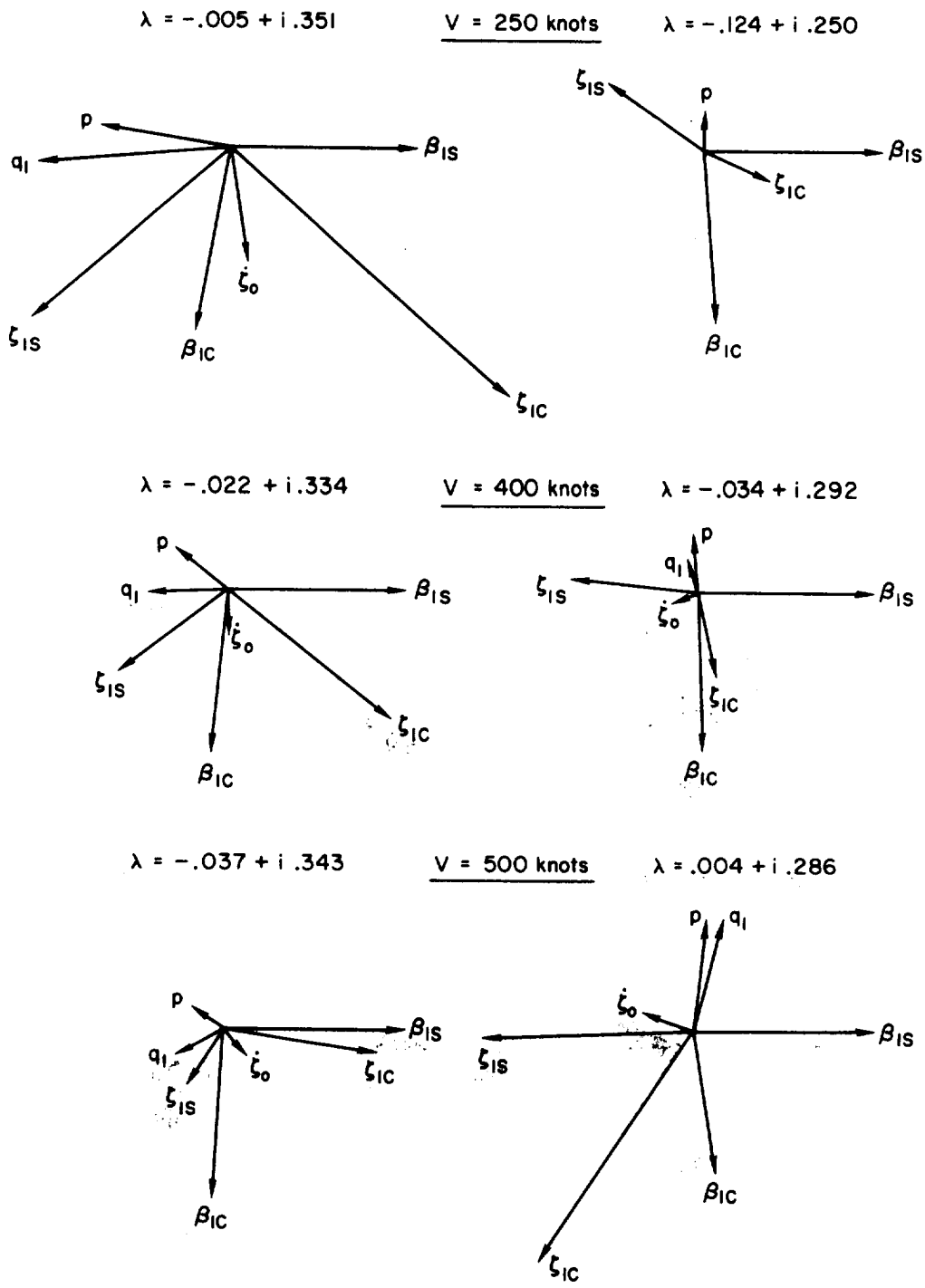

(d) Boeing rotor at Ω = 386 rpm; variation with velocity of predicted eigenvectors for wing vertical bending (q_1) and rotor flap (β - 1) modes.

Figure 34.- Concluded.

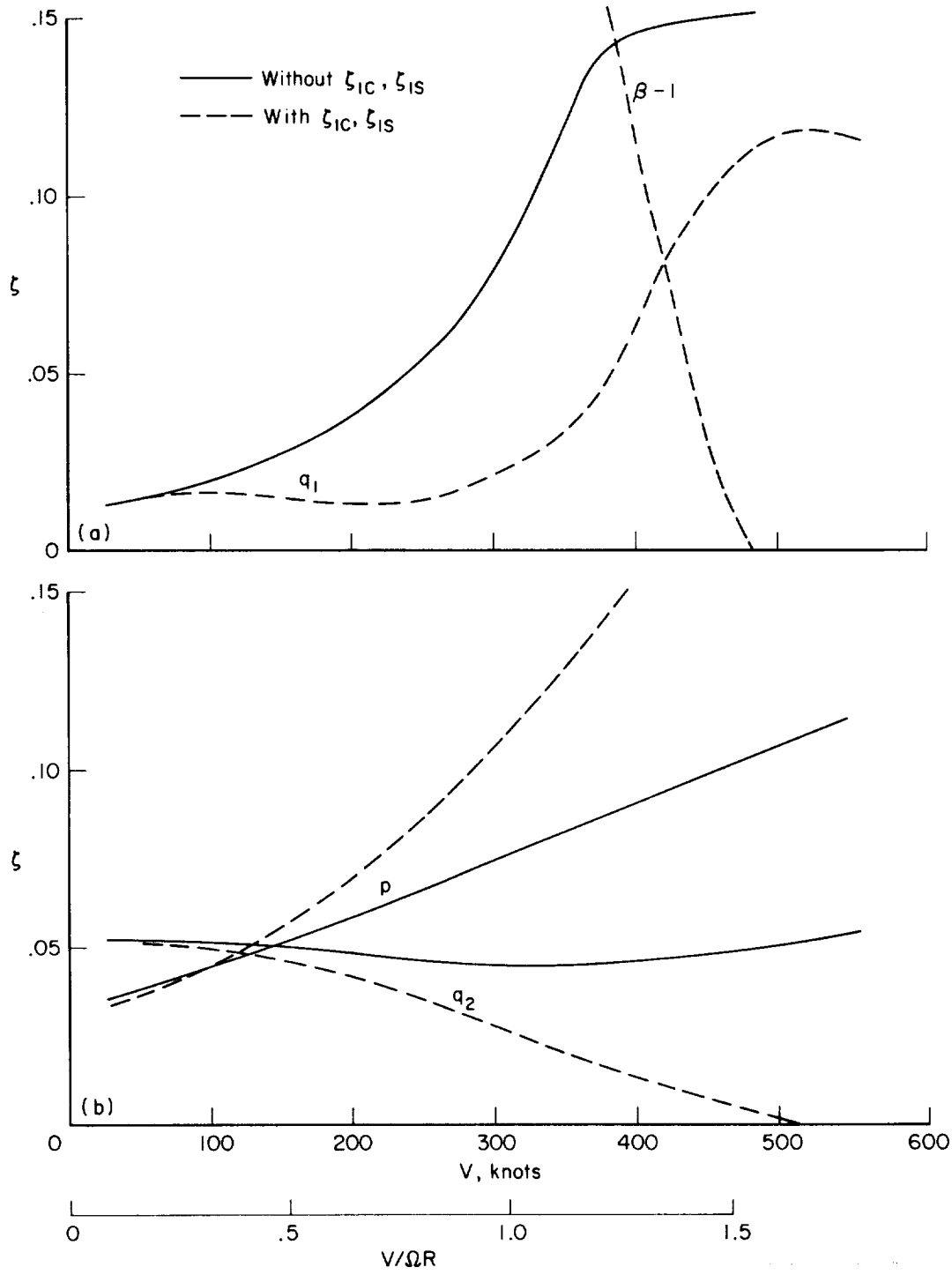

(a) Wing vertical bending (q_1) and rotor flap (β - 1) damping.
(b) Wing chordwise bending (q_2) and torsion (p) damping.

Figure 35.- Boeing rotor velocity sweep, Ω = 386 rpm; with and without ζ_{1C} and ζ_{1S} rotor lag motion.

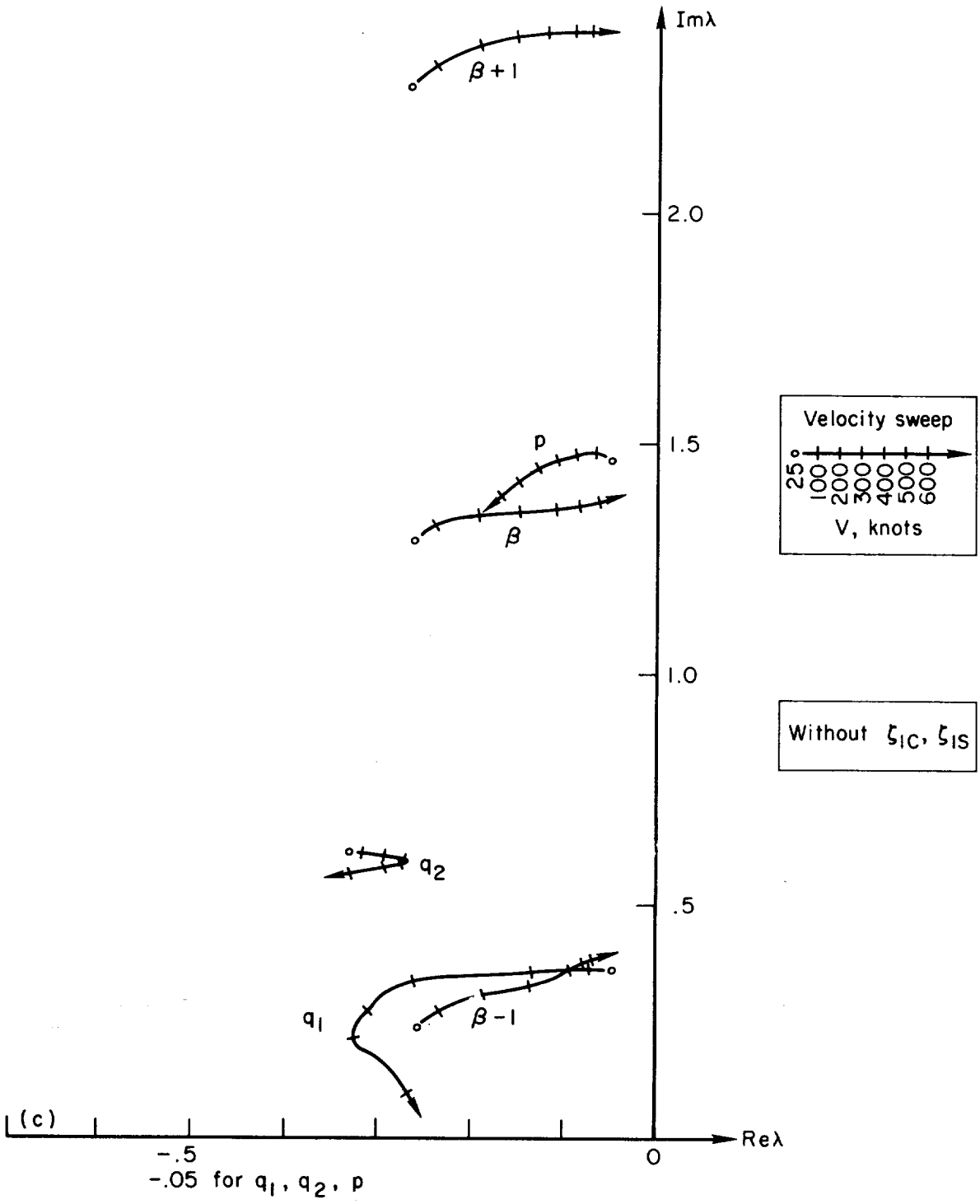

(c) Root locus.

Figure 35.- Concluded.

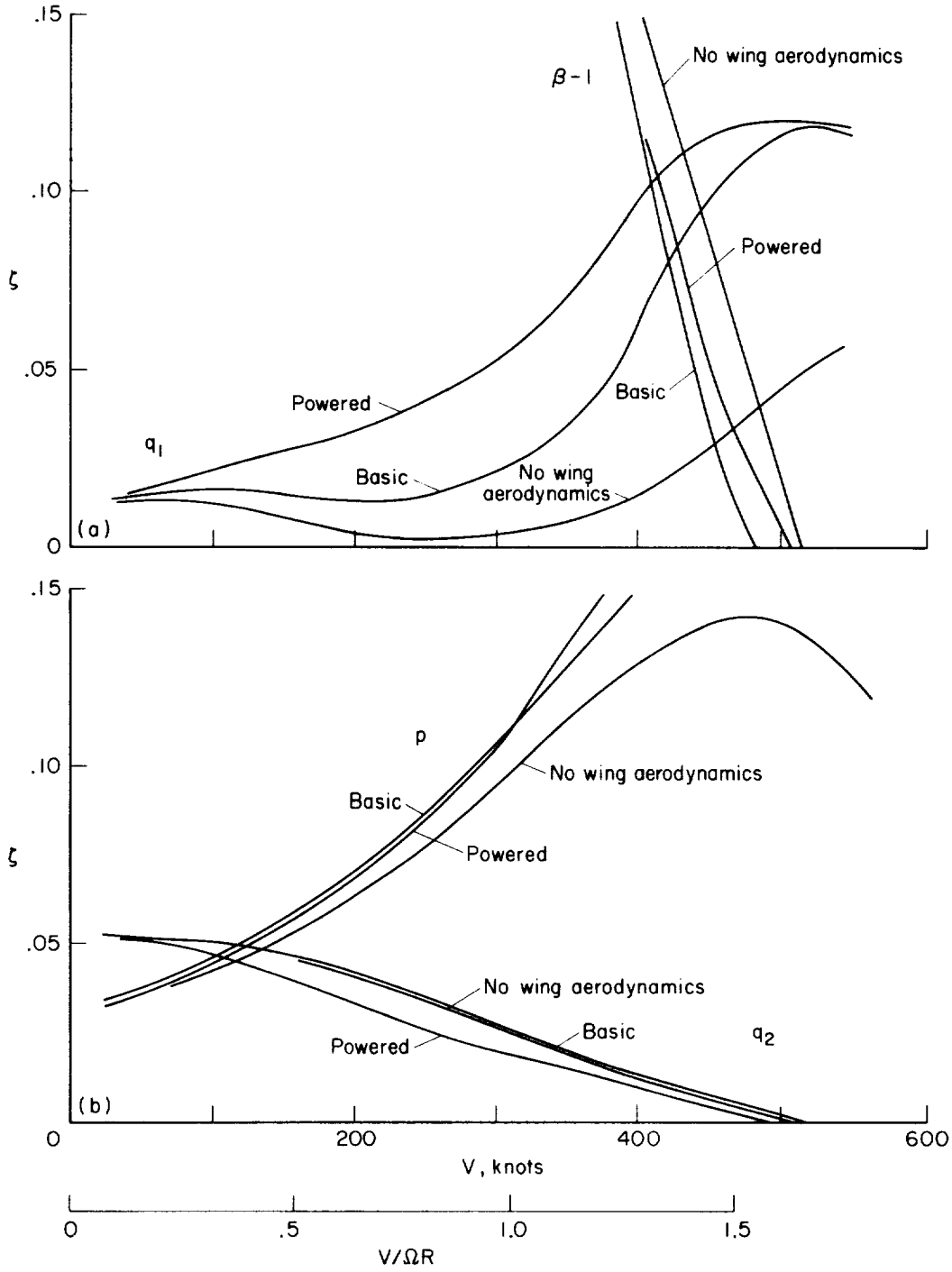

(a) Wing vertical bending (q_1) and rotor flap (β - 1) damping.
(b) Wing chordwise bending (q_2) and torsion (p) damping.

Figure 36.- Boeing rotor velocity sweep, Ω = 386 rpm; comparison of basic (autorotation and wing aerodynamics), powered, and no wing aerodynamics cases.

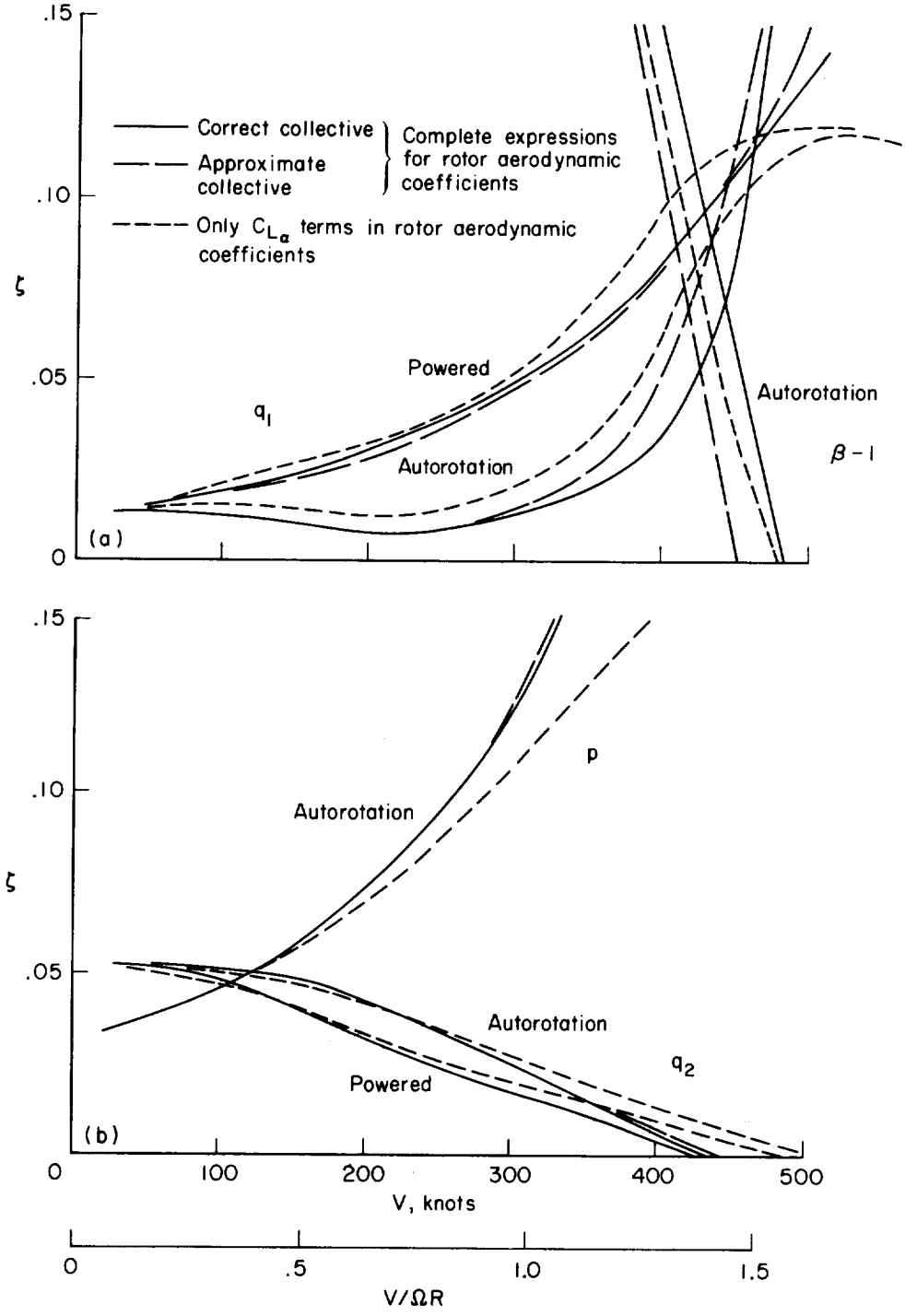

(a) Wing vertical bending (q_1) and rotor flap (β - 1) damping.
(b) Wing chordwise bending (q_2) and torsion (p) damping.

Figure 37.- Boeing rotor velocity sweep, Ω = 386 rpm; influence of the complete expressions for the rotor aerodynamic coefficients.

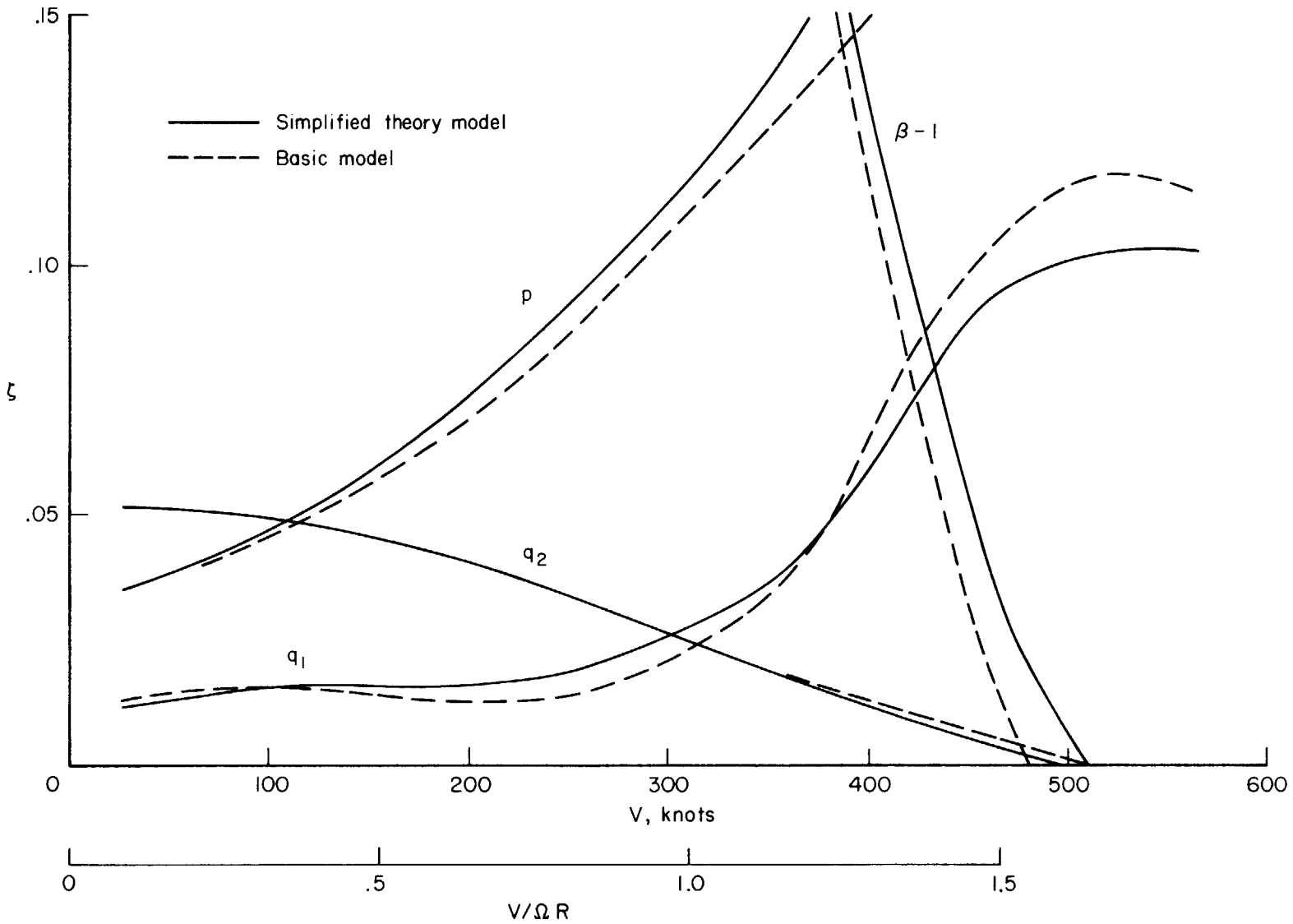

Figure 38.- Boeing rotor velocity sweep, Ω = 386 rpm; comparison of simplified and basic theoretical models; damping ratio for wing vertical bending (q_1), chordwise bending (q_2), torsion (p), and rotor flap (β - 1) modes.

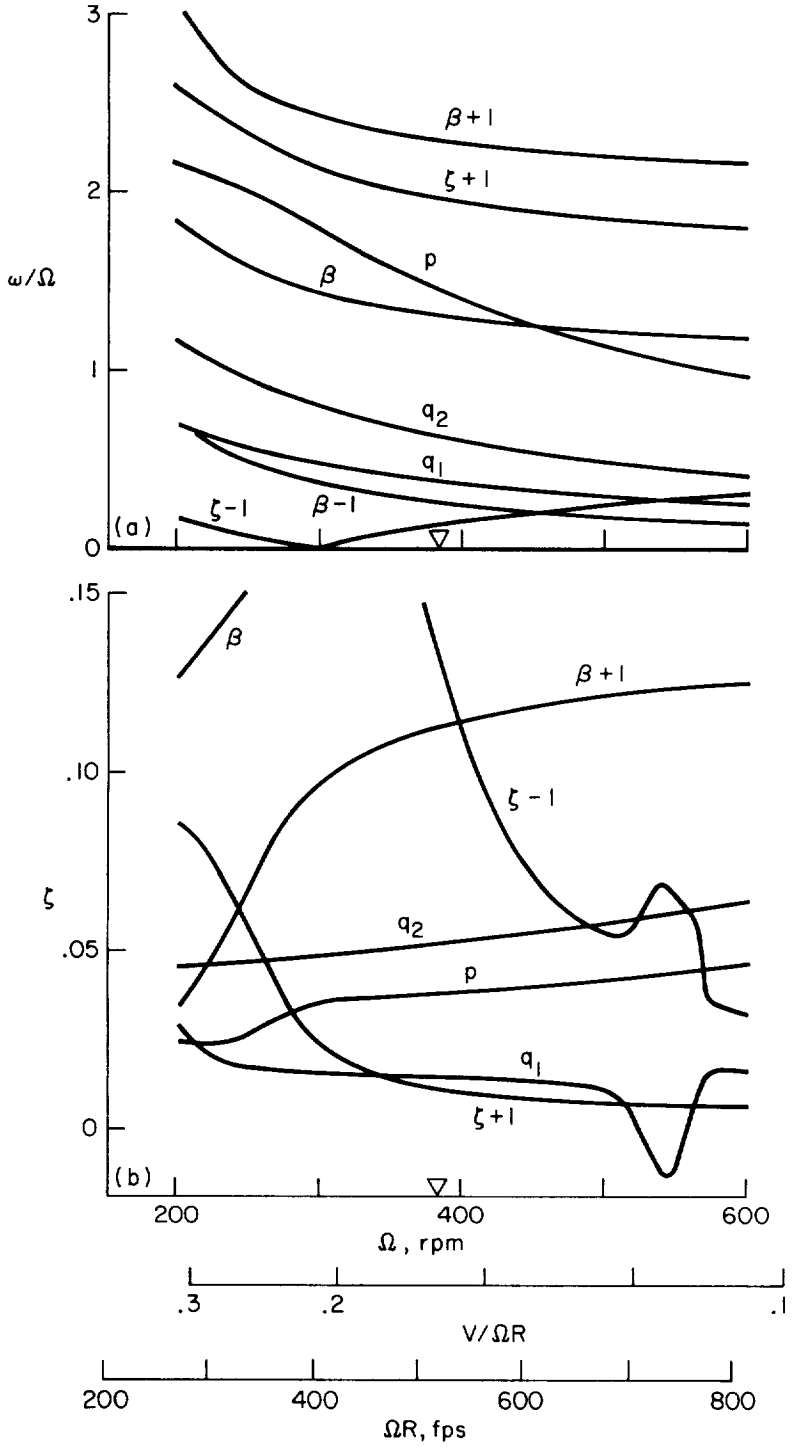

(a) Frequency of the modes.
(b) Damping ratio of the modes.

Figure 39.- Boeing rotor rpm sweep, V = 50 knots.

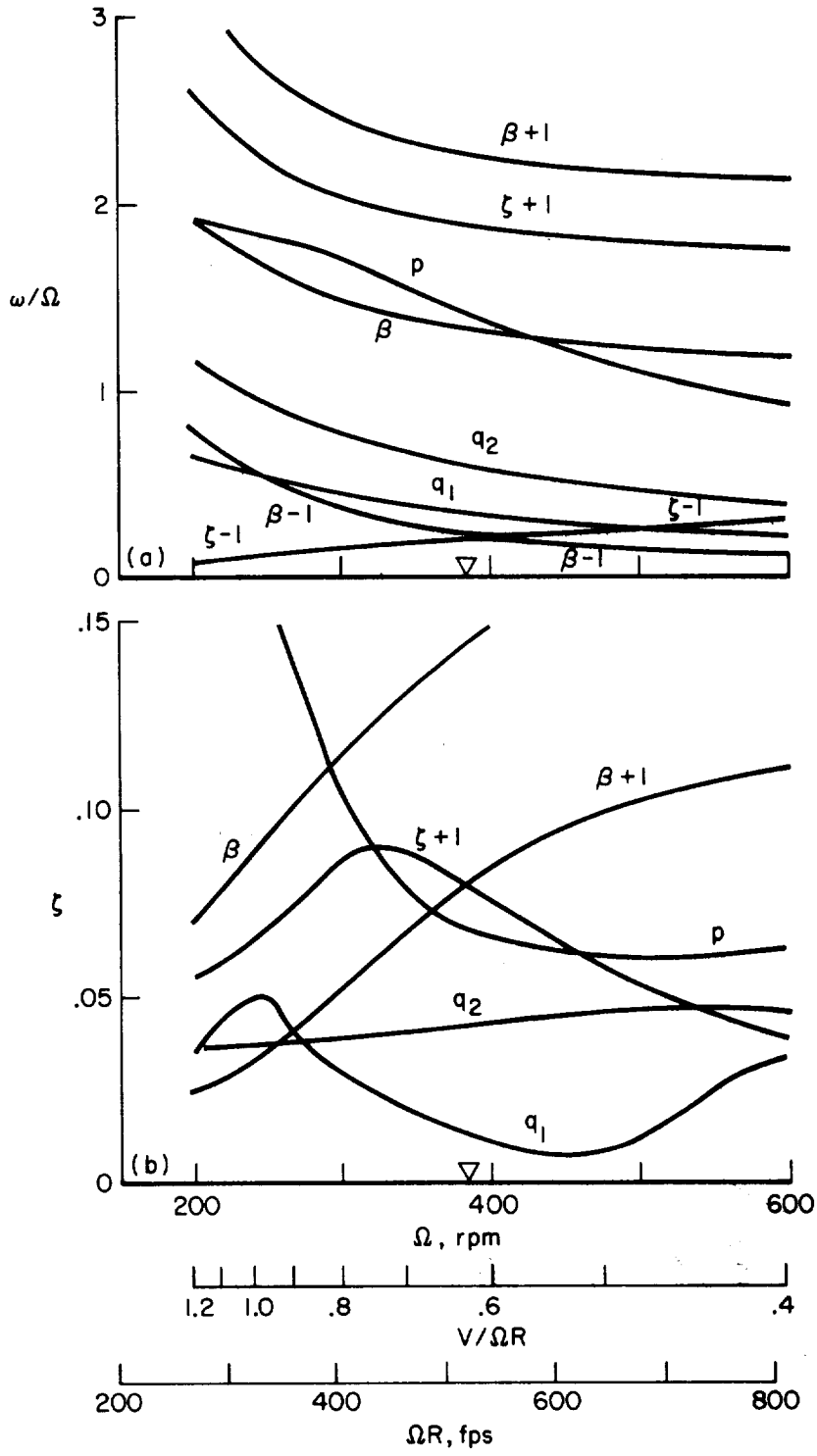

(a) Frequency of the modes.
(b) Damping ratio of the modes.

Figure 40.- Boeing rotor rpm sweep; V = 192 knots.

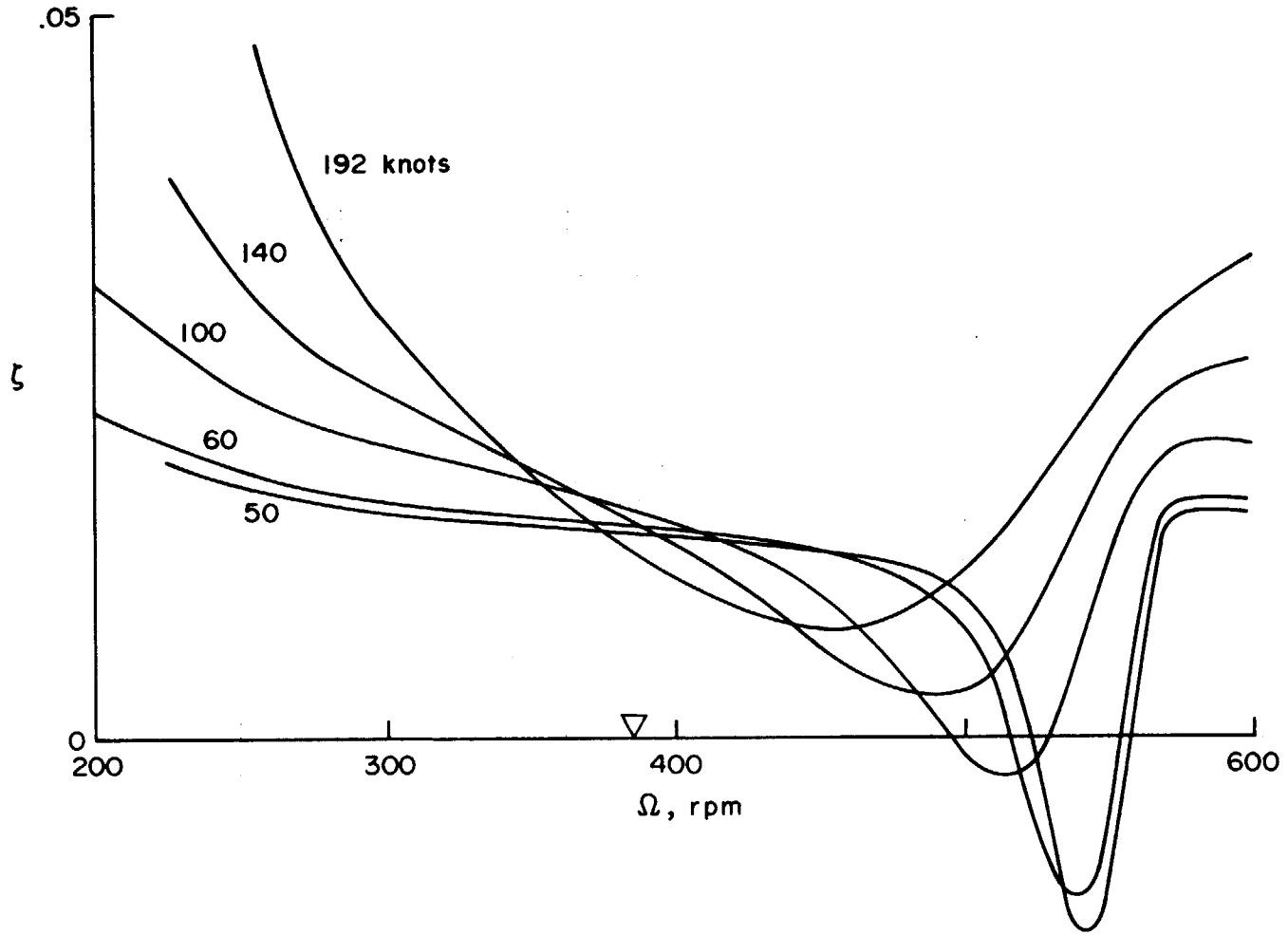

Figure 41.- Boeing rotor air resonance behavior; wing vertical bending (q_1) damping variation with rotor speed at V = 50 to 192 knots.

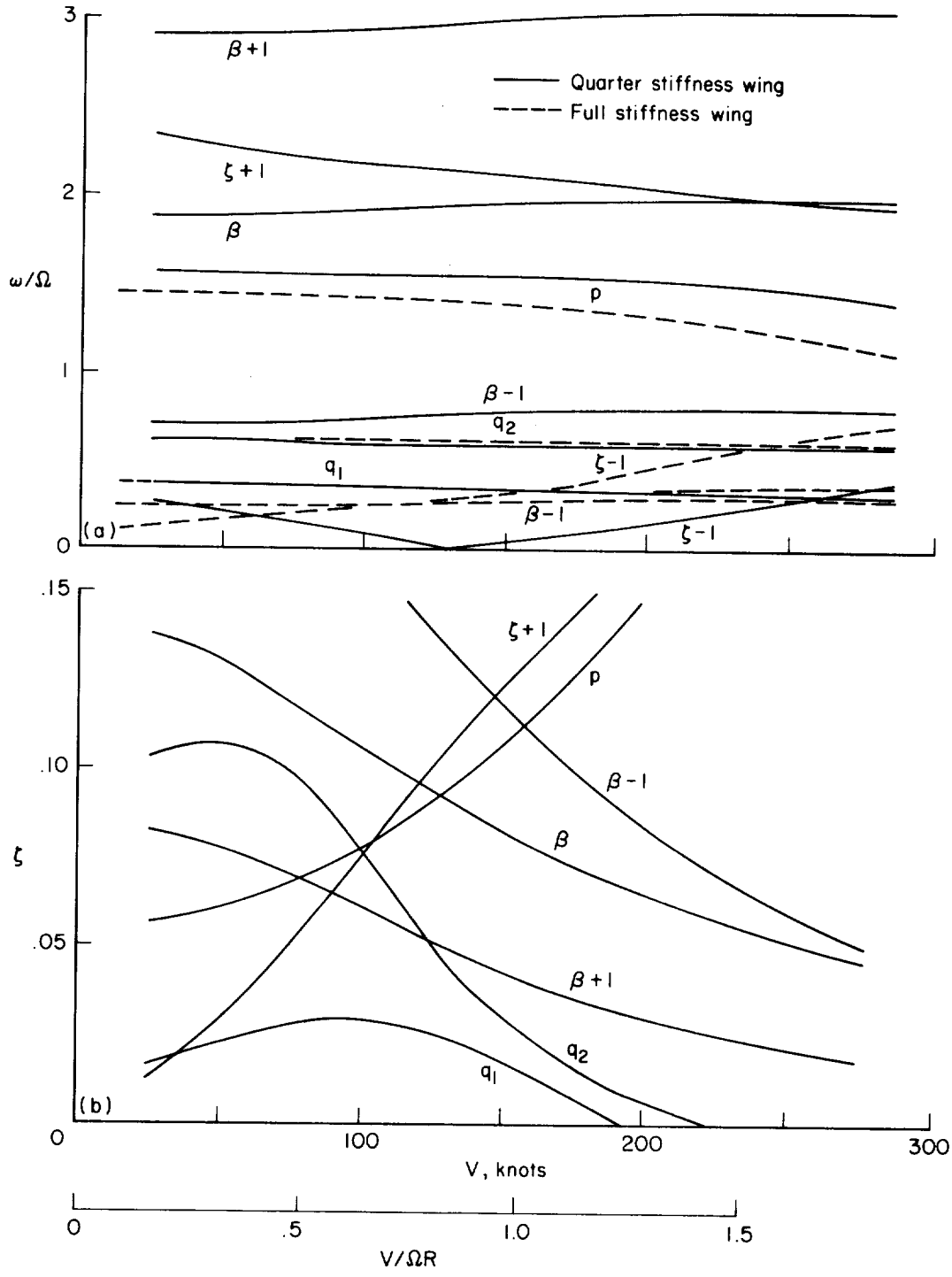

(a) Frequency of the modes.
(b) Damping ratio of the modes.

Figure 42.- Boeing rotor velocity sweep, quarter-stiffness wing, Ω = 193 rpm.

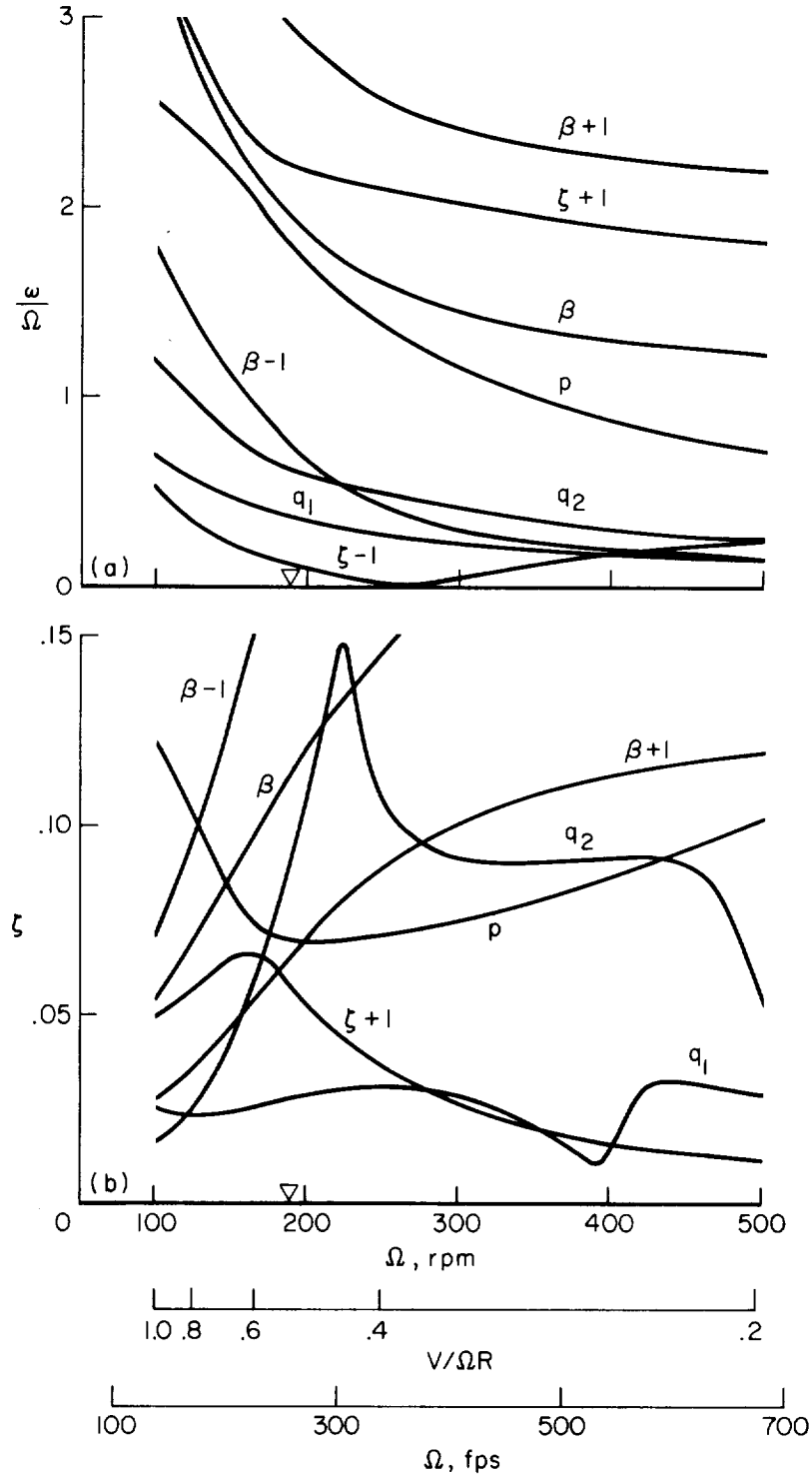

(a) Frequency of the modes.
(b) Damping ratio of the modes.

Figure 43.- Boeing rotor rpm sweep, quarter-stiffness wing, V = 80 knots.

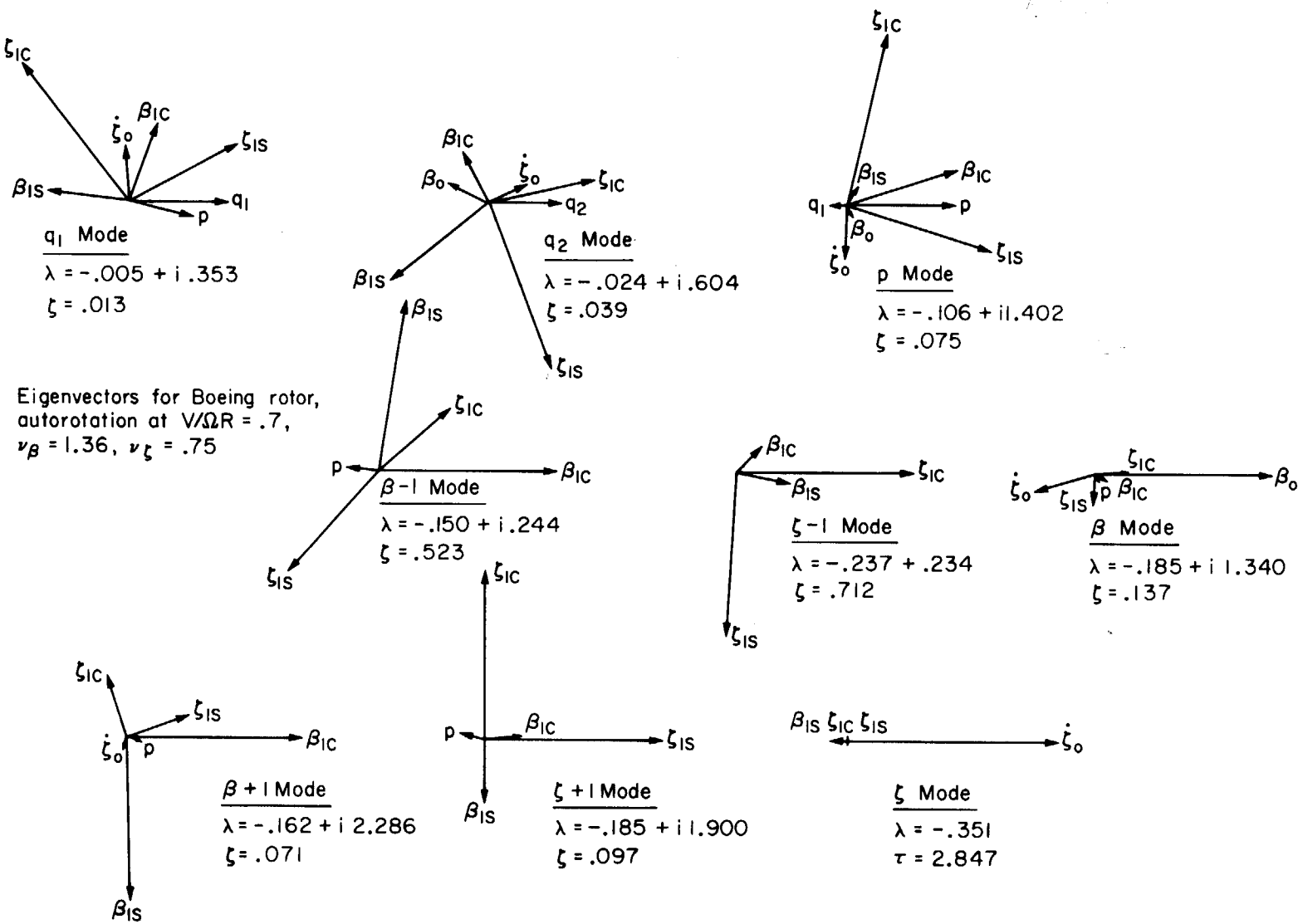

(a) Autorotation.

Figure 44.- Boeing rotor roots and modes at $V/\Omega R$ = 0.7, Ω = 386 rpm, V = 218 knots.

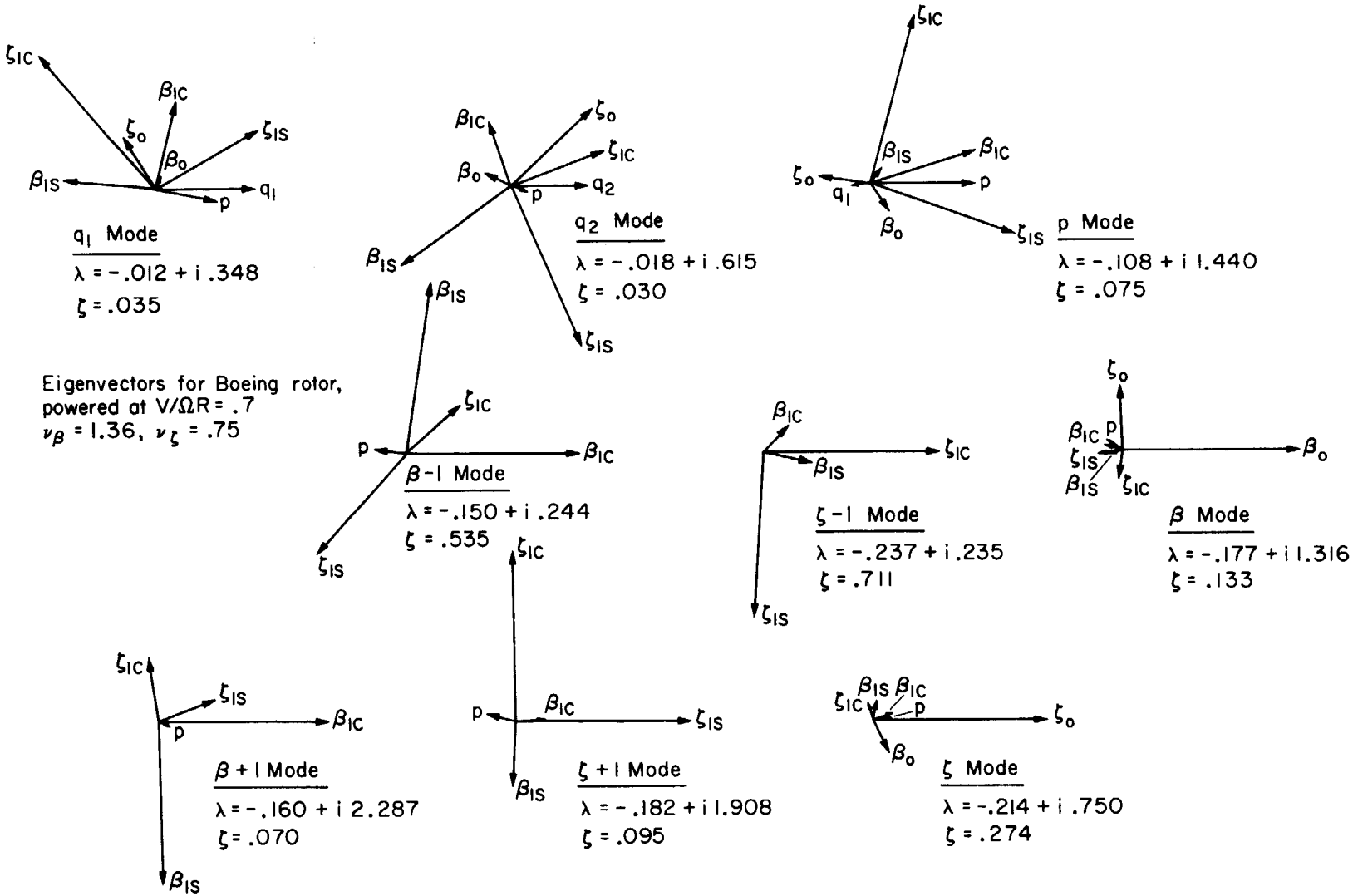

(b) Powered flight.

Figure 44.- Concluded.

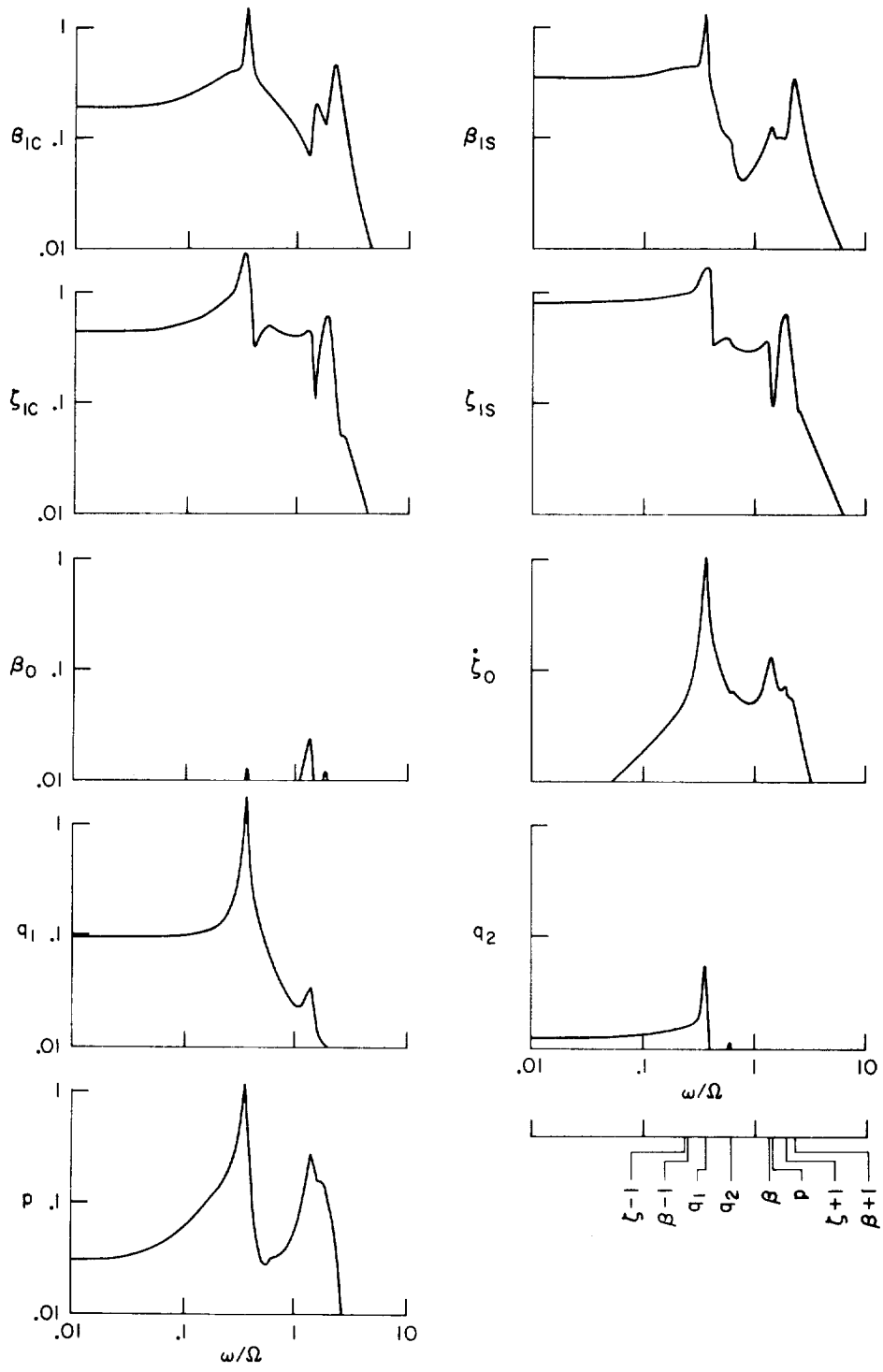

(a) Vertical gust α_G input.

Figure 45.- Boeing rotor in autorotation at $V/\Omega R$ = 0.7 (Ω = 386 rpm, V = 218 knots), magnitude of response of each degree of freedom to input at frequency ω.

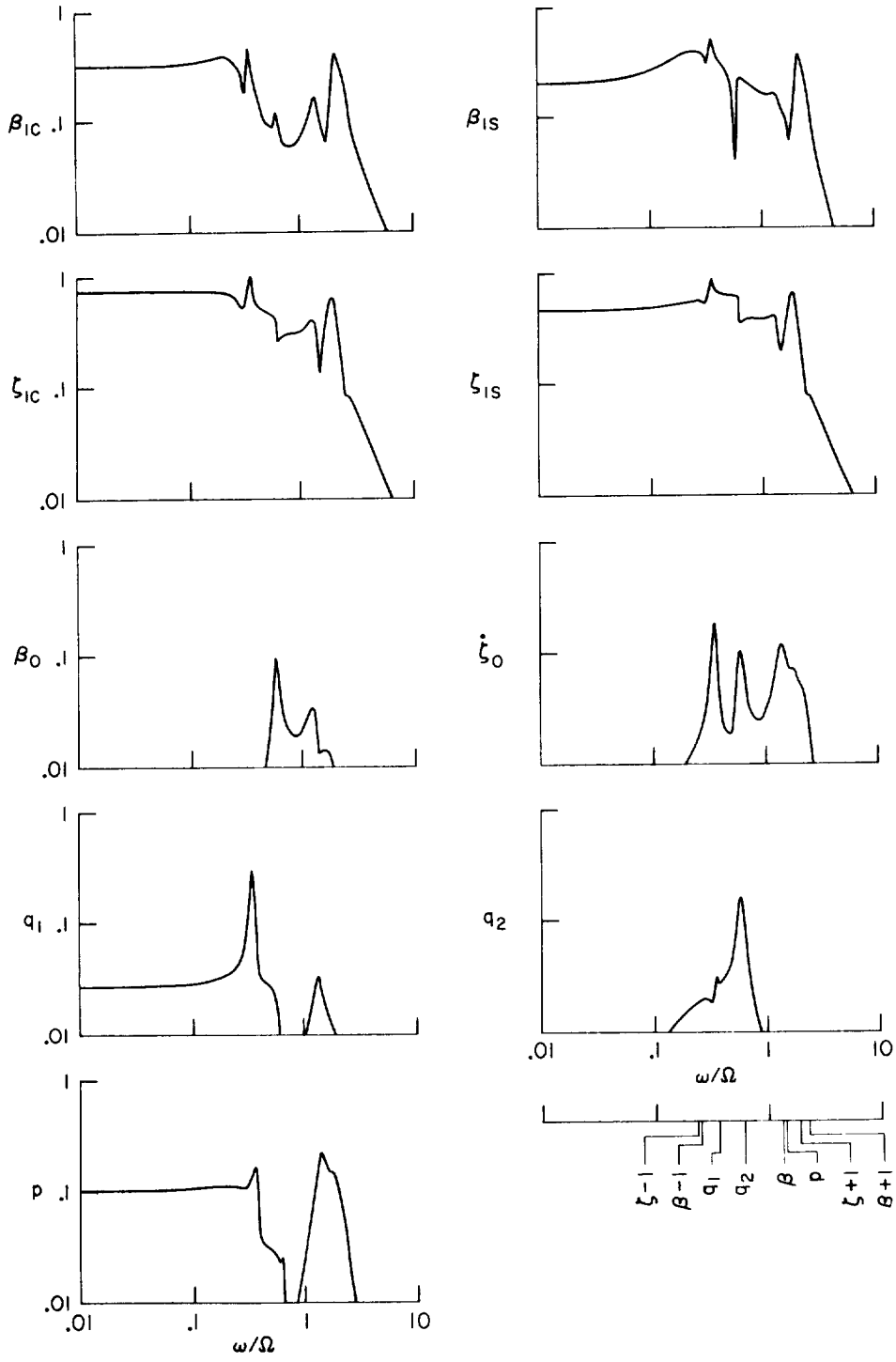

(b) Lateral gust β_G input.

Figure 45.- Continued.

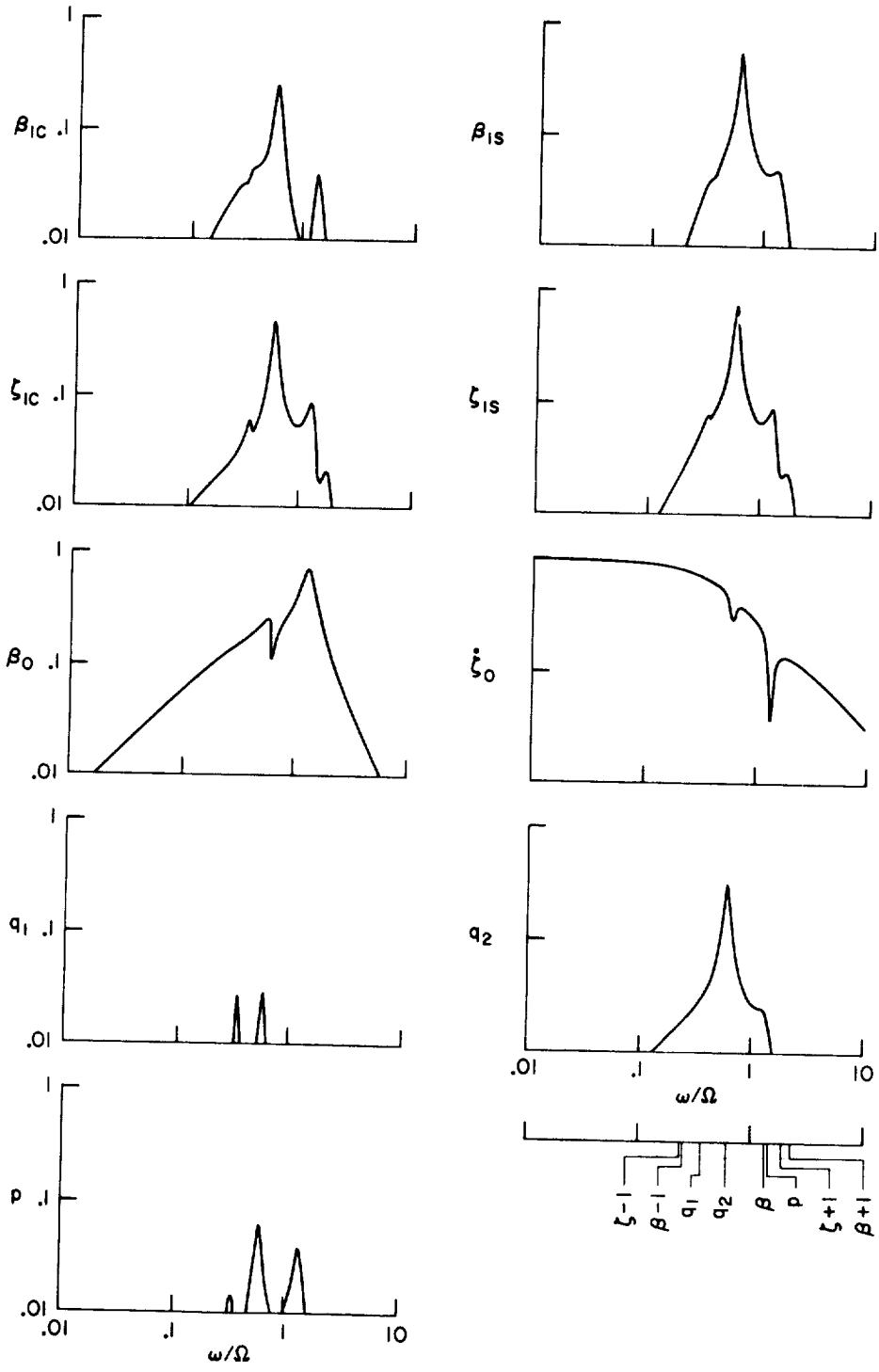

(c) Longitudinal gust u_G input.

Figure 45.- Continued.

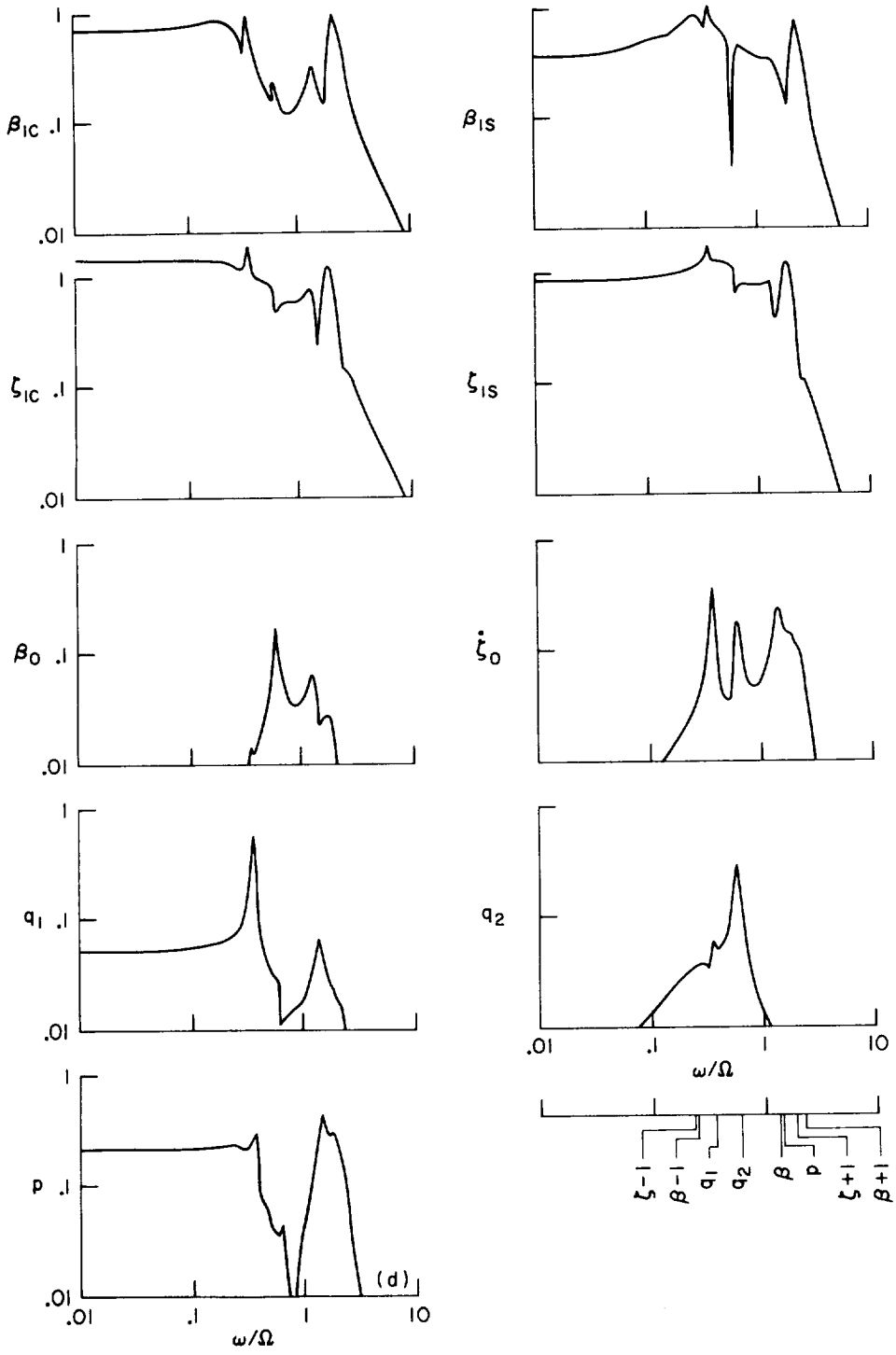

(d) Lateral cyclic pitch θ_{1C} input.

Figure 45.- Continued.

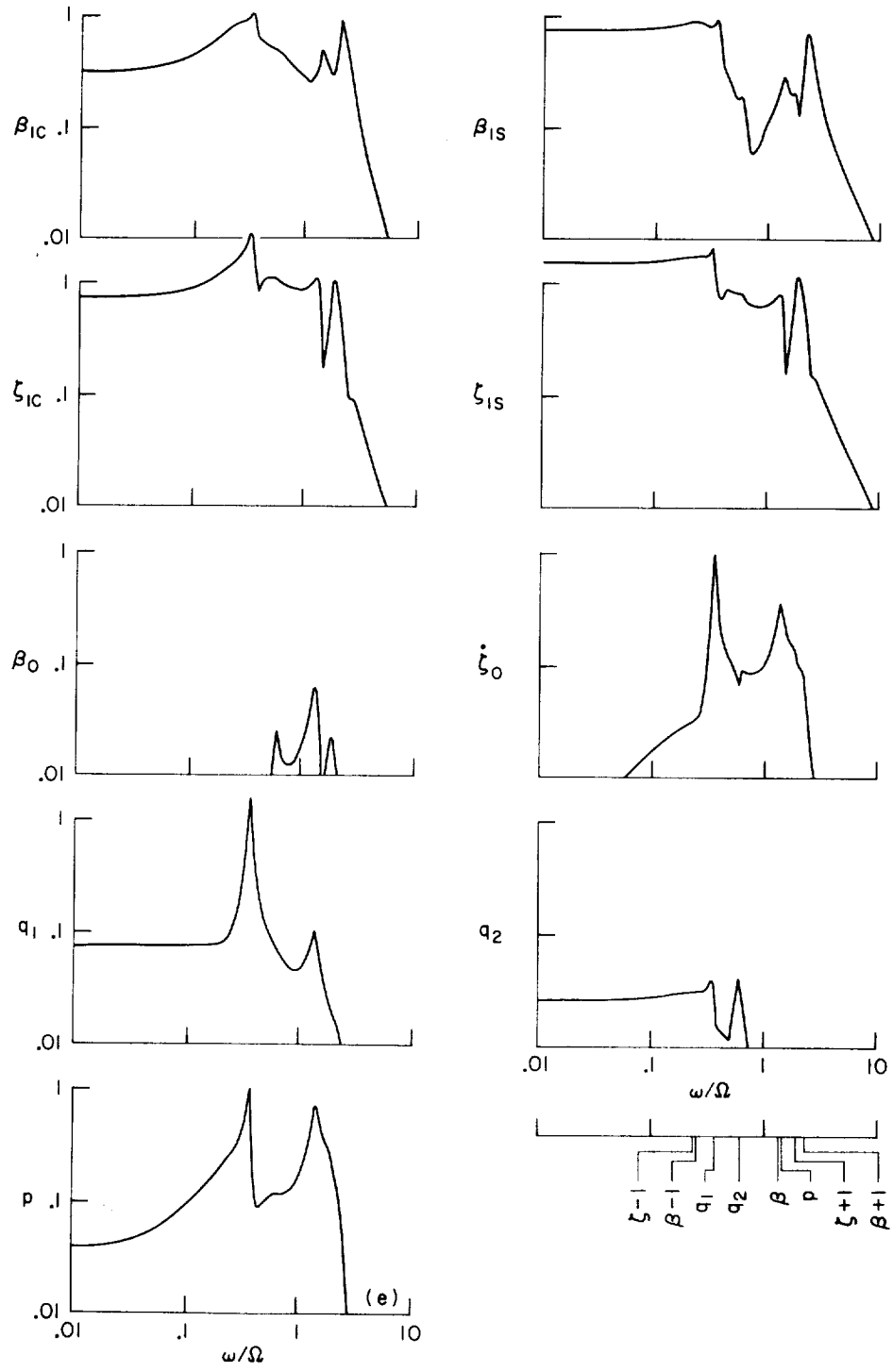

(e) Longitudinal cyclic pitch θ_{1S} input.

Figure 45.- Continued.

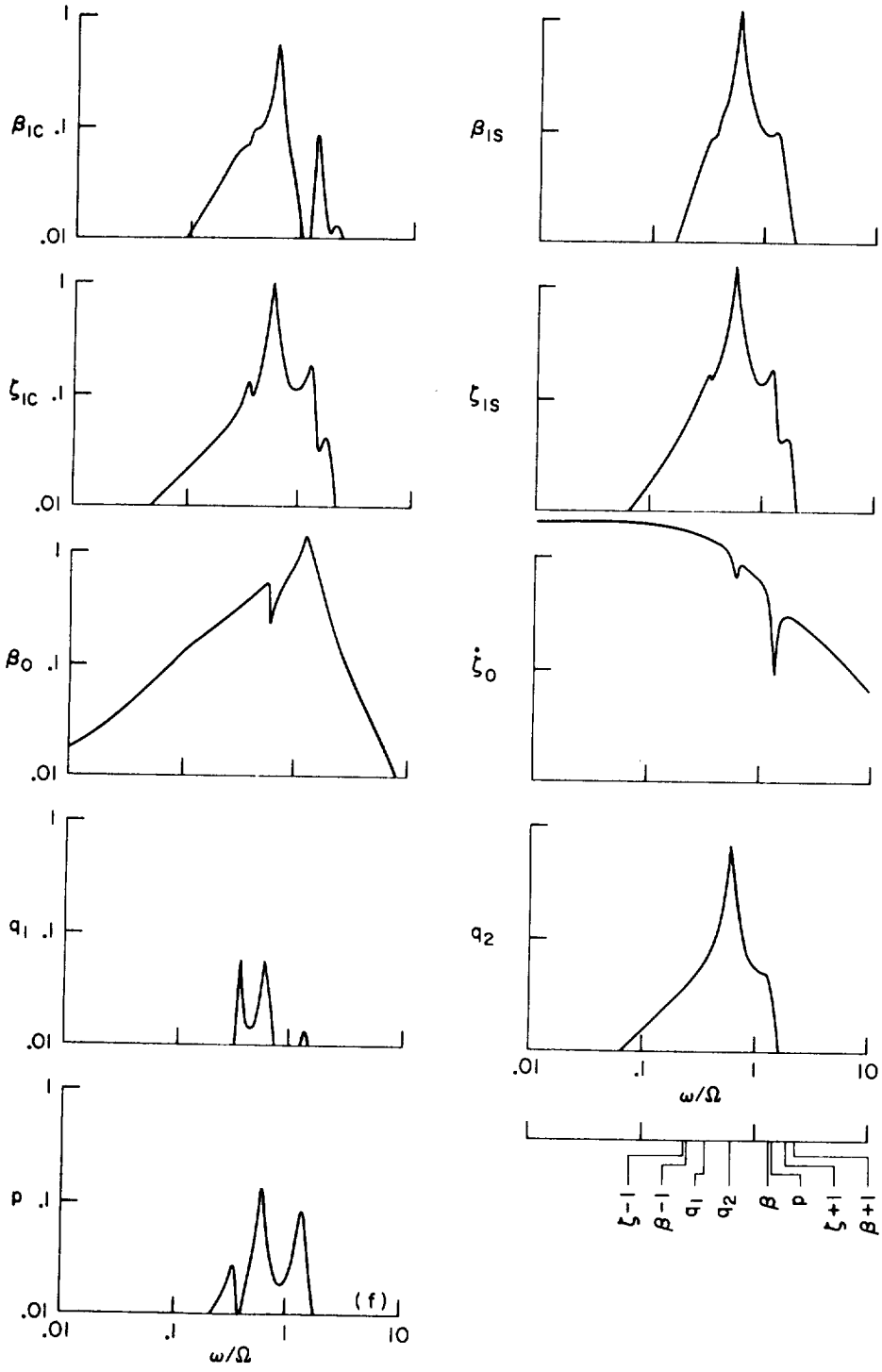

(f) Collective pitch θ_0 input.

Figure 45.- Concluded.

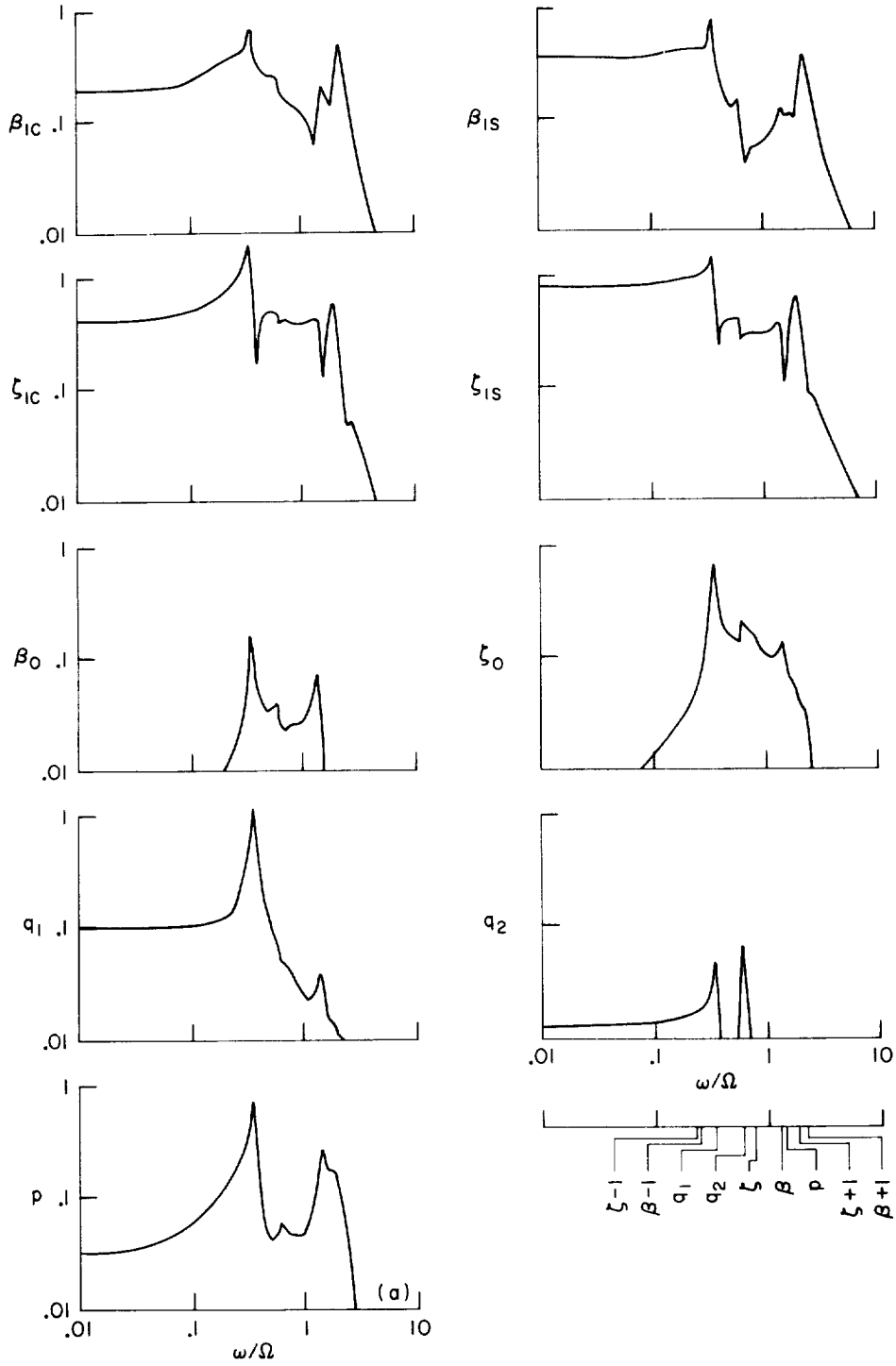

(a) Vertical gust α_G input.

Figure 46.- Boeing rotor in powered operation at $V/\Omega R$ = 0.7 (Ω = 386 rpm, V = 218 knots), magnitude of response of each degree of freedom to input at frequency ω.

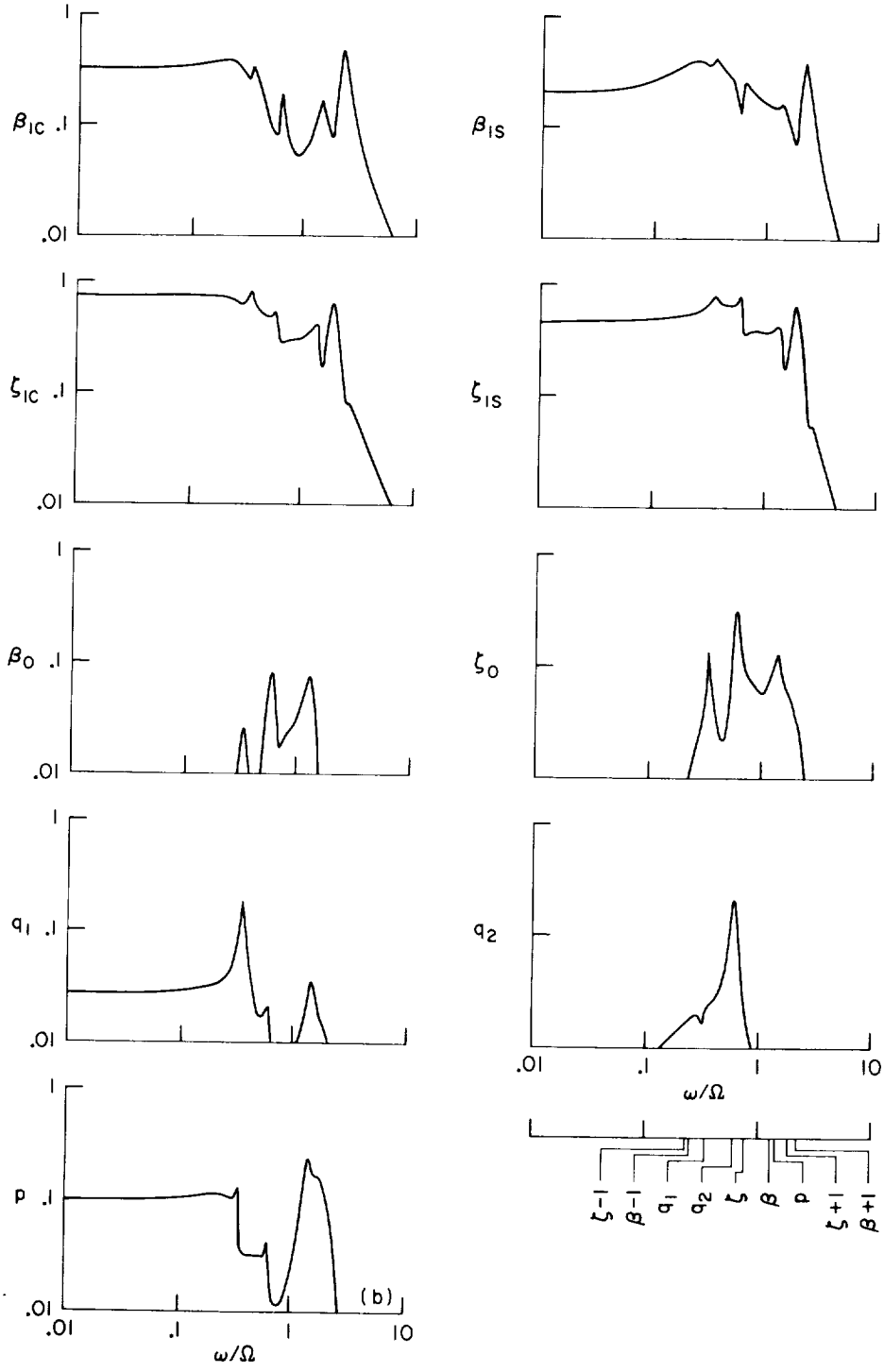

(b) Lateral gust β_G input.

Figure 46.- Continued.

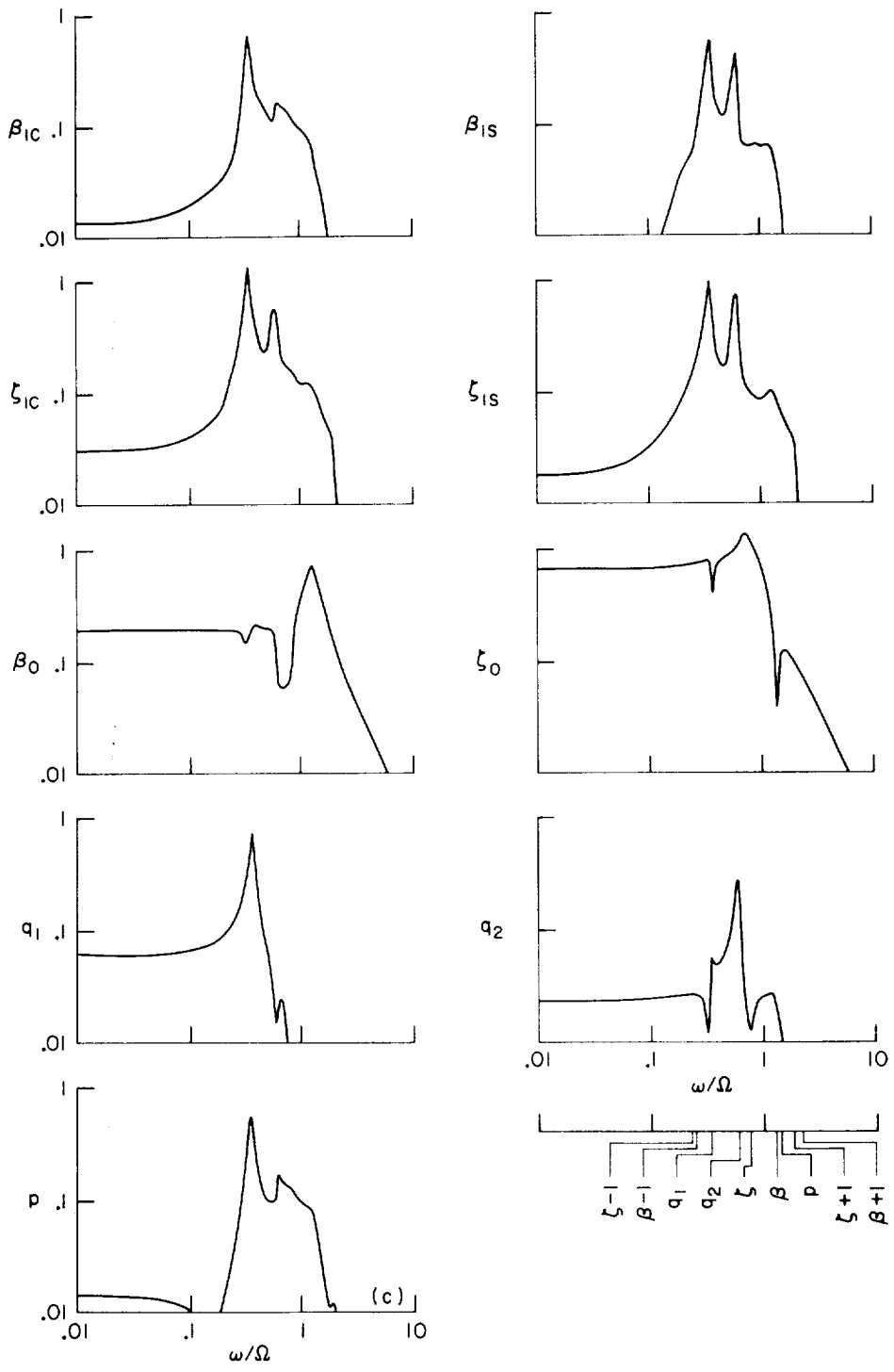

(c) Longitudinal gust u_G input.

Figure 46.- Continued.

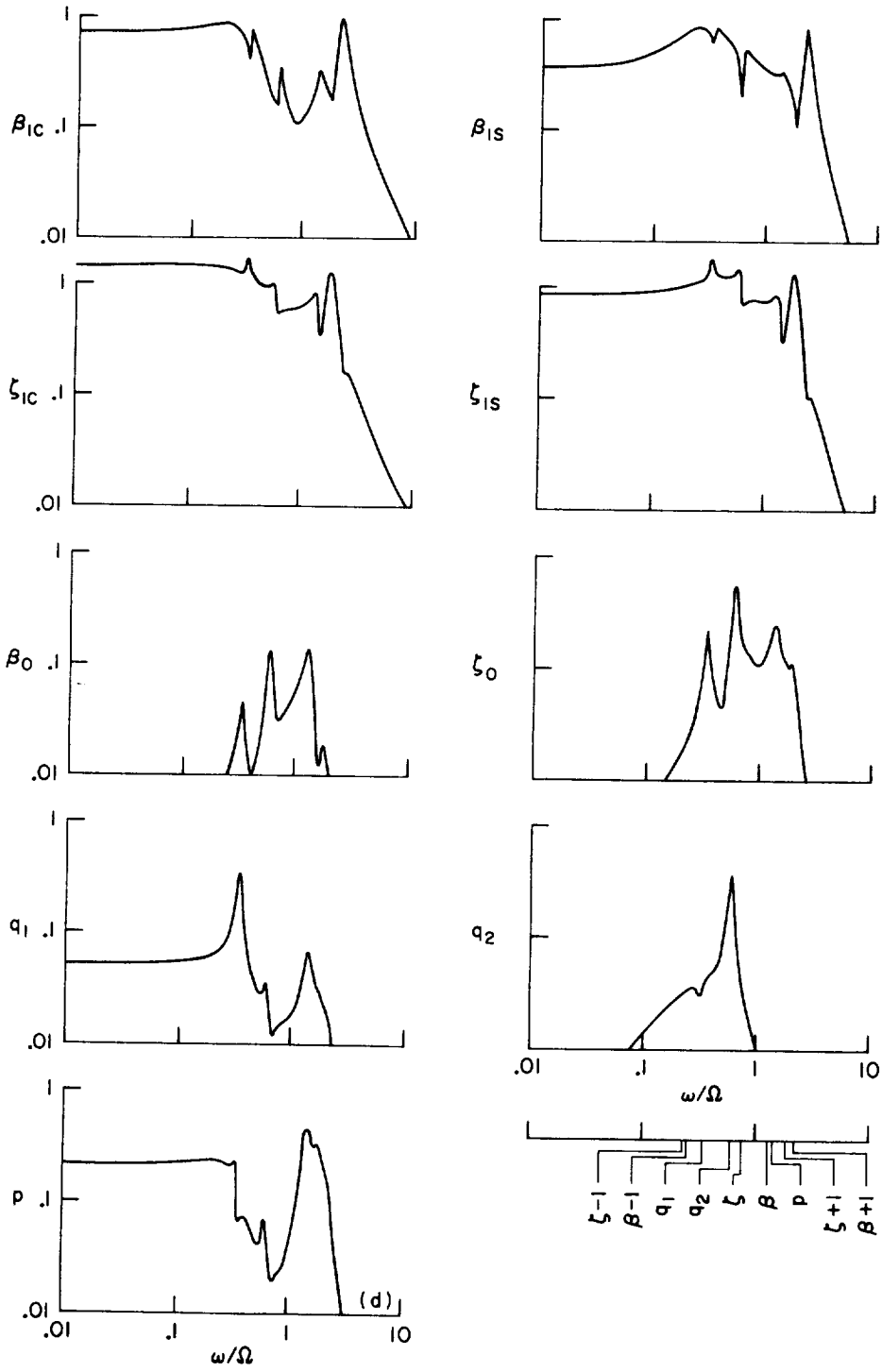

(d) Lateral cyclic pitch θ_{1C} input.

Figure 46.- Continued.

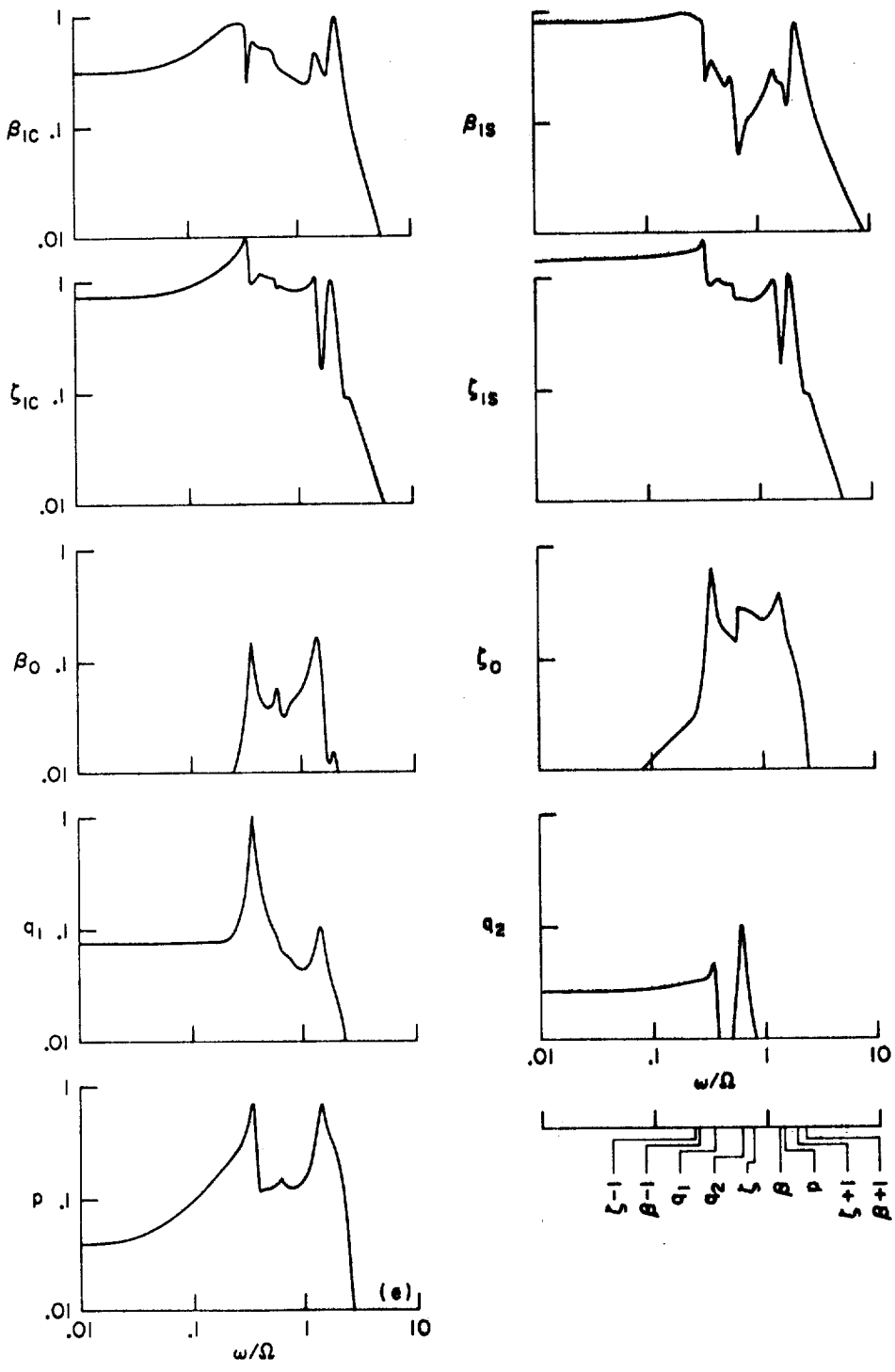

(e) Longitudinal cyclic pitch θ_{1S} input.

Figure 46.- Continued.

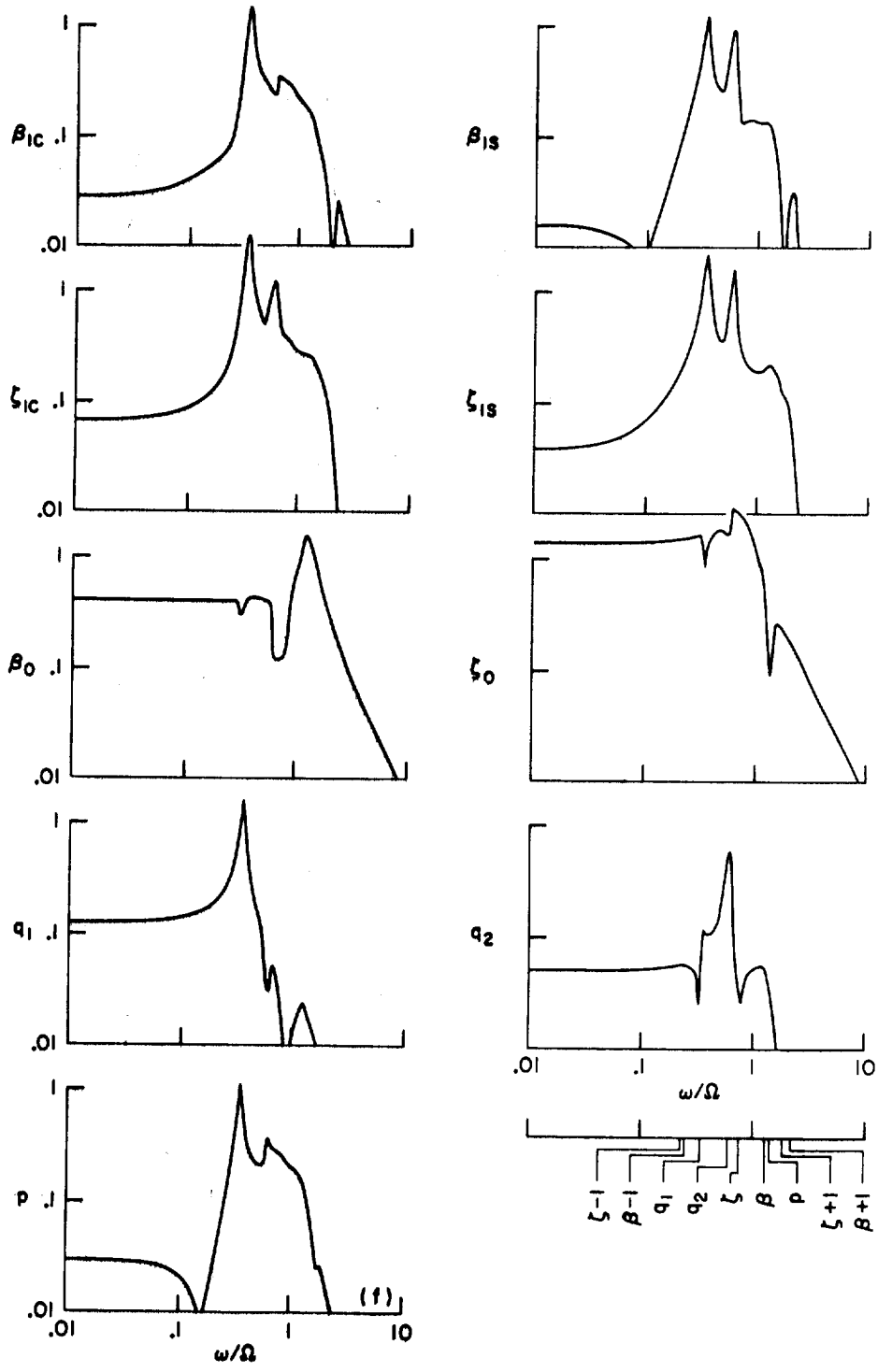

(f) Collective pitch θ_0 input.

Figure 46.- Concluded.

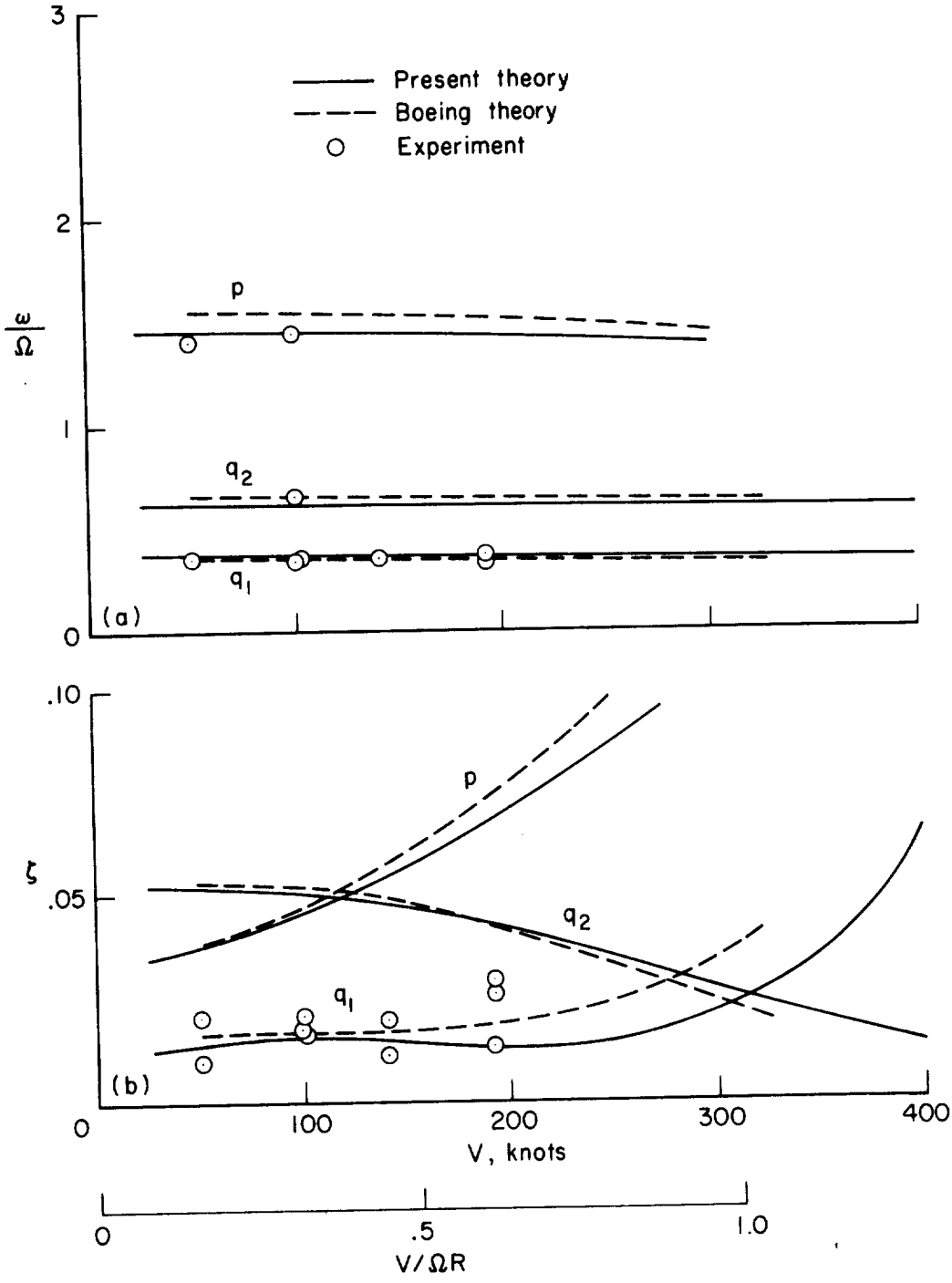

(a) Frequency of the modes.
(b) Damping ratio of wing vertical bending (q_1), chordwise bending (q_2), and torsion (p) modes; experimental data are for q_1 only.

Figure 47.- Boeing rotor velocity sweep at Ω = 386 rpm; comparison with full-scale experimental data and the Boeing theory.

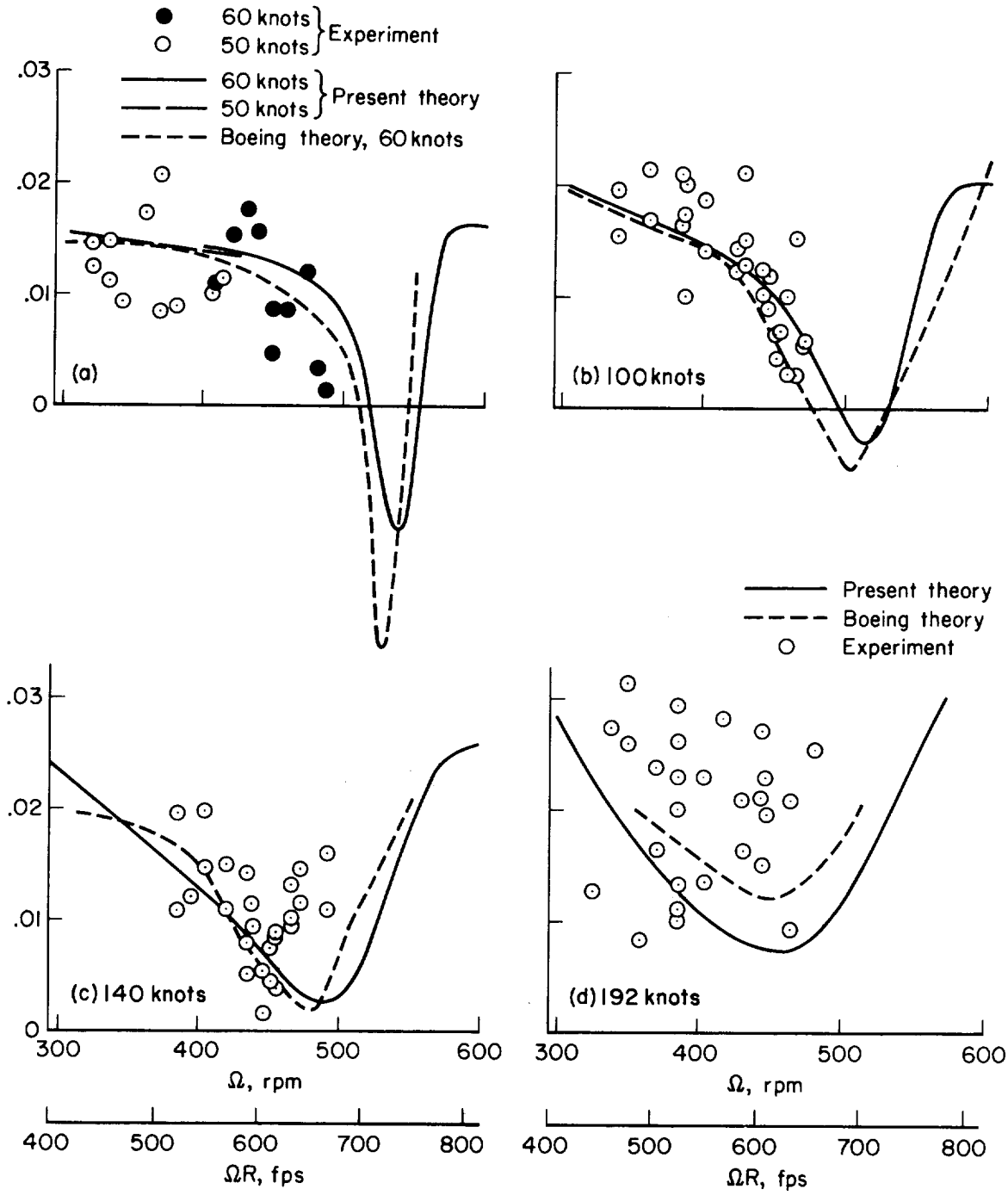

(a) Wing vertical bending damping (q_1) at 50 and 60 knots.
(b) Wing vertical bending damping (q_1) at 100 knots.
(c) Wing vertical bending damping (q_1) at 140 knots.
(d) Wing vertical bending damping (q_1) at 192 knots.

Figure 48.- Boeing rotor rpm sweep, comparison with full-scale experimental data and the Boeing theory.

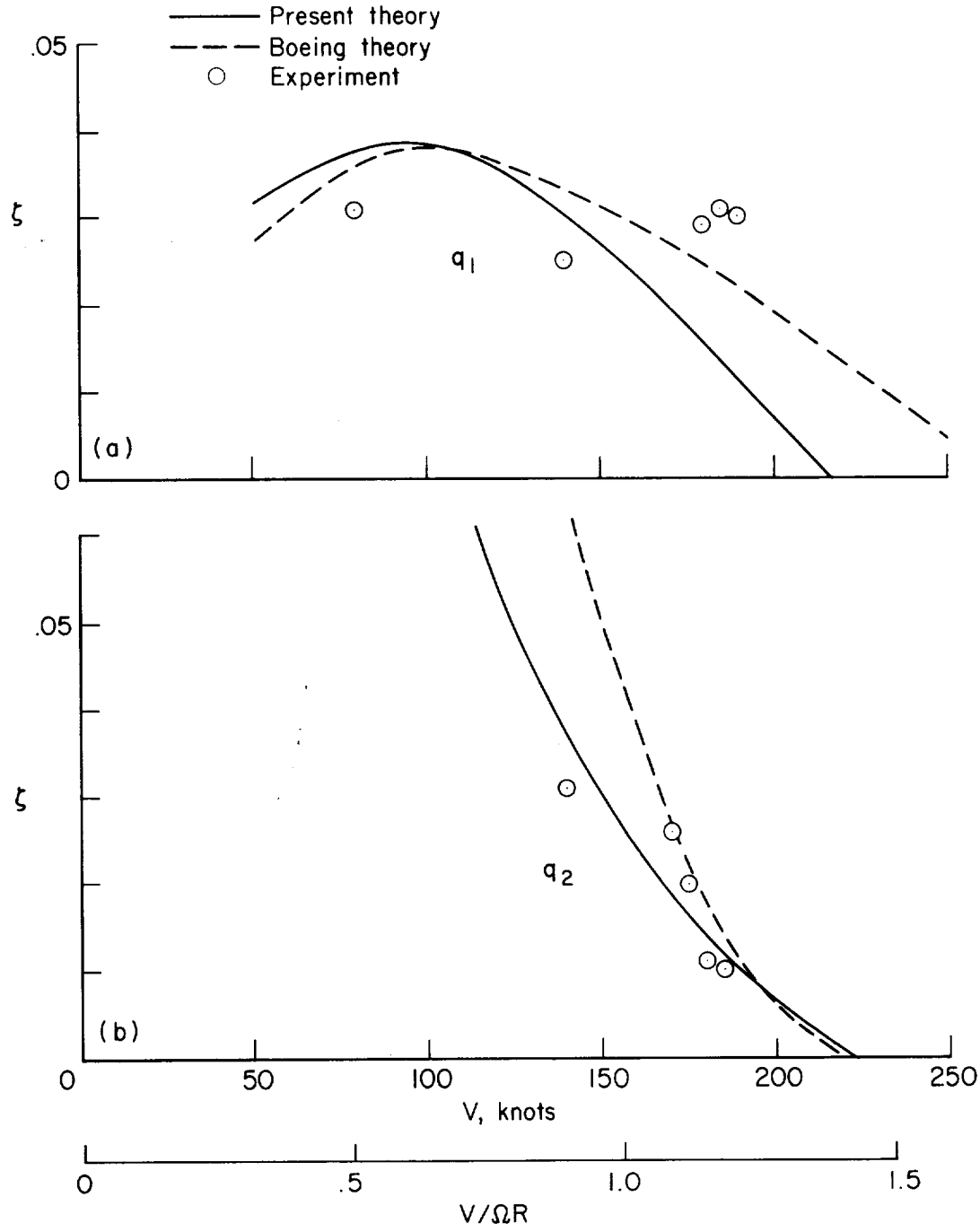

(a) Wing vertical bending damping (q_1).
(b) Wing chordwise bending damping (q_2).

Figure 49.- Boeing rotor on quarter-stiffness wing, velocity sweep at Ω = 193 rpm; comparison with full-scale experimental data and the Boeing theory.

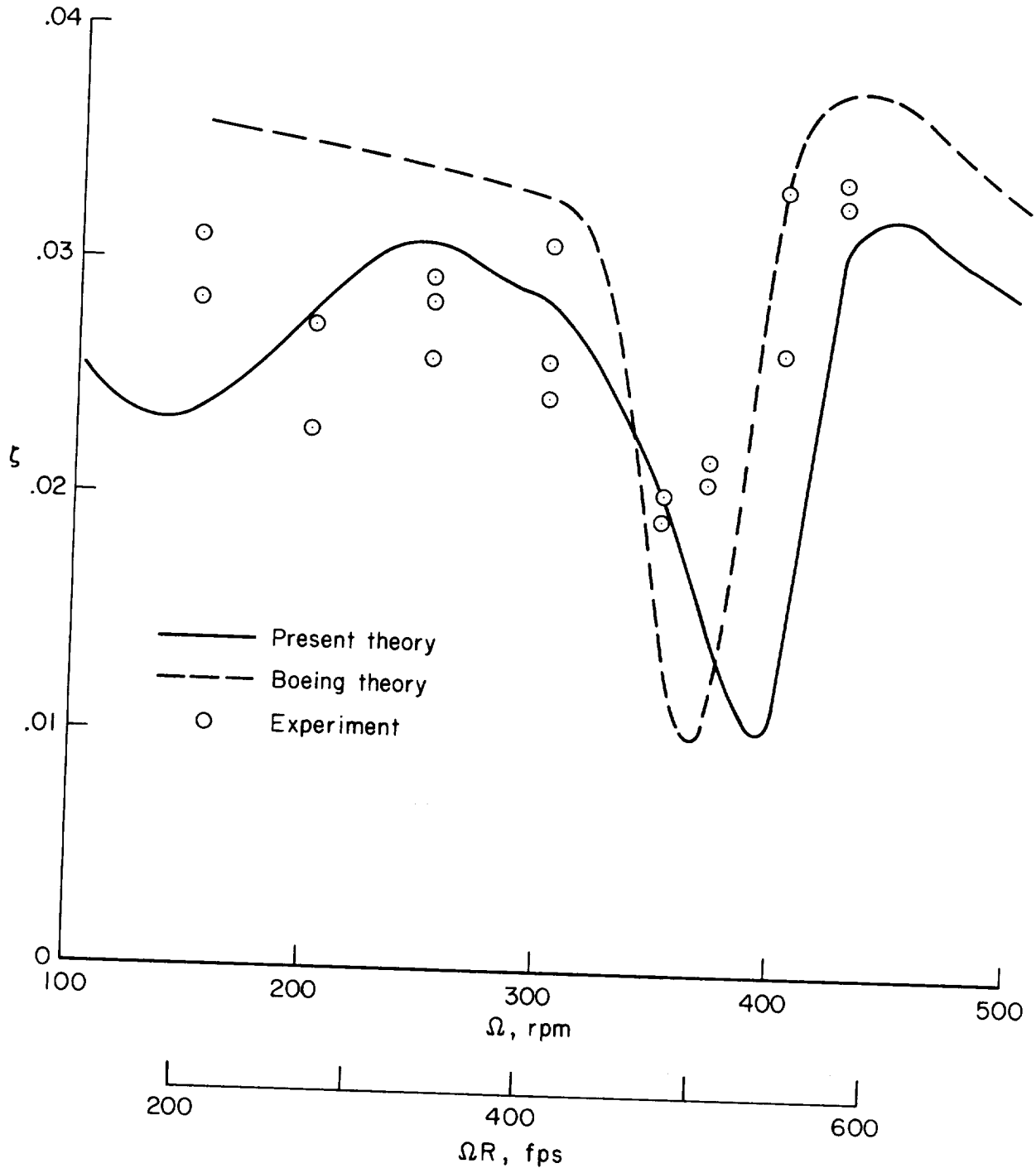

Figure 50.- Boeing rotor on quarter-stiffness wing, rpm sweep at 80 knots; comparison with full-scale experimental data and the Boeing theory; wing vertical bending (q_1) damping.

U.S. GOVERNMENT PRINTING OFFICE: 1974—739-160/130